Jacob W. M. Baars
Hans J. Kärcher

Radio Telescope Reflectors

Historical Development of Design and Construction

ASSL

Springer

Radio Telescope Reflectors

Astrophysics and Space Science Library

More information about this series at http://www.springer.com/series/5664

Jacob W.M. Baars • Hans J. Kärcher

Radio Telescope Reflectors

Historical Development of Design
and Construction

Springer

Jacob W.M. Baars
Max-Planck-Institut für Radioastronomie
Bonn, Germany

Hans J. Kärcher
MT Mechatronics - consultant
Karben, Germany

Cover figure: The 100-m Radio Telescope of the Max-Planck-Institut für Radioastronomie in Effelsberg, Germany. Credit: Norbert Junkes, MPIfR, Bonn, Germany

*To our numerous international colleagues
and friends in the Astronomical Community
and Industrial Companies.
Their contribution and dedication to our joint
tasks led to the realisation of many radio
telescopes.
It enabled us to write this book about their
achievements.*

Preface

This book deals with the conception, design and construction of large reflector antennas functioning as radio telescopes. Communication and deep space ground station antennas employ essentially the same technology. Both authors have devoted the major part of their professional life to this subject, be it from a rather different educational background or in a diverse professional activity.

Jacob (Jaap) W. M. Baars has been educated as an applied-physicist and has for 50 years been connected with the creation and execution of radio telescope projects while on the staff of the originating radio observatories. Thus, his main task has been to translate the science case of a project into the requirement specifications for the telescope and to manage the communication with and oversight of contractors and of in-house activities up to final acceptance, testing and astronomical commissioning.

Hans J. Kärcher is by education a structural engineer, a "bridge builder". He spent his professional life as a system engineer for large telescopes on the contractor side of the projects. This involved the full design of the telescope and the control over the contractual and financial aspects of the manufacturing, verification of its functionality and performance through testing and commissioning, in order to deliver a functioning telescope to the final users.

Physicists and engineers differ in the approach to their subject. The aim of physics is to describe the material world, including the Universe, by a limited number of theoretical assumptions and mathematical equations and test the resulting predictions by experiment in the laboratory or by observation through the telescope. The goal of engineering is to create material devices that fulfil the tasks required of them by the customers—in our case telescopes for astronomers. The engineer has a service function with respect to the astronomer. The astronomer is the originator of the project, defining the requirements to be fulfilled by the engineering effort of creating the telescope. Also, the astronomer has to convince the funding agencies, which often ultimately means the citizen taxpayer, to provide the funds. It is of interest to point out that science projects requiring advances in engineering capabilities often are looked at favourably by funding agencies because

the development of new technologies by industry may create wider commercial application.

The basic requirement of a telescope is to point to an astronomical source in a given direction, to follow the object along its path on the sky and to concentrate the received radiation effectively to the detector in the focal point of the reflector. The realisation of such an instrument involves aspects of structural and mechanical engineering, control systems, electronics and the theory of elasticity and electromagnetic waves. Our individual background and experience (HK in mechanics and control, JB in electromagnetism and radio astronomy) complement each other well, so that a comprehensive treatment of telescope design could be envisaged. The intention of our joint authorship is to convey a fuller picture of the overall subject to the reader than a single author would be able to do.

This book presents a narrative of the historical development of reflector telescopes and antennas up to the latest state-of-the-art projects. We highlight the progress in design methods and the resulting larger and more accurate reflectors by describing in some detail telescopes with significantly new and original design features and technical solutions. We emphasise the importance of a balance between the astronomical requirements and the technical feasibility of realising those under the prevailing financial and technical limitations. The interplay between structural imperfections and electromagnetic performance forms an essential aspect of any advance in the state of the art. Next to the general description of the technical advances by example of radio telescopes, we summarise the basic background of the mechanical, structural, electromagnetic and thermal aspects of telescope design. The mathematics is minimised in favour of physical explanation with the aid of graphical material. The description of some more specialised aspects has been separated from the main text in Addenda to the particular chapters.

An essential and increasingly difficult feature of highly advanced antennas and radio telescopes is the experimental confirmation of the structural and electromagnetic specifications. A fruitful approach has been the direct involvement of the future users, mostly radio astronomers, in the development and execution of the necessary test methods and accompanying equipment. Based on our joint experience in several projects, we add some remarks on the management and realisation of our projects.

We address a readership with interest in the progress of engineering solutions and/or the general development of ever larger and more accurate radio telescopes. As such it should be of interest to observational radio astronomers, structural, mechanical and control engineers, operational staff of radio telescopes and satellite ground stations as well as students in these areas. Also, our goal is to present the rather wide area covered here in a comprehensible and informative way to the non-expert while still providing sufficient detail to interest the expert in a particular field.

As the subtitle states, the emphasis of our book is on the history of design and construction of reflector telescopes. We do not present a history of radio telescopes or the science of radio astronomy.

   A considerable amount of work made by industrial contractors, especially in the area of structural mechanics and control systems, has not been published in a readily available form, if at all. Wherever possible we refer to original publications and reports to enable the reader to dive deeper into the subject of his interest. Several figures are not of a quality that one would desire. These are mostly copies of old, original drawings, made well before computer drawing became available and easy. Because of their historical flavour we decided to use them and we hope the reader will accept the lack of clarity.

   We owe our career-long association with the design and construction of telescopes to our employers. In the case of JB, these were radio observatories embracing projects that advanced the state of the art, while HK joined a company that created and maintained a strong foothold in the telescope business over more than 50 years. We have been fortunate to collaborate with many highly capable colleagues without whom the enormous progress in this field would not have materialised. They are too numerous to name. We express our gratitude and thanks for our joint experiences. In the preparation of this book, we have been helped by colleagues and librarian staff of several institutes for material too old to be in our private library. We extend a special thanks to Dennis Downes and Dave Morris (both colleagues of yore and now retired from IRAM) for their comments, corrections and suggestions on the style and contents of the book. JB thanks Mark Gordon of NRAO for presenting him with a copy of Strunk and White's *The Elements of Style*. The booklet is a gem! It turned the original text in what we hope is now reasonably proper English. Obviously, we are responsible for any remaining error and "Dutchism" or "Germanism".

Max-Planck-Institut für Radioastronomie, Bonn, Germany   Jacob W.M. Baars
MT Mechatronics - consultant, Karben, Germany   Hans J. Kärcher
June 2017

Contents

Chapter 1
Introduction

Archimedes and his "burning mirror" with which he putatively put the Roman ships to fire during the attack of Syracuse

According to legend, the paraboloidal reflector was first used by Archimedes to burn Roman ships attacking Syracuse. In 1636, Mersenne (1588–1648) suggested using a paraboloidal reflector as an astronomical telescope. Much later, in 1888 Hertz (1857–1894) selected a cylindrical paraboloid to demonstrate the existence of electromagnetic waves at radio wavelengths. In the twentieth century, the paraboloidal reflector played a dominant role in the birth and development of radio astronomy, radar, deep-space probe tracking and satellite and terrestrial communication. The improvements in size and accuracy of the reflector surface and in precision and stability of pointing direction have been inspired mainly by radio astronomy since the late 1930s. This has resulted in great advances in the design and fabrication of structures and control systems to cope with the unavoidable influences of gravity, wind and temperature variations on the performance of the telescope.

In a parallel development, the quality of the receiving electronics and the understanding and control of the electromagnetic parameters of the telescope systems have improved greatly. Many of these advances have been initiated by the need of radio astronomers for larger and more accurate telescopes operating at short wavelengths. They have found their way in applications for commercial satellite communication and for remote sensing, radar and space exploration.

In this book, we present the technical aspects of the advance in reflector antennas by following the historical path of the development of radio telescopes that started immediately after World War II. We describe the improvements in structural design through the introduction of finite element analysis and the homology design principle, as well as the technologies of fabrication and choice of materials, such as carbon fibre reinforced plastic (CFRP).

As introduction to the following chapters, we present here an imaginary dialogue that could have been held between a scientist or astronomer and a mechanical or structural engineer. Let us denote the scientist by the initials JB and the engineer by HK. They discuss a plan to build a large and precise radio telescope and in the process wander through the contents of this book.

Dialogue Between an Astronomer and an Engineer

JB: I want to develop radio astronomy and I need a large paraboloidal reflector to do this. What can you offer me?

HK: As you know, we engineers can design and build anything you specify, but I assume that there will be financial limitations. At some point your requirements may necessitate such new design and development that it becomes impossible to realise in a reasonable time and to find the required funds. So, it would be good if you could be more specific in the definition of your telescope.

JB: Well, actually I have never thought about telescopes, so I am in for any suggestions from you.

HK: You should perhaps start with reading Chap. 2 of this book. It wanders you through the early development of the astronomical telescope and introduces the technological challenges of radio telescopes. It will hopefully whet your appetite for understanding the basic requirements of a radio telescope. You should then be able to give me more precise specifications for the major parameters of your instrument.

JB: OK, reading that was useful. I see that the size of the reflector is not the only point. Also its precision is essential because it determines the shortest wavelength at which the telescope will be effective. Let me summarise my present wish: I want a fully steerable dish, so I can point in any direction and follow a radio source on its diurnal path along the sky. And I want the telescope to be efficient at 21 cm wavelength because that is where the spectral line of hydrogen was detected a while ago. Now, you are an experienced builder of bridges. Is this going to help you to design my telescope?

HK: Absolutely! My design will look like a bridge with the supporting arch underneath the road, in our case the curved reflector. This "bridge" will be hung between two towers that will be moved on a circular rail track on the ground and on the towers I will place a drive system to tilt the reflector in elevation. Look at Chap. 3 of this book and you will see that it is exactly what the design of the Jodrell Bank telescope looked like in the early 1950s.

JB: I looked through that chapter and was quite surprised by the different ways the designs of the early large radio telescopes evolved around 1960. If you look at the early Dwingeloo telescope, followed by Jodrell Bank and Parkes, you see large differences in the structural approach, in particular the odd, polar mounted 140-ft telescope in the USA. I am beginning to become quite excited of being the originator of a significant improvement in telescope technology. But I still need to gain a better insight in the basic quantities that determine the telescope performance and their influence on the design, construction and operation. I surmise that there must also be a close relation between the structural and mechanical design and the electromagnetic characteristics. After all the latter will determine how well my observational result will be useful for my astronomical purpose.

HK: We are getting close to the point where we will have acquired sufficient insight in each other's expertise that we can sit down and define a new telescope to your liking. The connection between structural and electromagnetic aspects that you just mentioned is important. The book summarises these in Chap. 8. For instance it shows the relation between reflector precision and loss in sensitivity and how structural deformations leading to shifts in the pointing direction influence the observation. It will help you to define the all-important parameters of reflector precision and pointing accuracy. It is obvious that both are dependent on the wavelength and basically determine the shortest wavelength at which your telescope will function satisfactorily.

JB: Indeed, I found that chapter useful. Now, looking at the state of the field around 1965 I would like to build a telescope of perhaps 100 m diameter that will perform satisfactorily at 1 cm wavelength. From what I have learned so far, this will give me an angular resolution of about 25 arcseconds. That will yield a lot of fine structure in observing galaxies and nebulae. At 1 cm wavelength the reflector surface will have to be a perfect paraboloid to within 0.5 mm rms error to achieve a good sensitivity of two-thirds that of a perfect reflector. And nothing is ever perfect!

HK: Your numbers are correct and I agree that it is hard to be perfect. But your requirement cannot be met with the usual design principle of providing enough stiffness against deformation. Even if we would manage that technically, it would become too expensive; too much material! But I have good news for you. Around 1965 an astronomer, of all alternatives, by the name of Sebastian von Hoerner, came up with a brilliant idea and he showed that it could be practically realised. It is introduced in Chap. 4 and goes by the short name of homology. The basic idea is to allow a moving structure to deform under gravitational load instead of assuring enough stiffness to avoid deformation. However, the design controls the deformations in such a way that the resulting reflector surface maintains a parabolic shape, be it with changing focal length. This is the definition of a homologous design. The principle was applied in the design of the 100 m diameter Effelsberg radio telescope in Germany. That telescope, operational since 1971, is even somewhat better than your specification and it is used at 3.5 mm wavelength. So your plan has already been executed. Wouldn't you rather go for something else? Perhaps dive into the millimetre waves where, as I understand it, there has been an enormous amount of action since the discovery in 1970 of copious amounts of carbon-monoxide (CO) in our Galaxy at 2.6 mm wavelength.

JB: Yes, you are right. Observing at millimetre and even submillimetre wavelengths has become perhaps the most productive branch of radio astronomy. I would probably not have managed to obtain the funds for another 100-m telescope. Actually the Americans built one around 2000 that is quite different in design from the Effelsberg telescope. You find it in Chap. 7 of the book, where other unusual telescope configurations are shortly reviewed. But may be I should go for a down- scaled version of Effelsberg and make it good for 1 mm wavelength. How big could it be?

HK: Well, you go down in wavelength by an order of magnitude, so the reflector should be ten times more precise. It follows that for the required deformation the area of the telescope should be about ten times smaller. That suggests a diameter of about 30 m. But let me warn you immediately for an operational consequence that you may not be willing to accept. Straightforward scaling of the Effelsberg design will preclude the use of a large receiver cabin behind the dish as in Effelsberg. And I guess you want that with the bulky cooled receiver systems you people are using.

JB: I see your point. We would need to cut the "cone" in the Effelsberg design and that is an essential part of the superior homologous behaviour. Is there a way around this? Can you create homologous behaviour without the dense cone and high symmetry of the Effelsberg structure?

HK: You are the first to ask and we can accommodate you. Look at Chap. 5, where we present a solution for a high accuracy 30 m diameter mm-telescope. The cone is replaced by a sort of "four-point" support of the reflector structure onto the elevation structure. It provides good deformation behaviour and allows for a large equipment room behind the reflector that moreover rotates only in azimuth, so you can get to your receivers in any position of the telescope. This four-point support has been used in several other telescopes that not necessarily rely heavily on homology. Some of these are also discussed in other chapters of the book.

JB: That all sounds good. I may be able to get funding for a 30-m mm-telescope. But as I look at the pictures in Chap. 5 I notice that some cladding or the like covers the entire telescope. I can see this as protection against rain, hail and snow. It occurs to me that at the high and sunny sites of these highly precise mm-telescopes you might run into problems of temperature variations leading to unacceptable deformations of the structure. Is that cladding also thermal insulation?

HK: Indeed, if you are trying to maintain a precision of less than 100 µm on a 30 m diameter reflector, you have to limit gradients and differences in the temperature of the structure to about 1 degree Celsius. This is an essential feature of that telescope and only by the temperature control system can the telescope be used at full capacity during day and night and independent of the seasons. Temperature effects have become an essential factor in the design of radio telescopes and a separate general discussion of this aspect is presented in Chap. 5. It may be useful for you to look at that.

JB: I'll certainly do that. I can use all the education I can get. We have reached the point where a sizeable telescope operates at 1 mm wavelength. The water vapour in the earth's troposphere increasingly absorbs the mm-wavelength radiation and therefore we are forced to place these telescopes at high sites where the atmosphere is much drier. I know that at the highest and driest places on Earth observations are possible to a shortest wavelength of about 0.3 mm. If I opted for a telescope to exploit that wavelength region, what are my options? Is it going to be worthwhile scientifically?

HK: People have asked themselves this question before. It has resulted in several telescopes that perform well near 0.3 mm wavelength. But it becomes extremely difficult to successfully confront the thermal effects. An important solution to ameliorate this problem is the use of structural material with a very low coefficient of thermal expansion. In the early 1980s the price of carbon fibre reinforced plastic (CFRP) decreased to a level where one could contemplate using it as material for

highly precise structures, for instance a telescope for submm wavelengths. CFRP has a thermal expansion coefficient typically more than an order of magnitude less than the usual materials steel and aluminium. Chapter 6 of the book is devoted to submillimetre telescopes that predominantly use this material. An early example is the Heinrich Hertz Telescope put into operation in 1993. The 10m-diameter reflector maintains its surface precision of 12 μm even when in sunshine. You certainly have heard about ALMA, the large array of 50 submillimetre antennas that operates on the 5000 m high Chajnantor plateau in northern Chile. This global collaborative project represents the current level of high precision reflector telescopes and you find it described in Chap. 6 of the book.

JB: Looking at the capabilities of that instrument you might wonder whether any further telescopes for (sub)-millimetre radio astronomy would be needed. One could think that observers will happily observe just with ALMA and forget about new instruments. But, as always, I believe there are some initiatives for specialised small telescopes concentrating on a very specific scientific goal. Do you know of these and other plans for large telescopes?

HK: I agree with you that ALMA is an enormous step forward and astronomers working in the (sub)-millimetre region will be happy with it for quite some time. To answer your question; yes I know about a few initiatives for single antenna instruments for wavelengths as short as 0.2 mm. These need to be located at the highest mountains to be effective. For still shorter wavelengths one needs to use a balloon or a highflying airplane to carry the telescope above the tropopause. The airborne telescope SOFIA that my group designed is a prime example of the latter. There is also a plan for a 50 m telescope for short mm-wavelengths. These projects are in an early stage and you will not find details on them in the book, which deals with the historical developments in design of radio telescopes.

Finally, you are certainly aware of the gigantic Square Kilometre Array (SKA), a global project in its first stages that may station between 2000 and 3000 reflector antennas of 15 m diameter all over southern Africa, most of them in South Africa. This telescope will not observe at wavelengths shorter than about 1.5 cm, so there is no issue with satisfying the antenna specifications with a relatively simple structural design. The challenge here is the transport, management, analysis and storage of the enormous mass of observational data and the realisation of a rock-bottom price for the mass production of the antennas.

JB: For me this was a useful conversation. I shall certainly read the book both for its historical content and to obtain a better view on the issues and solutions connected with the design and construction of radio telescope reflectors.

This book is an anthology of the development of large reflector antennas/radio telescopes in describing the advances in technology over the last 70 years, often developed for the specific requirements of a single instrument and later applied to

others. The material presented in this book describes the achievements of a large number of people. Most of these were engineers working in the project offices of the originating institutions and in the design and manufacturing departments of industrial contractors. Contrary to the situation of most scientists, the career of engineers normally does not depend on a published record of their work. In the less commercial context of the construction of state-of-the-art radio telescopes, the original contributions to engineering progress have often been summarised in the open literature by the originators of the project rather than the designers. In our research into the origins and execution of the projects described in this book, we have made an effort to identify original reports and papers by the design engineers. We refer to these at the appropriate place in the text and include the full reference at the end of each chapter. Although some of these are published in company publications with a limited distribution, which might be difficult to access, we feel that providing a record of publications should be part of a text that purports to present an historical review of the subject.

Chapter 2
Evolution of the Telescope
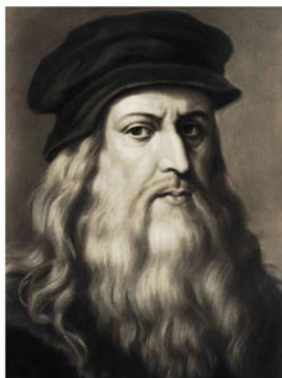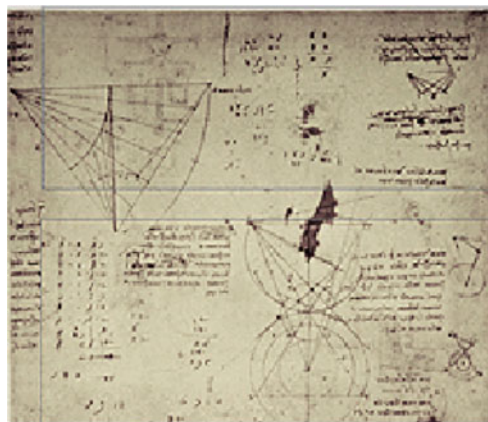
Leonardo da Vinci's Notebook with sketches of concave mirrors. Possibly a study towards a reflector telescope for observation of the Moon (1513) (Andrë Buys and Wikipedia)

2.1   Some History

2.1.1   Early Optical Telescope Efforts

Conic sections were first "discovered" by Menaechmus (380–320 BC) and fully studied by Apollonius of Perga (died ca. 190 BC), a contemporary of Archimedes. He introduced the common names *ellipse*, *parabola* and *hyperbola* for the three conic sections that serve as the defining curves for reflectors of electromagnetic radiation. Pappus of Alexandria (~290–350 CE) proved that a point on a conic exhibits a constant ratio of its distance to a given point and to a given line. This constant is known as the *eccentricity* of the conic; the fixed point is the *focus* and the line is called *directrix*. In polar coordinates (r, θ), the expression for any conic section, with its focus in the origin, is

$$r = f \frac{e+1}{e \cos \theta + 1}$$

where f is the focal length and e the eccentricity. We have for a parabola $e = 1$, an ellipse $e < 1$, a hyperbola $e > 1$ and a circle $e = 0$ (Fig. 2.1).

The parabola is the locus of points from where the sum of the distance to the focus and the directrix is constant. From this definition follows a most interesting characteristic: the parabola can be used as a focusing mirror. This is easily seen from Fig. 2.2. All rays in a plane wave travelling along the parabola's axis will upon reflection be directed to the focus and arrive there in phase.

The documents of Leonardo da Vinci (1452–1519) contain studies of geometrical optics and statements about using a concave mirror to obtain enlarged images of the Moon's surface (1513). It is possible that Leonardo constructed a reflecting
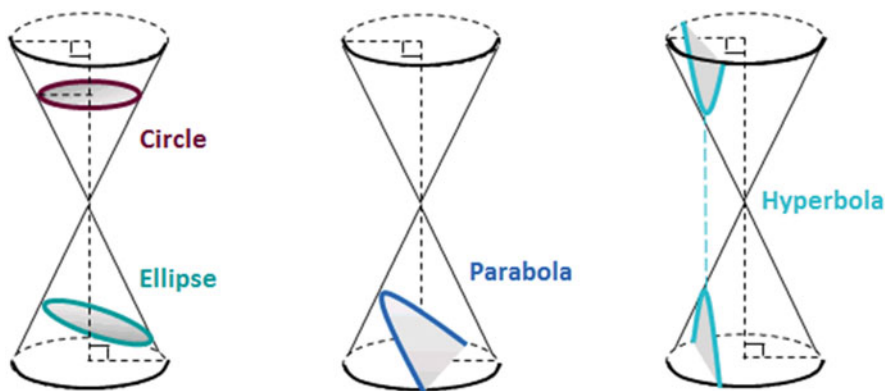
Fig. 2.1   The four conic sections. Depending on the angle of the section with respect to the axis of the cone, one obtains the curve of the *circle*, *ellipse*, *parabola* or *hyperbola* (Wikipedia, SheLovesMath)
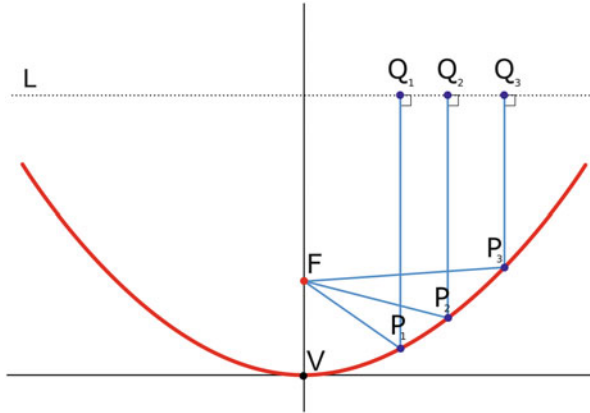
Fig. 2.2 Basic geometry of the parabola. The distance from any Q on the line L via reflection at P to the focus F is constant

Fig. 2.3 The first refractor telescopes. *Right* Lipperhey (courtesy The Robinson Library) and *left* Galileo (courtesy Amazing Space)

telescope in the early years of the sixteenth century but did not obtain useful observations because of the poor quality of the mirror. In the early seventeenth century, we see the development of the refracting telescope. The Dutch optician Hans Lipperhey (1570–1619) built the first telescope (called a "spy-glass") in 1609 by placing a concave and a convex lens in a tube. In the same year, Galileo Galilei (1564–1642) constructed a copy and used it for astronomical observations (Fig. 2.3). His observations of the moons of Jupiter formed a watershed in the understanding of the Universe confirming the heliocentric structure of the solar system as calculated by Copernicus.

The development of the refractor telescope created a renewed interest in the possibility of using reflectors to achieve similar magnifications. Marin Mersenne was the first to suggest (1636) the use of paraboloidal mirrors, but he did not construct one. Several decades later, in 1663, James Gregory (1638–1675) presented a design consisting of a parabolic primary mirror and an elliptical secondary reflector that sends the light backwards through a central hole in the

primary to the secondary focus. A variation on this dual-reflector design was introduced in 1672 by Laurent Cassegrain (~1629–1693) in replacing the elliptical secondary by a hyperbolic reflector. By locating one focal point of these conic sections in the focus of the parabola, the light reflected by the parabola was reflected to the second focus of the secondary mirror, which could be located in a convenient location. Despite some efforts, no optician was able to produce mirrors of these shapes to an acceptable quality for optical wavelengths. These proposals were far ahead of their time but are now commonly used for telescopes at all wavelengths.

Not being content with the lacking technology, Isaac Newton (1643–1727) set himself to produce a mirror telescope. He used a metal reflector, which he polished in a spherical shape. Although he tried, he was not able to figure the mirror in a parabolic shape and hence had to accept the spherical aberration of the spherical reflector. In order not to obstruct the light path when putting his eye in the focal point, he placed a small flat mirror in the telescope tube to direct the light sideways to the ocular, which was fixed to the outside of the tube (Fig. 2.4). This configuration is known as the *Newton telescope*. He presented this practical solution in 1668 despite its poor optical performance and has been given credit for the invention of the reflecting telescope: not entirely correct, but perhaps acceptable due to the ease of use and wide application of his solution.

In the eighteenth century, the technology of metal reflecting mirrors was gradually improved but remained unsatisfactory. William Herschel (1738–1822) constructed a large metal mirror of 1.2 m diameter in 1789, albeit with very limited success. In 1845, William Parsons (1800–1867), the third Earl of Rosse, Ireland, built a reflecting telescope with a bronze mirror of 1.83 m diameter, known as the Leviathan of Parsonstown (Fig. 2.5a). He developed grinding and polishing

Fig. 2.4 Isaac Newton and his first telescope with a 33-mm spherical metal mirror, donated to the Royal Academy in London in 1668 (courtesy The Robinson Library)
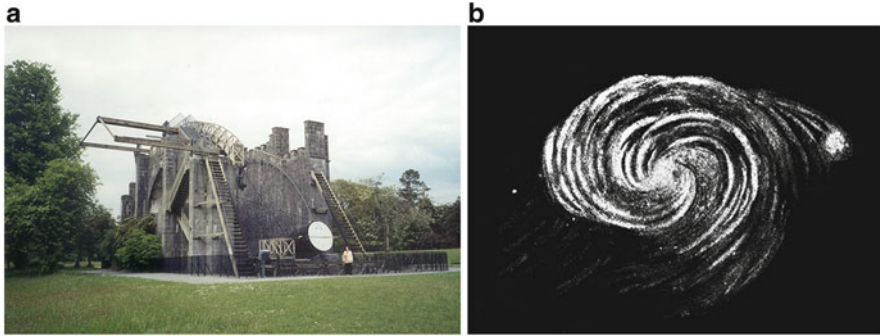
Fig. 2.5 (**a**) The 1.8 m diameter telescope of Lord Rosse in Birr Castle, Ireland, of 1845; (**b**) Rosse's sketch of the Whirlpool Galaxy, the first observation of spiral structure (courtesy H. Corwin, the NGC/IC Project and Wikipedia Commons)

methods to obtain a reasonably accurate paraboloid, which enabled him to resolve the spiral structure of the "Whirlpool Galaxy" (M51) (Fig. 2.5b) (Parsons 1850).

Significant advances in reflectors for optical astronomy only arose with the development of grinding large aspheric glass mirrors to the required precision, culminating in 1950 with the 5 m diameter Hale telescope on Palomar Mountain in California. Currently, the largest single blank glass mirrors have a diameter of about 8.5 m on the four Very Large Telescope (VLT) units of the European Southern Observatory in Chile, the Large Binocular Telescope (LBT) in Arizona, USA, and the Giant Magellan Telescope (GMT) with seven mirrors on a single mount that is under construction in Chile.

2.1.2   Emergence of Electromagnetic (Radio) Waves

Contrary to the optical domain, the use of radio waves for astronomy and communication has a short history of slightly more than one century. In the first half of the nineteenth century, the experimental work of Oersted, Coulomb and notably Ampère and Faraday demonstrated a close relation between electric currents and magnetic fields. Faraday's (1791–1867) discovery in 1845 of the rotation of the plane of polarisation of light under the influence of a magnetic field established an intimate relationship between light, considered a wave phenomenon, and electric and magnetic fields. On the basis of this groundwork, James Clerk Maxwell (1831–1879) developed the *dynamical theory of the electromagnetic field*, published in 1865. He unified electricity, magnetism and light into the concept of *electromagnetic (EM) waves* travelling through the ether with the speed of light c ($c \sim 300,000$ km/s).

The electromagnetic waves originating from Maxwell's equations are not limited to the wavelengths of light. The theory predicts the existence of EM waves at
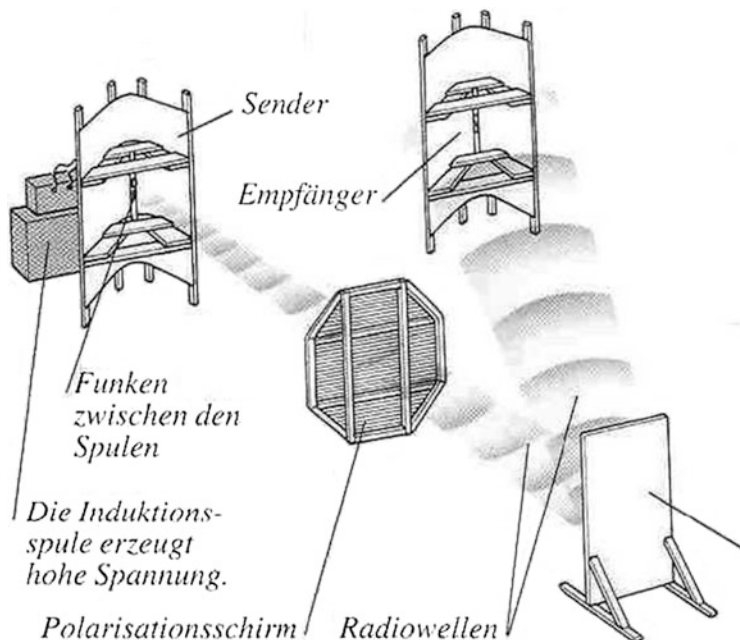
Fig. 2.6 Original sketch by Heinrich Hertz of his experiment to demonstrate the existence of electromagnetic waves. Parabolic cylinders concentrated the radiation from the transmitter (Sender) via a flat reflector (*bottom right*) onto the receiver (Empfänger). The polarisation grid allows the state of polarisation to be determined (Hertz 1888)

other wavelengths. Heinrich Hertz succeeded to demonstrate these *radio waves* in his experiments in Karlsruhe, published in 1888. The sketch of his experimental set-up is shown in Fig. 2.6 with original text in German (Hertz 1888). He used two cylindrical parabolic reflectors, placed in the background. Along the focal line of the transmitting mirror, he created high voltage sparks, correctly assuming that these would emit electromagnetic waves. Along the focal line of the receiving reflector, he observed tiny sparks coinciding with those emitted. Using a wire grid, Hertz demonstrated the polarisation state of the emitted radiation and conclusively showed that the characteristics of the waves conformed to Maxwell's theory. The wavelength of the experiment was about 66 cm. The original pieces of his experiment are preserved at the Physics Department of the University of Bonn, Germany. A picture of these, as placed during an exhibition in the Deutsches Museum in Bonn in 2013, is shown in Fig. 2.7.

Hertz's experiments aroused considerable interest in the new field of electromagnetic waves. It led to *wireless telegraphy* and to *radio broadcasting*. These developments used long wavelength (order of metres or longer) radiation transmitted and received by dipole and wire antennas. It led eventually to the birth of radio astronomy. *Radio Telescopes* are the major subject of this book.

Fig. 2.7 The original experiment, reconstructed after his move to the University of Bonn, is shown here while on display in the Deutsches Museum in Bonn (2013). The Ruhmkorff coil in front creates the sparks along the focal line of the cylindrical parabola on the left, which sends electromagnetic waves through the polarisation grid in the centre to an identical parabolic cylinder with receiver on the right (J. Baars, Deutsches Museum Bonn)

2.2 General Characteristics of Optical and Radio Telescopes

2.2.1 Introduction

Before we concentrate on radio telescopes, it is worthwhile to shortly discuss the major differences between optical and radio telescopes, particularly from the system engineer's point of view. These are caused by the difference of four to six orders of magnitude in the wavelength observed as illustrated in Fig. 2.8. The earth atmosphere limits transmission to *windows* near 1 µm wavelength (*visible* and *infrared*) and between roughly 1 cm and 10 m wavelength (*radio*). Consequently, there are great differences in the required precision of the optical parts of the telescope and in the character of the radiation detector in the focal plane.

The size of the *sensors* that are able to *detect* the radiation at the telescope will be in the range of its wavelength. This is illustrated by the fact that the size of the photoreceptors in the retina of our eye—the pixels of our biological CCD chip—is of the order of a micrometre, while the size of the receptors for the radio waves is in the range of decimetres to metres.

The early optical telescopes had no other receptors than the human eye, and therefore, up to the emergence of photographic techniques, the telescopes were just "magnifiers" for the human eye; the observation was made by looking through the telescope. The Sun is the energy source for the development of life on earth, delivering its energy by radiation in the visible window. Living creatures evolved using this radiation and in the process developed eyes. The natural energy output of
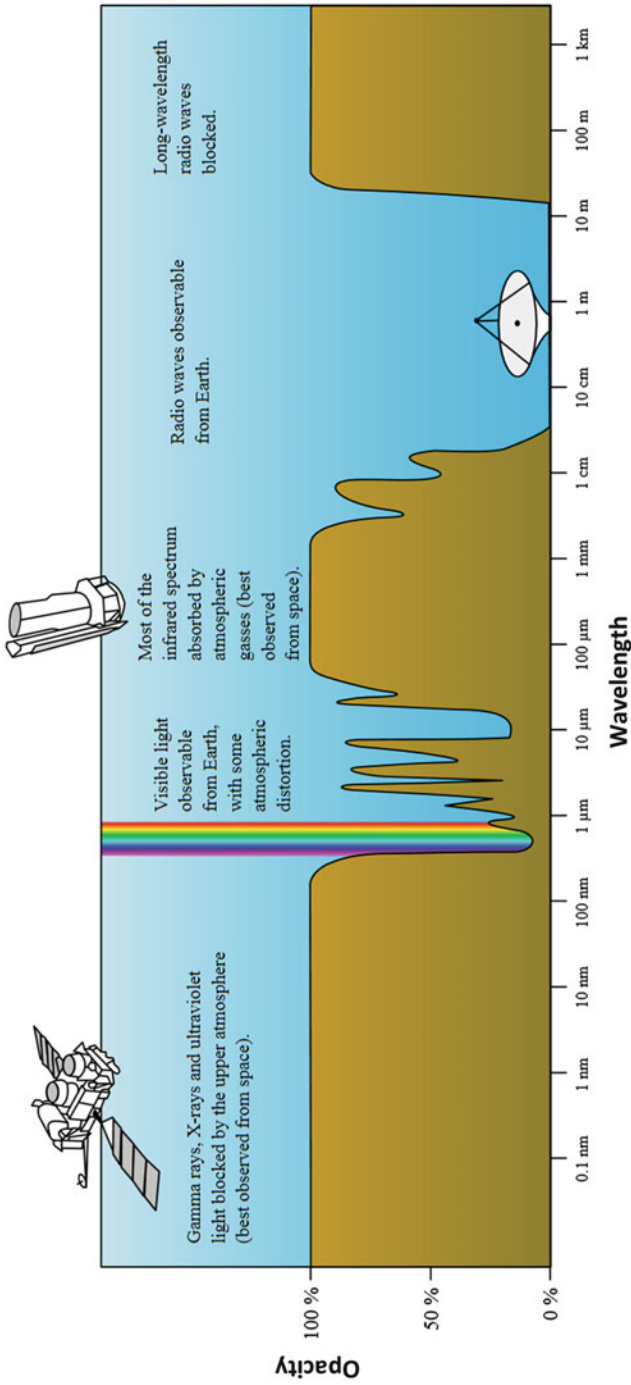
Fig. 2.8 The transmissivity of the earth's atmosphere as function of wavelength. Good transmission is only possible around 1 μm wavelength (visible and infrared) and in the radio window (about 1 cm–10 m wavelength) (Wikipedia)

the earth at its temperature of about 300 K is very small in the region of radio wavelengths. Hence, the discovery of radio radiation had to await the work of Maxwell and Hertz in the late nineteenth century. The cosmic radiation at radio wavelengths was discovered by chance in 1932 by Karl Jansky (1905–1950). We describe this in the next chapter.

After the introduction of the photographic plate in the second half of the nineteenth century, an important activity in astronomy became the imaging of extended objects, in particular nebulae in our Galaxy and external galaxies. The reflectors were relatively flat because a higher surface accuracy could be achieved in the grinding process of the paraboloidal shape. The resulting *f*-number, defined as the ratio of focal length to diameter (*f/d*), was significantly larger than one. This produced reasonably good images in the focal plane over a certain angular area before aberrations ruined the image. The situation is an order of magnitude better in the Cassegrain focus, and over the years, various optical configurations have been developed to enlarge the field of view to several square degrees on the sky (for instance, Schmidt and Ritchey–Chrétien telescopes).

When radio scientists and radar engineers turned their wartime radar antennas to the sky to start radio astronomy, their telescopes looked very different from an optical one. The reflectors were quite deep with focal ratios in the range 0.25–0.5 and a single feed illuminated them; they were *single pixel* telescopes. Imaging was out of the question with a single feed. Recently, new developments have produced so-called *phased-array feeds* (PAF) that allow the sampling of the prime focal plane to produce several tens of adjacent beams of good quality over a substantial angular area of sky. We return to this aspect in Chap. 8.[1]

In the early days of radio astronomy, there was rarely a well-defined science case that formed the basis for instrumental requirements with the exception of the spectral line of neutral hydrogen at 21 cm wavelength. Thus, progress during the exploratory period of the new science of radio astronomy was strongly determined by progress in mechanical and electronic engineering. At most radio observatories, the scientific staff was active in these fields.

The development of radio telescopes went along two routes:

1. Increase the size of the telescope aperture. Here, structural and financial limitations play a determining role in the available possibilities.
2. Shorten the wavelength of observation. Apart from the structural requirements for increasing reflector accuracy, the availability of radiation detectors of sufficient sensitivity is decisive for the feasibility of this option.

Structural and mechanical deficiencies will influence the electromagnetic performance in a negative way. It is important to have quantitative knowledge about

---

[1]The terms *illuminated* and *feed* originate with radar technology and have been adopted by radio astronomers, not least because many of the first generation were radar engineers. Actually, a radio telescope has a *reception sensor* (often a dipole or electromagnetic horn) in the focus to detect the radiation captured by the reflector and concentrated in the focus. A reciprocity theorem makes the transmitter terms physically admissible, albeit somewhat confusing to the uninitiated astronomer.

the relation between these quantities. We discuss these relations in Chap. 8. On this basis, we shall be able to define specifications for structural-mechanical parameters in order to obtain the required electromagnetic performance.

2.2.2 Types of Telescope Mount and Optics

Mount

At the time of the first radio telescopes after World War II, optical telescopes, the largest being the 100 in. (2.5 m) diameter telescope on Mt. Wilson near Los Angeles, were invariably attached to an *equatorial* (also called *polar*) mount with the polar axis placed parallel to the earth's axis at the site of the telescope. This allowed the *tracking* (following) of a star along its diurnal path by a rotation about the polar axis with the constant velocity of the sidereal clock. The declination (celestial latitude) of the star had to be set once at the beginning of an observation. Because the sky is dotted with sufficiently bright stars, weak objects of study could be tracked by the use of a small guiding telescope mounted on the main telescope and keeping a nearby bright star centred in its ocular. Turbulence in the atmosphere limits the angular resolution (sharpness of view) to about 1 arcsec from a good mountain site. Such a resolution at optical wavelengths (0.5 μm) is achieved with a reflector diameter of only 10 cm. Thus, larger telescopes could detect weaker objects but did not improve the angular resolution.

Because the "radio sky" was essentially empty to the first observers, it was not possible to use something similar to a "guiding star" to track a point on the sky against the rotation of the earth. Moreover, the radar reflectors were invariably attached to an *elevation–azimuth* (el-az) mount, because their targets also moved in this *local* coordinate system. To control the telescope in *celestial coordinates* (right ascension/hour angle and declination), a coordinate transformer was needed to obtain the required control signals to the elevation and azimuth drives for the position and path of the object. These could take the form of an extensive table of azimuth and elevation angle versus time for a certain celestial position[2] or preferably some electromechanical-optical device which would perform the transformation. We describe some examples of these later.

While a polar mounted telescope can track any sidereal object over its full daily path, the el-az mount runs into problems when the object transits through the local zenith. In that case, the azimuth velocity would approach infinity, which is obviously not realistic. Hence, an el-az telescope has a certain *cone of avoidance* around the zenith, where observations are not possible. The size of the avoidance angle is set by the capabilities of the drive system (maximum angular velocity and

---

[2]This basic mode was used by the author (JB) as late as 1977 in the calibration of the ESA ground station, for the Orbiting Test Satellite before a control computer had been installed. With only three strong radio sources available, it was a feasible, be it sometimes frustrating, method.

acceleration) and can normally be restricted to a few degrees, involving the interruption of observation by several minutes. It should also be noted that the el-az mount causes the field of view to rotate in the focal plane while a source is being tracked. The mechanical and structural complications of a polar mount are significantly greater than those of an el-az mount, especially for large reflectors. Thus, most radio telescopes have been realised with an el-az mount.

The first large radio telescopes in the Netherlands, Germany, England and Australia with diameters from 25 to 76 m, to be described in Chap. 3, were elevation–azimuth systems. In the USA, the first antennas of 26 m diameter at the Jet Propulsion Laboratory (JPL), University of Michigan and National Radio Astronomy Observatory (NRAO), built in 1958–1959, were polar mounted. At that time, the design of a large 140-ft (43 m) telescope for NRAO was being completed and here too the decision was made to use an equatorial mount. The main argument was that with the high pointing precision, specified for this telescope, analogue coordinate transformers would not perform well enough and computer technology did not (yet) allow a fully digital control system. We shall give more details of this telescope in Chap. 3. The polar mount has later only been used for a few aperture synthesis telescopes, which in principle operate with very long observations, up to 12 h, tracking the object under study over the entire daily hour-angle range.

Optics

The optical layout of the reflectors and detectors is driving the structural and mechanical design of a telescope. There are a number of different types of optical layout as illustrated in Fig. 2.9. In addition to the basic versions, with a primary, Cassegrain or Gregory focus, there are two widely used variations in the placement of the final focal point. The first is the Nasmyth configuration, named after the Scottish engineer James Nasmyth (1809–1890), who is known as the inventor of the steam hammer. Here, the beam returning from the Cassegrain or Gregory secondary reflector is directed sideways by a flat mirror, often through the elevation axis of the telescope. If one moves the mirror along with the elevation movement, one obtains a fixed focus outside, where the detector can be placed without the need to move it in elevation angle. A further set of mirrors can be used to create a Coudé focus[3] by guiding the beam along the polar or azimuth axis to a point, where the detector is stationary. In the field of communication, the Coudé arrangement is normally called *beam waveguide*, particularly useful in case of a transmitting station, where the bulky transmitter can have a stationary location in the basement of the antenna. Sometimes the off-axis mirrors are curved to avoid a too narrow beam or to create an extra focus position. These solutions are widely used on satellite communication and deep space ground stations. Some radio telescopes have adopted the beam waveguide, notably the Nobeyama Millimeter Telescope (Chap. 5) and the Sardinia Radio Telescope.

---

[3]Note that this last name derives from the French word for elbow, to indicate the path of the light, contrary to the gentlemen who gave their name to the other configurations.
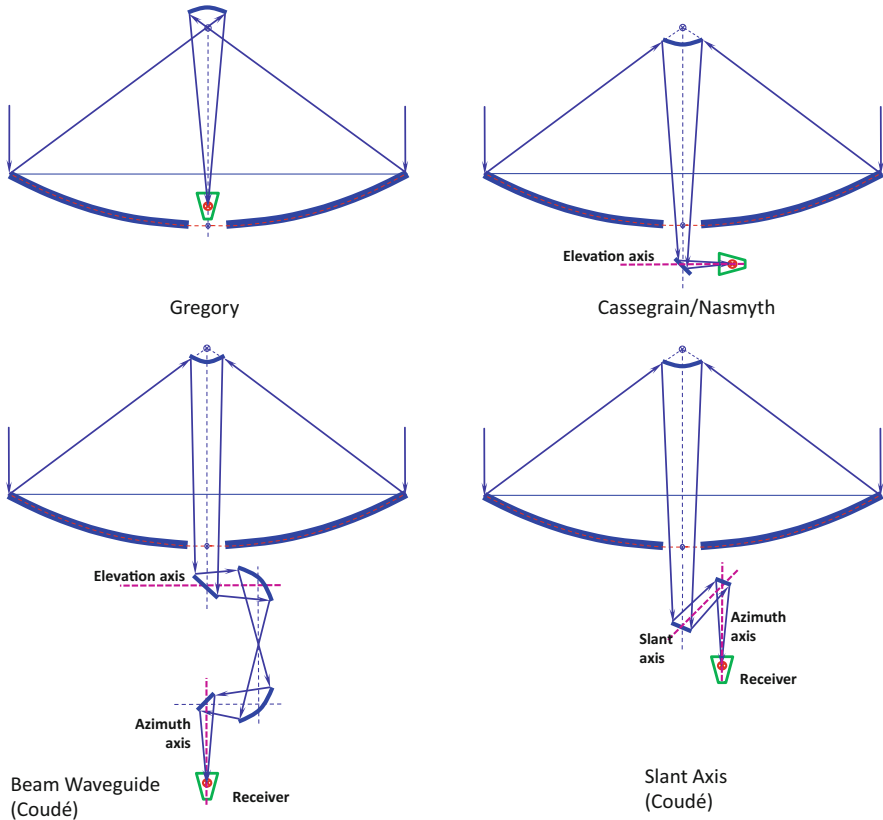
Fig. 2.9 The major geometries of astronomical telescopes. Cassegrain (*upper right*) and Gregory (*upper left*) introduced a hyperbolic and elliptical secondary mirror, respectively, to move the focus to the back of the primary reflector. The Nasmyth variety (*upper right*) deflects the beam sideward by a flat mirror, placed on the elevation axis. More mirrors can be used to bring the focus to a stationary position, called coudé focus (lower sketches)

Any radio telescope project will start with the definition of the optical layout. It will be influenced by the specific scientific goals and the available technology and funds.

Usually, the diameter of the primary reflector will be chosen first. This choice is of course strongly determined by the available funds, but considerations of the astronomical goals are at least as important. For instance, the envisaged minimum wavelength determines the necessary precision of the reflector surface. This is a major cost driver and it influences the affordable reflector diameter. The dependence of the cost of the antenna as function of reflector diameter is of particular interest. Meinel (1979) has suggested a relation $cost \propto D^{2.5-2.7}$ based on structural mechanics and empirical data (van Belle et al. 2004). This relation should be used with caution, because it depends on a number of influences that are not considered, in particular the relation between reflector panel precision and cost.

In the addendum to this chapter, we present the geometrical aspects and discuss the advantages and disadvantages of the Cassegrain and Gregory configuration in general terms. This will aid the reader when he encounters the descriptions of the actual telescopes in later chapters.

The Gregory configuration preserves the real focus of the main reflector. It is rather easy to change between *primary* focus and *Gregory* focus operation by moving the prime focus receiver to the focal point without changing the position of the secondary reflector. The *Cassegrain* configuration has only a virtual main reflector focus, and for prime focus operations, the secondary reflector has to be removed. The distance between the main and the secondary reflector of the Gregory configuration is considerably larger than that of the Cassegrain configuration. This renders the Cassegrain configuration more compact and eases the structural challenge for the support of the secondary reflector. These aspects have to be weighed in the definition process of the optical system.

The different configurations to realise a convenient focal point have all been widely used for optical telescopes since more than 200 years, and they have been adopted for radio telescopes. In radio astronomy and telecommunication, the antenna system usually consists of a paraboloidal main (primary) reflector and a hyperboloidal (Cassegrain) or ellipsoidal (Gregory) secondary reflector to create a secondary focus near or behind the vertex (central lowest point) of the main reflector. Some radio telescopes and many communication ground stations locate the receiver in a tower inside the primary reflector. To avoid excessive loss of reflector area, such a tower should be narrower than the secondary reflector. For ease of access, only very large antennas would be likely to select this option. An example is the Effelsberg 100-m telescope (Chap. 4).

2.2.3   Alternative Geometrical Configurations

A method to avoid problems caused by aperture shadowing is the use of *offset reflectors* (Fig. 2.10). Instead of the rotational symmetric dish, only a segment of a larger virtual paraboloid is used. The segment may be circular as sketched, but could be also elliptic or similar, depending on the opening ("illumination") angle of the related feed horn.

The unobstructed aperture provides advantages in the area of beam quality and overall sensitivity. The diameter of the virtual paraboloid is more than twice than that of the real reflector, resulting in about twice the distance of the focal point from the virtual vertex, which causes structural challenges for the support of the focus equipment. The geometry is widely used in the small dish antennas for the private reception of satellite TV. The largest offset antenna is the Green Bank Telescope of 100 m diameter that we describe in Chap. 7.
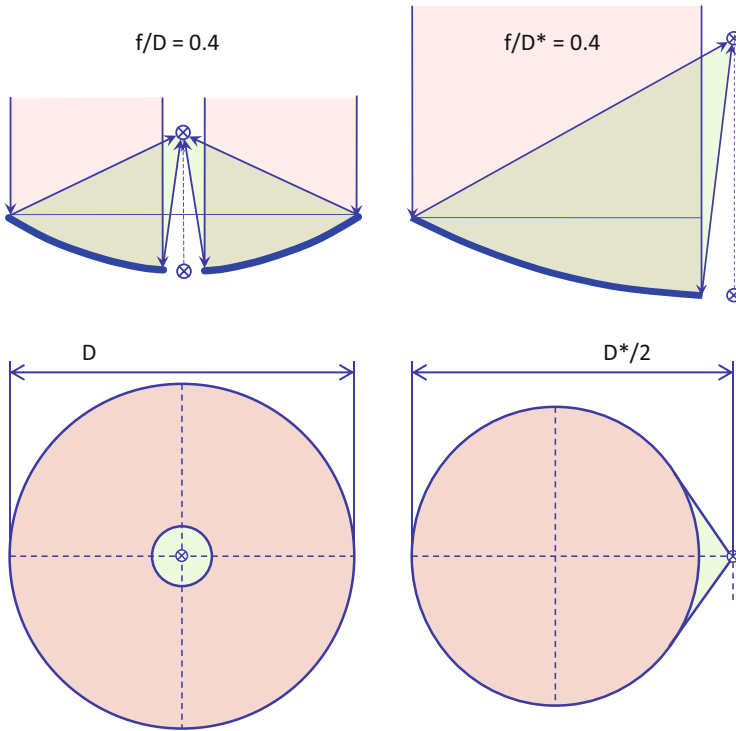
Fig. 2.10 The symmetrical and offset geometry of the reflector

2.3 Technological Challenges for Radio Telescopes

Clearly, the long wavelength at which radio telescopes operate significantly eases the requirements on the structural accuracy and stability. On the other hand, both the poor angular resolution and the faintness of the radio sources push for large reflectors. Because the telescope functions as a single pixel detector with one radio receptor in the focal point, there is no pressing need for a large *f*-ratio. Actually, small *f*-ratios are preferred because of the smaller size of the receptor in the focal point. The resulting reduction in the length of the structure is attractive to the structural designer. The choice of the focal ratio is therefore a primary driver of the design, both in relation to the receiving equipment and even more to the overall structural layout. Two competitive aspects are of importance: the curvature of the reflector and the length of the structure. Both features have a decisive influence on the structural design and will be discussed in detail in later chapters.

The opening angles, the angle from the focus to the edge of the reflector, of the optical telescopes are in the range of below 30° up to 60° (*f*-ratio > 1), whereas the opening angles of the radio telescopes are in the range of 100–180°. Most radio telescopes have a focal ratio between 0.30 and 0.45. Interestingly, the first two large

telescopes selected somewhat extreme values of 0.25 (Jodrell Bank) and 0.50 (Dwingeloo). We shall see in their description in Chap. 3 that there were good reasons for those choices.

Optical telescopes are invariably placed in an enclosure, called *dome*, which partially opens towards the sky during observations. The dome protects the telescope during inclement weather and also avoids excessive solar heat on the telescope structure during the day. Radio telescopes, being much larger than optical telescopes, are normally placed fully exposed to the environment. Consequently, the telescope structure must be designed for survival under extreme weather conditions such as storm and heavy snowfall or icing. In addition, the telescope is subjected to the daily and seasonal variations in ambient temperature that will cause significant temperature variations and gradients in the structure. These cause differential expansion, which may easily lead to deformations beyond the specified values. As a consequence, the thermal control of the telescope has become an essential part of the design effort for the highly accurate telescopes of the last few decades. If such control is successful, the radio astronomer has the advantage that he can observe also during the daytime contrary to his colleague in optical astronomy.

Radio telescopes also differ from optical ones in the layout of the reflecting surface. Metallic reflectors of a single piece, similar to the usual glass blanks of optical telescopes, are rare in radio astronomy, although we shall meet a few later on. The reflector is normally composed of a set of surface elements, which we call *panels* that are supported by a sufficiently stiff *backup structure*. The usual pattern of the reflector layout is in concentric rings of trapezoidal panels, although a pattern of hexagonal panels has also been applied. Each panel is attached to the backup structure by a number of adjustable screws. After completion of the surface, the panels must be adjusted to the paraboloid with the required accuracy. Thus, the development of measuring methods and equipment is part of the basic task of the radio telescope designer.

A final challenge is the control of the telescope pointing to and following (*tracking*) of the object of observation. A radio telescope must perform an *absolute pointing* to a selected direction and follow this point on the sky against the earth rotation. This must be accomplished under influence of the wind. In terms of overall performance, the quality and reliability of the position control system is as critical as the precision of the reflector surface. These aspects will receive considerable attention in this book.

2.4   Basic Specifications of a Reflector Radio Telescope

In the early days of radio astronomy, it was not easy to define the performance specifications, and hence the structural and mechanical specifications, for an instrument with which one would essentially enter no man's land in a new area of astronomy. The diameter of the reflector and the shortest wavelength of observation

are the primary determinants of the mechanical and structural requirements for the telescope. The reflector must point to and follow the object along its diurnal path and concentrate the received radiation in the focal point. Thus, the reflector is attached to a mount structure that provides accurate pointing while maintaining the parabolic shape under changing attitude angle, i.e. varying gravitational force. Hence, the two major specifications of the telescope are precision and stability of both the reflector surface and the pointing direction. It is easy to see that both quantities determine the shortest wavelength at which the telescope can be effectively used.

2.4.1 Reflector Precision

Radio reflectors normally consist of a set of surface panels, which are placed on a support structure. Here, the imperfections in the individual panels, the precision of their placement on the support structure and the differential deformation within the support constitute the major deviation of the surface from the desired form. In 1952, John Ruze (1916–1997) presented a *tolerance theory*. It is a quantitative probabilistic analysis of the effect of relatively small-scale aperture phase errors on the radiation pattern. We will discuss this in Chap. 8. The major result is that the efficiency of the antenna η_s decreases according to the following equation:

$$\eta_s = \exp\left[-\left(\frac{4\pi\varepsilon}{\lambda}\right)^2\right], \tag{2.1}$$

where ε is the rms deviation from the perfect reflector and λ the wavelength. Thus, for an error of only one-sixteenth of the wavelength, the sensitivity is reduced to half of maximum; to limit the loss to 10%, the error must be no larger than one-fortieth of the wavelength.

2.4.2 Pointing Precision

The angular resolution of the telescope, which we designate as the *half-power beam width* (HPBW) of the antenna, is determined by the ratio of wavelength λ to reflector diameter D. The HPBW θ_A, in radian, is given by

$$\theta_A = a\frac{\lambda}{D} \tag{2.2}$$

where $a \approx 1.0 - 1.3$, depending on the illumination of the aperture (see Chap. 8). For instance, an antenna of 25 m diameter operating at 21 cm wavelength has an

HPBW of ~30 arcmin, the size of the full Moon. In Chap. 8, we show that a pointing error of one-tenth of the HPBW causes a signal loss of about 3–4%. In practice, this is acceptable, but it should be noted that in this example it means a pointing error of about 3 arcmin. This is very large compared to the optically determined positional accuracies of astronomical objects.

Summarising, the two basic specifications for a radio telescope are:

– Reflector rms precision is a small part of the wavelength (typically $<\lambda/16$).
– Absolute pointing and tracking precision is not worse than one-tenth of the HPBW.

We add to these an operational condition:

– These specifications must be obeyed at the shortest design wavelength and under all operational environmental conditions such as temperature variations and wind forces.

2.5   Summary

The structural engineer is faced with the task of supporting two essential components: the reflector or mirror, and the sensor or receiver in the focal plane. The support of the optical focus devices at a long distance from the main mirror requires a different structural layout (e.g. a Serrurier-type *tube*) from the support of the focus equipment in radio telescopes with a shorter distance to the main reflector (e.g. a *quadripod*).

The type of supporting system for the main mirror or reflector is dependent on its size and composition. Whereas the main mirror of the Palomar telescope is one monolithic piece of glass, supported by the so-called *mirror cell*, the main reflector of a radio telescope is normally composed of reflector panels, supported by *a backup structure* (BUS). Some of the extremely large optical telescopes also apply the *segmented mirror* approach, supported by a BUS, often called in the traditional manner mirror cell. The backup structures of the large reflectors will be trusses, whereas the mirror cells and mounts of the traditional optical telescopes are mostly hollow box-type structures. Thus, the cells and mounts belong more to the art of *machine tool* design, while the BUS falls in the category of the art of *structural mechanics* (bridge building) (Kärcher 2008). Once the size of the reflector reaches diameters of 50–100 m, operating even at millimetre wavelengths, the challenge for the structural engineer is stronger than for a bridge because of the requirement of high precision.

Modern large optical telescopes use a real or artificial guide star to sample the wavefront in the telescope aperture and use this to adjust some of the optical elements to correct for the measured disturbance in real time. Unfortunately, adaptive optics in a closed loop manner is not feasible for radio telescopes, because

the small focal plane field normally does not contain a suitable source for wavefront sensing to provide the signal for a closed loop correction.

Several modern large radio telescopes incorporate error correcting systems, which are applied in an open loop, designated *active optics*. The active optics of radio telescopes uses corrections of the reflector surface by motorised actuators, and corrections of the telescope direction (pointing) via look-up tables or sensor readings. Active optics is a more complicated challenge for the system engineer than adaptive optics, because it requires a reliable prediction of the telescope deformations, not necessary for the adaptive optics. This prediction may be based on the readout of sensors distributed over the telescope structure and an extrapolation of the measured data by a finite element-based *deformation state model*. This method is called *flexible body control* (FBC) and will be discussed in Chap. 5.

Addendum: Geometry of Optical Configuration

In this addendum, we present the geometry of the Cassegrain and Gregory reflector antenna with an emphasis on the optical parameters that dominate the structural and mechanical design (see also Baars 2007). Once the diameter has been selected, the focal length is the only remaining free parameter for primary focus operation. The great majority of radio telescopes have a primary *f-ratio* between 0.3 and 0.5 with extremes of 0.25 and 0.8. Since the early 1970s, preference has been given to *dual-reflector* geometries in the form of a *Cassegrain* or *Gregorian* optical layout. The dual-reflector configuration offers flexibility in the choice of the defining parameters and the resulting geometry of the telescope. In addition to the primary diameter, three parameters fully determine the geometry of the system. Normally, these are chosen to be the *primary focal length*, the *position of the secondary focus* with respect to the vertex of the primary and the *magnification*, denoted m, of the dual-reflector system. This term originates with the magnification of the observed object in the first simple optical telescopes. The virtual *equivalent parabola* has a focal length of m times the primary focal length as illustrated in Fig. 2.11. Thus, the magnification is the ratio of the *effective focal length* of the Cassegrain/Gregorian system to the focal length of the primary. An important aspect of the dual-reflector geometries (Cassegrain, Gregory) is the improved optical quality in the secondary focal plane due to the large effective focal length.

The geometry of the dual-reflector systems is shown in Fig. 2.12. The Cassegrain employs a hyperbolic secondary reflector with one of its foci coinciding with the primary focus. The second focus of the hyperbola provides the focal point of the telescope system. Normally, the final *secondary focus* is located behind the vertex of the primary reflector; the distance from the primary vertex to the secondary focus is called the *back focal distance*, which we denote by the symbol b. The dual-reflector system's focal length is the distance between the two foci of the secondary reflector, denoted here by the symbol f. With F denoting the primary focal length, we have $f = F + b$, where b is reckoned positive if the focus is behind the primary

P – primary reflector, parabola
S – secondary reflector, hyperbola, ellipse
EP – equivalent primary parabola
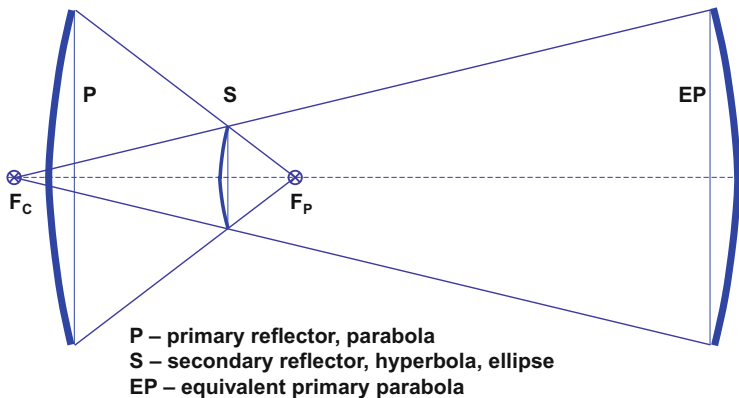
Fig. 2.11 Illustrating the concept of the equivalent paraboloid E-P. The focal length of E-P is m, the magnification, times that of the primary paraboloid f. Lines from F_C past the edge of the secondary reflector S project E-P at a distance $m \cdot f$ from F_C
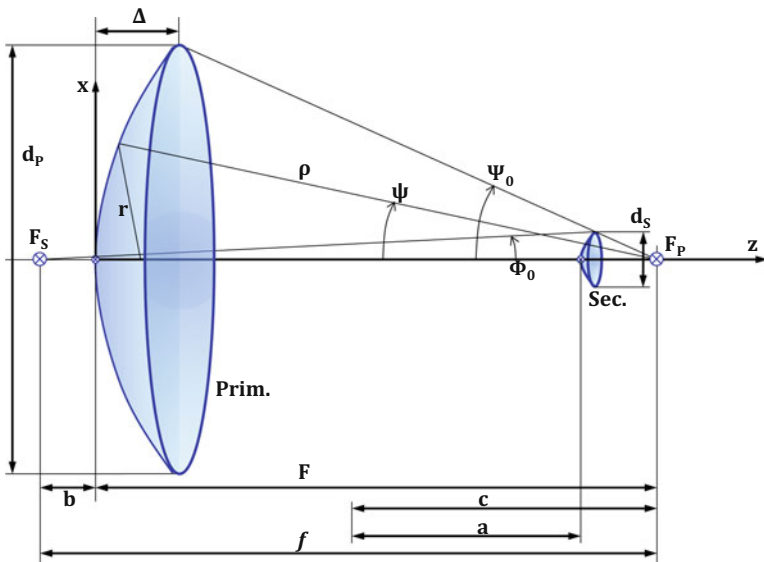
Fig. 2.12 Geometry of the Cassegrain Reflector antenna

vertex. Using the variables for the geometry given in Fig. 2.12, we summarise the geometrical relations in Table 2.1. The defining constants of the secondary reflector are parameters c and a; their ratio is called the *eccentricity e* of the reflector. The eccentricity is determined by the chosen magnification m (Eq. 2.9). When the Cassegrain focus is in the vertex of the parabola, we have $f = F(b = 0)$, and it follows that $m = d_P/d_S$, where d_P and d_S are the diameter of the primary and

Table 2.1 Geometrical relations of the Cassegrain/Gregory telescope

Parabola in polar coordinates	$\rho = F\sec^2\dfrac{\psi}{2}$	(2.3)
Parabola in Cartesian coordinates	$r^2 = 4F(F+z),\ \tan\dfrac{\psi}{2} = \dfrac{r}{2F}$	(2.4)
Hyperbola (Cassegrain)	$r_S = \dfrac{c^2 - a^2}{a + c \cdot \cos\phi}$	(2.5)
Ellipse (Gregory)	$r_S = \dfrac{c^2 - a^2}{c - a \cdot \cos\phi}$	(2.6)
Opening angle of primary reflector P	$\tan\dfrac{\Psi_0}{2} = \dfrac{d_P}{4F}$	(2.7)
Angle of equivalent paraboloid E-P	$\tan\dfrac{\Phi_0}{2} = \dfrac{d_P}{4mF}$	(2.8)
Eccentricity of secondary reflector e	$e = \dfrac{c}{a} = \dfrac{m+1}{m-1},\ m = \dfrac{e+1}{e-1}$	(2.9)
Diameter of secondary reflector S	$d_S = 2f/(\cot\Psi_0 + \cot\Phi_0)$	(2.10)
Distance between reflectors	$d = (mF - b)/(m+1)$	(2.11)
Distance between foci of secondary reflector	$f = F + b$	(2.12)
Depth of paraboloidal reflector	$\Delta = f\left(\dfrac{d_P}{4f}\right)^2$	(2.13)
Surface area of paraboloid	$S = \dfrac{8\pi}{3}f^2\left[\sec^3\left(\dfrac{\Psi_0}{2}\right) - 1\right]$	(2.14)
Conical constants of the Ritchey–Chrétien telescope		
Primary mirror	$K_P = -1 - 2[(d+b)/d] \cdot m^{-3}$	(2.15)
Secondary mirror	$K_S = -1 - 2[m(2m-1) + (d+b)/d] \cdot (m-1)^{-3}$	(2.16)

secondary mirror, respectively. This simple relation does not apply to the Gregory system.

Some recent radio telescope proposals apply a *Ritchey–Chrétien* optical layout to exploit the *coma-free focal plane* that allows the use of large two-dimensional detector arrays over a large field of view. The Ritchey–Chrétien employs two hyperboloidal mirrors. The expressions for the *conical constants* K_P and K_S of the coma-free optical system are also given in Table 2.1. The eccentricity of the mirror is equal to the square root of the absolute value of its conic constant. From Eqs. (2.15) and (2.16), we see that the eccentricity is larger than one; hence, both surfaces are *hyperboloids*. The full theory of the RC optics can be found in Wilson (1996).

The electromagnetic treatment of the reflector antenna defines the collection area of the primary reflector as the area of the plane aperture through the outer edge of the reflector. The physical area of the reflector (Eq. 2.14) is larger by an amount depending on the focal ratio, shown in Fig. 2.13. The physical area must be
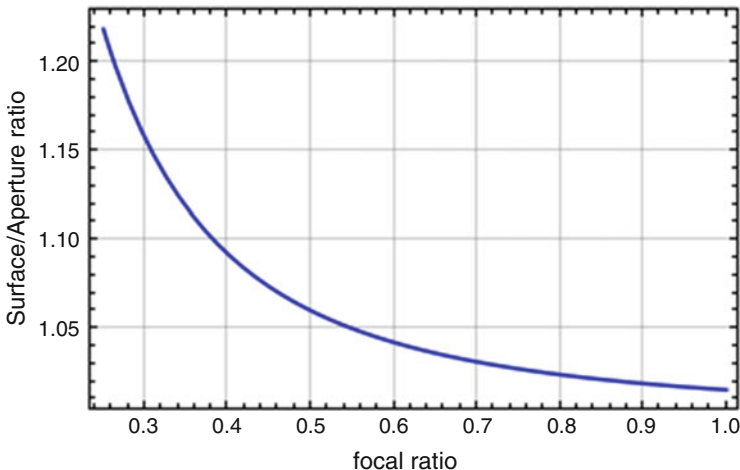
Fig. 2.13 Ratio of the true physical area of the reflector to the aperture area as function of the focal ratio

fabricated and hence a deep reflector will be more expensive. In practice, based on electromagnetic, structural and manufacturing arguments, most antennas and radio telescopes have a primary f-ratio between 0.3 and 0.5, with a surface "surplus" between 16% and 6%.

The choice of the primary focal ratio is a compromise between structural and electromagnetic requirements. The f-ratio determines the opening angle of the reflector (Eq. 2.7). This angle must be matched by the beam width of the feed horn in the focus. Input from the receiver engineer is necessary here. There exist a wide variety of feeds. A useful rule of thumb is that the angular width of the feed beam at the -10 dB level must equal the opening angle of the reflector (see Eq. 8.1). For a basic horn feed, this means an aperture width of about 0.5–1.0 wavelengths for f-ratios from 0.25 to 0.60. It is obvious that the horn aperture will increase with decreasing opening angle because a larger aperture creates a narrower beam, just as a larger reflector will produce a narrower antenna beam. In a dual-reflector system, the opening angle of the secondary reflector is much smaller than that of the primary reflector and the feed will be significantly larger.

The choice of location of the secondary focus determines the back focal distance. It is typically between 0.2 and 0.4 times the primary diameter to accommodate large receiver units in an equipment room behind the backup structure at for instance a Nasmyth focus. This sets the distance between the primary and secondary focus (Eq. 2.12), which we call the *focal distance* of the dual-reflector system. We can now choose either the diameter d_S or the opening angle Φ_0 of the subreflector with Eq. (2.10) to finalise the geometry of the telescope. The resulting full opening angle of the secondary reflector is normally of the order of $10°$.

References

Baars, J.W.M.: The Paraboloidal Reflector Antenna in Radio Astronomy and Communication. Springer, Berlin (2007)

Cassegrain, L.: Journal des sçavans. J.-B. Denis edt. **7**, 71–74 (1672)

Da Vinci, L.: Codex Atlanticus, p. 59(b) (1513)

Faraday, M.: Faraday's Diary, vol. IV, pp. 7504–7718 (1845)

Gregory, J.: Optica Promota (1663)

Hertz, H.: Über Strahlen elektrischer Kraft. Wiedemans Analen. **36**, 769 (1888)

Kärcher, H.J.: Large telescopes and the art of bridge building. Proc. SPIE. **7012**, 4K1–12 (2008)

Maxwell, J.C.: Dynamical theory of the electromagnetic field. Philos. Trans. R. Soc. Lond. **155**, 459–512 (1865)

Meinel, A.B.: Cost-scaling laws applicable to very large optical telescopes. Opt. Eng. **18**, 645–647 (1979)

Parsons, W.: (Earl of Rosse), Observations on the Nebulae. Philos. Trans. R. Soc. **140**, 499–514 (1850) (PDF online)

Van Belle, G.T., Meinel, A.B., Meinel, M.P.: The scaling relationship between telescope cost and aperture size for very large telescopes. Proc. SPIE. **5489**, 563 (2004)

Wilson, R.N.: Reflecting Telescope Optics, p. 90 ff. Springer, Berlin (1996)

Chapter 3
Birth of Radio Astronomy

The first large, fully steerable radio telescope (25 m) at Dwingeloo, the Netherlands. Built in 1955/1956, it has been declared a National Monument. Completely refurbished it is operated by CAMRAS, an organisation of amateur astronomers and radio enthusiasts, for outreach and research (J. Baars, ASTRON)

3.1   Early History of Radio Telescopes

In Germany in 1904, Christian Hülsmeyer used a copy of Hertz's apparatus to demonstrate the reception of radiation reflected from a ship, thereby introducing a first primitive version of radar, albeit without range information. In the early years of the twentieth century, the ingenious inventor Guglielmo Marconi (1874–1937) was instrumental in the development of radio communication and broadcasting at long wavelengths of deca- and hectometres. The antennas were wire dipoles. In the early 1930s, Marconi used parabolic dishes of 3 m diameter in a demonstration of telephony across the English Channel at a frequency near 1.7 GHz. Radar was developed in several countries in the late 1930s and was put to use intensely in World War II, using paraboloidal reflectors at decimetre wavelengths. Great secrecy surrounded these latter activities.

3.1.1   *Jansky's* Bruce *Antenna*

A major activity in radio was the emergence of short-wave intercontinental communication, typically at wavelengths of the order of 10 m. It was soon discovered that weather phenomena, in particular remote thunderstorms, could interfere with the communication. At the Bell Telephone Laboratories in Holmdel, New Jersey, USA, physicist-engineer Karl G. Jansky (1905–1950) was given the task to systematically determine the occurrence of such interference as function of time and direction. In 1932, he constructed a so-called Bruce antenna for 14.6 m wavelength (Fig. 3.1) and placed it on a platform, which rotated in azimuth to identify the direction of any interference. In the process of his experiment, he noticed from a certain direction in azimuth the daily appearance of a significant increase in the noise level of the receiver.

The maximum signal moved in azimuth angle by about 4 min of time per day, and Jansky correctly concluded that the origin of the noise was located outside the solar system. He identified it as cosmic noise coming from the direction of the centre of our Milky Way (Jansky 1933). This first radio telescope was nicknamed Jansky's merry-go-round, and its azimuth mechanism is the first appearance of a mechanical component still used in modern radio telescopes, called the wheel-on-track configuration. Jansky proposed the construction of a large radio telescope, but this was not granted and his bosses moved him to other work in the mid-1930s.

3.1.2   *Reber's Transit Paraboloidal Reflector*

Jansky's discovery did not create a reaction from the astronomical community, but another radio engineer and ham-amateur Grote Reber (1911–2002) was inspired by it. In his backyard in Wheaton, Illinois, he built a parabolic reflector of 9.6 m diameter with a focal ratio of 0.6, shown in Fig. 3.2. Expecting that the radiation
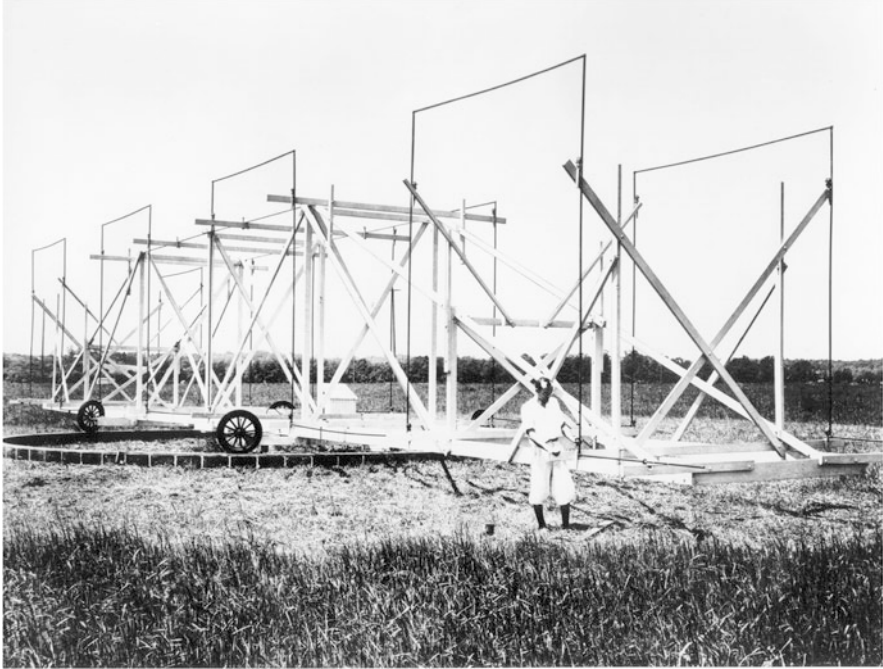
Fig. 3.1 Karl Jansky in front of his merry-go-round antenna 1932 at the Bell Labs in Holmdel, New Jersey. A copy of the antenna is located at the entrance of the National Radio Astronomy Observatory in Green Bank, West Virginia, USA (Courtesy AT&T)
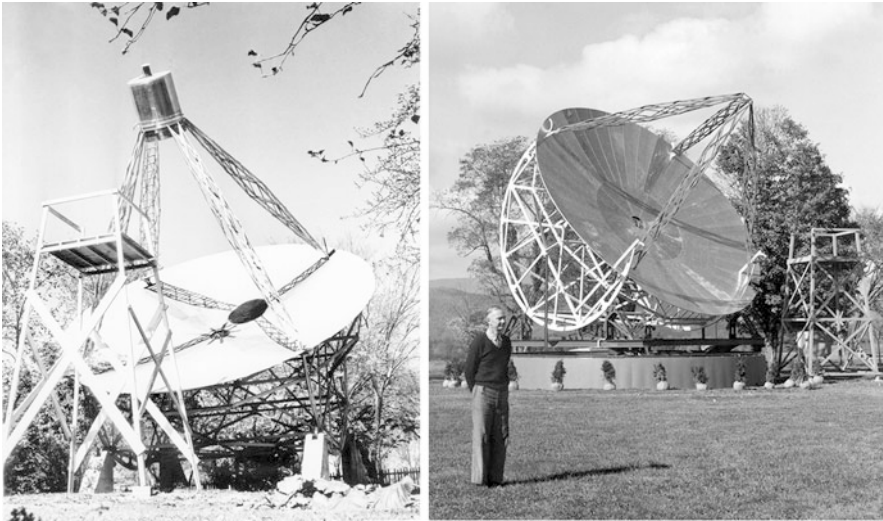
Fig. 3.2 *Left* the 9.6-m diameter parabolic transit reflector built by Grote Reber in his backyard in Wheaton, Illinois, in 1936–1937. *Right* Reber standing next to his antenna at the entrance of the National Radio Astronomy Observatory in Green Bank, West Virginia. An azimuth track has been added for full movement (NRAO/AUI/NSF)

would be of thermal origin, he made his first observations at the highest frequency of about 3 GHz (10 cm wavelength) where equipment was available at that time (1937). He did not detect any signal. His next experiment at 910 MHz also failed to produce a result, so he finally settled at 160 MHz (wavelength 1.9 m) and there he was successful. Thus, after Jansky's original discovery, radio astronomy was put on a solid footing with the first maps of galactic radio emission collected by Reber (1940a, b). He worked throughout the war and published several papers with his observations. These indicated that the dominant radiation at radio wavelengths was not of thermal origin but rather showed a spectral behaviour of being stronger at longer wavelengths. This component of radiation was totally unknown at visible wavelengths. Its origin, synchrotron radiation from free electrons spiralling in the magnetic field of the Galaxy, was described theoretically only in the early 1950s by Kiepenheuer (1950) and Shklovski (1952) on the basis of the radio observations.

The structural design of Reber's antenna is astonishingly modern, with a rocking chair concept for the elevation section: used in a very similar manner in current extremely large optical telescopes designs (the 30-m TMT and the 39-m E-ELT). The rotating elevation structure consists of three subsystems: the reflector, the elevation cradle and the quadripod. The system design is excellent and excites the admiration of a modern structural engineer. It is miraculous how Reber conceived of his design ideas, particularly when we look at the evolution of later large radio telescopes, where sometimes detours were taken that proved to be unsuitable. The original telescope was a transit instrument rotating only in elevation. It was equipped with a cavity drum receiver at the focus (visible in Fig. 3.2). Reber donated his telescope in the 1960s to NRAO in Green Bank, where it was reinstalled under his supervision on an azimuth turntable (Fig. 3.2). Visible is also a service tower for the installation and maintenance work at the receiver on top of the quadripod. It is an amazingly good design.

3.1.3   Würzburg Riese Radar Antenna

During World War II, many parabolic dishes were deployed for radar, both on ships and on the ground. At the retreat of the German army in the spring of 1945, the European Atlantic coast was dotted with radar antennas of 7.5 m diameter, called Würzburg Riese. The German word "Riese" means giant and it is indicative of the state of the art in parabolic reflectors at that time. Several of the antennas were "adopted" by radio astronomy groups in statu nascendi in England, France, Scandinavia, the USA and the Netherlands. If the antenna was in good condition, one could use it at wavelengths as short as 10–20 cm.

Figure 3.3 shows the Dutch Würzburg antenna, located at the short-wave transmitting station in Kootwijk. This antenna was used for the first extensive mapping of the distribution of neutral hydrogen atoms in our galaxy at a wavelength of 21 cm. This spectral line had been predicted to be observable by Henk van de Hulst (1918–2000) during a wartime colloquium in Leiden in April 1944 (van de Hulst 1945). It was detected in 1951 at Harvard University by Ewen and Purcell
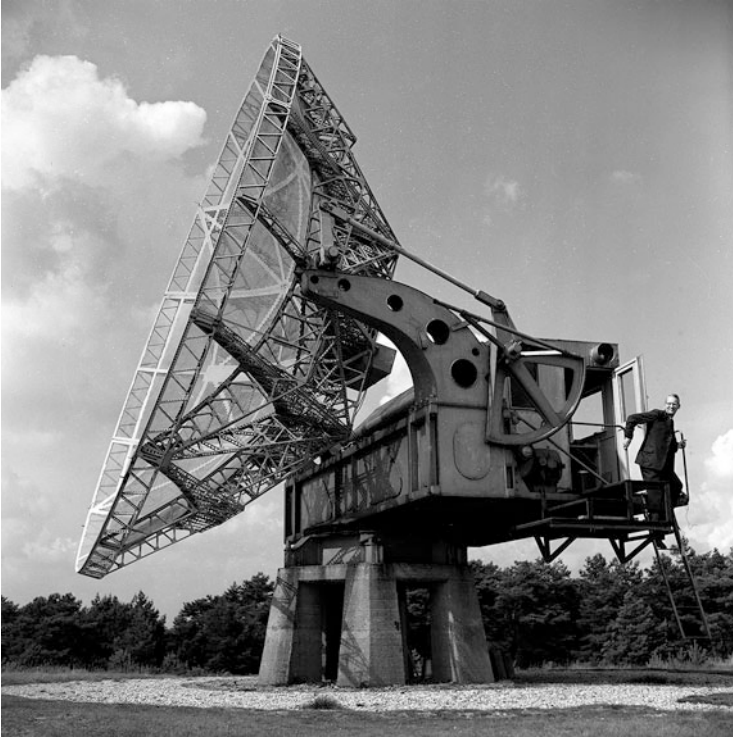
Fig. 3.3 "Würzburg Riese" German radar antenna of 7.5 m diameter, relocated after the War to the Kootwijk radio transmitting station, with which the 21-cm hyperfine line of neutral hydrogen in our Galaxy was detected in 1951 by Lex Muller (on the stairs) (Arie Hin, ASTRON)

(1951), 6 weeks later confirmed in Kootwijk by Muller and Oort (1951) and shortly afterwards in Australia by Christiansen and Hindman (1952).

Depending on the observing program for the antennas, they were used with different types of mount (Fig. 3.4). The Dutch group used the original alt-azimuth mount of the radar antenna, whereas the solar physicists in the Netherlands changed to an equatorial mount for ease of tracking the Sun, thereby avoiding painstaking coordinate transformations. The group in Cambridge, UK, used two antennas as transit interferometer for source position determination. The three examples give some hints to the importance of the telescope mount and its complexity from the mechanical and structural engineer's point of view.

Looking at the Würzburg reflectors, we see design features, which show clearly that they originate from an aircraft manufacturer (Zeppelin). The porous reflector consists of punched-hole aluminium sheets, and the latticed truss system shows its origin from aircraft stringers. The location of the hard points, where the reflector is attached to the elevation bearings, is arranged between the reflector edge and the centre. This distributes gravitational deformations somewhat evenly over the reflector, which is desirable. We elaborate on this in detail later.
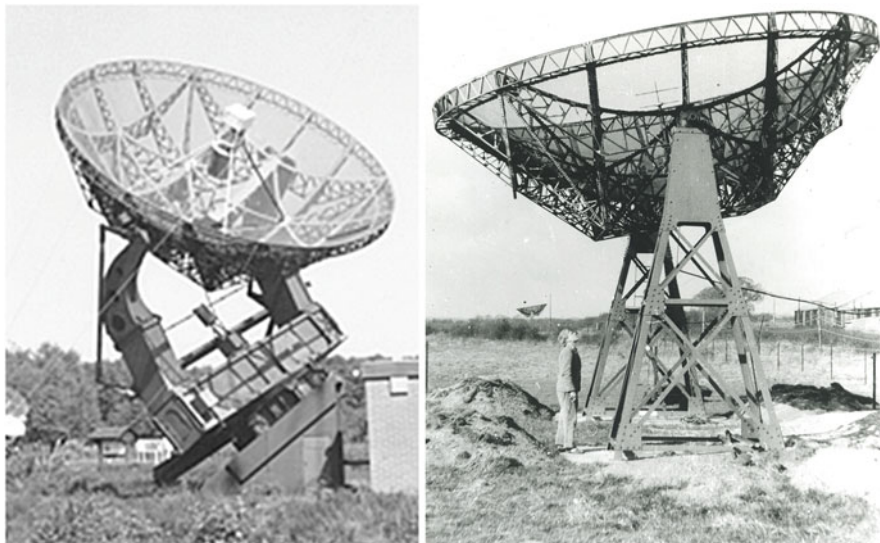
Fig. 3.4 Würzburg antennas employed different types of mounting. *Left* Polar mount for solar tracking in Dwingeloo, the Netherlands. *Right* Meridian transit with movement in elevation only, inspected by F. Graham Smith in Cambridge, England (1951). Note the second antenna of the interferometer in the distance

3.2 The First Large Radio Telescopes

The US Naval Research Laboratory (NRL) 50-ft (15 m) was constructed in 1950 but became fully operational only in 1954. Its aluminium reflector had an astoundingly high surface accuracy of 1 mm. However, the dish was attached to a gun mount of insufficient stiffness and the pointing errors did not allow exploiting its use at short cm wavelengths. This unbalance between pointing and surface accuracy has hampered more telescopes to be fully utilised. We address this aspect further in the discussion of other telescopes.

In the spring of 1956, the 25-m telescope of the Netherlands Foundation for Radio Astronomy in Dwingeloo, the Netherlands, began operation, the following year followed by an equally large antenna of the University of Bonn, Germany, placed at the Stockert in the Eifel Mountains near Bonn. These antennas were designed and constructed parallel to each other but without contact between the designers. Two completely different basic designs emerged, and each type has been selected later for large telescopes. For this reason, we shortly describe both instruments.

3.2.1 Dwingeloo (NL) and Stockert (BRD) Telescopes

3.2.1.1 Dwingeloo

Soon after the end of the war, Prof. Jan Oort (1900–1992) at Leiden Observatory in the Netherlands initiated a plan for a large radio telescope with a reflector diameter of 25 m. It was completed in 1956 in Dwingeloo in the northeast of the country. The telescope shows in its layout some influence of the Würzburg antenna, particularly in the appearance of the asymmetric shape of the azimuth frame and the arrangement of the elevation bearings in the rear between the edge and the centre of the reflector backup structure.

Some new features can be identified (Fig. 3.5):

1. The azimuth load is distributed over four outer wheels on a circular track and a central pivot bearing of 2.5 m diameter that carries half of the vertical load and includes the drive gearing.
2. The reflector surface and backup structure have a triangular topology in contrast to the rectangular of the Würzburg reflector. This also leads to triangular reflector panels.

The telescope was designed for operation at 20 cm wavelength (van de Hulst et al. 1957). The reflector surface consists of wire mesh with 15 mm spacing and 1.5 mm thick wires. The mesh is attached to triangular flat frames with a side length of 0.9 m. Thus, the surface is a mosaic of flat facets and the maximum deviation from the paraboloid is 3 mm, which is acceptable for the planned operational wavelength range. The rather large focal ratio of 0.5 was chosen to enable this solution for the surface. A deeper dish would have resulted in too large an error with flat surface facets and necessitated either more expensive curved facets or smaller ones needing additional support structure.

Particularly interesting in the pre-computer analogue era is the solution for the transformation from celestial to earth-bound elevation–azimuth coordinates to enable tracking of an astronomical source. The coordinate transformer consists of two coupled two-axis mechanical bracket systems (Fig. 3.6) that can be driven by servo control. The celestial coordinate (hour angle and declination) bracket is driven to the required position and the coupled azimuth–elevation bracket servos deliver the control signals to the telescope azimuth and elevation drives to point in the desired celestial direction. The maximum error of the system could be limited to 0.02°.

From the mechanical point of view, the telescope can be considered the *exemplary prototype* for all wheel-on-track telescopes built later all over the world. It was the first telescope designed by B. G. Hooghoudt (1924–1995), who would later put his mark on the design of many telescopes, for both radio and optical astronomy, among them several that we will describe in this book. Werkspoor executed detailed design and construction.

Fig. 3.5 The Dwingeloo 25-m radio telescope in the Netherlands was the biggest in the world for about a year, when the 76-m Jodrell Bank telescope overtook it. The alt-azimuth design employs a "wheel on track" for the azimuth movement. The central mast carries the dipole feed in the focal point and a small receiver package behind the focus (ASTRON)

The telescope was upgraded in the early 1970s by a more accurate surface, enabling observations at 6 cm wavelength, computer control for automated observing and a quadripod for support of cryogenically cooled receivers at the primary focus. It was decommissioned in 1999 but saved from demolition by being declared a National Monument in 2009. It is now operated by CAMRAS, an organisation of amateur astronomers and ham-radio enthusiasts, and it plays an important role in public outreach (http://www.camras.nl/). The chapter picture shows the telescope in its present form.

Fig. 3.6 The analogue coordinate transformer to control the telescope in celestial coordinates (ASTRON)
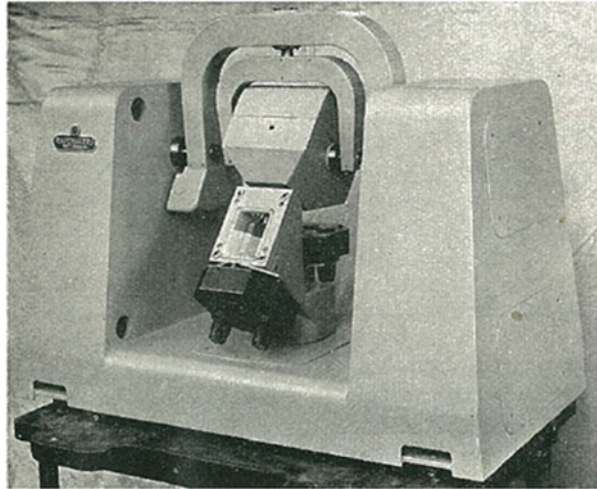
3.2.1.2   Stockert

The Stockert antenna (Fig. 3.7) is placed on top of a conical concrete tower (Pederzoni 1956). The telescope was designed and built by Zeppelin Metallwerke, Friedrichshafen, and the reflector backup structure shows similarities to the Würzburg reflectors, but with a radial arrangement of the main trussed girders, supported by an inner circular hub and an outer trussed hoop (Fig. 3.7).

It has a very compact elevation–azimuth structure, reminiscent of a canon mount. One might surmise that the designers possessed considerable experience with this type of two-axis mount. The reflector is supported by a central ring and cantilevered outwards in a self-supporting structure. The surface is made of a perforated aluminium skin with 10 mm diameter hole at 12 mm interval. The pre-assembled backup structure is shown in Fig. 3.8.

The mount of the Stockert telescope is very different to the mount of the Dwingeloo telescope. It is a so-called *king-post mount*. The king-post is a construction element used since medieval times in cranes and windmills. The main feature of the central king-post is to stabilise the system against wind-induced overturning moments by horizontal reaction forces in two bearings. In the wheel-on-track mount, the overturning moments are taken very differently by vertical reaction forces in the bogie wheels (Fig. 3.9).

The king-post design allows, in relation to the reflector diameter, the use of rather small ball bearings, available at the time of the Stockert construction (Fig. 3.8, right). Currently, much larger roller bearings are available (so-called slewing bearings), which are able to take large overturning moments in the bearing plane, without the need for a king-post and a second reaction bearing. Considering the "load transfer in bearings" aspect, the wheel-on-track design is equivalent to a segmented slewing bearing; it takes the overturning moment in one reaction plane. The segmentation into four azimuth bogies was imposed by size restrictions in the

Fig. 3.7 The Stockert 25-m radio telescope of the University of Bonn, Germany, employs a compact "king-post" mount design for the axes movements. Also here originally a central mast for the feed was used; it was later replaced by a subreflector to form a Cassegrain configuration (Astron. Inst. Univ. Bonn)

manufacturing of slewing bearings. However, such bearings are now available in non-segmented configuration from specialised fabricators in diameters up to 8 m. The Stockert-type mount with a conical concrete tower and only one single slewing bearing for azimuth is called *turning-head mount* and has regularly been used for telescopes up to 50-m reflector diameter. The Stockert telescope may be considered an early prototype for this type of mount. Unusual in the Stockert layout are the large offsets between the elevation and azimuth axes and between the reflector and elevation axes. This has implications for the transformation between the celestial and elevation–azimuth coordinates. The Stockert team used for this purpose the same analogue coordinate transformer as used in Dwingeloo. In 1966, the focal
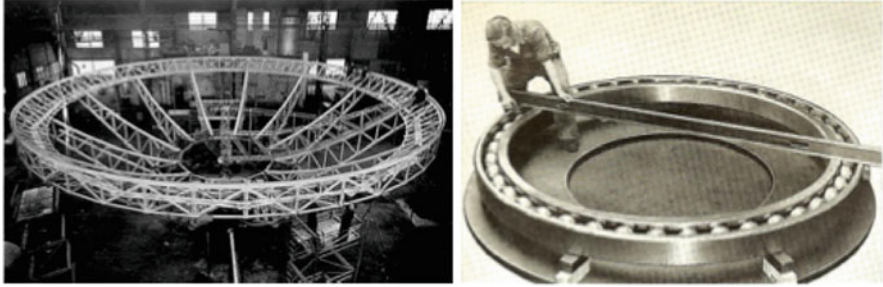
Fig. 3.8 *Left* Pre-assembled backup structure in the Zeppelin workshop. *Right* the 2.6-m diameter ball bearing from SKF for the azimuth movement (Astron. Inst. Univ. Bonn)
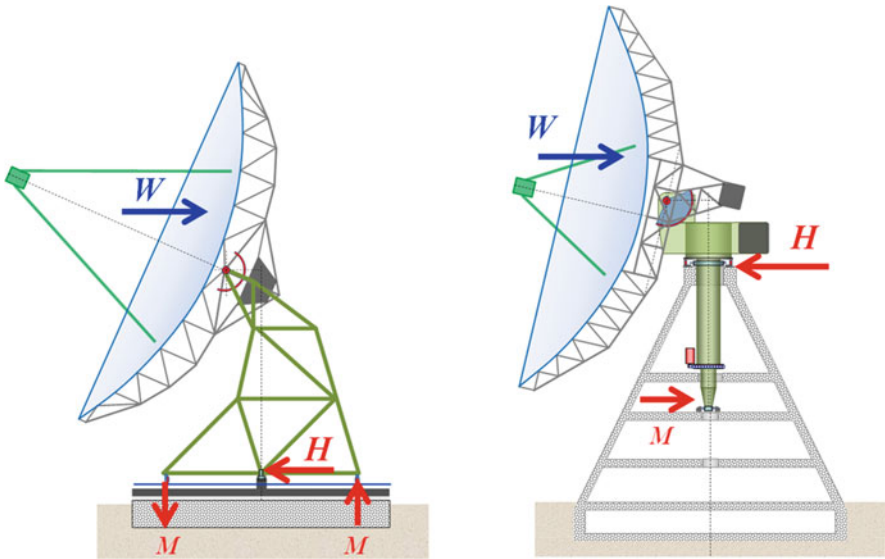
Fig. 3.9 Comparison of two mount concepts. *Left* the wheel-on-track configuration of the Dwingeloo telescope; *right* the king-post solution of the Stockert telescope

arrangement was changed from primary focus to a Cassegrain layout with a subreflector of 2.5 m diameter.

After the Effelsberg telescope came into operation in the early 1970s, the telescope was used for long-term surveys until operation was stopped in 1993. Similarly to the fate of the Dwingeloo telescope, it was salvaged by the designation of Monument, and it is now operated by an organisation of amateurs and educators (Verein Astropeiler Stockert, http://netcom-bonn.de/).

3.2.2   A Comment on Accessibility of the Focal Point

Both large antennas mentioned here, and the Jodrell Bank antenna, to be discussed next, use a central pole to support the feed in the primary focus of the paraboloid. This was the usual way to "feed" the dish in the case of radar, where the bulky transmitter was located behind the reflector. Initially, the early radio telescopes just replaced the transmitter by a receiver and accepted the loss in the coaxial cable from the dipole feed to the receiver input. In some cases, a small receiver front end with a mixer and some intermediate frequency amplification was placed on top of the central mast. Later, with the development of low-noise electronics, often cooled to cryogenic temperatures, the tripod and quadripod were introduced to support the bulky front-end equipment at the focus. Of course, also the Cassegrain or Gregory variety of basic optics requires the stable arrangement for the relatively large secondary reflector near the primary focal point. While the use of the central mast severely limits the amount of equipment near the focal point, it has its advantages. First, the asymmetric loading of the reflector support structure by a quadripod complicates the structural design of the support structure. Second, the aperture blocking of the quadripod with its negative influence on the gain and the side lobe level of the antenna (see Chap. 8) is effectively avoided by the use of the central mast. Notwithstanding significant alterations to its design, the Jodrell Bank telescope has maintained the central tower to support the prime focus receivers, even including heavy cryogenic systems. The blocking by this central structure of the very large aperture remains small, comparable to the best quadripods. On smaller reflectors, this would cause an unacceptably large blocking.

3.2.3   Jodrell Bank (UK): Lovell Telescope (76 m)

After the war, Bernard Lovell (1913–2012) assembled a group of scientists and radar engineers at the University of Manchester to make radar studies of cosmic ray air showers and meteor trails. He obtained permission to place the radars at the field station of the Botany Department in Jodrell Bank about 30 km south of Manchester. Once out in the countryside, where the level of interference was much lower than in Manchester, Lovell developed the idea of a giant dish capable of swinging around the whole sky and extending the research to the new field of radio astronomy. In 1947, he approached the renowned manufacturer of optical telescopes Grubb Parsons in Newcastle upon Tyne for an engineering proposal but without success. The engineering challenges for the radio telescope were too different from those of optical telescopes. In 1949, Lovell engaged Henry Charles Husband, from
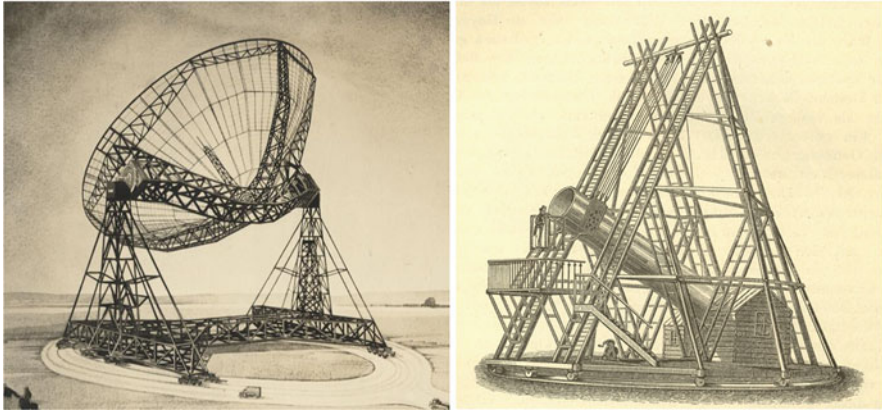
Fig. 3.10 The first sketches by Husband for an alt-azimuth telescope of 200 ft diameter, with a wire-mesh reflector surface, to operate at wavelengths longer than 1 m (Jodrell Bank Observatory). On the right is Herschel's large alt-az optical telescope of 1789 (Wikipedia)

profession a bridge designer, and asked him to produce design concepts including cost estimates for a telescope with a diameter of some 200–250 ft. Based on Husband's input, Lovell convinced the scientific boards of the UK of the importance of his project and a first design study by Husband was financed. Husband's design approach is very well documented in the *Blue Book* (1951). His first design sketch of 1951 (Fig. 3.10) shows the influence of his education as bridge builder with two huge towers supported by a turntable on a curved railway track and a catwalk-type beam between the elevation bearings, carrying a wire-mesh reflector. Another inspiration may have been the telescope built by William Herschel in Slough in 1789. Any influence of a Würzburg reflector design is not apparent in his concept.

Husband started with a cost estimate of £100,000 for a 200-ft telescope. In the end after a number of engineering and financial crises, the telescope did cost nearly £500,000. It also looked very different from the first design sketch. Husband was able to overcome the engineering problems, and Lovell managed to convince the Nuffield Foundation to cover the cost overruns. Husband's approach used modern design methods, starting with a conceptual design (as described in the Blue Book) followed by preliminary and final design phases that resulted in what is now known as a Preliminary Design Review (PDR) and a Final Design Review (FDR). It is possible that these reviews were actually just discussions during afternoon tea in Bernard Lovell's office.

New results in radio astronomy, in particular the detection of the neutral hydrogen line at 21 cm wavelength, necessitated a change of the shortest wavelength down to 20 cm. This required considerable design adjustments, and the appearance of the completed telescope in 1956 is very different from that of the first concept (Lovell 1957). During the detailed design phase, significant changes were made to the reflector surface and the backup structure (Fig. 3.11).

Fig. 3.11 The original 250-ft telescope of 1957. The central bicycle wheel damps structural resonances and does not carry loads (David Darling-photopedia.com)

The reflector surface is solid, made of welded steel sheets, and is part of the load-bearing structure. This increased the impact of wind on the structure considerably. Another change is the transition from the catwalk girder between the elevation bearings to a lightweight space truss on the reflector rear with a large outer hoop, which houses the attachment brackets for the elevation bearings and drives. Interesting is the central "bicycle wheel", which does not carry any load, contrary to a structural engineer's first assumption, but provides damping of structural resonances. We see here the first indication of the importance of dynamic features in the structure of large radio telescopes.

The reflector is a very deep "bowl"; the f-ratio is only 0.25, which means that the focal point of the paraboloid lies in the aperture plane of the reflector. As in the case with the Dwingeloo telescope, this is not an arbitrary choice. First of all, the receptor in the focal point is now quite well shielded from the environment; it hardly "looks over the edge" of the reflector. Thus, there is less risk for receiving interfering signals from human activity in the surroundings such as motor traffic and electrical equipment. This was a serious concern in the industrialised region of Manchester, contrary to the rural and specifically protected "interference free zone"

environment of the Dwingeloo telescope. Secondly, this configuration allowed the entire reflector to be turned downwards to the nadir for convenient access from the ground to the receiver equipment at the focal point. As in the Dwingeloo telescope, a central mast supports the feed at the focus.

The 250-ft (76 m) telescope of 1956 looks to the structural engineer as a lightweight and progressive achievement. As one could expect from such a pioneering project, problems arose over time that led to an extensive refurbishment after about 15 years of use. The problems were related to performance as well as survival issues. Adding diagonal bracings to stiffen the azimuth towers against sideward wind loads solved them. Also the very light "bicycle wheel" was replaced by two sturdy load carrying support wheels. These lift the centre of the reflector structure and reduce thereby the sag of the original structure, which had resulted in a large astigmatism deformation of the reflector surface. The wheels also relieve the loads on the elevation bearings and reduce the risk of fatigue in the steel structure. The telescope was named the "Lovell Telescope" in 1987 and further enhanced in 2002 with a new surface of higher accuracy, enabling observations at higher frequencies. The focal ratio has been increased and the focus sticks out over the reflector edge. However, the central tower for the support of the focal instruments has been maintained (Fig. 3.12). The entire elevation rotating structure is balanced about the elevation axis without the need for additional balance weights.

The telescope is still in full use and evokes admiration from a contemporary structural engineer for the early pioneers of radio telescope design. It will be used in
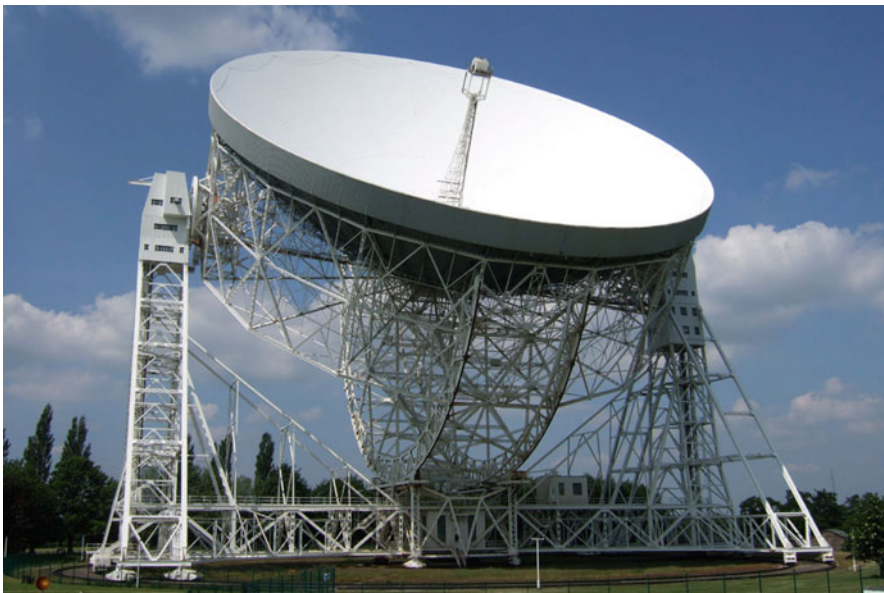
Fig. 3.12 The Lovell Telescope at Jodrell Bank, England, in its present form (Jodrell Bank Observatory)

Fig. 3.13 A model of the Mark V design of 400 ft diameter that was never realised (Jodrell Bank Observatory)

the sequel as an example for the explanation of some fundamental features of structural mechanics in telescope design.

The original large telescope at Jodrell Bank was called "Mark I", an indication that Lovell did not rest after its erection but developed plans for even larger telescopes. The model of a plan for a 400-ft telescope called Mark V (Fig. 3.13) provides some insight into the evolution of structural ideas in the engineering group at Jodrell Bank. Immediately obvious is the addition of a sturdy cross connection between the tops of the azimuth towers. This is probably a result of the scary experience with the Mark I under a heavy gale as described by Lovell in his biography (Lovell 1985).

The reflector backup structure in the Mark V model has no longer the large outer hoop. It is not supported at the edge of the reflector but fourfold on two cross beams shifted somewhat to the centre. Additional support is provided by two wheels arranged about two-thirds from the axis centre. The whole space is filled with a huge number of latticed steel struts, an indication that the design concept was driven more by fear of structural failure than by a systematic structural concept.

A similar dense strut system is used in the Green Bank Telescope (see Chap. 7). It reminds one somewhat of the design approach by the builders of the Gothic cathedrals, more pragmatic and empiric than systematic and based on theory. We shall discuss this in more detail in the chapter on homology design (Chap. 4).

Funding for the Mark V remained unsuccessful, not least because considerable expenses were needed for the necessary refurbishing of the Mark I that one did want to salvage. What one owns is better than what one perhaps might acquire.

3.2.4 Parkes (Australia) 64 m Telescope

At CSIRO in Australia, Edward (Taffy) Bowen (1911–1981) launched a plan in the 1950s for a giant radio telescope as a national entrance into "big science". Funds were obtained not only from Australia but also from the Carnegie and Rockefeller foundations of the USA. The design and management approach of the proposers differed from Lovell's and Husband's in Jodrell Bank. They solicited design concepts from renowned engineering firms from Australia and overseas and received several unconventional proposals (Fig. 3.14). From a mechanical point of view, the concepts show interesting features, but none has any resemblance to the telescope as actually built.

On a trip to London in 1955, Bowen came in contact with Barnes Wallis (1887–1979), who had previously designed the WWII Wellington bomber for the Royal Air Force and invented the "dam buster" bomb for destroying German dams. He showed Bowen a design concept for a large telescope (Fig. 3.15, left) that contains the germ for the evolution to the final Parkes telescope (Fig. 3.15, right). Wallis' reflector shell looks very lightweight like an aircraft hull, with spiral purlins. He believed that the reflector diameter could be extended up to 1000 ft (300 m). A cannon turret probably inspired his mount.

The final design is the opposite to the broad-based mount of the Lovell telescope but is quite reminiscent of the Stockert telescope. Freeman Fox of the UK, a famous engineering firm for bridges and roadways, carried out the detailed design. After an
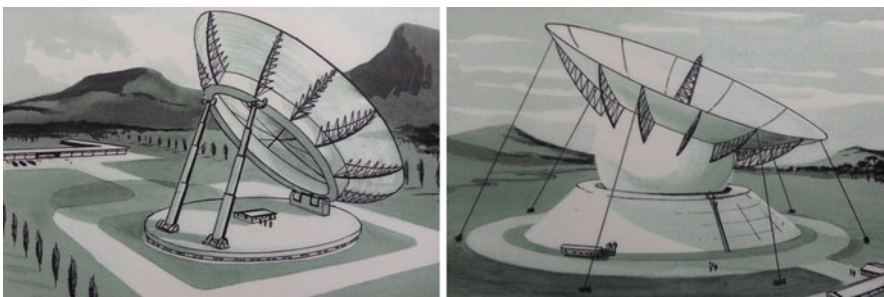
Fig. 3.14 Some entries of a design contest for the large Australian radio telescope [Credit: CSIRO Radio Astronomy Image Archive (RAIA)]
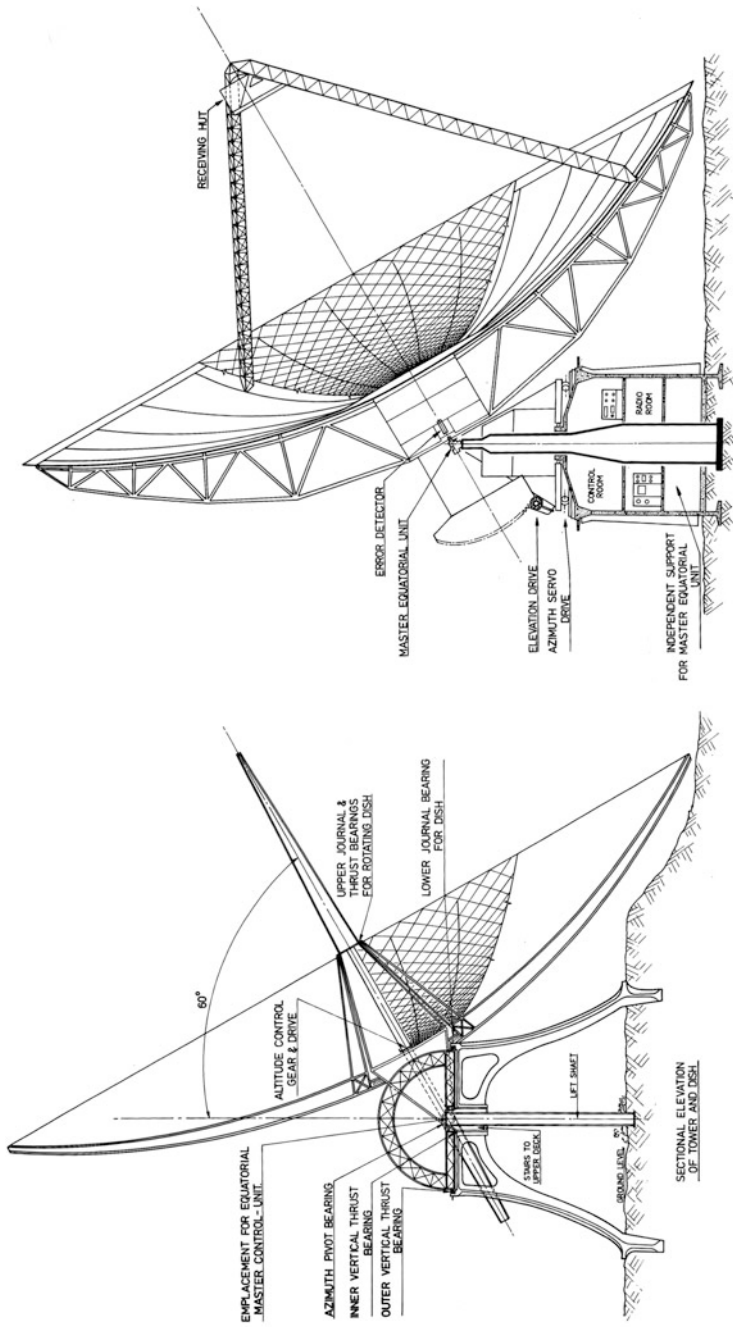
Fig. 3.15 Historical sketches: *left* design concept of Barnes Wallis for a giant radio telescope of up to 300 m in diameter; *right* cross section of the final design of 64 m diameter (CSIRO RAIA)

Fig. 3.16 The 64-m diameter radio telescope in Parkes, Australia, in operation since 1961 (CSIRO RAIA)

international bidding process, the construction contract was awarded in 1959 to the West German firm MAN Gustavsburg, at that time one of the world's leading producers of steel bridges. A complete trial assembly of the turret and the reflector hub, including the azimuth and elevation bearings and drives, was executed on the assembly yard of MAN. The final erection of the steel structure was executed with a huge derrick, now seldom used while replaced by a large mobile crane. The availability and cost of such a crane is sometimes one of the design drivers for the steel structure of a telescope, especially for a site in a thinly inhabited region, which is often the case. The telescope was located in Parkes, NSW, and came into operation in 1961 (Bowen and Minnett 1962; Bolton 1963; Robinson 2011). The telescope (Fig. 3.16) looks quite filigree and resembles many of the features of the original Wallis' concept. Only the supporting pole for the receivers in the focus has been changed from a maypole to a tripod, and the reflector backup structure is a space truss instead of the ribs and stringers of Wallis' aircraft hull, but the spiral purlins were kept.

The reflectors of the 64-m Parkes telescope and its 46-m twin in the Algonquin Park, Canada, are supported on the rear by a solid steel hub of small diameter on a turret-type mount (Fig. 3.16). The turret design doesn't allow full sky coverage like the Lovell telescope but is restricted to elevation angles above about 45°. The central hub prevents the use of an elevation cradle with interfaces to the backup structure further outwards that are necessary to avoid coma-type deformations under lateral forces dominating at lower elevation positions of the reflector. This

structural design philosophy is the opposite of that of the Lovell telescope with its elevation bearings arranged on the outer hoop of the backup structure. While the Lovell telescope suffers large sag of the reflector in the centre and a related strong astigmatic deformation at high elevation angles, the main problem of the Parkes' approach is a large S-type bending of the reflector centre at low elevation position resulting in a coma-type reflector deformation. The optimum is obviously something in between as chosen for the Dwingeloo reflector.

The Parkes telescope employs a mechanical coordinate transformer, called "master equatorial", not externally located as in Dwingeloo, but mounted on a separate central tower in the crossing point of the telescope axes inside the turret (Fig. 3.17). A large effort was devoted to this task with a major impact on the structural design that in our computer era is no longer necessary. As with the Dwingeloo telescope, the equatorial axes can be driven in celestial coordinates providing the control signals to the elevation and azimuth drive motors for positioning or tracking the desired point on the sky. The Parkes instrument goes one step further in that it places a flat optical mirror exactly on the crossing point of the axes of both the master equatorial (declination and hour angle) and the telescope (elevation and azimuth). A second mirror is attached to the rear of the radio reflector near the centre. An optical autocollimation system is created between these two mirrors that provides a closed loop correction for any small variation in the viewing direction of the reflector caused by external circumstances such as wind gusts. This solution improves the stability of pointing and tracking with respect to the open loop system.

Over its more than 50 years of life, the Parkes telescope, as well as its smaller twin at Algonquin Park in Canada, has been improved and modernised but was never subjected to the drastic changes in the structural system that happened to the Jodrell Bank telescope (Fig. 3.18). The design approach with the turret and extremely narrow central reflector hub was rarely followed up by subsequent radio telescopes. We will return to this subject after we have gained a better insight into the structural mechanics of large reflectors in a later chapter. There a comparison of the Parkes design approach with the Lovell approach will give us a deeper insight into the structural design issues of radio reflectors. These will lead to general design guidelines.

3.2.5   NRAO (USA): 140-ft and 300-ft Telescopes

For the last examples of the early, large telescopes, we turn to the 140-ft (43 m) and 300-ft (92 m) antennas of the *National Radio Astronomy Observatory* (NRAO) in Green Bank, WV, USA. The telescopes described above employed alt-azimuth mounts. The designers of these telescopes were driven by practical considerations, using existing bearing and drive technology and being aware that the alt-azimuth-type axes arrangement results in the simplest structural subsystem. A mechanical coordinate transformer achieved the transformation between alt-azimuth and
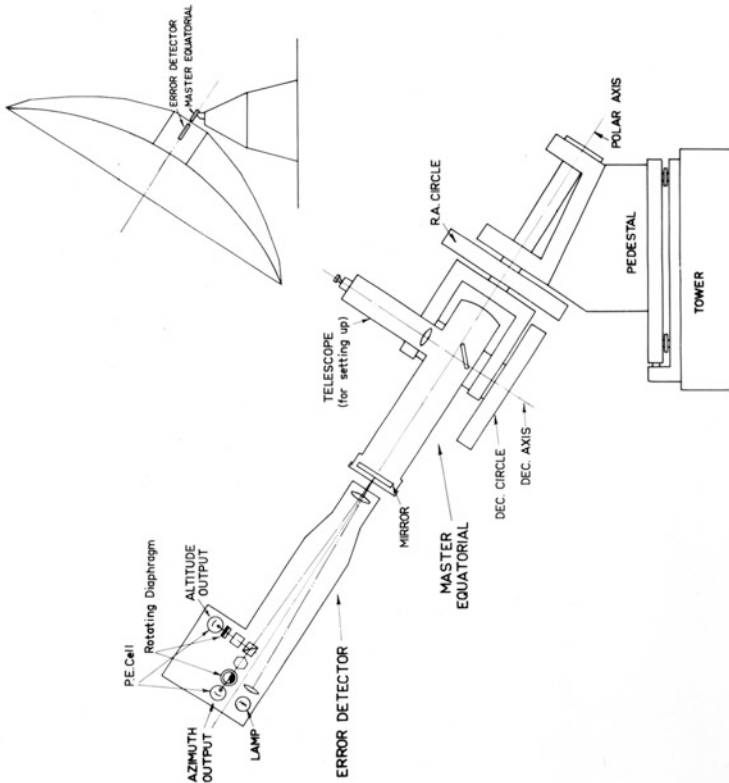
Fig. 3.17 The master equatorial is mounted on a separate central tower in the crossing of azimuth and elevation axes. An autocollimation system (*top left* in drawing, *top* in photo) corrects for small pointing errors in real time (CSIRO RAIA)

Fig. 3.18 The Parkes telescope in its current situation with a partially closed surface and a larger focus cabin (CSIRO ATNF)

celestial coordinates. In Chap. 2, we discussed the differences between the equatorial and alt-azimuth mount and mentioned that during the design discussions of the 140-ft telescope in the late 1950s the decision was taken to select an equatorial mount. This decision had grave consequences for the detailed design and the fabrication of the telescope. A considerable part of the structure had to be fabricated twice and the completion was delayed by more than 5 years to July 1965. The telescope has remained a "one-off" product, but the technical novelties and its eventual success as probably the most productive radio telescope during its lifetime warrant a description. The book *But it was fun* (Lockman et al. 2007) offers an account of NRAO's first 40 years in Green Bank with detailed reports on the two telescopes to be described now.

3.2.5.1 NRAO 140-ft Equatorial Telescope: An Expensive and Slow Project

The basic requirement for the telescope was unimpeded performance at a wavelength of 3 cm under the specified operational conditions. With a beamwidth of 3 arcmin at that wavelength, the pointing and tracking precision requirement was set at better than 20 arcsec. The surface precision was specified at 1 mm rms. These were specifications that no antenna of any diameter had achieved at the time. Several conceptual designs were presented and studied during 1955–1958.

Husband, the designer of the Jodrell Bank telescope, suggested to carry out a complete design, perhaps looking at several alternatives, before deciding on construction.

In July 1955, it was decided to design an alt-azimuth antenna of 140 ft diameter. Any larger dish, planned for the future, would need to be supported by that type of mount, and experience obtained with the 140-ft would be invaluable. Despite this sound argument, in 1956 the equatorial alternative was again brought into the design discussions despite the fact that several outside experts estimated a 25–50% increase in cost. Several designs, both alt-azimuth and polar, were reviewed in October 1956 and declined. E.L. (Ned) Ashton (1903–1985) was given the task to make a better equatorial design. Not having worked with telescopes, he seemed a good choice to present something original. Ned was professor at the University of Iowa and quite famous for his designs of several bridges across the Mississippi River, one of them being the first all-welded aluminium bridge. His design clearly was inspired by the 5-m Hale telescope on Mount Palomar in the use of hydrostatic bearings, and the welded aluminium backup structure for the reflector was a first in radio telescopes. In January 1957, a final decision was taken in favour of a polar mounted telescope of the Ashton design. A last-minute argument by an influential (solar) astronomer led to the extreme requirement of "being able to observe the Sun at any time when it is above the horizon". This required an excessively large hour-angle range of ± 8 h with serious structural and cost consequences. But Ashton said it could be done and was told to commence the detailed design phase.

A comparison of the 140-ft with the Stockert telescope (Fig. 3.19) shows that the polar axis can be interpreted as a king-post tilted into the direction of the earth axis.
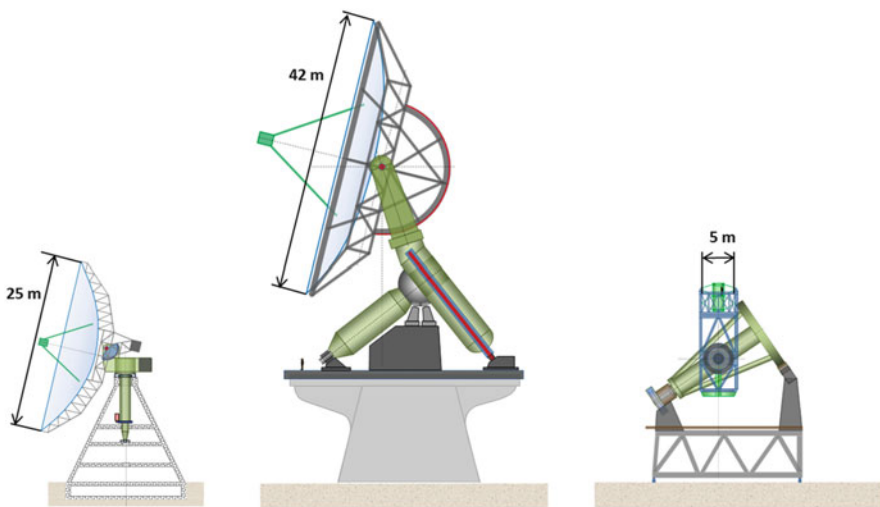
Fig. 3.19 Comparison of the mounts of the Stockert radio telescope with a king-post mount, the 140-ft and Palomar optical telescope with polar mount (to scale)
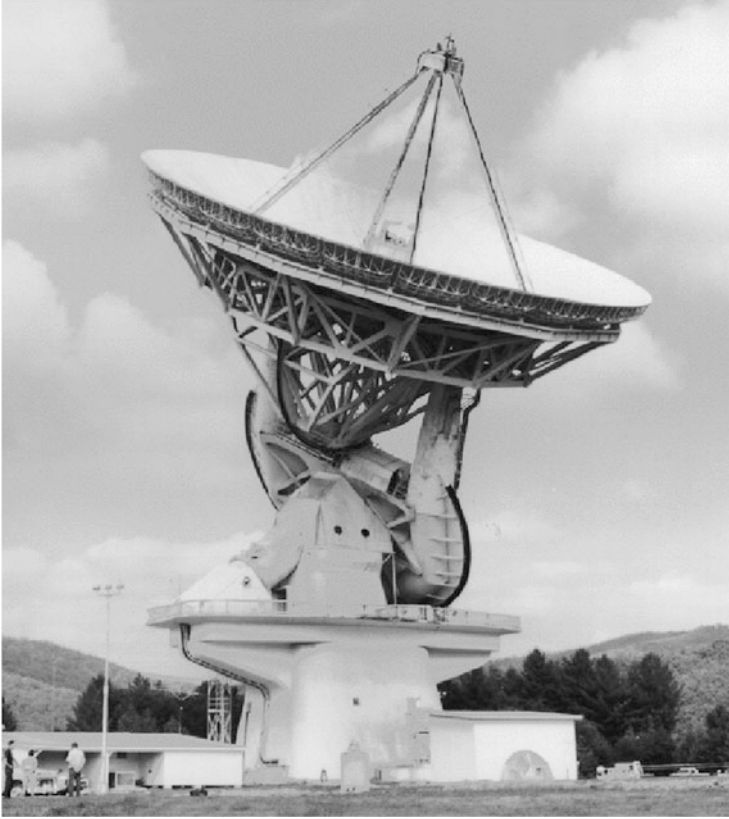
Fig. 3.20 The equatorially mounted 140-ft reflector at NRAO in Green Bank, WVA, USA, shortly after its completion in 1965. The sphere of the polar bearing is shielded by the cabin with two port holes. Later, the polar axis and yoke were covered with thermal insulation (NRAO/ AUI/NSF)

A comparison with the 5-m Hale telescope on Mount Palomar shows similarities in the design of the mount particularly in regard to the bearings. Hydrostatic bearings were not used in any radio telescope at the time. At the top of the polar axis, a 5-m diameter sphere rests on the hydrostatic bearing, which carries the load of the entire moving part at a weight of 2700 t.

A large and massive yoke supports the declination structure and carries the hour-angle gear rack. The reflector backup structure is a welded aluminium space truss structure with a central large gear rack in the back for the declination drive. Three rings of large aluminium-welded surface panels of average length of 7 m form the primary reflector. Because of the extremely large hour-angle range of 8 h at either side of the meridian, the telescope has a concrete support tower of almost 20 m height (Fig. 3.20). The telescope is very heavy and has nearly the same weight as the 100-m Effelsberg telescope; its overall weight per collecting area of about 2000 kg/m^2 is about five times that of Effelsberg (Chap. 4).

Bids went out in August 1957 and the Bliss Company of Ohio received the order in June 1958 for a fixed price of $4.75 million and a completion time of 2 years. In 1962, the company Stone and Webster replaced Bliss and redesigned and fabricated large parts of the steel section (polar axis, bearing and yoke). From early 1962, work progressed but still slowly. For the transportation of the bulky and heavy steel sections from the factory to the site, a few bridges needed to be strengthened and the clearance in some railway tunnels was not more than a few centimetres. The aluminium backup structure was welded on the site. During the hoisting of the backup structure, a cable broke and disaster was avoided because it happened early and the BUS dug into the ground without being damaged. In 1963, NRAO took over all supervision with Maxwell Small of Brookhaven Laboratory as on-site Project Manager. The telescope was finally finished in mid-1965, a 5 years delay, and at a total cost of $13.5 million, almost a factor three over the original contract (Small 1965).

The telescope started observations in the summer of 1965 and quickly made several outstanding discoveries. Because of its excellent suite of receivers, in particular at the short wavelengths below 10 cm, observers from all over the USA and abroad heavily subscribed it. With increasing experience, the users noticed several less agreeable aspects of the telescope. These were caused both by the changing gravitational load with varying viewing angle and by differential deformation due to temperature variations and gradients. This last problem was identified as early as July 1961, well before any site assembly had been performed, exemplified by the following remark in the quarterly Director's Report: "a study should be made of thermal deflection due to solar heating and other causes". This however was only undertaken after the problem arose during early operation.

Thermal and gravitational deformation of the large surface panels led to astigmatism and serious pointing errors. In the early 1970s, Sebastian von Hoerner and Woon-Yin Wong (1975) made extensive studies of these effects and realised several significant improvements in the telescope's behaviour. Among other measures, all exposed metal parts of the support structure were covered with a layer of thermal insulation, not yet the case in the early picture of Fig. 3.20.

Despite its shortcomings, the 140-ft became a highly productive telescope due to its state-of-the-art receiver systems and very flexible mode of operation. In 1999, financial constraints forced NRAO to decommission it. From 2005 to 2010, it has been used by MIT as a receiving antenna for bistatic radar experiments. In 2012, it has been given a new life as data ground station for the Russian VLBI space-borne antenna Radio-Astron, still serving radio astronomy.

3.2.5.2 NRAO 300-ft Transit Telescope: A Cheap and Quick Deal

When the long delay in the completion of the 140-ft became clear in 1960, NRAO proposed to design and build a "quick and dirty" (John Findlay) very large telescope of limited sky coverage to bridge the time gap and provide NRAO and the community with observing capabilities that were competitive with the emerging

large dishes in Europe and Australia. Under the leadership of John Findlay (1915–1994), a proposal for a 300-ft (92 m) transit instrument for 21 cm wavelength was presented and funded by the NSF in a record short time of a few months.

Bob Hall (1922–2010), who had also designed the early 85-ft polar mounted antennas mentioned in Chap. 2, carried out the basic design in the fall of 1960 and the detailed design and planning was ready in February 1961. The project foresaw a construction time of 12 months, an estimated cost of less than $500,000 and a lifetime of 5 years. The contract was awarded to Bristol Steel and Iron of Richmond, Virginia. Contrary to the initial experience with the 140-ft, this company turned out to be capable and a pleasure to work with, so John Findlay referred to them as the "Virginia Gentlemen". Field assembly started in August 1961 and first observations were made on 20 September 1962. The final cost was $850,000 (Findlay 1963).

The space truss structure of the reflector is supported at about two-thirds of the radius by two towers (Fig. 3.21). A central wheel enables the movement in declination driven by a pinion-chain gear. Two legs in the meridian plane held in place sideways by tension cables position the prime focus feed. The surface of panels of aluminium mesh was placed on the structure by adjustable spacer rods. Through a trench in the ground on the southern side, the elevation coverage was increased by about 5°.

Fig. 3.21 The original NRAO 300-ft transit telescope. The reflector structure is supported by two towers. The elevation drive is realised through a centre wheel with pinion and chain (J. Baars, NRAO/AUI/NSF)

There is an aspect to the operation of this telescope that is worthwhile to mention. Because the structure was designed to be as light as possible with a rather short planned lifetime of 5 years, it could not possibly survive the regular heavy snowfall during the Green Bank winter. The solution was found in the acquisition of a surplus air force jet engine that in times of snow blew its warm exhaust through the antenna mesh and avoided ice and snow buildup. The roar of the engine could be heard throughout the entire Deer Creek Valley!

From the start, the telescope was intensively used. Tests at 10 cm wavelength in late 1963 (in which one of us (JB) participated) showed the feasibility of high-frequency observations. Around 1970, an improved surface was installed and a "travelling feed" enabled tracking an object for about 5 min. Sky surveys were carried out to a highest frequency of 5 GHz.

After a highly productive life of 26 years, material fatigue in an essential gusset plate caused the telescope to collapse on the evening of 15 November 1988 (Fig. 3.22). Its loss opened the way for the 100-m GBT (Green Bank Telescope) to be described in Chap. 7.

3.2.6   *The 120-ft* **Haystack Antenna** *of MIT Lincoln Laboratory*

In the period 1960–1964, approximately parallel in time with the NRAO 140-ft, Lincoln Laboratory of MIT carried out a project of a radome-enclosed, high accuracy antenna of 120-ft (36.6 m) diameter for the US Air Force. It was envisaged as an advance in the development of high-frequency antenna systems. The resulting design of the antenna contains several original ideas that are worthwhile to shortly mention here.

The Haystack radio telescope is a fully steerable parabolic antenna, enclosed in a large space-frame radome. The radome is 46 m in diameter, and its 932 triangular membranes are made of 0.6-mm thick Tedlar-coated Dacron cloth manufactured by ESSCO of Concord, Massachusetts. The antenna is located at the Westford Site of MIT Lincoln Laboratory in Massachusetts, USA.

The telescope has a Cassegrain configuration with a planned maximum operational frequency of 8 GHz. The original major purpose was for planetary radar. The choice of a radome was made to assure continuous, weather-independent operation of the antenna. This removed the need to design the telescope to survive extreme weather conditions. Thus, the specifications could be limited to those required by the scientific operation. The major specifications were a reflector surface rms error of 0.8 mm and a pointing precision of 18 arcsec.

Astronomers did not influence the telescope layout, and, contrary to the case of the NRAO 140-ft telescope, an elevation–azimuth mount was selected from the outset. The designers embraced the latest advances in computers and software, in particular the use of finite element analysis with STAIR and FRAN. They also

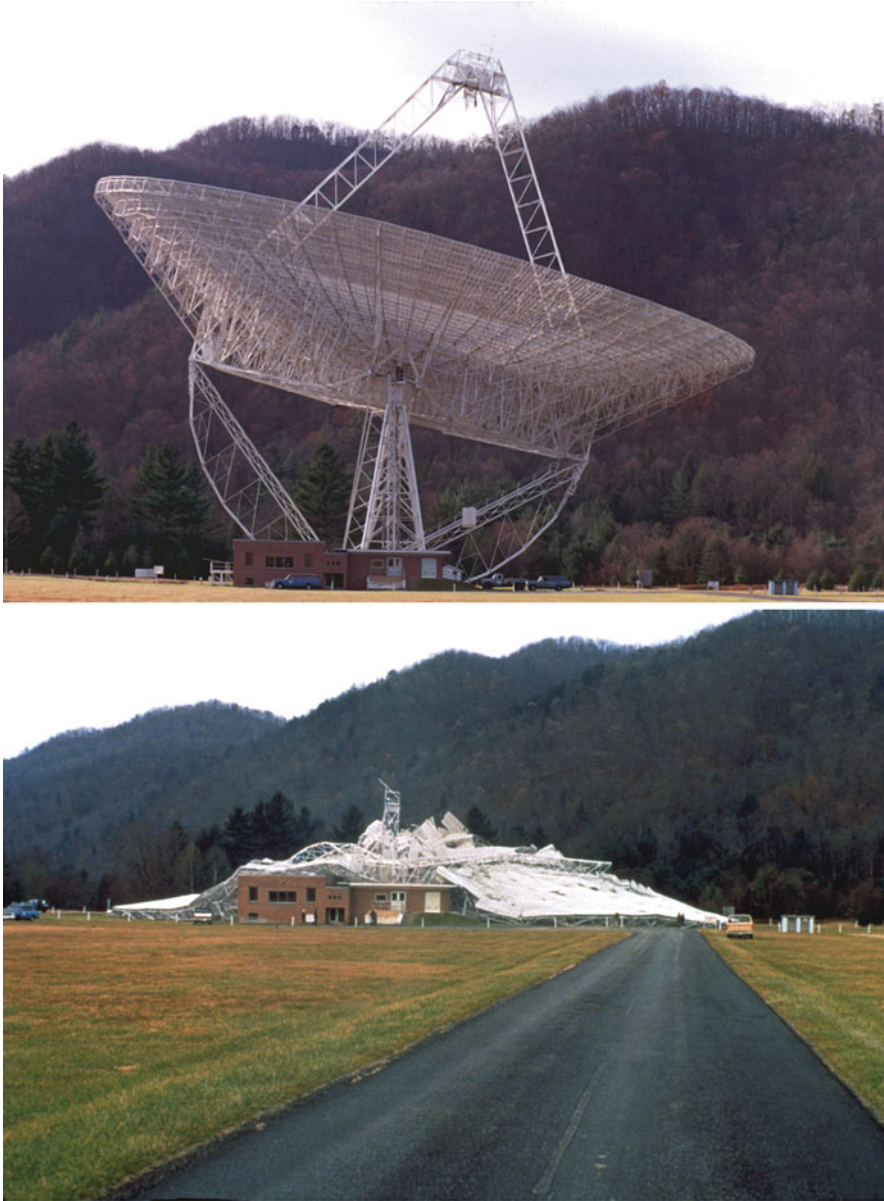**Fig. 3.22** *Top* the 300-ft at NRAO on 14 Nov 1988. *Bottom* the remains after its collapse on 15 November 1988 (Richard Porcas, MPIfR and NRAO/AUI/NSF)

incorporated some control features in the antenna beyond the basic axis movement (Fanning 1966).

The radome prevents one to make a picture of the antenna. In Fig. 3.23, we show a computer rendering of the facility with a "cut-away" to offer a glance in the
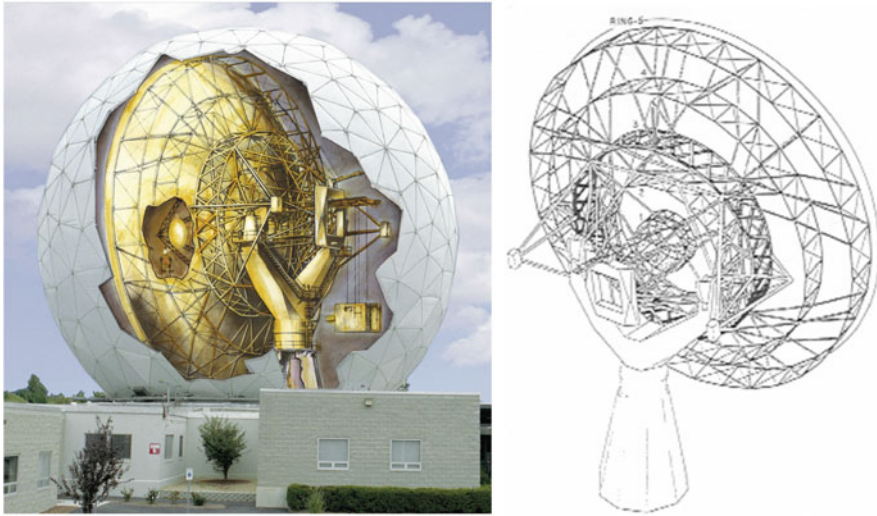
Fig. 3.23 The Haystack radome-enclosed antenna of MIT Lincoln Laboratory in Westford, Massachusetts. (Courtesy Haystack Observatory) "Cut-away" view of the installation (*left*) and basic structural layout (*right*) (from Ingals et al. 1994)

interior of the radome and also a drawing of the basic structural layout of the antenna. A central concrete tower supports the antenna through a hydrostatic azimuth bearing of 1.8 m diameter. The yoke structure for the support of the elevation bearings is made of steel. The reflector and its support structure to the elevation bearings are realised in aluminium. The elevation bearings are of the standard roller type. From there, planar trusses create a "four-point" support for the reflector backup structure. This structure consists of five stiff ring trusses (Fig. 3.23, right) connected to each other by pre-tensioned radial thin rods of 10–25 mm diameter. This concept is very different from the usual stiff radial beams and thinner circumferential connections.

The backup structure is connected to the four-point support at the third ring. As we will show in the next chapter, this is advantageous in view of the gravitational deflections with varying elevation angle. The quadripod for the support of the subreflector is also attached at these four points, thereby remaining completely free of the reflector support. A system of three cables attached to ring 4 of the backup structure together with some pendulum counterweights enable a partial correction of the gravity-induced large-scale deformations as function of elevation. This ingenious method is a first example of *active control* of deformations in a radio telescope.

The reflector surface is made of 96 sandwich panels of aluminium that are preloaded to act as a shell, thereby adding stiffness to the overall structure. The results of the finite element calculations were applied to "bias rig" the setting of the surface in the zenith position in order to provide the most precise surface at intermediate elevation angles, where the bulk of observations are made.

The original performance of the antenna is summarised by Weiss (1966). Over the years, many improvements were carried out and the antenna can be operated with acceptable performance at 3 mm wavelength, more than an order of magnitude smaller than the original specification (Ingalls et al. 1994).

3.3   Conclusion

We conclude here our general description of the first generation of large parabolic radio telescopes. By the mid-1960s, the emphasis of radio astronomy shifted to interferometric arrays, so-called *synthesis telescopes*, to obtain maps of source brightness distribution with high angular resolution. After the discovery in 1969 of carbon monoxide (CO) in the Galaxy by its spectral line at 2.6 mm wavelength, interest towards higher frequencies into the short millimetre wavelength region increased considerably. Concurrently, some new and highly original structural design and fabrication methods were developed that led to the construction of large and simultaneously highly accurate reflector telescopes. These design methods and their application are the subject of the following few chapters.

References

Bolton, J.G.: Radio astronomy with Australian 210-foot telescope. Proc. IEEE. **51**, 1464–1470 (1963)

Bowen, E.G., Minnett, H.C.: The Australian 210-ft radio telescope. J. Br. IRE. **23**, 49–53 (1962)

Christiansen, W.N., Hindman, J.V.: A preliminary survey of 1420 Mc/s line emission from galactic hydrogen. Aust. J. Sci. Res. **A5**, 437–455 (1952)

Ewen, H.I., Purcell, E.M.: Radiation from galactic hydrogen at 1420 Mc/s. Nature. **168**, 356 (1951)

Fanning, W.R.: Mechanical design of the Haystack antenna. Design and construction of large steerable aerials. IEE Conf. Publ. **21**, 100–104 (1966)

Findlay, J.W.: The 300-foot radio telescope at Green Bank. Sky Telescope. **25**, 68 (1963)

Ingalls, R.P., et al.: Upgrading the Haystack radio telescope for operation at 115 GHz. Proc. IEEE. **82**, 742–755 (1994)

Jansky, K.G.: Eletrical disturbances apparently of extraterrestrial origin. Proc. IRE. **21**, 1387–1398 (1933)

Kiepenheuer, K.O.: Cosmic rays as the source of general galactic radio emission. Phys. Rev. **79**, 738–739 (1950)

Lockman, F.J., Ghigo, F.D., Balse, D.S.: But it was fun – the first forty years of radio astronomy at Green Bank. NRAO, Green Bank (2007)

Lovell, A.C.B.: The Jodrell Bank radio telescope. Nature. **180**, 60–62 (1957)

Lovell, B.: The Jodrell Bank telescopes. Oxford University Press, New York (1985)

Lovell, B., Husband, H.C.: Blue Book (1951). Downloadable from Jodrell Bank Observatory site: http://www.jb.man.ac.uk/aboutus/lovell/bluebook/

Muller, C.A., Oort, J.H.: The interstellar hydrogen line at 1420 Mc/s and an estimate of galactic rotation. Nature. **168**, 357–358 (1951)

Pederzoni, T.: Radiosternwarte Stockert. Telefunken Zeitung. **29**(113), 157–181 (1956)

Reber, G.: Cosmic static. Proc. IRE. **28**, 68–70 (1940a)

Reber, G.: Cosmic static. Astrophys. J. **91**, 621–624 (1940b)

Robinson, P.: An Australian icon – planning and construction of the Parkes telescope. Science with Parkes @ 50 years young (2011)

Shklovski, I.S.: On the nature of the radio radiation of the Galaxy. Astron. Zh. (Russ). **29**, 418–449 (1952)

Small, M.M.: The new 140-foot radio telescope. Sky Telescope. **30**, 267 (1965)

van de Hulst, H.C.: Radiogolven uit het wereldruim. Nederlands Tijdschrift voor Natuurkunde. **11**, 210–221 (1945)

van de Hulst, H.C., et al.: De radiosterrenwacht te Dwingeloo. de Ingenieur. **69**(3), 1–20 (1957)

von Hoerner, S., Wong, W.-Y.: Gravitational deformation and astigmatism of tiltable radio telescopes. IEEE Trans. Antennas Propag. **AP-23**, 689–695 (1975)

Weiss, H.G.: Performance measurements on the Haystack antenna. Design and construction of large steerable aerials. IEE Conf. Publ. **21**, 95–99 (1966)

Chapter 4
Structural Design of Reflector Antennas: Homology
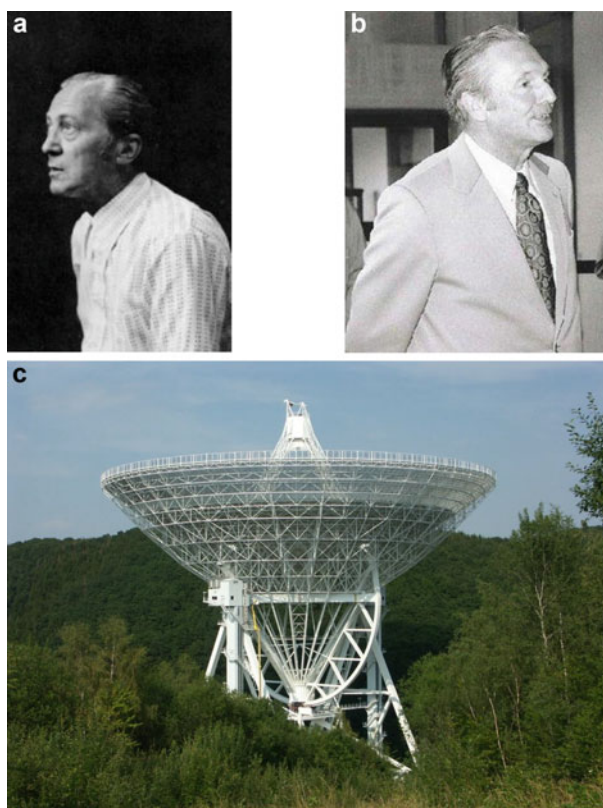
(**a**) Sebastian von Hoerner Theory of Homology (**b**) Otto Hachenberg Practice of Homology (**c**) The 100-m Radio Telescope at Effelsberg, Germany (Courtesy, NRAO and MPIfR)

4.1   Introduction

The two large telescopes built in the 1950s at Jodrell Bank and Parkes were pioneering pieces of technology. Astronomers developed the ideas for the telescopes and industrial engineers and companies executed the design and erection. For the engineers the task was new, not comparable to their work on bridges or aircraft structures. They worked in the pre-computer era in an experimental way with the limited analysis tools for structural mechanics as graphical statics and slide-rule computation. The performance of the telescope was adequate for the observation of long wavelengths (metres to decimetres), and the deformation behaviour of the telescope structure was of limited importance.

While the large reflectors in Jodrell Bank and Parkes were predominantly aiming at an increase in sensitivity, the NRAO 140-ft was designed to extend observations to the short wavelength of 3 cm. Working at shorter wavelengths improves the angular resolution proportional to the wavelength, but it requires an increased precision of the reflector under operating conditions. In the centimetre- and millimetre-wavelength regime, the required reflector precision reaches the magnitude of the natural structural deformations or beyond. As noted earlier, this became obvious in the operation of the 140-ft telescope by the large gravitational deformations as function of the attitude angle of the reflector and by temperature variations in the structure.

Clearly, improvements in the structural design methods would be needed for the realisation of large and highly accurate reflectors. Fortunately by the mid-1960s, *finite element analysis* and computing power had advanced to a level, where iterative, computer-supported design optimisation methods became possible. In addition, a completely new approach to the gravitational deformation problem was introduced, the *principle of homologous deformation*. In this chapter, we present a non-mathematical explanation of this principle. It was applied in the design of the Effelsberg Radio Telescope. With its diameter of 100 m and short-wavelength limit of 7 mm, a new era of radio astronomy was started. The description of this instrument forms the main part of this chapter. We also discuss less rigorous applications of the homology idea in the form of the *four-point support*.

4.2   The Design of Homologous Structures

In 1962, Sebastian von Hoerner (1919–2003), a German theoretical astrophysicist and cosmologist, joined NRAO in Green Bank, where ideas for a very large telescope were regularly discussed. Von Hoerner presented a plan for a giant telescope of 200 m diameter, operating at relatively long wavelengths for the observation of occultations of extragalactic sources by the Moon. This technique, known from optical astronomy, enables the very precise measurement of the source's celestial position by the timing of the occultation and is not sensitive to

the telescope beamwidth or precise pointing direction. Being ignorant of structural mechanics, von Hoerner attacked the problem of designing the cheapest possible large telescope from first principles. This led to his theory of *homologous deformation*, which we will summarise now. This theory shows that, for a given amount of material, a homologous designed telescope would work to at least an order of magnitude shorter wavelength than with a structure based on a classical, stiff design.

Von Hoerner introduced his homology ideas in *Design of Large Steerable Antennas*, a paper published in the Astronomical Journal (von Hoerner 1967a). This paper gives inspirational insights into the lucidity of his thinking. He completed his theory to a level, where practising engineers could apply it (von Hoerner 1967b and NRAO/LFST reports).

He based his investigation on an octahedron, which he used as engineering model for hand calculations of design limits (Fig. 4.1). The use of the octahedron as representation of an antenna seems daring, and an engineer would probably never come up with such an ingenious idea. It is the first time that the octahedron occurs in telescope design, and it inspired the elevation cradle of the Effelsberg telescope, which was designed around that time.

First von Hoerner derived *three basic natural limits* to the size of a structure with a specified geometrical precision, for instance a reflector. The *gravitational limit* is unavoidable. The deformation of a structural member under gravity is proportional to the product of its length and mass, divided by the stiffness. Under the reasonable assumption that the cross section, that is, the mass per unit length, is proportional to the length, we obtain the following expression for the gravitational deformation:

$$\delta_g \propto \left(\frac{\rho}{E}\right)D^2, \tag{4.1}$$

where ρ is the density and E the modulus of elasticity of the material, while D is the reflector diameter. If we define the shortest operational wavelength as 16 times the rms reflector deformation (see Chap. 8), we find

$$\lambda_g \approx 70\left(\frac{D}{100}\right)^2, \tag{4.2}$$

with λ in millimetres and D in metres.

Fig. 4.1 *Left* Octahedron diagonals. *Right* Deflections (cm) in the horizontal plane of an octahedron of 100 m diameter, as seen from the top of the octahedron (von Hoerner, in Astron. J., 1967)
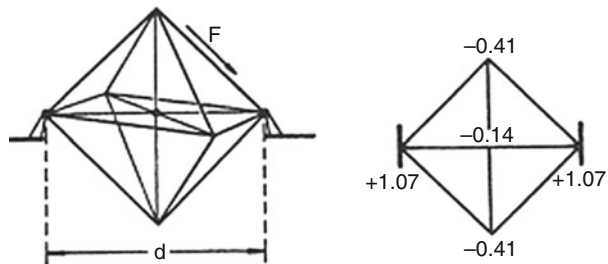
The thermal deformation is proportional to the length of the structural member and the temperature variation:

$$\delta_T \propto C_T \cdot D \cdot \Delta T, \tag{4.3}$$

where C_T is the coefficient of thermal expansion and ΔT the temperature difference with respect to the surrounding. Under similar assumptions as above, we find for steel the *thermal limit* at the minimum wavelength

$$\lambda_T \approx 6\left(\frac{D}{100}\right) \cdot \Delta T, \tag{4.4}$$

with ΔT in Kelvin, D in metres and λ_T in millimetres. For aluminium, the value is twice as large.

So, if we build a 100-m telescope of a design based on stiffness and made of steel, our smallest useful wavelength will be about 7 cm. With a typical temperature gradient of 5 Kelvin, the thermal limit is 3 cm, hence not critical. On the other hand, a 20-m reflector will be limited to a shortest wavelength of 6 mm by thermal effects, while gravity would allow operation down to 3 mm.

A third natural limit is the *stress limit*, where the structure collapses under its own weight. For steel, this is about 600 m, practically beyond the financial means of an observatory.

Von Hoerner plotted the natural limit relations in a diagram of diameter against shortest wavelength, together with the data of existing radio telescopes (Fig. 4.2). The "classical" designs all lie under the gravitational limit. The millimetre-

Fig. 4.2 Three natural limits for conventional tiltable telescopes. Existing telescopes are indicated for comparison. Note: No.1 is in a dome (von Hoerner, in Astron. J., 1967)
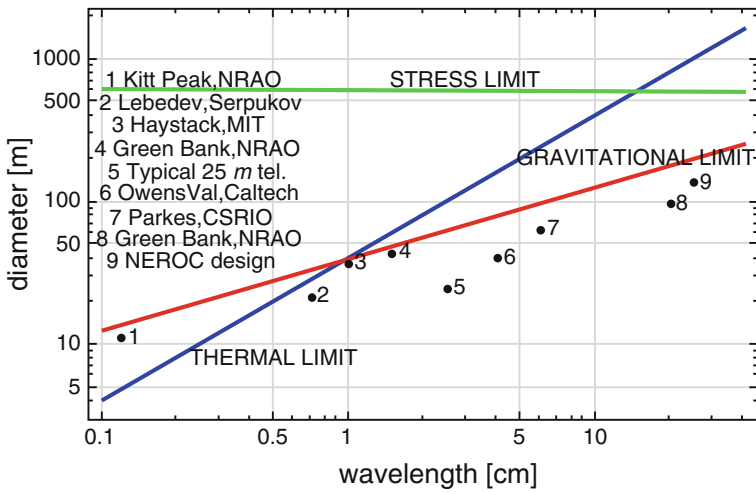
wavelength telescope (No. 1) will be limited to a shortest wavelength of 3 mm due to thermal effects.

The diagram is based on absolute deformations when tilting the octahedron antenna from zenith to horizon without any best-fitting. In the second half of his paper, von Hoerner discusses how to *pass the gravitational limit*. He introduces four possible strategies, which have not lost their validity:

1. *Avoid the deformations by not moving in elevation angle.*
   This design strategy was used in the early days of radio astronomy by the hole-in-the-ground parabolic dishes at Jodrell Bank, UK (1952), and Dover Heights, Sidney (1953). The prominent example is the 300-m Arecibo telescope (1963). A modern version is the 500-m FAST telescope in Guizhou, China, completed in September 2016 by NAOC of Beijing, China (Chap. 7).
2. *Fight the deformations with strong motors in the structure.*
   Von Hoerner mentions the Sugar Grove reflector with a diameter of 600 ft. Its construction was terminated in 1959 due to management and engineering problems after several thousand tons of steel were delivered to the site. Von Hoerner qualifies the method as too complicated and expensive. The recently developed methods of Active Optics, discussed later in this book, could also be ranked under this category. Instead of strong motors in the structure, small motors on the structure are used that actively control the position of the reflector surface panels. However, this is also complicated and expensive as correctly pointed out by von Hoerner.
3. *Cancel the deformations with levers and counterweights.*
   This is the method used for the isostatic support of optical mirrors. Von Hoerner is aware of this and correctly mentions two drawbacks that are not acceptable in most radio telescopes: too much weight is added and the structure becomes soft against wind deformations. These drawbacks are also applicable to the big active mirrors of modern very large optical telescopes. The Haystack antenna (Chap. 3) applies a simple form of this correction.
4. *Allow deformations that do not hurt the performance.*
   This is von Hoerner's preferred approach, which he calls homology. In analogy to the isostatic supports of the optical mirrors, he could have called it also iso-deflective support principle. *Homology*, defined as a classification of figures with certain topological properties, is an apt name and the community of radio telescope engineers has accepted it. Not all are aware of the analogy to the isostatic principle used for optical mirrors.

In the second part of the paper, Von Hoerner describes his approach to homology with a goal of achieving realistic and practical design rules. First, he defines the basic homology principle; in his own words: "*The laws of physics tell us that a structure, under the influence of gravitation, deforms in a state of minimum energy; the centre of gravity must move down. The material constants ρ and E tell us the amount by which it must move down. But there is no law of nature telling us that a parabolic surface must deform into something different from a parabolic surface.*

We thus look for a structure which deforms down whatever it must, but still gives a perfect paraboloid of revolution for any elevation angle".

Second, he explains the principle of equal softness by a now famous sketch (Fig. 4.3), where the print-through of the two lower supports on the deflection of the upper truss structure is eliminated by the addition of two "mattress" layers.

Third, he shows the existence of exact solutions for the problem of homologous deformations in the mathematical sense. An engineer would not approach his tasks in this way, but would try to find solutions empirically not caring about existence of an exact solution. Figure 4.4 shows the two-dimensional model that von Hoerner used for the proof of existence. Seeing its complexity, the engineer's first reaction might be to wonder whether this method may lead to the best practical design. We will not elaborate this point and leave it to the reader to reach an understanding.

Von Hoerner's complete description of the homology mathematics is presented in a second paper (von Hoerner 1967b). He developed an algorithm with which he could optimise, that is, homologise, a realistic three-dimensional telescope structure with available computer power. However, he did not rely on existing external software sources. In the 1960s, the first commercial finite element analysis (FEA) programs were available. These were used in a trial and error manner, for instance in the design of the large German telescope to be described below. He was aware of the FEA software but preferred his rigorous mathematical method for obtaining exact solutions. So he wrote his own FEA program with an integrated homology optimisation algorithm.

Based on the calculation power of contemporary computers, he restricted his FEA algorithm to space truss-type structures with only strut-type structural

Fig. 4.3 Elucidating equal softness (von Hoerner, in Astron. J., 1967). (**a**) Conventional design with hard (h) and soft (s) surface points. (**b**) Deformation of surface in zenith position. (**c**) Structure where all surface points have equal softness
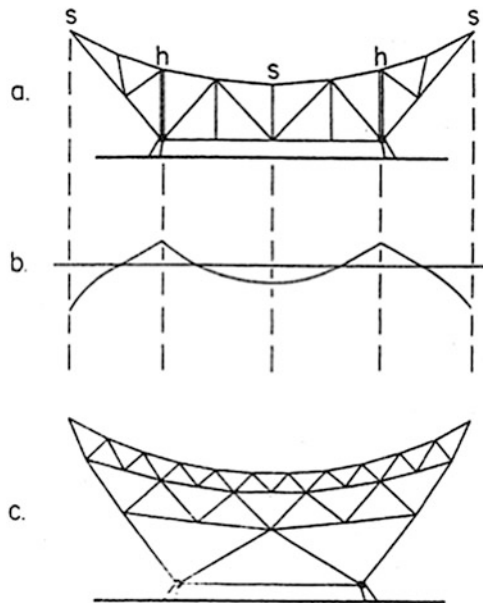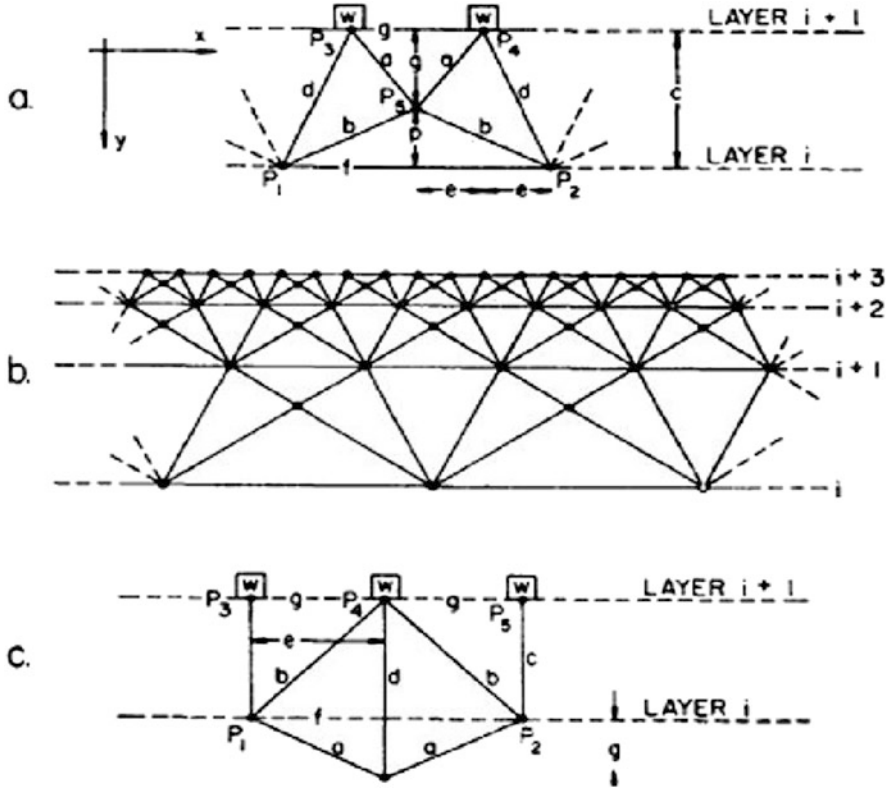
Fig. 4.4 Two types of cells, where layer $i + 1$ is parallel to layer i for any elevation. (**a**) Most simple type, general solution. (**b**) Particular solution ($c = 2e = 3q$) of same type, three layers. (**c**) Pressure-stable cell, which keeps height constant if P_1P_2 is compressed (von Hoerner, in Astron. J., 1967)

members, fixed geometry and topology, leaving the cross sections of the struts as optimisation parameter. Again he showed the existence of an exact solution for the three-dimensional systems by comparing the number of free optimisation parameters (cross sections of the struts) with the number of physical conditions (elasticity equations described by the stiffness matrix). His homology optimiser was based on the partial derivatives of the stiffness matrix elements with respect to the cross sections of the struts. The equation system was very large, of the order of the number of node deflections plus cross sections. Thus, he was restricted in flexibility by the memory capacity of the computer.

In Green Bank, John Findlay, on the basis of his experiences with the construction of the NRAO telescopes, increased the capabilities of NRAO's structural design group with the goal to turn von Hoerner's theoretical homology solutions into practically realisable structures. He embraced the new tools of FEA algorithms. A young engineer, Woon-Yin Wong, well versed in these new methods, joined the

group around von Hoerner and Findlay. Colleagues of the engineering department of the University of Virginia also participated. Several design studies were made, in particular for a large millimetre-wavelength telescope of 65 m diameter.

4.3 The Design of a 65-m Homologous mm Telescope

Von Hoerner and his colleagues applied the theory to numerical trials for some simple structures. Originally, memory capacity limited the calculation power to 100 structural members. Therefore, they started with a very simple model (Fig. 4.5, left) with a hexagonal net representing the reflector shell, two "anchor" points and upper and lower guying. Optimisation criteria were the homology of the "surface points" of the hexagonal network in horizontal and zenith position. This worked perfectly and the team was excited. They were, however, aware that the example was too simple to represent a real telescope, and so they made their model more sophisticated, still under the restrictions of the memory capabilities of their computer, and after some further steps they achieved the structure in the middle of Fig. 4.5, which has a first resemblance of a telescope. The final result was the structure on the right in Fig. 4.5, which shows the major structural subsystems characteristic of a complete Elevation Rotating Structure (ERS) consisting of:
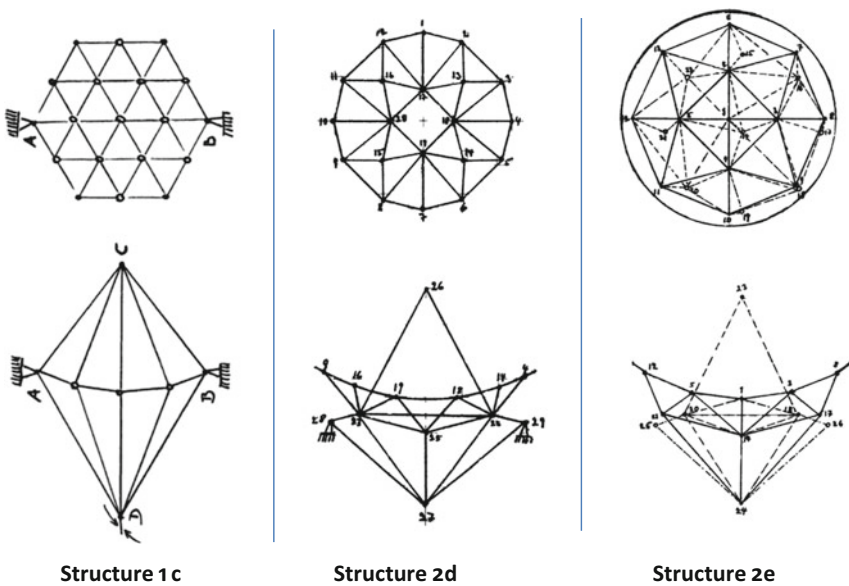

Fig. 4.5 The evolution of the homologous design of a 65-m telescope (NRAO Report, 1972)

1. The reflector Backup Structure (BUS)
2. The Cradle (CD)
3. The Reflector Surface (RS)

Let us look in more detail into the essence of homologous telescope design. We need to understand not only the geometrical issues of the design but also the deformation issues, which inevitably includes the understanding of the forces that cause the deformations.

Currently, highly sophisticated computer-aided tools are available: the modern Computer-Aided Design (CAD) tools for the geometrical issues and the related FEA programs for the force and deformation aspects. These tools are ideal for analysis, but they don't help at the beginning of the design process. Particularly in the early conceptual phase, it is necessary to understand the basic mechanics of deformable bodies. For instance, one has to know the difference between longitudinal deformation and bending, or between a latticed truss and a framework. One starts the design process by making some hand calculations.

In Fig. 4.5, the BUS is a space truss system, which carries on top the reflector surface (RS), indicated only in the upper sketch on the right by the surrounding curved line. The cradle (CD) is indicated in the lower sketch by dashed lines. It consists of the octahedron existing in the design concept from the start and an inverted umbrella cone (see also Fig. 4.6). The CD penetrates the BUS structure freely, the only connection being at dedicated interface points between the umbrella cone and the rear of the BUS.

The octahedron/umbrella cone design concept is a very basic result of von Hoerner's theoretical efforts. It was used for the design study of a 65-m telescope, and we find it also in a modified form in the final design of the 100-m Effelsberg telescope. In the "flat" outline drawings (Fig. 4.6) of the study report for the 65-m
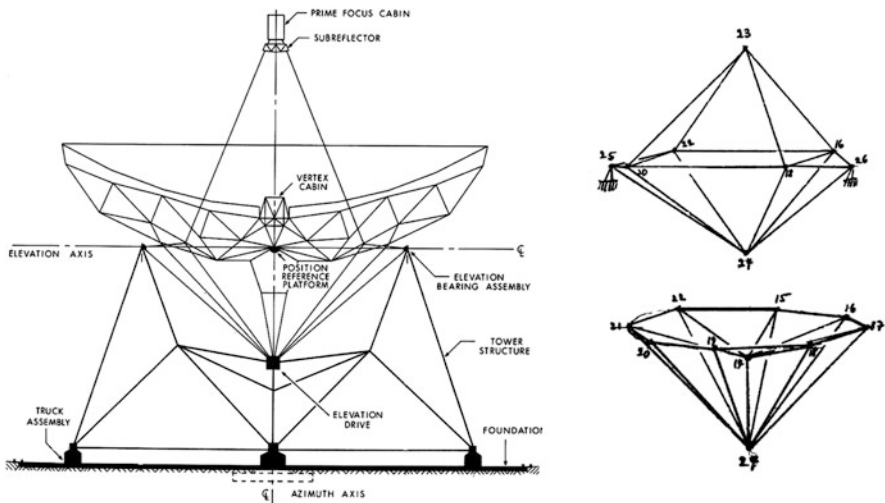
Fig. 4.6 The 65-m millimetre telescope design (NRAO Report, 1972)

telescope (Findlay and von Hoerner 1972), the umbrella cone and octahedron are difficult to identify, but the isometric sketches on the left help to imagine them in the drawing; clearly visible is the separation of the elevation bearings from the BUS structure. Later NRAO designed a 25-m diameter telescope for short millimetre wavelengths. The drawing of this antenna in Fig. 4.7 gives a good impression of the application of the homology principles.

The work by von Hoerner and his colleagues demonstrated the potential of the homologous design procedures. It enabled the achievement of superior telescope performance with a significantly lighter and consequently cheaper structure. Unfortunately, NRAO could not realise the promising 25-m millimetre telescope concurrently with the Very Large Array that was constructed in the decade 1970–1980. The homology ideas were however incorporated in the design development of the 100-m Effelsberg telescope in Germany. We turn now to a description of this instrument.
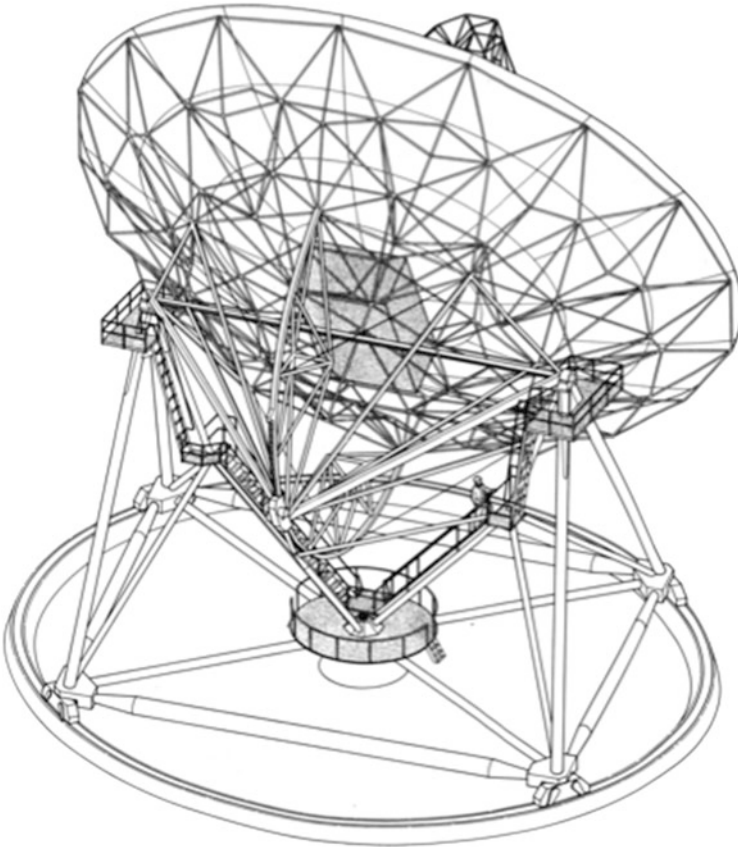
Fig. 4.7 Drawing of the NRAO design for a 25-m telescope for short mm wavelengths (NRAO Report, 1977)

4.4   The Effelsberg 100-m Radio Telescope

4.4.1   The German Proposal for a Giant Radio Telescope

In Germany, after the erection of the Berlin Wall, Otto Hachenberg (1911–2001) transferred in 1962 from the Heinrich-Hertz-Institut in East Berlin to the University of Bonn. He had been director of the institute since 1951 and had built a 36-m diameter transit telescope for solar observations. In 1963, he and his colleagues Wolfgang Priester and Friedrich Becker at the Astronomical Institute presented a proposal for a 60–80-m diameter radio telescope to the State of Nordrhein-Westfalen (NRW) government. A year later, they applied to the Stiftung Volkswagenwerk (VW-Foundation) for a grant to finance an 80-m telescope. First design studies for an 80-m telescope were made by the companies Fried. Krupp and MAN. The Radio Astronomy Institute at the university lacked structural design capacity.

There followed a rather confusing period in the development of radio astronomy in Germany. Around the time the request from Bonn University for funding arrived at the VWF, another proposal was received from Sebastian von Hoerner on behalf of the University of Tübingen for the funding of a 160-m telescope for lunar occultations. This occurred in the context of a professor appointment at Tübingen for von Hoerner. The VWF signalled a willingness to fund both projects, each with 18 million DM, provided that the institutes could convincingly demonstrate to be able to finance the operation and further development of the telescopes. Neither university could fulfil this requirement. Now the Max-Planck-Society (MPG) resolved to establish a *Max-Planck-Institut für Radioastronomie* (MPIfR) with both telescopes and Hachenberg and von Hoerner as directors. Agreement on the location of the MPIfR could not be reached. Von Hoerner insisted on the neighbourhood of Tübingen for his long-wavelength telescope that would be very sensitive to man-made interference. This would supposedly be less serious in the thinly populated Schwarzwald than in the industrialised surroundings of Bonn. Hachenberg, with support from the government of Nordrhein-Westfalen, argued for Bonn. Eventually, von Hoerner declined his appointment to Tübingen and withdrew his proposal to the VWF. In 1966, the MPG confirmed the establishment of the MPIfR in Bonn, appointed Hachenberg as its first director and announced the appointment of a second director in due time. The VWF accepted the MPG decision and made the full sum of 36 MDM available for a large telescope. By that time, the goal for the diameter had grown to 90 m. During the conceptual design it became apparent, not least through the application of the new homology principles, developed by von Hoerner, that a 100-m telescope capable of operation at 3 cm wavelength would be feasible for the available funds.

Hachenberg's design strategy was different from von Hoerner's. He did not focus on one idea such as von Hoerner's homology principle, but looked first at what others had done. The 1964 proposal for an 80-m telescope to the Volkswagen Foundation included budgetary estimates. They were based on design sketches that were obviously derived from previous telescope designs: the Stockert telescope near Bonn and the Lovell telescope at Jodrell Bank. The Stockert concept (Fig. 4.8,
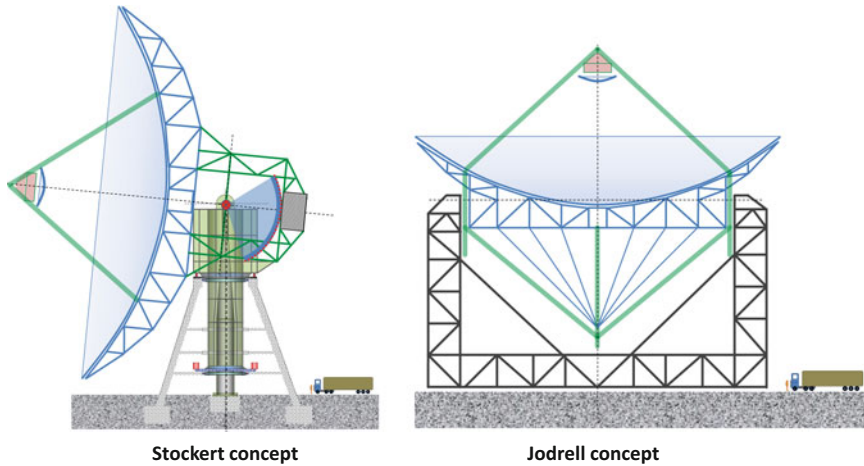
Fig. 4.8 Our rendering of the original sketches for an 80-m radio telescope from Krupp and MAN: *left* Stockert and *right* Jodrell concept

left) shows the king-post on a conical tower, with a separate internal column for the independent support of a master equatorial as in Parkes. The Lovell concept (Fig 4.8, right) shows the characteristic wide support of the reflector backup structure, the "bicycle wheel" and an alidade with two towers on both sides of the reflector. The drawings probably formed the basis for weight and cost estimates; the latter was 18 million DM.

After the VWF agreed in principle to finance a large telescope, the Astronomical Institute of the University of Bonn contracted in 1965 under Hachenberg's direction competing design studies at the two most renowned steel construction companies in Germany, "Krupp Stahlbau" in Rheinhausen and "MAN" in Gustavsburg near Mainz. Their main fields of activity were steel bridges and hydraulic structures. MAN had gained experience in the construction of the Parkes telescope, which however was designed by others.

Hachenberg did not dictate a design concept but encouraged the engineers to develop new concepts. The basis of the study was what is known as a performance specification, not a design specification. A performance specification describes only the functionally and scientifically necessary requirements. It avoids the prescription of items not related to functionality or performance.

For the definition of the performance requirements, Hachenberg formulated his own version of the homology principle. He was aware that the absolute deformations of such big structures would be far above the required accuracy of the reflector surface. Thus, he formulated the performance request as a best-fitting process: the deviations of the reflector surface against a best-fitted paraboloid should be in the range as required by the shortest operational wavelength. It was allowed that the best-fitted paraboloid changes its position and even its focal length. It was also allowed that the individual reflector areas could deviate from the fitted shape but within the limits dictated by the shortest operational wavelengths. This is essentially the definition of a homologous structure. Von Hoerner had a different

strategy, as we have seen. In the real world, both approaches achieve similar results, because material and geometrical tolerances are unavoidable in both. Hachenberg's approach conforms more to the thinking of engineers than von Hoerner's, because it takes these tolerances into account in the design process. However, von Hoerner included in his theory and algorithms the concept of *deviation from pure homology* as caused by, for instance, the choice of standard member dimensions and imperfections in the geometry and stiffness of the nodes. In practice, this means that perfect homology will not be achieved and both gentlemen were well aware of this.

4.4.2   A Comment on the Homologous Behaviour of a Structure

The homologous design of the NRAO 65-m telescope was never realised in hardware. As we indicated in the previous paragraph, the approach for the design of the German large telescope applied the principles of homology without using the mathematical apparatus established by von Hoerner. In this context, it is interesting to note that, once the principles of homology became known among telescope designers and operators, a certain *homologous behaviour* could be discerned in some existing telescopes. Probably, the earliest awareness of this occurred during the testing of the NRAO 85-ft telescope at the very short wavelength of 2 cm by Mezger and one of us (JB) in 1964. We found a significant change in focal length as function of elevation angle and by refocusing the efficiency of the telescope could be optimised. This is one clear aspect of homologous behaviour and von Hoerner was pleased with this observation. The same phenomenon was measured on the Parkes and other telescopes enabling the instrument to be effectively used at shorter wavelengths than originally envisaged by the simple act of refocusing. This shows that a well-designed truss-frame structure can exhibit a deformation behaviour mimicking homology. Most telescopes have been designed without homology principles in mind, but many behave partially homologously, a welcome surprise to the users.

4.4.3   The Industrial Design Proposals

The two industrial studies resulted in very different design concepts, both fulfilling and even exceeding the requested performance. A comparison of the two concepts gives us insight into the principal courses of a design process.

The MAN study (led by Winfried Schönbach) resulted in a so-called four-point design concept, where the elevation cradle—the interface structure connecting the

reflector shell with the elevation bearings—is reduced to two elevation wheels. They contain also the counterweights needed for balancing the weight of the reflector shell. The reflector bowl is supported only on the four corners of these elevation wheels. These four corners carry the quadripod for the secondary reflector (Fig. 4.9). MAN had used this design concept for 25-m class antennas for communication. It was also applied in the Westerbork Synthesis Radio Telescope in the Netherlands. Later, it was used with some variations and improvements in a number of 30–50 m telescopes, for instance the 30-m MRT Spain, the 40-m IGN Yebes and the 50-m LMT Mexico. We discuss these later in this chapter.

The four support points cause large-scale deviations in the reflector surface that we discuss in detail later. The remaining overall surface error of about 0.6 mm rms is within the limits of the specification. The maximum deviations at the edge of the reflector are only about 3 mm relative to the best-fit paraboloid! The absolute deformations are much larger, in the range of several centimetres.

The Krupp study (led by Helmut Altmann) resulted in a rather different design concept with similarities to von Hoerner's proposal. It shows an umbrella cone and an octahedron as described in von Hoerner's LFST reports of 1965–1966. Von Hoerner mentions in these reports his contacts with the people in Bonn and one can assume that the design group at Krupp knew his reports. There are some differences between von Hoerner's octahedron and Altmann's "Tragkorb" (support basket, the yellow structure in Fig. 4.10, left). In von Hoerner's design (Fig. 4.6), the octahedron legs are arranged in the 45° planes, and the backup structure is connected to the four points of the octahedron similar to the four points of the MAN design. In
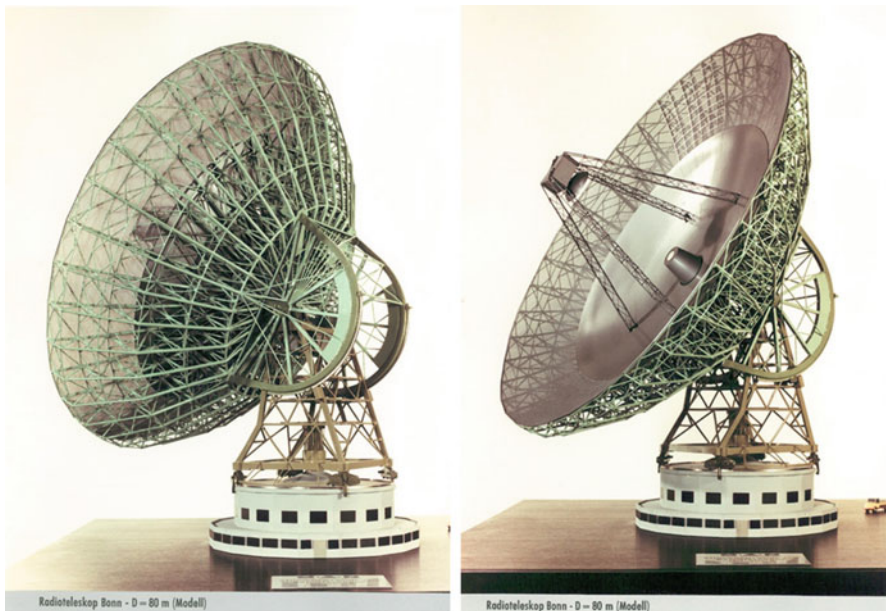

Fig. 4.9 A model of the MAN design concept for an 80-m telescope with four-point reflector support (MAN)

the Krupp design, the octahedron is rotated by $45°$. One of the diagonals is parallel to the elevation axis (the first model shows only a rudimentary octahedron with one of the legs cut away, and the final design shows the full one), and the backup structure is not directly connected to the four points, but only to two points in the centre and the rear of the umbrella cone. By this construction, the print-through of the four points is avoided, and the weight of the reflector bowl is transferred in zenith position almost perfectly by the final 48 umbrella struts (right figure; the left figure has only 12 umbrella struts) to the rear tip of the Tragkorb, the octahedron.

The Krupp design leads to a strong coma-type deviation in horizon position. This is caused by the push–pull forces balancing the weight of the reflector, which is the sacrifice of the two-point central support concept similar to the print-through areas of the MAN four-point support in the zenith. The remaining overall surface error of the Krupp design is 0.6 mm rms, equal to the MAN design.

Hachenberg was extremely pleased by the outcome of the studies and the cost estimates allowed him to change the plans to a 90-m or 100-m telescope. Both companies amended their studies accordingly. In these amendments, Krupp stayed with its design concept and just scaled up the size, whereas MAN changed to an umbrella cone system, probably on the basis of its superior performance.

Fig. 4.10 Models of the Krupp design for an 80-m telescope with separate elevation cradle. First proposal on the *left* and final design on the *right* (Krupp)
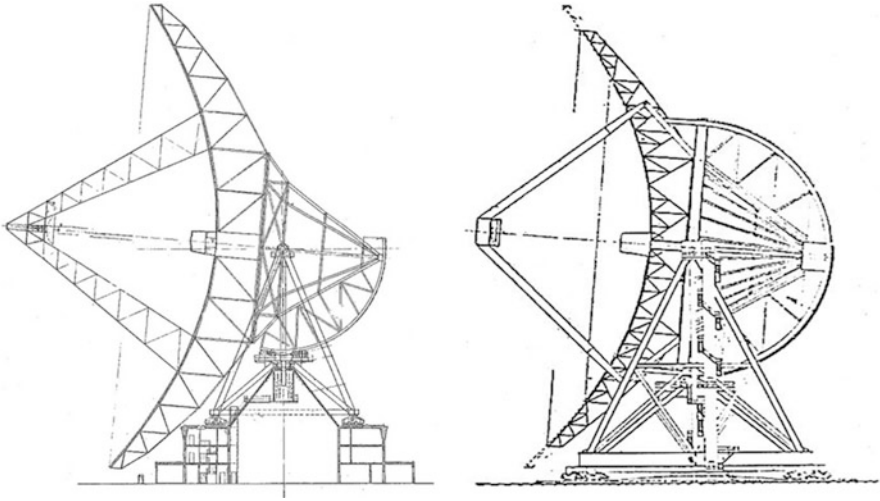
Fig. 4.11 The final 90/100-m diameter designs by MAN (left-90 m) and Krupp (right-90/100 m) (Krupp, MAN)

The designs are different in three points (Fig. 4.11):

1. The diameter of the elevation wheel of the Krupp design is much larger than that of MAN.
2. The quadripod for the secondary is in the MAN design attached to the backup structure; in the Krupp design, it is attached to the octahedron completely separate from the backup structure.
3. The MAN design has an elevated azimuth track, resting on a circular three-story building.

4.4.4 The Final Design and Realisation

Hachenberg's evaluation report discloses that the final reflector deviations of the MAN design were twice that of the Krupp design, which was due to the different choices for supporting the quadripod. In the MAN design, the loads of the quadripod could not be distributed in the BUS in a homologous way, leading to a higher rms reflector deviation. In his evaluation report of the designs, Hachenberg concluded that Altmann's design was the better one. The intelligence of this design and the resulting better reflector accuracy gave him the decisive argument for the choice of the Krupp solution. An impression of the telescope structure is shown in Fig. 4.12.
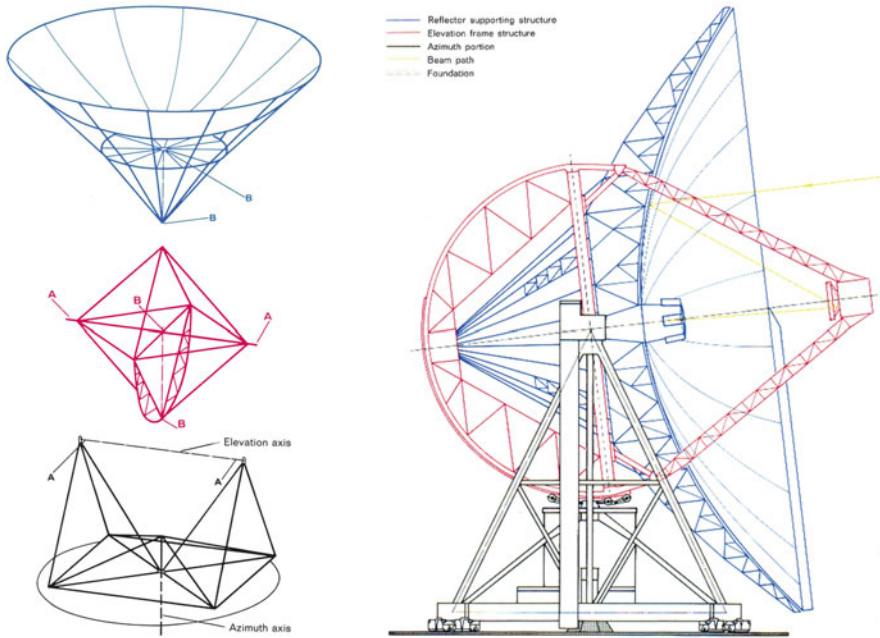
Fig. 4.12 The three basic building blocks and a cross section through the Effelsberg telescope (MPIfR)

The realisation of Hachenberg's dream went very smoothly. The Volkswagen Stiftung granted the money for the 100-m version, and the competing companies were persuaded to form a joint venture (ARGE Star) with Krupp as leader for design and manufacture, and MAN leading the on-site assembly and erection (Fig. 4.13). The 100-m telescope was inaugurated on May 19, 1971, and a description with measured system parameters appeared in 1973 (Hachenberg et al. 1973). The telescope is a beautiful structure (see front picture of this chapter) with an astounding performance.

The initial operation however was hampered by a serious problem in the servo-drive system. It caused the elevation structure to vibrate and go into oscillation endangering the structure. It took a long time to resolve the problem. The final solution was very simple: two of the four elevation drives were disconnected and all vibration stopped. Fortunately, the power of the remaining two drives was sufficient for the specified operational modes. After about 10 years, the surface plates of the panels delaminated from the honeycomb core. They were exchanged for aluminium cassette panels. Also the azimuth rail track had to be replaced. The overall performance of the telescope remained unchanged.

In 2006, a new "active" subreflector of 6.5-m diameter with a surface error of 60 μm was installed. Its 96 surface panels are individually adjustable and the effect of non-homologous large-scale deformations of the main reflector can be

Fig. 4.13 The Effelsberg 100-m radio telescope during its erection in 1970 (MPIfR)

counteracted in real time. This is an example of *active optics* mentioned in Chap. 2. Specifically, it means that the telescope can be used at 3 mm wavelength with a stable sensitivity over the entire elevation range. Clearly, this is a much more economic method than equipping the 2300 panels of the primary reflector with motorised actuators.

4.5 Backup Structure and Deformation Patterns

The three early large radio telescopes, Lovell (before the 1976 refurbishment), Parkes and Effelsberg are so different in their structural design that they are good examples for the discussion of general structural design issues (Fig. 4.14). In all three cases, the axes arrangement is elevation over azimuth (EL/AZ), but the support of the reflector backup structure (BUS) on the alidade is significantly different:

– The BUS of the Lovell telescope is supported at the outer rim. (The red wheel in the centre is only for damping purposes and does not take loads.) A central pole supports the receivers in the prime focus.
– The BUS of the Parkes telescope is supported at the central hub. The receivers in the prime focus are supported by a tripod mounted directly on the BUS.
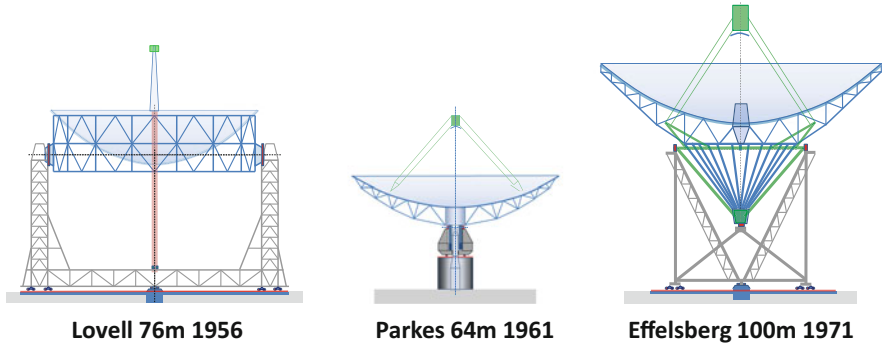
Lovell 76m 1956   **Parkes 64m 1961**   **Effelsberg 100m 1971**

Fig. 4.14 The three reference telescopes for discussion of structural design issues

– The BUS of the Effelsberg telescope is supported between the centre and the rim. It has an additional intermediate structure, the elevation cradle, not existing in the other telescopes, that also carries the quadripod for the receivers without any connection to the BUS (green).

It will be clear that these differences in BUS support cause rather different gravitational deformation patterns over the range of elevation angle. In the following section, we illustrate by simple graphical means how the gravitational forces act on the structure and lead to systematic deformation patterns.

4.5.1   The Design Approach of the Effelsberg Backup Structure

Before we go into the details of the structural layout of the BUS, we consider some basic structural effects. We use the simplest structural model for deformation calculations: the elastic beam (Fig. 4.15). It is clear that a beam supported at its ends has its maximum sag in the centre (left sketch) and that a centrally supported beam has its maximal sag at the edges (middle sketch). The simplest method to reduce the sag is obviously to support the beam somewhere in between. Some simple calculations show that for a beam with constant cross section the optimum support locations lie at 63% of the overall length.

The Effelsberg BUS follows such a strategy, although the chosen distance is somewhat smaller than 63%. We do not know why Husband at Jodrell Bank and Freeman Fox at Parkes didn't apply such very simple considerations. Probably, they were not aware of the magnitude of the deformations, or they were aware and the estimated magnitude of the deformations was much smaller than the wavelength that the radio astronomers intended to receive. The designers of the Dwingeloo telescope did support the BUS close to the optimised radius. It appears that Sebastian von Hoerner was the first who thought systematically about the gravity-induced deformations (see the similar sketch from his basic paper on homology in
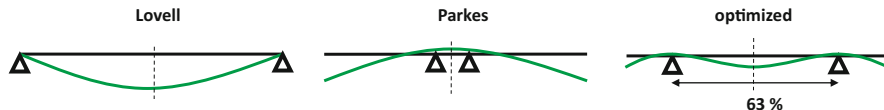
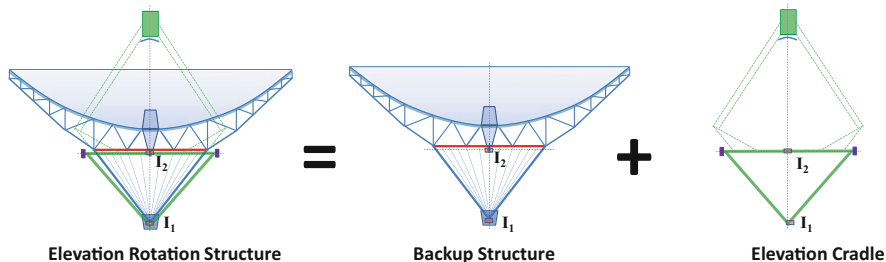**Fig. 4.15** Bending behaviour of an equivalent beam

Fig. 4.16 The elevation rotation structure is split into backup structure and elevation cradle

Fig. 4.3, above). A first conclusion of these very basic structural considerations is that the *choice of the distance between the elevation bearings*, which defines the distance of the BUS supports, has a major influence on the overall structural layout and hence the appearance of the telescope.

The Effelsberg reflector is a good example to study the structural design issues of backup structures in more detail. First, we see that the Effelsberg designers split the Elevation Rotation Structure (ERS) into two separate subsystems: the Backup Structure (BUS) and the Elevation Cradle (ELC), which are connected to each other only at two interface points I1 and I2 placed on the rotation axis of the main reflector (Fig. 4.16). The introduction of the ELC seems at first rather artificial and is against the usual approach in bridge design, where the designers always try to get the largest possible load transferred directly to the support points. In contrast to a bridge, the weight of the Effelsberg BUS is first transferred to two points on the *z*-axis, about which the main reflector and the BUS are rotationally symmetric, and from there transferred onto the elevation bearings via diagonal struts of the ELC.

Why would one make these large detours in the load transfer? We will see that the main mechanical argument for the detour in the load paths is to avoid the print-through of the large forces at the elevation bearings onto the reflector shape (Eschenauer and Brandt 1972).

When we look into the archives of the Effelsberg design phase, we see also that the designer, Horst Altmann, was influenced not only by mechanical arguments but also by his professional background as structural engineer of that time. He was well experienced in hand calculations based on graphical statics and the slide rule, without the help of computers. The BUS is a three-dimensional space truss-type structural system of complex shape and therefore not easily accessible to hand

calculations. The easiest way, the reduction of the dimensions from three to two, is achieved by the introduction of symmetry, in the case of a radio reflector obviously rotational symmetry about the reflector axis. By doing so, the structure becomes accessible to two-dimensional graphical statics on the drawing board, and this is exactly what Horst Altmann did as shown in one of his sketches (Fig. 4.17) (Altmann 1972).

In the left sketch, he shows the gravity-induced forces (the weights, which he called G (Gewicht) in German) in zenith position. The sketch shows also another arrangement of forces, related to the stiffening contribution of the circumferential hoops R (for the German Ring). The two interface points of the BUS to the ELC are indicated by the letters A and B, where B takes both vertical and lateral and A only lateral forces, which are zero in the zenith load case. The right sketch shows the load distribution in horizontal position, a weight list at the truss nodes and the graphical evaluation of the forces in the struts of the radial BUS girder by a force (Cremona) diagram. Altmann used this basic type of static considerations at the beginning of the Effelsberg design process; later his team analysed their structural designs in three dimensions with the computer-aided FEA tools that were becoming available at that time. We may not repeat Altmann's graphical statics, but we can use his method to get a basic understanding of the load transfer and the related deformation features of the Effelsberg reflector system.
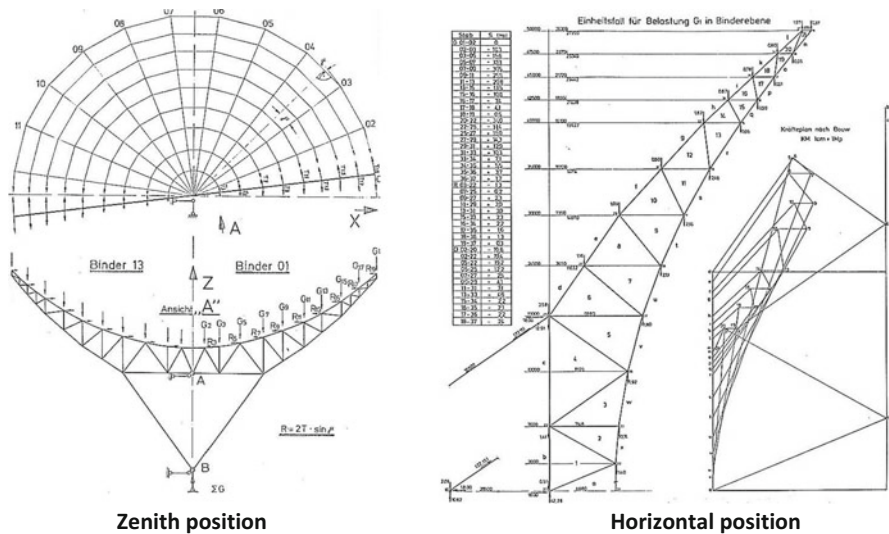

Zenith position   **Horizontal position**

Fig. 4.17   Horst Altmann's static considerations in 1968 (in Der Stahlbau 1972)

4.5.2 Interpretation of the Load Cases of the Effelsberg Reflector

4.5.2.1 Zenith Position

First we look at the load paths in zenith position (Fig. 4.18). The BUS has the appearance of an inverted umbrella, and the cone of the umbrella is part of the BUS, not part of the ELC. The red arrows indicate the external forces g^{BUS} on the structure introduced by gravity. They are applied here for simplicity only at the nodes of the BUS trusses and represent the weight of the structure proper as well as dead loads from the weight of the reflector surface. They have to be in equilibrium with the reaction force G^{BUS} at the supporting point of the BUS at the tip of the umbrella cone, which is the only interface to the ELC that is taking vertical loads. The related *equilibrium condition* reads

$$G^{\mathrm{BUS}} = \sum_i g_i^{\mathrm{BUS}} + G^{\mathrm{BAL}}$$

where G^{BAL} is the weight of the ballast needed for balancing about the elevation axis in horizontal position (discussed below for the horizontal load case). The internal load transfer of the forces g_i^{BUS} at the nodes through the struts of the girders is not shown in the sketch. The load transfer in the cone is indicated by the forces in the cone struts S^{CONE} and the radial struts R^{CONE} at the interface of the cone to the radial girders. The sketch shows only one pair of opposite radial girders. Due to the rotational symmetry, all other girders have the same behaviour, and the ballast G^{BAL} and the reaction force G^{BUS} are related to the sum of all radial girders.

In the ELC, the incoming reaction force G^{BUS} has to be transferred to the elevation bearings by the forces $S^{P\&P}$ in the diagonals called *Peter & Paul* (traditional names), which create a reaction force $R^{P\&P}$ in the EL axis strut.
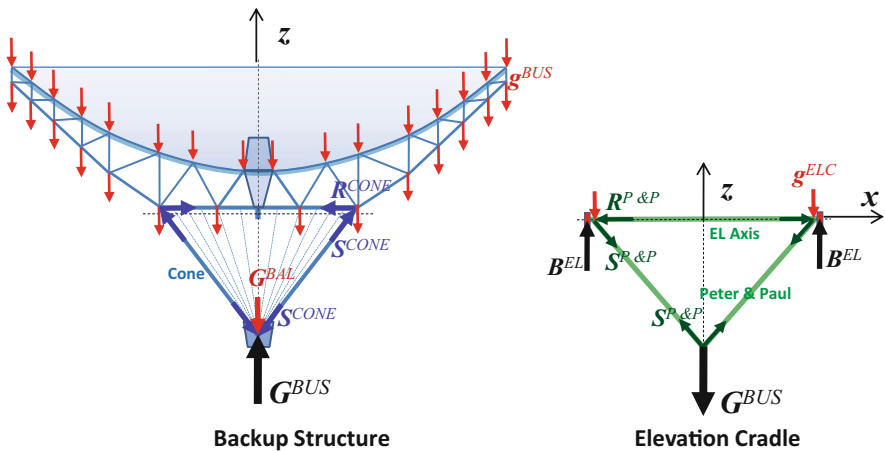
Fig. 4.18 Load paths zenith position

These forces are huge; they put the full weight of the ERS on the elevation bearings. The structural strength in the elevation bearing area is the most critical in the telescope, whereas the stresses in the BUS radial girders and circumferential hoops are less critical. The relief of the reflector truss from the direct impact on the elevation bearings is the main mechanical argument for the Effelsberg design approach with the *inverted umbrella* and explains the extremely low weight of the Effelsberg BUS.

4.5.2.2   Horizon Position

Now we consider the load paths in horizontal position (Fig. 4.19). As in the zenith case, we look at the BUS and the ELC separately. Again the whole weight of the BUS is transferred at only one point to the ELC, this time at the centre of the radial girders. The sketch shows also that the forces introduced into the nodes of the BUS trusses are not balanced about the elevation axis (contrary to the zenith load case). Therefore, a counterweight is needed which is arranged at the end of the umbrella cone. The related equilibrium condition for the vertical forces is

$$G^{\mathrm{BUS}} = \sum_i g_i^{\mathrm{BUS}} + G^{\mathrm{BAL}}$$

Fig. 4.19   Load paths horizontal position

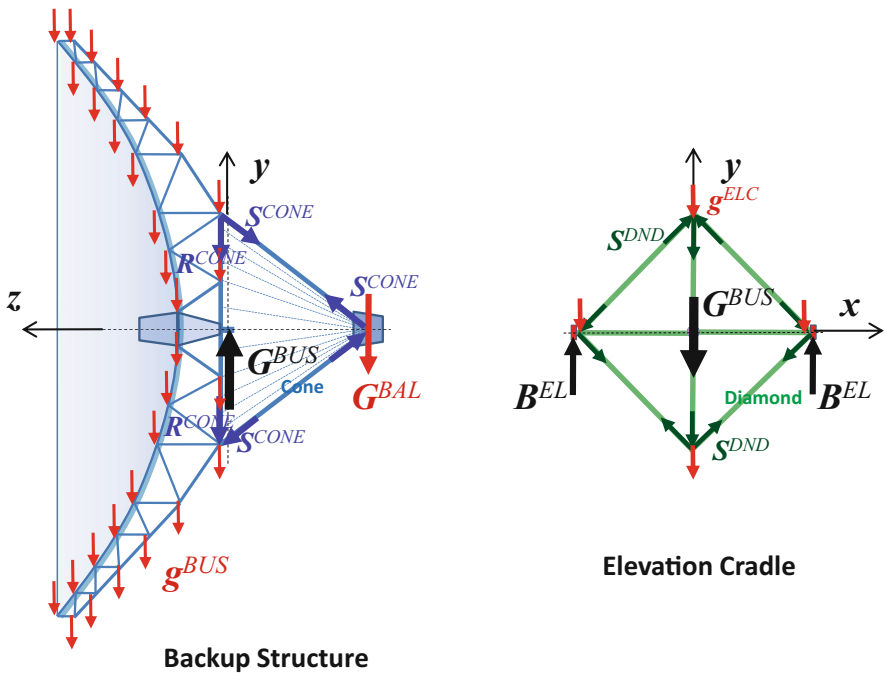Contrary to the zenith load case, the horizontal load case is not rotationally symmetric. The structure itself is still rotationally symmetric, but the loads are skew symmetric about the x–z plane. Therefore, the internal load transfer in the radial girders varies with the cosine of the girder location in a cylindrical coordinate system about the z-axis. The sketch may be interpreted as showing the maximum case in the vertical girders; the stresses in the horizontal girders are zero, and their weight is transferred to the vertical girders by the circumferential hoops.

In the ELC, the incoming reaction force G^{BUS} has to be complemented by an equilibrium condition for the tilt moment, which leads to

$$z^{\text{BUS}} \cdot G^{\text{BUS}} = -\sum\nolimits_i z_i^{\text{BUS}} \cdot g_i^{\text{BUS}}$$

The reaction force G^{BUS} is transferred to the elevation bearings B^{EL} by a diamond-type arrangement of struts (right sketch in Fig. 4.19). The forces S^{DND} in the diagonals transfer the full weight to the bearings without any axial load in the elevation axis. They are half of the forces $S^{P\&P}$ in *Peter & Paul* for the zenith load case, because there are four diamond diagonals instead of two Peter & Paul diagonals.

4.5.3   Load Case Superposition

The gravity vector changes its direction with respect to the rotating ERS only in the y–z plane. Therefore, the gravity vector can be decomposed into two components: one symmetric g^z in the direction of the co-rotating z-axis and one skew symmetric g^H in the direction of the co-rotating y-axis, whereby

$$g^H = g \cdot \cos \text{EL} \ \ \text{and} \ \ g^z = g \cdot \sin \text{EL}$$

The skew symmetric component g^H and the symmetric component g^z are equivalent to the gravity load case in horizontal and zenith position, respectively (Fig. 4.20).

This means that all gravity deformations are composed only of the contributions of two basic load cases: the symmetric one in zenith position and the skew symmetric one in horizontal position. *This simplifies tremendously the assessment of the deformation behaviour and the related quality of the design of the ERS structure. It is sufficient to optimize only the two reference load cases and elevation-dependent deformations are a superposition of these two load cases as a function of the elevation angle.*

For the superposition, we have to take into account the influence of the erection and alignment procedure on the final shape of the reflector. The structural engineer's approach in the application of the gravity loads is switching on the gravity in the zenith and horizon position. It does not directly describe reality, because the
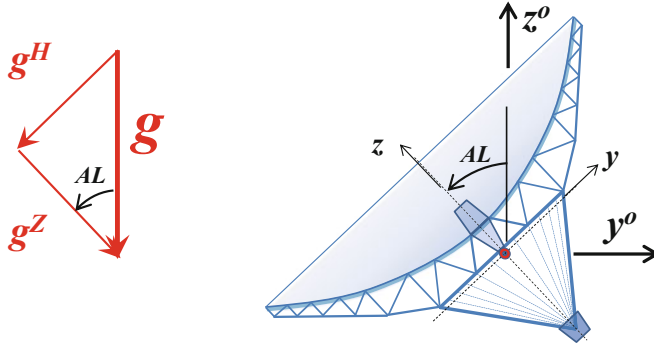
Fig. 4.20 Decomposition of the gravity vector in a symmetric and a skew symmetric component

structure is assembled under the influence of the gravity forces during the erection process. This has to be taken into account in the superposition process. Normally, the reflector is aligned to the desired paraboloid at some intermediate elevation angle EL_0. At this position, the gravitational deformations have been removed by the alignment procedure. Now the deformation $\delta_i(EL)$ at any point i of the elevation rotating structure is found from the following superposition formula:

$$\delta_i(EL) = \delta_i^H \cdot (\cos EL - \cos EL_0) + \delta_i^z \cdot (\sin EL - \sin EL_0), \qquad (4.5)$$

where δ_i^H and δ_i^z are the calculated gravitational deformations in horizon and zenith position, respectively. This equation is valid for all vector components in the co-rotating coordinate system. For a fixed global coordinate system, the vector components have to be subjected to the appropriate coordinate transformation equations.

4.5.4 The Deformation Behaviour of the Effelsberg Reflector

After these preparations, we now deal with the deformation features of the Effelsberg BUS that drive the design. We look again into the archives of the Effelsberg project and use the contour plots as found in the 80 m studies and shown in Fig. 4.21. The Krupp study introduced the "umbrella" concept, as used later for the final design of the real telescope. The first MAN study ended up in a "four-point" design not used for Effelsberg, but applied in some other realised telescopes discussed below.

First we note that the engineers used different kinds of display in the two studies. The contour plots of the MAN study show the basic *gravity switched on* load cases as explained above. The Krupp study showed an *aligned case*, that is, the reflector
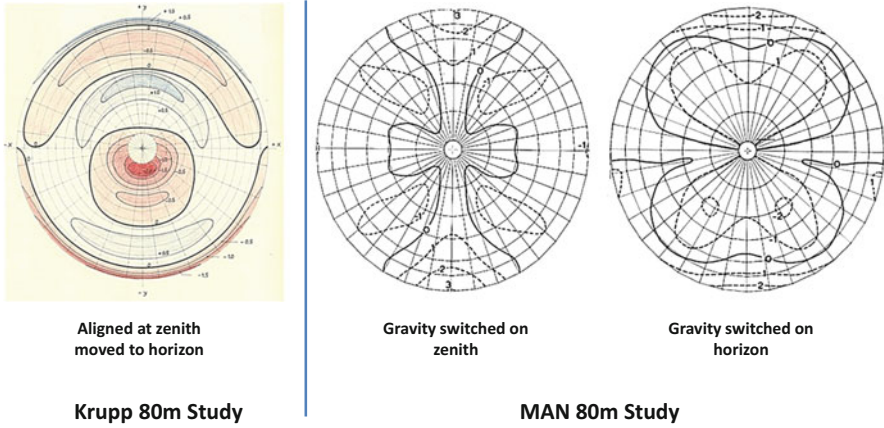
**Aligned at zenith   Gravity switched on   Gravity switched on
moved to horizon   zenith   horizon**

Krupp 80m Study   **MAN 80m Study**

Fig. 4.21 Contour plots from the Effelsberg 80 m studies

aligned to zero deviations in zenith position (taking into account the real situation during erection), and then moved to horizon. With our superposition formula (Eq. 4.5) this means that the deformations in the Krupp contour plot are those combined of the two basic load cases as:

$$\delta_i(0) = \delta_i^H \cdot (\cos 0 - \cos 90) + \delta_i^z \cdot (\sin 0 - \sin 90) = \delta_i^H - \delta_i^z. \qquad (4.6)$$

Thus, the Krupp contour plot shows the deformations of the basic load case *gravity switched on horizon minus gravity switched on zenith*. The figure shows a very specific deformation pattern, and we'll now try to understand why it has this shape. Encouraged by von Hoerner's very simple structural models used in his basic paper, we reduce the plane calculation model of Altmann further by replacing the radial trussed girders by bending beams, avoiding the necessity to use Cremona plans for hand calculations.

In a first step (Fig. 4.22, centre), the radial girders are represented by a curved beam in the centre line of gravity of the trussed girders. The offset between the bending beam and the corner of the umbrella cone has to be modelled by a virtual beam element. In a further simplification step (right sketch), we reduce the curved beam to a straight beam. We will see that this simple model is sufficient to understand some of the basic features of the Effelsberg bending behaviour. First, we consider the zenith load case (Fig. 4.23).

The gravity-induced forces G^{BUS} (left) have to be transferred by our bending beam to the umbrella cone interface, which causes bending moments (centre) with a maximum M^Z at the interface to the umbrella cone. The reaction forces at the cone interface have then to be transferred through the cone diagonals to the interface with the ELC (centre). The bending moments cause typical sag of the beam (right) with the maximum downward sag at the edges and in the centre and peaks above the cone interface (green). Best-fitting of a reference plane (right) results in a typical
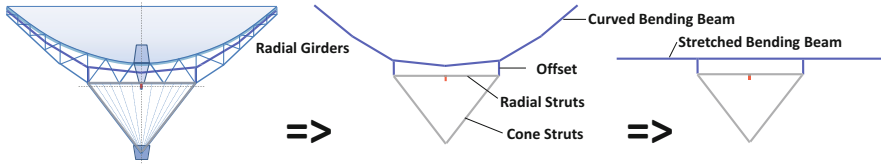
Fig. 4.22 Most simple model for the interpretation of the deformation behaviour
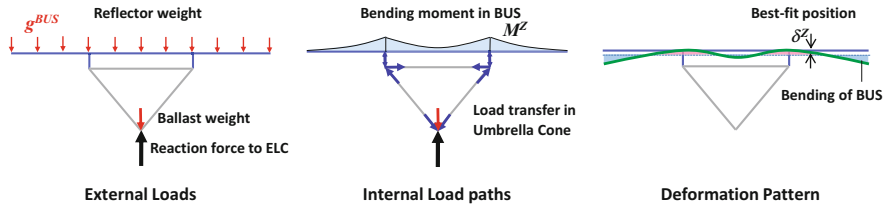
Fig. 4.23 Interpretation of the deformation pattern for zenith load case
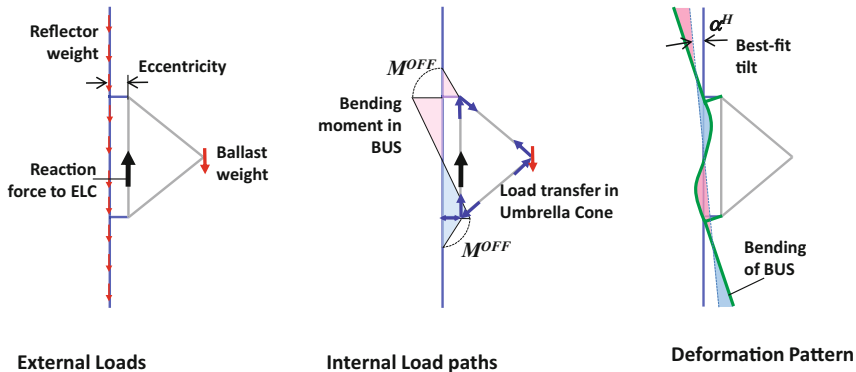
Fig. 4.24 Interpretation of the deformation pattern horizon load case

deformation pattern with upward deviations around the interface (red) and downward deviations at the edges and in the centre (blue). The magnitude of the deviations depends on the stiffness/weight ratio of the reflector truss system that the beam model represents.

Second, we look at the basic horizon load case (Fig. 4.24). Here, the gravity loads act directly in the centre line of gravity of the model beam (left) and cause no direct bending! But at the interface to the umbrella cone, there is an eccentricity that causes skew symmetric reaction forces at the umbrella cone and related skew symmetric bending moments in the middle section of the model beam with the maximum M^H at the cone interface (centre). The related deformations are also skew symmetric (right), with back deviations (blue) at the upper centre and the lower edge, and front deviations (red) at the lower centre and upper edge. The best-fitted reference plane has a tilt α^H against the absolute coordinate system.

The two types of deformations in the two basic load cases have a very different quality:

1. The bending in the zenith load case is natural and cannot be avoided. It depends on the stiffness-to-weight ratio of the BUS structure and could only be reduced by the use of lightweight materials as e.g. carbon fibre composites or by von Hoerner's method of introducing secondary trusses with related artificial flexure.
2. The bending in the horizon load case is related to the manner in which the interfaces between the BUS and the ELC are designed. The effects are not natural but artificial and should be avoided by a smart structural design.

Before we investigate how to avoid the bending in horizon position by an adequate BUS/ELC interface design, we compare the deformations of our simple beam model with those in the contour plot of the Krupp 80 m study (Fig. 4.25). We see a similar skew symmetric shape as in the simple beam model. Only at the edges are some deviations visible, which are probably caused by a hoop effect of the space truss system not reflected in our simple model. The symmetric zenith load case has a minor influence on the deformation pattern and may be responsible for the upward shift of the central zero.

Reflecting on the load paths in the Effelsberg structural concept reveals what should be done to avoid the secondary bending in horizon position (Fig. 4.26). In the actual configuration (left), the central reaction force G^{BUS}, which is equivalent to the whole weight of the BUS including umbrella cone and the ballast, is transferred by the radial cone members R^{CONE} to the BUS/CONE interface, and from there as offset force L^{OFF} into the BUS, represented by the beam model.
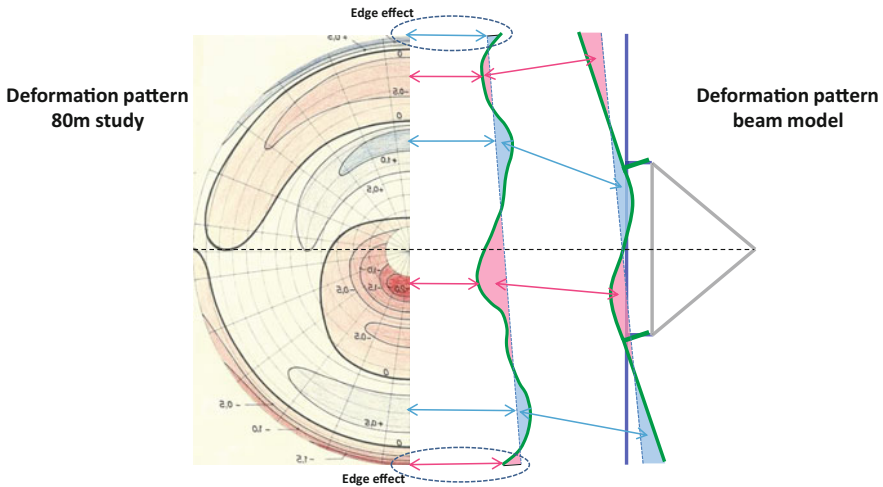

Fig. 4.25 Interpretation of the shape of the Effelsberg 80-m study contour plot in horizon position—*centre* shows projection of the contours and *right* our beam model
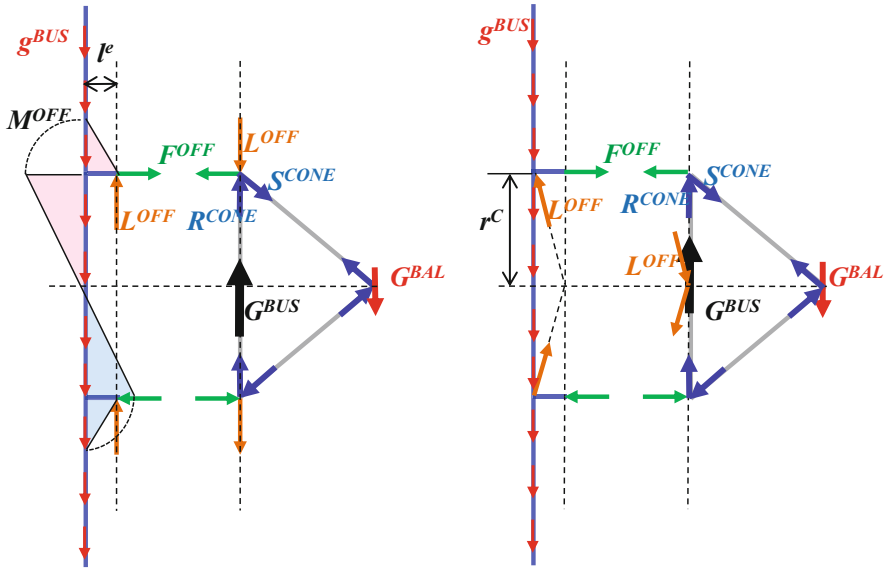
Fig. 4.26 Remedy for the bending in the horizon load case of the Effelsberg system

A remedy for the secondary bending is the separation of the central load transfer between BUS beam and cone. The vertical weight of the BUS beam should be transferred directly to the central pivot at G^{BUS} without the detour across the cone. The direction of the tilted load transfer elements L^{OFF} should be chosen such that they are in equilibrium with the forces F^{OFF} that transfer the offset moment of the BUS weight against the elevation axis to the ballast weight. Thereby, the bending is avoided.

The designers of the Effelsberg reflector system were probably not aware of this effect and did live with their results. The overall performance of the design was overwhelmingly better than all the previous telescopes of similar size, even surpassing the basic specifications. We leave the question how the details of the Effelsberg central interface should look to avoid the bending as an exercise to the reader.

But with the requirements becoming tougher for more accurate telescopes, also the horizon load case has to be optimised to a similar level as the zenith case, and this is what the designers of the 30-m Millimetre Radio Telescope (MRT) did. Also in the early design phase of this telescope, the horizontal load case showed similar deficiencies to those explained above. The introduction of a precisely tilted central interface achieved the same quality as the zenith load case. We shall discuss this in some detail in the description of this telescope in Chap. 5.

4.5.5   Performance Limits of the Effelsberg Reflector Principle

To conclude this section, we summarise a systematic approach to the deformation behaviour and performance limits of Effelsberg-type reflectors. We use modern FEA computations of a reflector structure with similar design features as the Effelsberg reflector as illustrated in Fig. 4.27. The only difference is the quadripod, which is attached directly to the BUS truss, not separately to the ELC as in Effelsberg. This is of course a significant departure from the homology idea behind the Effelsberg solution.

The computed contour plots of reflector deformations in the zenith and horizon orientation under different layouts of the quadripod are shown in Fig. 4.28. The figure also lists the calculated rms surface error under the influence of gravity for a reflector diameter of 100 m.

1. The upper two diagrams show the results for the two basic gravity load cases without any influence of a quadripod. As such, it is representative of the real Effelsberg telescope. The zenith load case (left) shows a very favourable 324-μm rms surface deviation. The dominating effect is the print-through of the umbrella cone rim visible as red annulus in the diagram. The horizon load case (right) shows much less favourable deviations with a magnitude of 2084 μm rms. The deformation pattern is exactly the same as discussed and identified in the previous section as secondary bending introduced by the forces at the central BUS/ELC interface.
2. The middle two diagrams show the results for the same load cases but including the weight of the quadripod, supported by the BUS. The deformation behaviour is now strongly dominated by these additional loads and presents a prohibitive
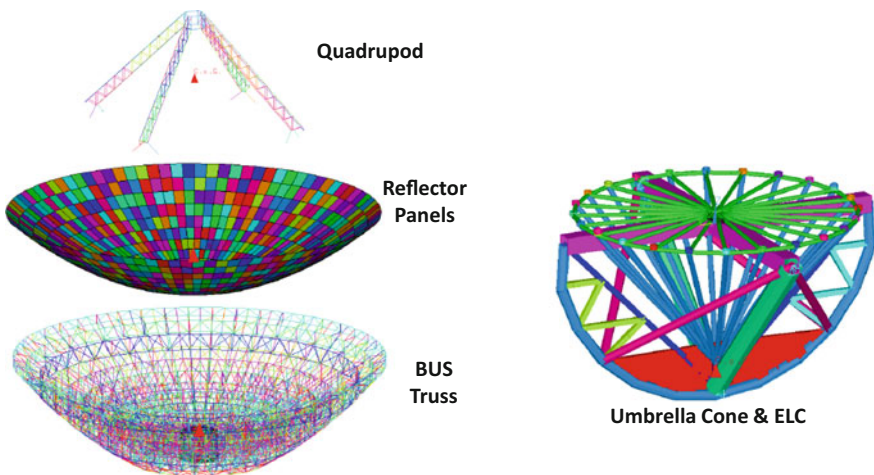
Fig. 4.27   FE model of an Effelsberg-type reflector structure used for parameter studies

σ^Z = 324μm rms   σ^H = 2084 μm rms

Contourplots no quadrupod

σ^Z = 1424μm rms   σ^H = 3191μm rms

Contourplots including quadrupod

σ^Z = 1424μm rms   σ^H = 3191μm rms

Contourplots quadrupod ± 45° orientation

Fig. 4.28 Contour plots of gravity-induced deformation for different layouts of the quadripod. *Left* zenith, *right* horizon position

design solution without additional measures, such as local strengthening, in the connection to the BUS.

3. A change in the orientation of the quadripod by $\pm 45°$ (lower diagrams) does not change the magnitude of the computed rms deviation despite the different deformation pattern over the reflector area. While in the zenith position the pattern is simply rotated by $45°$, the deformation pattern looks quite different in the horizon position. The "push and pull" of the lower and upper two legs is clearly visible.

From this exercise, we can draw the following conclusions. If the design of the structural system of the telescope aims at ultimate performance, the following points need to be considered:

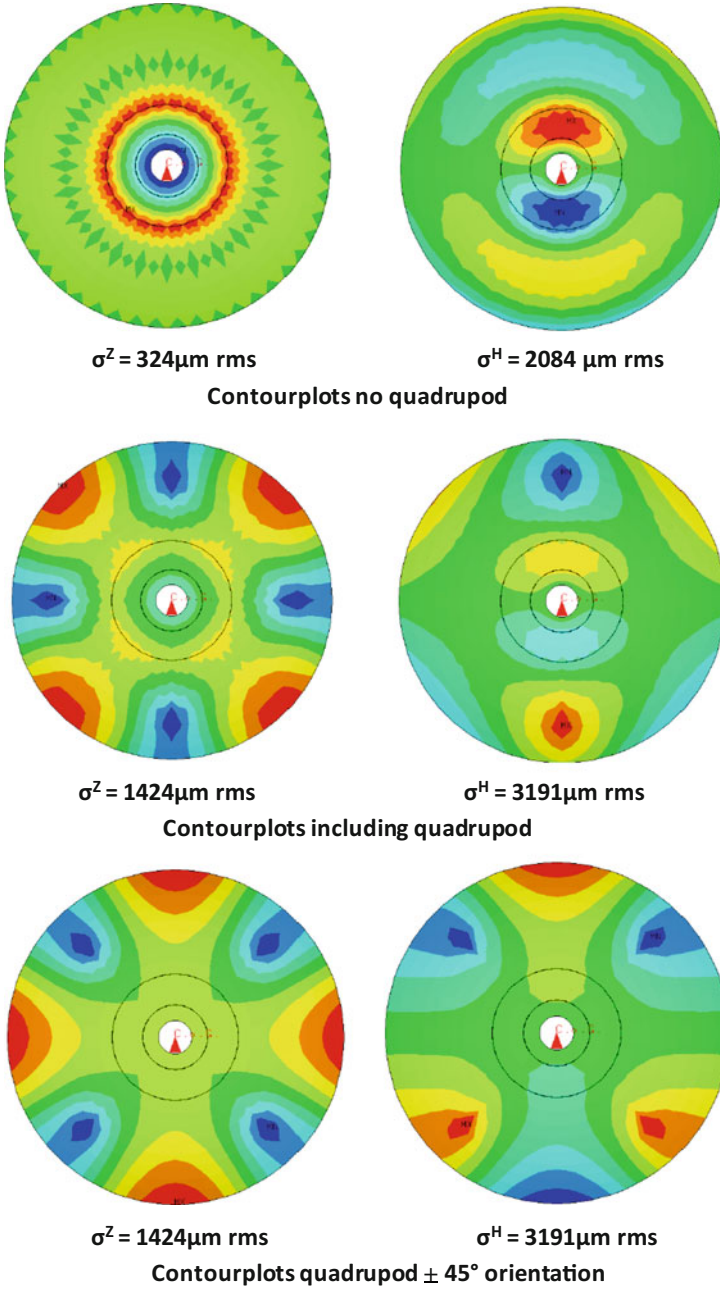1. The quadripod should have a separate support independent from the BUS. Otherwise, the BUS must be strengthened in the area of attachment of the quadripod. This will unavoidably lead to loss of the rotational symmetry of the BUS with possible consequences for the reflector accuracy. However, a successful example of this choice is the MRT, to be described in the next chapter.
2. The central BUS/ELC interface has to be designed according to the method described in the previous section in order to eliminate the secondary bending in the BUS-ELC interface.

With these provisions, it seems feasible for a 100-m reflector to reach accuracies of the order of 300 μm rms for both basic load cases. The remaining deviations are caused by natural bending of the reflector truss system between the ELC interfaces and could be further reduced only by the introduction of sub-truss systems in the sense of von Hoerner's homology principles. But before doing this, we have to look if this is worthwhile in the context of the overall system, particularly by comparing the achieved accuracies under gravity loads with other disturbances, such as the impact of environmental effects of wind and temperature and the actual fabrication accuracy of the surface panels. We deal with these effects in later chapters. Here, we want to illustrate the influence of the alignment process on the accuracy. From Eq. (4.5), we know that the deviations in any elevation position can be assessed by a sine/cosine combination of the two basic gravity load cases. The same is valid for the accuracies but in a root-sum-squared manner as shown by von Hoerner and Wong (1975), which leads to:

$$\sigma^2(\mathrm{EL}) = \sigma_H^2 \cdot (\cos \mathrm{EL} - \cos \mathrm{EL}_0)^2 + \sigma_Z^2 \cdot (\sin \mathrm{EL} - \sin \mathrm{EL}_0)^2, \qquad (4.7)$$

where EL_0 is the elevation angle at which the surface was adjusted to the prescribed contour. As an example we take the case at the top of Fig. 4.28, the actual Effelsberg telescope. The plot in Fig. 4.29 shows the reflector error as function of elevation angle for the cases of alignment in horizon, zenith and two intermediate elevation angles of $30°$ and $60°$. By choosing an adjustment angle of $60°$, we can balance the large difference between zenith and horizon and thereby halving the maximum surface error.

Fig. 4.29 Influence of the alignment angle on the overall reflector accuracy. *Full* and *dash-dotted curves* pertain to adjustment in horizon and zenith position, respectively. *Dashed* and *dotted curves* result from adjustment at 30° and 60°, respectively
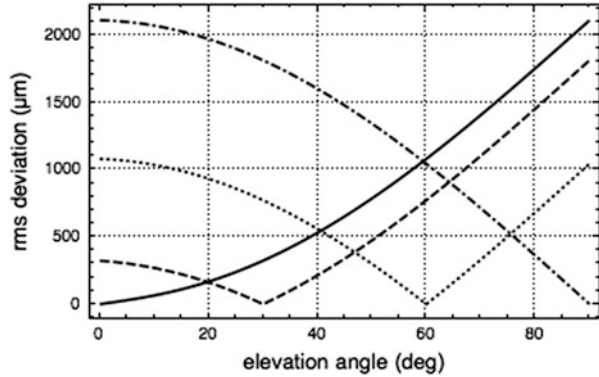
We conclude here our discussion of the method of homologous design and its major application to the Effelsberg telescope. Different requirements on the layout of a telescope may make the rigorous application of the homology principles difficult if not impossible. Such is the case in a few large millimetre-wavelength telescopes that will be described later. There exist "semi-homologous" designs; in particular the *four-point reflector support*. We present the evolution of this alternative support in the following section by example of a few medium-sized telescopes.

4.6   Four-Point Reflector Support

4.6.1   Introduction

When the highly symmetric *umbrella* of the Effelsberg telescope is to be used for smaller telescopes, one quickly runs into a serious problem of accessibility of the space behind the vertex of the primary reflector. With the increase in size of cryogenically cooled receiver systems, the preferred choice for a new telescope became the dual-reflector (Cassegrain) geometry with the final focal point in the neighbourhood of the primary vertex, often in a Nasmyth configuration (see Chap. 2) behind the vertex. This essentially rules out the application of the umbrella support. An alternative is needed between the two-point support of the telescopes described in Chap. 3 and the umbrella solution. An important improvement in deformation behaviour of the reflector can be achieved by dividing the load of the BUS to four points of the elevation cradle (ELC) before transferring this load to the two elevation bearings. In this section, we discuss the development of the *four-point support* by the example of three telescopes. The 25-m antennas of the Westerbork Synthesis Radio Telescope (WSRT) were designed in the mid-1960s by B. G. Hooghoudt. The ELC is a square cradle cantilevered on the elevation axis and supporting the BUS on its four corners. In the mid-1970s, one of us (HK) was

involved in the design of several Intelsat ground stations of 32 m diameter, where a four-point support was introduced. This solution was subsequently used in the 32-m MERLIN antenna of Jodrell Bank Observatory, which we discuss here. A more elaborate design was realised by Krupp/MAN in the late 1970s to satisfy the high requirements for the 30-m Millimetre Radio Telescope (MRT), which we describe in detail in Chap. 5. Finally, here we summarise the Yebes 40-m antenna of the early 2000s, in which HK applied some further developments of the four-point support.

4.6.2   The Westerbork Array of 25-m Antennas

The *four-point support* was applied in the antennas of the Westerbork Synthesis Radio Telescope (WSRT), together with some original design and fabrication methods that are worthwhile to mention. This telescope operates on the principle of *aperture synthesis*, in which the outputs of a set of interconnected antennas are combined to synthesise a picture of a celestial source with an angular resolution determined by the largest distance between the telescope's elements. Normally, this involves the tracking of the source over long periods to provide angular resolution in all directions. The early synthesis telescopes, among them the WSRT, used an *equatorial mounting* for the antennas for ease of sidereal tracking.

The WSRT consists of 14 equatorial antennas of 25 m diameter, placed on an E-W line and located in the northern part of the Netherlands. It began its operation in 1970 (Baars et al. 1973). The design was guided by the requirement to produce highly identical antennas in a cost-effective series production with minimal erection procedures in the field. Any differences in the geometry of the mount between the individual antennas needed to be limited to less than 1 mm. The reflector surface precision was specified at 4 mm rms (Baars and Hooghoudt 1974).

An assembly hall was built on the observatory site with templates to assemble the three major sections of the antenna in a controlled environment. Referring to Fig. 4.30, the polar-axis house and the declination cradle were welded in their respective templates, assuring dimensional precision and reproduction of better than 1 mm. The support ring for the reflector was delivered from the shop in four pre-welded sections and completed by connecting these in its template to form the ring girder. Surrounding the ring girder is the template, set to 0.2 mm accuracy, for the assembly of the reflector, which consists of 98 panels, divided over three rings. The panel frames, while resting on the support points of the template, were bolted together to form the load-bearing reflector. The inner section of the surface is a shell-like membrane structure supported by the support ring girder at its inner radius only. The outer panel ring is attached to the outer radius of the ring girder and receives additional support at about 80% of the radius by a hoop cantilevered from the ring girder. Non-load-bearing small panels cover the area above the ring girder.

Fig. 4.30 Exploded view of the major sections of the WSRT antenna. The reflector is connected to the support through a pin socket filled with epoxy. The reflector support connects to the declination cradle at the four corners. The polar axis is in a straight line with the rear pentapod support leg (in Baars and Hooghoudt 1974)
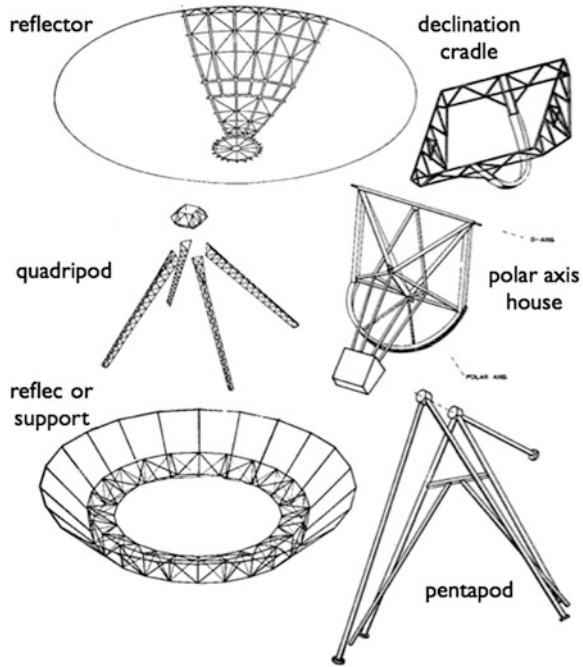
The ring girder with reflector is connected to the four corners of the declination cradle by four bolts each. As we will elucidate in detail below, the four-point support reduces gravitational deformation in the reflector by about an order of magnitude compared to a two-point support directly at the declination bearings. This could be considered a first significant step towards homology, although at the time of design this principle had not yet been published.

A novel solution was introduced for the connection of the reflector to the ring girder. At each connection point, a pin from the reflector panel is protruding into a socket on the ring girder. The socket is filled with epoxy resin to realise a fixed connection. This arrangement allows for normal manufacturing tolerances of the steel girder, and the use of epoxy avoids any stress to be exerted on the reflector surface while connecting it to the support ring, thereby maintaining the intrinsic high accuracy of the template assembly. After assembly of the reflector on the template, it was raised by 10 mm, supported on the four corners to the cradle and its deformation measured. Figure 4.31 shows that the deformation in zenith position is a factor two below the calculated value. The careful assembly in the templates enabled the achievement of a higher than specified surface precision of 1.4-mm rms, allowing operation with good efficiency at the short wavelength of 6 cm, a factor three smaller than envisaged in the original design.

The reflector surface is a stainless steel mesh of 8 mm spacing, 0.8 mm wire thickness, epoxy bonded to the panel frames. The extensive use of epoxy was a novel aspect of the antennas. Actually, after about 10 years in the field, the mesh
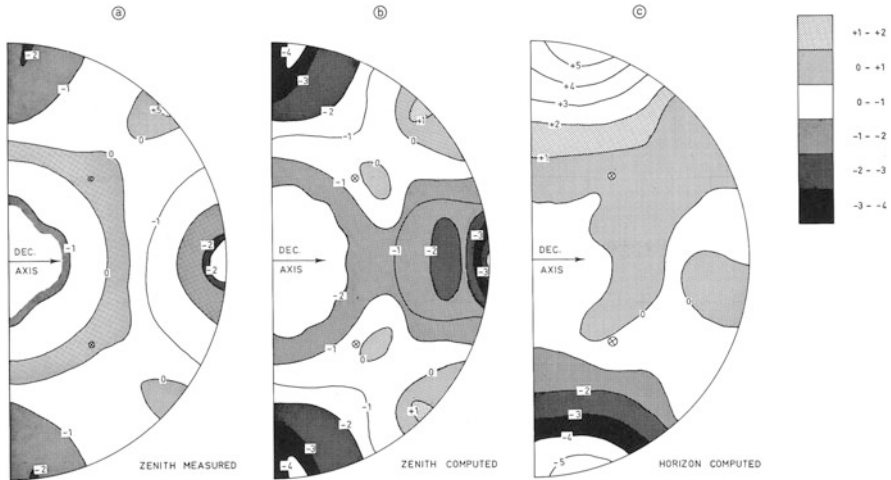
Fig. 4.31 Plots of the measured zenith (*left*) and computed zenith and horizon (*right*) deformation under gravity. The measured values are a factor two smaller than computed (in Baars and Hooghoudt 1974)

started to delaminate from the frames requiring a labour-intensive repair activity that has remained stable for more than 30 years. The bonding between reflector and support rings has not shown any deterioration over more than 40 years.

The erection activities in the field required only a small number of hoisting manoeuvres; two antennas could be assembled with one crane in 3 days. Figure 4.32 shows the antenna array. In the original layout of the array, 10 fixed antennas were placed along an E-W line at 144 m interval. This baseline was extended by 300 m of rail track, on which two antennas could be moved and located at any position. The signal from these two antennas was correlated with that from each of the ten fixed ones, delivering 20 tracks of visibility measurements on increasing baselines. In 1980, another rail with two additional antennas was located 1.5 km westward. Thus, 40 baselines over 3 km baseline were covered. The instrument is still in full operation. Recently, it has been equipped with *phased-array feed* (PAF) systems providing wide bandwidth, multi-beam operation for wide field mapping at L-band (Sect. 8.8).

4.6.3   The MERLIN Antenna with a Perfect Four-Point Support

The 32-m MERLIN antenna in Cambridge, UK, was built in 1990 as part of a radio telescope array, the Multi-Element Radio Linked Interferometer Network
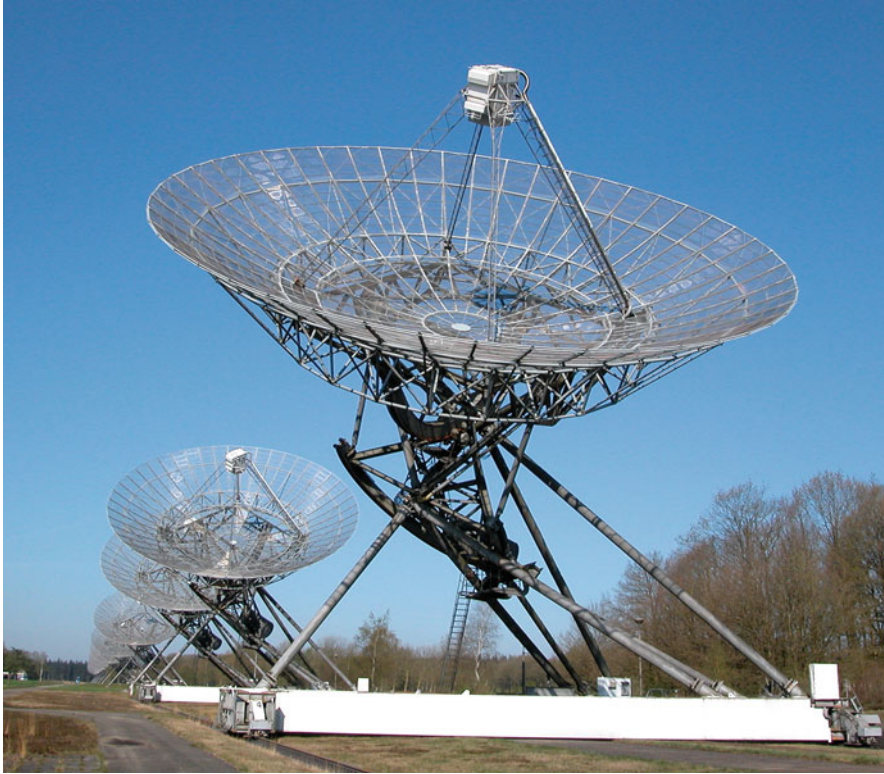
Fig. 4.32 The WSRT with its sleek and astoundingly simple and economic design of the 25-m equatorial antennas. The polar axis is in one line with the southern support leg (ASTRON)

(MERLIN) of the Jodrell Bank Observatory (Fig. 4.33). It operates from 151 MHz to 24 GHz, and the antenna in Cambridge is the largest radio reflector built in the UK since the 76-m Lovell. Contrary to the Lovell telescope, this time only performance specifications and a cost ceiling were stipulated. The design team of MAN based the design on work in 1977 for Intelsat communication ground stations of the same size. These employ a basic *four-point* reflector support.

At that time, structural analysis was executed by finite element programs running on IBM mainframe computers, which were fed in batch mode by punch cards. The results were delivered as tables printed by matrix printers, to be evaluated by hand. The plots in Fig. 4.34 shows deformation patterns printed in black and white with colour added by hand. The diagram on the left of Fig. 4.34 shows the typical deformation pattern of a two-point support in zenith position as mentioned in the example of the Lovell telescope in Chap. 3. It is dominated by astigmatism caused by the sag between the two elevation bearings. The deformations at the edge of the 32-m reflector are in the range of 10 mm.

Fig. 4.33 The 32-m antenna of the MERLIN array in Cambridge, UK (H. Kärcher)

The design idea for the avoidance of this astigmatic sag is the transition to a four-point support by the use of an additional ring girder (Fig. 4.34, right). This involves the introduction of a new structural subsystem, which we have called elevation cradle ELC in Sect. 4.5, and here takes the form of the ring girder. (Don't confuse this with the ring girder of the WSRT reflector. There the cradle is the equivalent of the ring girder here.) The location of the four interface points on the 45° symmetry lines results in perfect isostatic behaviour of these four points, and the resulting deformation pattern (right sketch) shows the desired symmetry about both the x–y-axes and the 45° directions. The resulting rms value is an order of magnitude smaller than that of the two-point support. We mentioned a similar improvement for the WSRT antennas earlier. Also here the main strategy for the improvement of the deformation behaviour should be the elimination of large-scale deformation by understanding the load transfer issues at the interface points between the reflector backup structure and the elevation cradle.

Two effects dominate the remaining deformations of the four-point system in the right diagram: the print-through of the four interface points and the sag of the
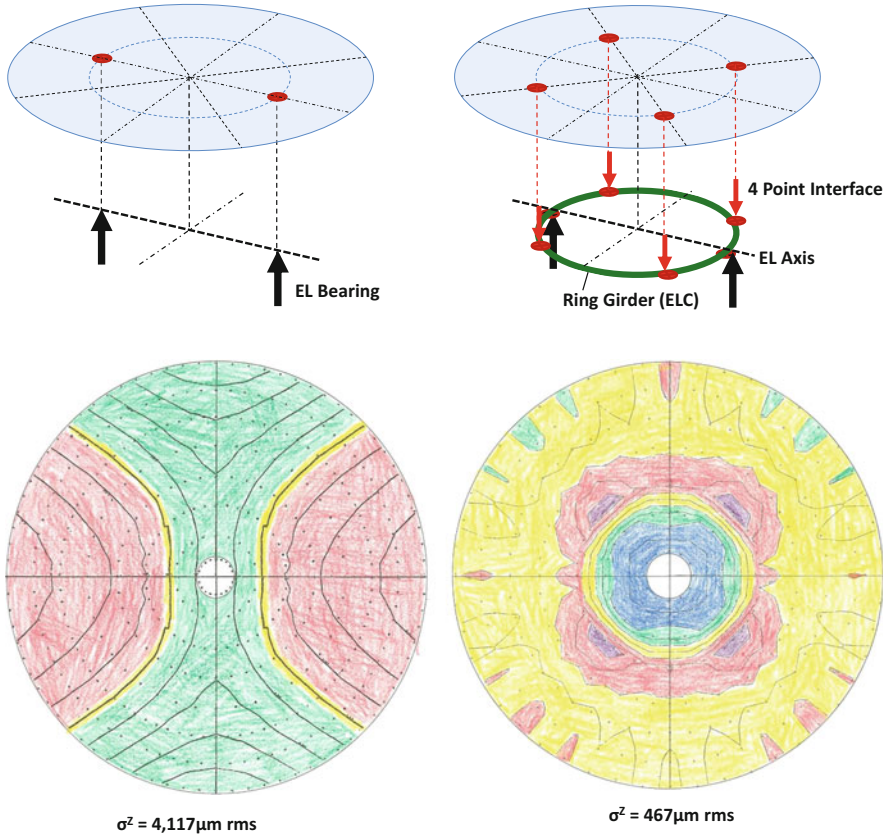
Fig. 4.34 Top: basic geometry and force paths for the two-point (*left*) and four-point (*right*) reflector support. Bottom: Gravitational deformation patterns in zenith position of both layouts. The astigmatism of the two-point is effectively removed by the four-point solution

reflector centre. The astigmatism is completely removed. The design details of the system are shown in Fig. 4.35.

In this design, the ring girder is not placed behind the backup structure as e.g. the similar yoke-type elevation cradle of the MRT (Chap. 5), but is integrated "contact free" into the backup structure. The reason for this arrangement is the deformation behaviour in horizontal position, where otherwise a second-order coma will arise, as explained for the Effelsberg design concepts.

In the horizontal load case, the four-point support behaves much better than other concepts. The rms value in horizon is even lower than in zenith position (Fig. 4.36, right). Also here, the deformation behaviour is dominated by the print-through of the four interface points and a tilt of the reflector centre. A remaining second-order coma can be identified in the pattern, indicating that the lateral load
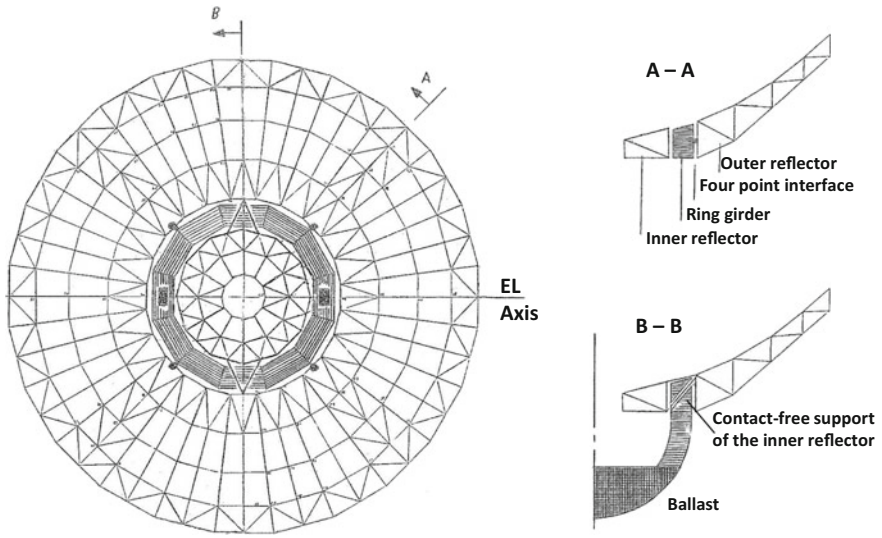
Fig. 4.35 Design concept of 1977 for the four-point support with integrated contact-free ring girder. It was used for the 32-m MERLIN antenna in 1990
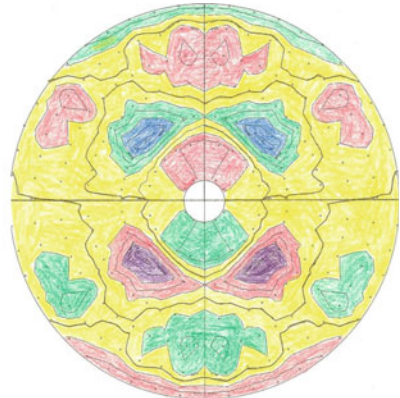
$\sigma^H = 341\mu m$ rms

Fig. 4.36 *Left* Detail of the four-point support with 4 flexure rods connecting to the upper and lower truss nodes (H. Kärcher, MAN). *Right* Gravitational deformation in horizon position. The rms deviation is 341 μm

transfer at the interface points is not perfectly centred with respect to the centre of gravity of the backup structure.

The picture in Fig. 4.36 (left) shows details of the support interface. The inner hoop of the backup truss is completely separated from the outer wall of the ring girder. One of the four interface points is visible (centre) with its four flexure-type

Fig. 4.37 Comparison of measured (*left*) and computed (*right*) gravitational deformation between elevation angles of 35° and 90°. Note that the measured value contains the panel and measurement error

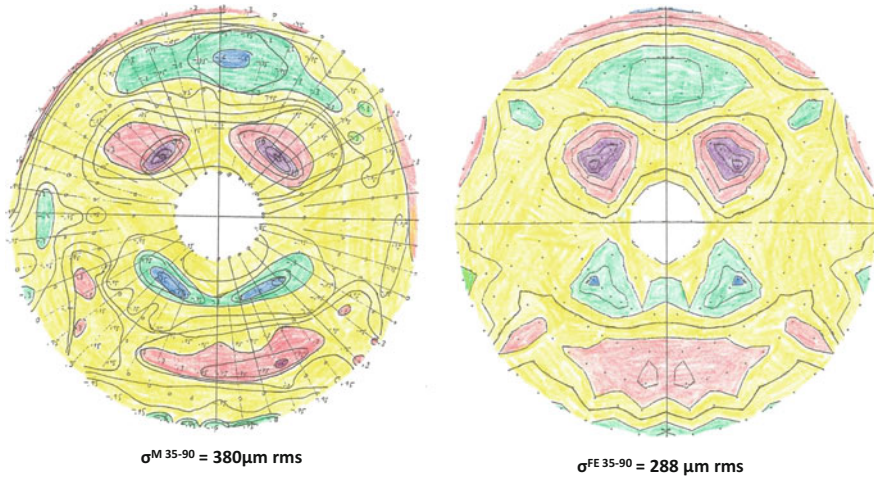rods connecting to the adjacent two upper and lower truss nodes. Their flexibility in radial direction facilitates the decoupling of the backup structure from the ring girder under thermal expansion.

The reflector panels of the telescope are standard aluminium cassette panels with an rms fabrication error of 170 μm. The measurement and setting of the surface was accomplished with an accuracy of 190 μm. The surface was adjusted at 35° elevation angle and measured at zenith position. In Fig. 4.37, we show the measured and computed gravity deformations between these two elevation angles. The measured rms contains the contributions of the panel fabrication and adjustment error. Correcting for those, we obtain a gravity component of 282 μm, remarkably close to the calculated value and a confirmation of the high reliability of the FEA.

4.6.4   The Joined Four-Point Support of the IGN 40-m Telescope

The Spanish Instituto Geografico Nacional (ING) operates the 40-m radio telescope in Yebes, named ARIES XXI. It was built in 2001–2005, based on design studies, which started in 1992. The main purpose of the telescope was for VLBI observations up to 22 GHz, but operation at frequencies to 90 GHz was planned and 200-μm rms overall surface accuracy was specified. A picture of the telescope is shown in Fig. 4.38.

Fig. 4.38 The 40-m diameter radio telescope of IGN at Yebes, Spain (H. Kärcher)

The requirement of a spacious receiver cabin between the elevation bearings naturally led to the adoption of a yoke geometry for the elevation cradle (ELC). The corners of the yoke offer themselves as a four-point support for the reflector. In the 40-m telescope, the ring girder of the MERLIN design is combined with the yoke to form a *joined four-point support* (Fig. 4.39).

From the structural point of view, the corners of the ballast arms provide a joined four-point interface between the ELC, constituted by the yoke with ballast arms and ring girder, and the backup structure trusses. The corner points of the ballast arms, as indicated in the figure, are the equivalent to the ideal four-point interface of the 32-m MERLIN antenna.

The deformation patterns of the optimised structure (Fig. 4.40) show that the zenith load case is dominated by the print-through of the quadripod legs. This is caused by the rather large opening angle of the legs for minimising the aperture blockage. The horizon load case shows the characteristic second-order coma pattern, but the overall rms value in horizon is smaller than in zenith. The optimisation was finished at this stage because the requested accuracy had been achieved.
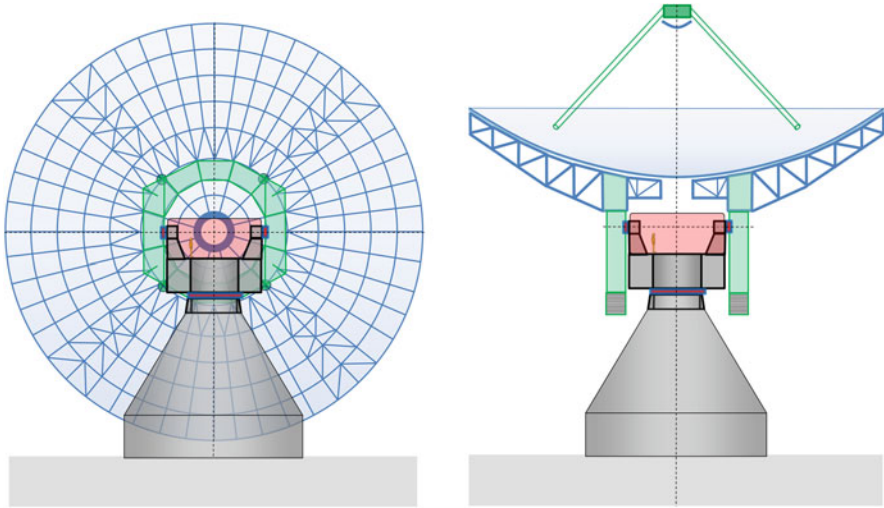
Fig. 4.39 Views of the IGN 40-m telescope design. In the sketch on the left, one notices the dotted four-point connection of the BUS to the ring girder (*green*) of the yoke. On the *right*, the ring girder is placed on top of the yoke arms. The inner section of the surface is not connected to the girder, as in the MERLIN antenna. Receiver cabin is in *pink*

$\sigma^Z = 316\mu m$ rms $\sigma^H = 215\mu m$ rms
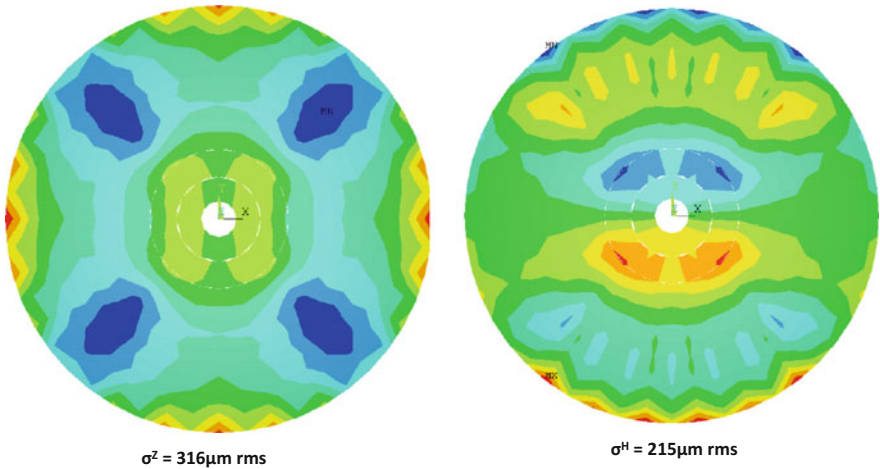
Fig 4.40 Gravitational deformation patterns of the 40-m telescope. *Left* zenith situation with strong effect of quadripod (*blue*). *Right* horizon position with second-order coma as large-scale deformation

4.7   Conclusion

In this chapter, we have introduced design methods that go well beyond the classical methods of bridge building. An essential step was the development of the concept of homologous deformation, introduced by von Hoerner. It allowed the design of antenna structures with "controlled" gravitational deformations that resulted in a reflector surface an order of magnitude more precise without requiring more material. The Effelsberg 100-m telescope remains the prime example of a thorough application of the homology principle. In the late 1970s, attention shifted to the realisation of large telescopes for millimetre wavelengths that required reflector precision of better than 0.1 mm. Requirements beyond pure structural design often did not allow the strict application of the Effelsberg principles. In the next chapter, we discuss the "semi-homologous" and additional methods developed to satisfy the performance and operational requirements of the major millimetre telescopes.

References

Altmann, H.: Die Stahlkonstruktion des 100-m Radioteleskops in Effelsberg. Der Stahlbau. **41**, 321, 360 (1972)

Baars, J.W.M., Hooghoudt, B.G.: The synthesis radio telesscope at Westerbork. General lay-out and mechnical aspects. Astron. Astrophys. **31**, 323–331 (1974)

Baars, J.W.M., van der Brugge, J.F., Casse, J.L., Hamaker, J.P., Sondaar, L.H., Visser, J.J., Wellington, K.J.: The synthesis radio telescope at Westerbork. Proc. IEEE. **61**, 1258–1266 (1973)

Eschenauer, H., Brandt, P.: Über die Optimierung der Tragstrukturen von Parabolantennen. Tech. Mitteilungen Krupp. **30**, 2 (1972)

Findlay, J.W., von Hoerner, S.: A 65-meter telescope for millimeter wavelengths. National Radio Astronomy Observatory, Charlottesville (1972)

Hachenberg, O., Grahl, B.H., Wielebinski, R.: The 100-meter radio telescope at Effelsberg. Proc. IEEE. **61**, 1288–1295 (1973)

von Hoerner, S.: Design of large steerable antennas. Astron. J. **72**, 35–47 (1967a)

von Hoerner, S.: Homologous deformations of tiltable telescopes. J. Struct. Div. Proc. Am. Soc. Eng. **93**, 461–485 (1967b)

von Hoerner, S., Wong, W.Y.: Gravitational deformation and astigmatism of tiltable telescopes. IEEE Trans. Antennas Propag. **AP-23**, 689–695 (1975)

Chapter 5
Emergence of Millimetre-Wavelength Telescopes

The 30-m millimetre-wavelength radio telescope of IRAM, located on Pico Veleta, Spain, is the largest telescope for operation down to 1 mm wavelength. It started operation in 1985 (J. Baars, IRAM)

5.1 Into mm Wavelengths

As mentioned in Chap. 2, a major cause of frustration to the radio astronomer is the extremely poor angular resolution compared to what is provided in the optical domain. One way to overcome this handicap is the use of interferometers or synthesis telescopes. However, there also remained the desire to extend the frequency range of single reflectors to very high frequencies with as large a size as possible, which would both improve the resolution and widen the available window in the electromagnetic spectrum. It led to activities in the development of mm-wavelength detectors and the realisation of reflector antennas capable of observing at wavelengths as short as 1 mm. This posed new challenges to the structural design engineer and to manufacturing, particularly of highly accurate reflector surface panels. We describe the results of these efforts in this and the following chapter by example of some of the telescopes dedicated to the millimetre- and submillimetre-wavelength range.

We recollect that two numbers express the basic specification for a radio telescope:

1. The rms deviations of the reflector surface from the prescribed geometric form must be smaller than 5–6% of the shortest operational wavelength. From the Ruze formula (Chap. 8), an error of this magnitude lowers the aperture efficiency from its long-wavelength value by a further 35–45%. Thus, for a shortest wavelength of 1 mm, the surface error should be smaller than 60 μm.
2. The precision and stability of pointing and tracking should be smaller than one-tenth of the half-power beamwidth. For a telescope of 25 m diameter, operating at 1 mm wavelength, the beamwidth is about 10 arcsec. Thus, the pointing accuracy must be of the order of 1 arcsec.

These specifications must be maintained under operational conditions, notably under the influence of wind forces and variable thermal loading by the Sun, as well as the diurnal variation in ambient temperature.

At mm wavelengths, the earth's troposphere increasingly attenuates the radio radiation with increasing frequency. The main culprit is water vapour. The density of water vapour decreases by about a factor three with every 2 km height above sea level. Thus, mm telescopes are preferentially placed on a high mountain and in a climate with abundant clear sky. As a consequence, there will be full solar irradiation in the daytime and significant radiative cooling at night. In addition, one might expect relatively strong wind on such a high site. The design should be able to cope with these variable loads and preferably the telescope should be available both during day and night.

In the early 1960s, the first antennas specifically built for millimetre wavelengths were the dishes at the University of Texas in Austin (4.9 m diameter) and the Aerospace Corporation in California (diameter 4.6 m). Their original purpose was for atmospheric studies, but in both cases radio astronomers quickly obtained access to explore the "mm sky".

In 1962, NRAO in Green Bank submitted a proposal to the NSF for the construction of a mm telescope of 36 ft (11 m) diameter, usable to a shortest wavelength of 1 mm. The proposal was accepted despite the fact that at the time its outstanding characteristic was the uncertainty of both technical and scientific viability. The design and construction of the telescope required new solutions to achieve the extremely high surface precision of only 50 μm, which had not been reached before even on smaller reflectors. A "state of the art" in receiving components did not exist. First, experimental germanium diodes suitable for this wavelength range were just becoming available and the circuitry had to be developed. But even if the new technology would perform well, what was there to observe? At NRAO, Peter Mezger surveyed the situation in early 1964 and concluded: "*on the basis of our current knowledge we may expect to observe the planets, compact HII-regions, some quasars and perhaps recombination lines of ionised hydrogen*". Nevertheless, the observatory received the go-ahead in 1964 and $1 million to realise the 36-ft telescope at an altitude of 1920 m on Kitt Peak in Arizona. At least, the atmospheric quality at this high and dry site would be an asset for its operation.

First observations from 1968 onwards produced some results along the lines of Mezger's report. Then, in early 1970 a group from the Bell Labs brought its own receiver and detected the spectral line of carbon monoxide (CO, $J = 1 > 0$) at 115 GHz in our Galaxy (Wilson et al. 1970). The importance of this detection lies in the fact that the concentration of CO in interstellar space is directly related to the density of molecular hydrogen, which is the most abundant substance in the universe. Unfortunately, hydrogen molecules do not radiate in the radio and optical wavelength regime, and consequently, their density can only be inferred from observations of other molecules. Carbon monoxide provides this link.

After the detection of CO, the telescope was oversubscribed with observing requests—more than any other radio telescope in the entire USA. NSF's gamble of $1 million paid off and millimetre astronomy became a "hot" field. Mark Gordon has told the story of the 36-ft operation in his book "Recollections of Tucson Operations" (2005). The situation in 1970 is summarised by short descriptions of ten mm telescopes of size between 4.5 and 22 m in a special issue on Millimeter Wave Antennas of the IEEE Transaction on Antennas and Propagation (Cogdell et al. 1970).

5.2 The NRAO 36-ft Antenna

We now present the major features of the 36-ft telescope. The Rohr Corporation in Chula Vista, California, made a feasibility study in 1964 with the conclusion that "a 36-ft telescope with 0.002 in. (50 μm) surface precision should be possible". Later that year, Rohr received a contract worth $600,000 to construct and erect the 36-ft on Kitt Peak.

At NRAO, there were strong differences of opinion about the geometrical layout of the antenna. Up to that time, Frank Low had made mm-wavelength test

observations at 1 mm with a bolometer of his own design attached to a 3-m searchlight. The feed of his receiver worked best at a long focal length, and hence, he requested that the *f*-number of the antenna would be equal to one ($f/D = 1$). This greatly upset the "cm-wavelength" astronomers, who were used to the observatory-wide value of $f/D = 0.42$. They wanted the same number for the 36-ft, which would enable a simple scaling of feed designs to the shorter wavelengths. Moreover, the very long focus support legs would certainly impede the dynamical behaviour and pointing accuracy. Some astronomers even argued in favour of a Cassegrain system. A compromise was reached for prime-focus operation at $f/D = 0.8$. As is obvious from Fig. 5.1, the telescope looks quite different from the examples shown earlier.
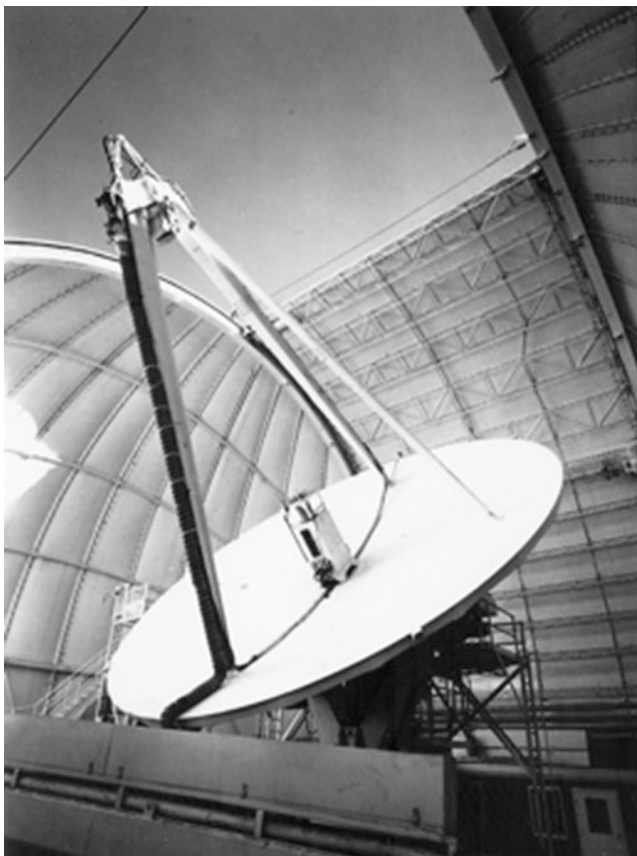

Fig. 5.1 The original NRAO 36-ft millimetre-wave telescope in the dome. Note the unusually "flat" surface and long feed support legs in this $f/d = 0.8$ configuration. The dome fabric is not transparent to the mm waves and observations are carried out with an opened dome (NRAO/AUI/ NSF)

The contractor decided to machine the full surface on a large milling machine after the 11 m diameter dish had been welded together from several sheets of aluminium. This skin was attached to a backup structure of steel. The machining process was quite frustrating in that a carefully made cut, when measured several hours later, would show unexpected and excessive deviations from the required shape. Eventually, it was discovered that the tide of the nearby Pacific Ocean moved the entire milling machine out of the vertical, which led to machining and measurement errors. Thus, machining was restricted to the hours where the influence of the tide was minimal. The telescope reached a surface error of 0.1 mm, a factor two worse than specified.

The bimetallic nature of the aluminium skin and steel backup pulled the reflector out of shape with varying temperature. Some of the gain loss caused by these large-scale deformations could be corrected by a refocusing of the feed. But successful observing was normally restricted to the night-time, avoiding any solar influence. The turret-type alt-azimuth mount required a computer-based positioning and servo system. A direct drive was realised with torque motors, an advanced but trouble-prone system.

The antenna was placed in a protective enclosure, which could be opened over the width of the reflector. The dome removed the need to design the antenna for survival in extreme weather conditions. In addition, clever planning of the observations by looking in the downward direction decreased the influence of wind. But the dome did not significantly ameliorate the temperature effects.

Despite a noticeable amount of difficulties, the telescope became heavily used. In the early 1970s, it was the largest mm telescope with state-of-the-art receivers in the world. Several tens of molecules in the interstellar space were discovered with it, demonstrating the relevance of the mm-wavelength range for astrophysics.

By the middle of the 1970s, plans for large mm telescopes were being made in Europe (Germany, France and the UK), Japan and at NRAO, where a proposal for a 25-m antenna was advanced. Its design was based on an earlier in-house 65-m telescope study (see Chap. 4). While this proposal went its very slow way through the administrative process, NRAO replaced the 36-ft dish in 1983 with a new 12-m diameter reflector in Cassegrain configuration with a panelled surface on a truss-frame backup structure (Fig. 5.2). This telescope operated with significantly increased efficiency until it was decommissioned in 2003.

There are parallels between the story of the 36-ft and that of the 140-ft, told in Chap. 3. In both cases, NRAO initiated a plan for a revolutionary radio telescope that the contractors did not manage to realise on specification, cost and schedule. Nevertheless, both instruments opened new regimes of observation and NRAO worked successfully to ameliorate the shortcomings of the telescopes by providing the best possible receivers and observer support. Both telescopes were among the most productive instruments during their lifetime.

The proposed 25-m antenna was never built and NRAO concentrated its further efforts on the realisation of a large millimetre-wavelength synthesis array. Both in Europe and Japan, large mm telescopes were constructed in the early 1980s. Some of these included major technology advances that enabled millimetre-wavelength

Fig. 5.2 The second-generation surface of the NRAO mm telescope. The size of the dome allowed a diameter of 12 m. Surface panels from EESCO are supported by a truss-frame BUS designed at NRAO. The focal ratio was reduced to 0.42 and the system operates in Cassegrain mode (NRAO/AUI/NSF)

astronomy to become a major field of research and discovery. We describe some of these instruments in the following sections.

5.3   The IRAM 30-m Telescope (MRT)

5.3.1   Introduction: Performance Specification

By the time the large Effelsberg radio telescope became operational, the Max-Planck-Institut für Radioastronomie had grown to its planned size with three directors: Peter Mezger (1928–2014) and Richard Wielebinski joined the founding director Otto Hachenberg in 1970. Mezger had participated in the initiation of millimetre-wavelength research at NRAO and was keen to expand the observing capabilities of the Institute into the millimetre-wavelength range, well beyond the capabilities of the Effelsberg telescope. In 1973, he proposed to build a 30-m diameter telescope for millimetre wavelengths, located at an atmospherically excellent site. This proposal was accepted in the context of the German government's program *Grossprojekte* (Big Projects) and funded in 1976 by a grant from the Volkswagen Foundation.

A contemporary initiative in France towards the construction of a millimetre interferometer array led to an international collaboration and resulted in the creation of the French-German *Institute for Radio Astronomy in the Millimeter Range* (IRAM) in 1979. The German contribution, a 30-m millimetre radio telescope, was placed at 2850 m altitude near the Pico Veleta in the Spanish Sierra Nevada near Granada, while the array of three antennas of 15 m diameter was located at 2550 m altitude on Plateau de Bure in the French Alps between Grenoble and Gap (see also Chap. 6).

Based on the excellent success of their joint effort in the design and construction of the Effelsberg telescope, the MPIfR invited the companies *Krupp Industrietechnik* and *MAN Gustavsburg* to form a consortium for the design and realisation of the mm telescope. The 30-m telescope was constructed between 1979 and 1984. In this project, the authors collaborated for the first time, JB as MPIfR project manager and HK as lead engineer of MAN. We describe now the design and performance of this instrument, which is one of the most productive mm telescopes of the last 30 years.

Similarly to the Effelsberg project, the MPIfR issued a compact Performance Specification and a Statement of Work (SOW, *Pflichtenheft*) for a study of four alternative design concepts. One concept should follow the Effelsberg design principles. A second should provide a large receiver cabin with convenient access. Alternative concepts were allowed to follow individual ideas of the engineers in the companies.

Experience with other telescopes, notably the NRAO 140-ft and the new Effelsberg 100-m telescope, had indicated the necessity of controlling the environmental effects of wind and temperature and in particular the need to match the surface quality with the pointing requirement. Thus, in the specification of the new mm telescope, the equal importance of surface and pointing accuracy was put forward as the major requirement for the design. This led to several novel structural design ideas. The instrument was to satisfy the following performance specifications:

1. Alt-azimuth mounted 30-m diameter telescope, primary focal ratio 0.35.
2. Operational environmental conditions of 10 m/s stationary wind with a gust factor of 20%; thermal loading during day (solar heating) and night (radiation towards clear sky) at a site above 2000 m.
3. Unimpeded performance at 2 mm wavelength with a goal of acceptable performance at 1.3 mm under the defined environmental conditions. This was quantified to: reflector precision <100 μm, pointing and tracking precision and stability <2 arcsec.
4. Control of thermal effects during operation and extreme environmental situations.
5. Cassegrain optics with a large receiver cabin, preferably with a Nasmyth focus.
6. Survival in 200 km/h winds together with an ice load on the telescope of 30 cm.

The SOW prescribed the design process and can be seen as a model for other projects. After the drafting of the different concepts, the two most promising would

be selected for a detailed engineering analysis. This included the definition of the design load cases, a computer-aided deformation analysis by finite element analysis (FEA), a dynamic analysis for the assessment of the structural resonances and error budgets for surface and pointing precision. In addition, the layout of the motors and drives, an interior forced air circulation system to control thermal gradients and a heating and de-icing system, including an energy budget, was required. Finally, a cost estimate for the alternatives should be presented. At the end of this conceptual part, one of the alternatives would be selected for final design and realisation.

The final design phase then had to cover the specification and design of all subsystems, wind tunnel tests for the selected configuration, detailed subsystem verification by calculation or tests and manufacturing, installation and commissioning plans. The whole design process can be taken as exemplary for a well-organised project with unprecedented requirements.

The companies formed the ARGE-MRT (*Arbeits-Gemeinschaft-Millimeter Radio Teleskop*) for the design and construction of the new millimetre telescope, which we refer to with the acronym MRT. Each of the companies presented three conceptual designs, of which one was selected almost without change. Its structural design, while aiming at homologous behaviour, departs significantly from the Effelsberg homologous design. The major and essential deviation from the "umbrella" support structure resulted from the requirement to provide a large, easily accessible receiver cabin. With the size of the reflector of 30 m, the umbrella had to be abandoned and other means for obtaining a homologous structure had to be found. The chosen solution is of general interest and has been used in several later telescopes.

5.3.2 The Design Selection

Cross-sectional views of the conceptual proposals are shown in Fig. 5.3.

– Version 1 represents the attempt to scale down the Effelsberg design concept from 100 to 30 m concurrently with the arrangement of the requested receiver cabin of at least 3 m diameter behind the main reflector vertex. For this purpose, the designers arranged a long central steel tube behind the reflector from the vertex to the elevation wheel, which allowed in a virtual way the arrangement of the BUS and ELC pivots on the symmetry axis of the elevation structure as requested by the Effelsberg principle (see Chap. 4). The diameter of the elevation wheel looks disproportionate compared with the reflector structure, and the whole design makes a rather clumsy impression.
– Version 2 was only a slight variant of version 1, which we do not show here.
– Version 3 uses the same design concept with the central steel tube behind the reflector but changes the elevation cradle ELC to a four-point concept with two sideward elevation wheels of much smaller diameter similar to the original MAN design concept for Effelsberg. The size of the alidade is reduced by
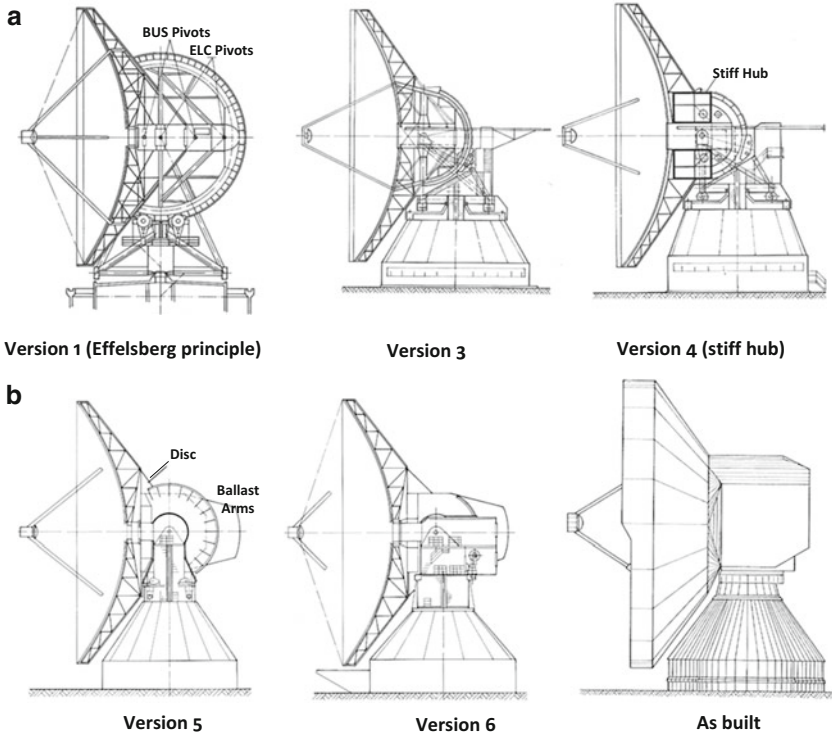
a

BUS Pivots
ELC Pivots

Stiff Hub

Version 1 (Effelsberg principle)   Version 3   Version 4 (stiff hub)

b

Disc

Ballast
Arms

Version 5   Version 6   As built

Fig. 5.3 (**a**) First design variants of a 30-m diameter mm telescope. (**b**) Final variants—Version 5 was realised with an insulating cladding covering the entire telescope

placing the azimuth track on a conical tower, resulting in a large offset between the elevation and azimuth axis. The design looks better but not mature.

– Version 4 is similar to version 3 but introduces a stiff hub, which allows the placement of one central elevation wheel of much smaller diameter than in version 1. The stiff hub shows some resemblance to the hub of the Parkes telescope. MAN applied it to several communication antennas with a lower reflector accuracy (Chap. 4). A structural optimization was executed and showed the feasibility of the design including the demanding 100 μm rms requirement. But the concept was abandoned for reasons of access to the receiver cabin in the hub area.

– A breakthrough was achieved in Version 5 with a new concept that solved the arrangement and access problems for the receiver cabin. The major step in version 5 was to abandon the Effelsberg cone and substitute it by a slender disc. The disc is carried on the rear by two sideward-arranged elevation wheels similar to version 3, which carry also the ballast; we call these *ballast arms*. The space between the ballast arms allows the arrangement of a receiver and drive cabin with excellent access and without any hindrance by reflector supporting structures.
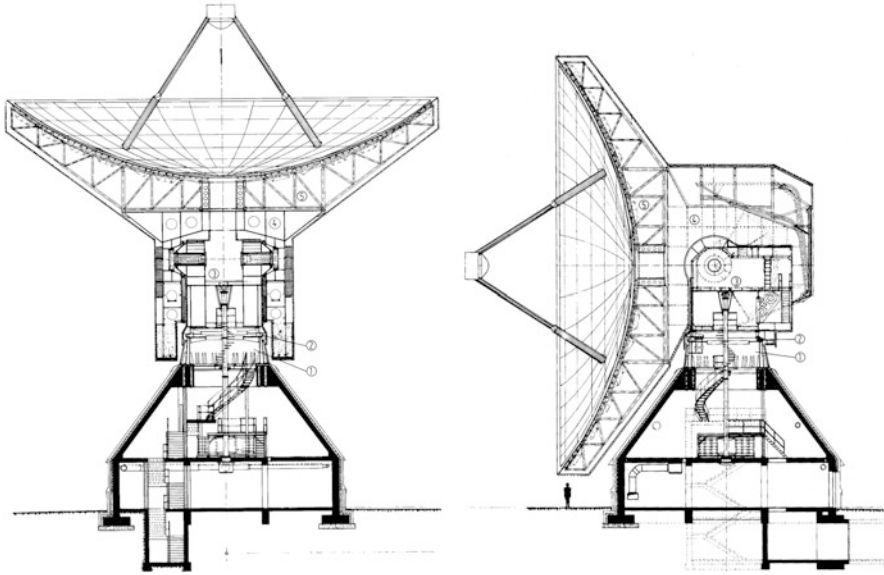
Fig. 5.4 Cross sections of the 30-m millimetre telescope—MRT

– Version 6 is similar to version 5 with improvements in the area of the alidade and a larger receiver cabin. This design has been realized. The last sketch in the figure on the right shows a view of the telescopes with its outside cladding, protecting all load carrying structures against wind, sunshine, rain, snow and ice.

Cross sections of the final design are shown in Fig. 5.4. The antenna is of the *turning head* type with the azimuthally rotating part supported on a concrete tower. The upper part of the elevation yoke structure is a cone section ending in a round and flat plate of 14 m diameter. The homologous reflector backup structure in the form of a steel truss frame is supported at 20 points on the periphery of the flat plate.

Contrary to the Effelsberg solution, the quadripod for the support of the secondary reflector is directly connected to the backup space frame and, most importantly, included in the finite element analysis (FEA) of the reflector in order to achieve an optimum behaviour of both surface and pointing precision. Above the pedestal and behind the reflector is a two-storey cabin, which houses the drive systems on the lower floor and provides a large cabin for the receivers at the Nasmyth focus. A picture of the MRT is shown in Fig. 5.5.

The reflector consists of 420 panels in 7 rings, made by Dornier. The panel is a composite of aluminium honeycomb core of 40 mm thickness to which top and bottom sheets of 1.5 mm thick aluminium are epoxy bonded. The paraboloidal form is obtained by stretch forming on a mould. Based on the experience with similar panels on the Effelsberg telescope, great care was taken in assuring hermetically sealed panels to avoid penetration of humidity, which tends to delaminate the bond.

Fig. 5.5 The MRT is covered on the outside with thermal insulation. The skin of the cladding can be heated to avoid ice deposit. The extended rim at the top of the reflector avoids ice or snow to fall onto the reflector surface (IRAM)

Two panels of approximate size 1×2 m^2 are placed on an intermediate support frame that is mounted on the BUS through adjusters on its four corners (Eschenauer et al. 1980). The panels are attached to the frame by 15 adjusters, preset in the shop on an accurate 3D measuring machine. The MPIfR actively participated in this effort. An average accuracy of 27 µm per unit was achieved, a factor two better than specified.

The subreflector of 2 m diameter is one of the first accurate reflectors to use CFRP as the outer skin of a composite panel with an aluminium honeycomb core, made by Dornier Systems. The reflecting side was metallised by flame spraying a thin layer of aluminium. This has proven to be a reliable solution. After 30 years of use, the reflector does not show deterioration in mechanical or electromagnetic behaviour.

A widely used method to suppress atmospheric fluctuations is to make differential observations between neighbouring patches of sky. This can be achieved by nutating the subreflector between two radial positions. The MRT nutator, designed by one of us (HK), allows the antenna beam to switch between directions several arcminutes apart on the sky at about 1 Hz frequency.

The requirements for accuracy and stability of pointing and tracking of ~1 arcsec posed a challenge to the designers. A state-of-the-art system was developed in collaboration between Krupp, the University of Bochum and the MPIfR. Special

hardware to improve the resolution of the best available angle encoder was developed at MPIfR. Commissioning took time, but the required performance was achieved.

To summarise, the major novel aspects of the 30-m MRT are:

1. Nasmyth configuration with large, continuously accessible receiver cabin
2. Inclusion of the quadripod in the structural design of the BUS and the resulting small pointing variation. Simultaneous optimisation of both surface and pointing quality
3. Active thermal control, including insulation, heating/cooling with air circulation in BUS
4. Intermediate panel frames with pre-adjusted panels
5. Axis control system with state controller
6. Nutator for a 2-m diameter secondary
7. Lightweight subreflector of CFRP/Aluminium honeycomb composite.

The specified and actually achieved parameters of the MRT are assembled in Table 5.1.

5.3.3   The Structural Concept of the MRT

A sketch of Effelsberg and the MRT to the same scale (Fig. 5.6) shows the difference in size, which illustrates immediately the issues with the arrangement and access of the Cassegrain focus and receiver cabins. Effelsberg is so large that it allows a receiver cabin behind the reflector and within the cone structure with enough space for people to walk around. For the size of the MRT, a similar cone would completely block the possibility for the placement of an accessible cabin.

But how can we realise a homologous behaviour of the reflector structure? The designers of version 6 solved this question by cutting the cone into four quarters and lifting the cone pivot to four points in the corners of a square disc (Fig. 5.7). Together with the ballast arms, the disc forms a yoke-type structure that is equivalent to the elevation cradle ELC of Effelsberg and leaves in the centre the necessary space for the arrangement of the receiver cabin.

The disc is extended up- and outwards to a circular size of 14 m diameter (Fig. 5.8). The truss-frame BUS is supported at 20 points on the circumference of the disc and homologous deformation behaviour is thereby achieved (Brandt and Gatzlaff 1981). We explain this below in some detail.

The MRT design process resulted in a transition from a wheel-on-track design to a turning head or turret design. This has notable implications for the design of the reflector supporting structure but also of the alidade, in particular the azimuth axis mechanisms. In regard to functionality, the turret-type pedestal is more appropriate for smaller telescopes, where the homology requirement is less stringent. The design of the MRT demonstrates that such a layout can be realised successfully with large reflectors of very high surface accuracy.

Table 5.1 Specified and achieved characteristics of the MRT

| Characteristic	Specification	Actual	Unit
Primary reflector diameter	30	30	m
Secondary reflector diameter	2	2	m
Focal ratio primary/secondary	0.35/7.0	0.35/7.0	
Overall reflector rms accuracy	100	70	μm
Subreflector rms accuracy	25	15	μm
Pointing/tracking accuracy	2	1–2	arcsec
Lowest structural natural frequency	3	2.8	Hz
Panel fabrication accuracy (rms)	50	27	μm
Backup structure deformation (rms)	50	50	μm
Wind (12 m/s) deformation (rms)	35	30	μm
Temperature differences in structure	<1	~1	K
Quadripod geometrical blocking	<7	4	%
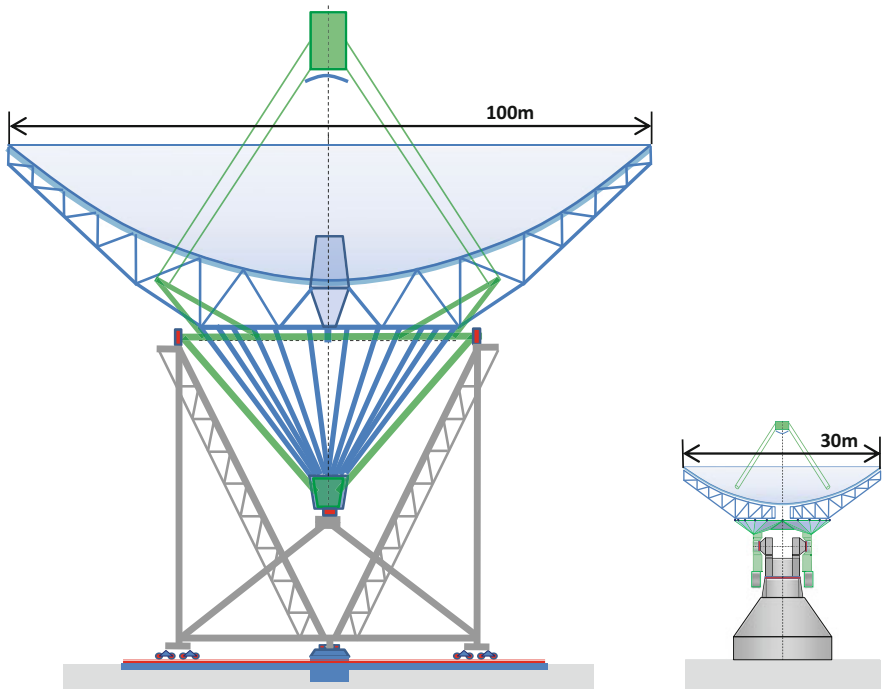
Fig. 5.6 The concepts of the 100-m Effelsberg and the 30-m MRT drawn to the same scale. Colour code: *blue*—reflector backup structure, *green*—elevation cradle and *grey*—alidade
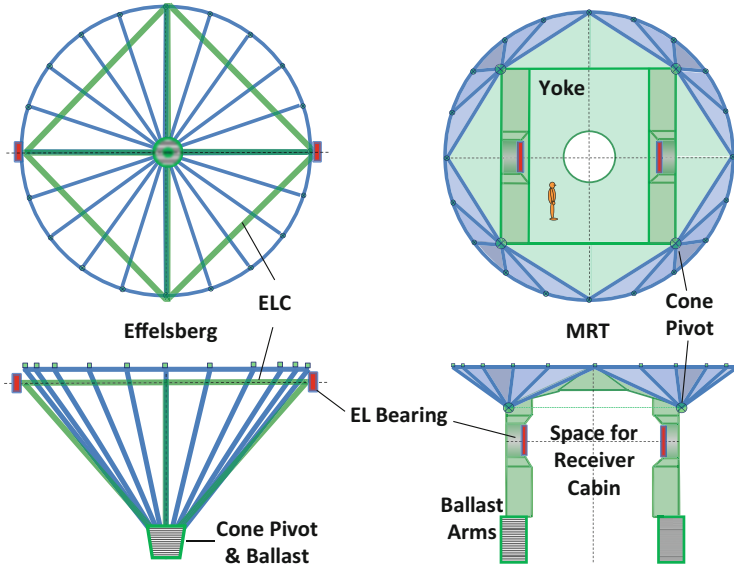
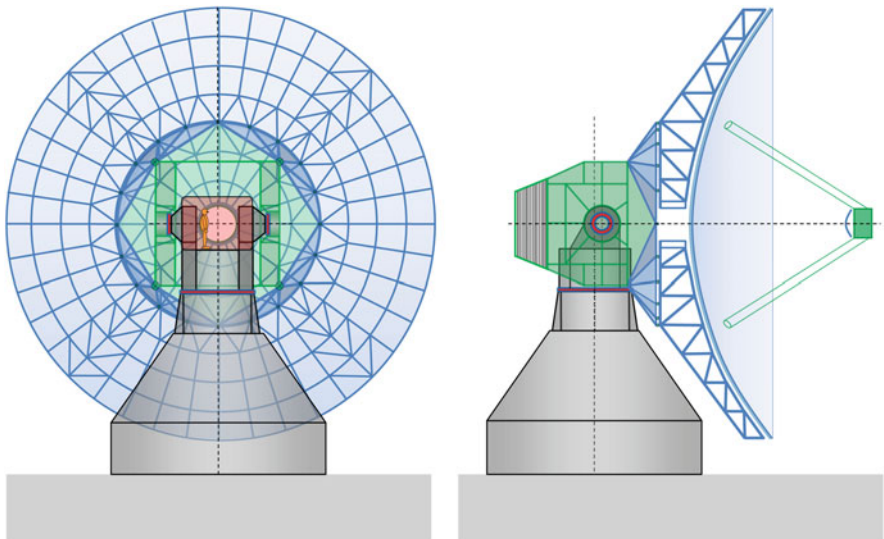**Fig. 5.7** BUS/ELC interface in Effelsberg and MRT (not to same scale)

Fig. 5.8 Rear and side view of the structural arrangement of the MRT

5.3.4   The Deformation Behaviour of the MRT

The feasibility of the four-quarter cone concept was verified by computer-aided structural optimization based on finite element calculations. The examination of the deformation patterns of the two basic gravity load cases gives some insight into the remaining homology issues.

5.3.4.1   Load Case in Zenith Position

A look into the calculation sequences as described in the project documents shows that favourable values in zenith position were reached by a trick with the ballast location in the ballast arms (Fig. 5.9). At the beginning of the optimisation process, the ballast was arranged directly under the centre of the elevation bearings (left sketch), and the deformation pattern showed a large astigmatism, caused by the bending of the yoke between the bearings. This could be counteracted by an offset arrangement of the ballast against the bearings (right sketch). The calculations showed that an offset of 1.35 m would compensate this astigmatism very well, leaving a small spherical aberration. The rms error could be diminished from 96 to 44 μm!

The details of the deformation pattern in zenith (Fig. 5.10, a hand-drawn rendering of the FE results) give some hints on the remaining structural disturbances. First, we can see the circular print-through of the 20 support points of the BUS girders on the yoke disc (20 green dots in the figure). Also some remaining influence of the four pivot points of the yoke is visible, which causes on the outer rim of the reflector the four humps on the 45° axes and the four valleys on the horizontal and vertical axes. On the whole, the level of homology is quite good and, as in Effelsberg, much better than that for the horizontal load case.

Fig. 5.9 Optimisation of the ballast position with respect to the centre of the bearing. This counteracts the astigmatism, lowering the gravitational deformation from 96 to 44 μm rms
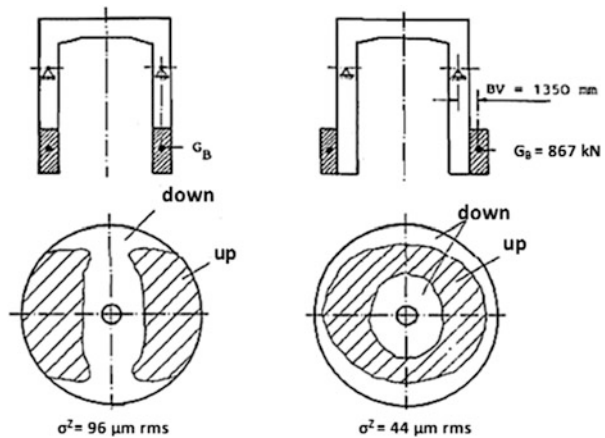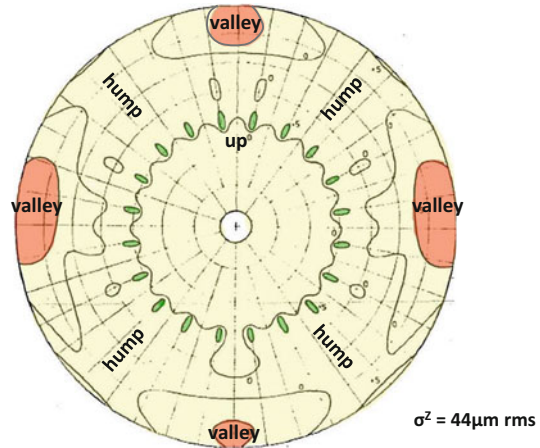
Fig. 5.10 Gravitational
deformation pattern in
zenith position after
structural optimisation of
Version 6. The resulting rms
error is 44 μm

5.3.4.2   Load Case in Horizon Position

At this stage of the optimization process, the deformation at the horizon showed an
rms of 105 μm, more than twice the zenith value. The deformation pattern shows a
higher order coma (Fig. 5.11) and is very similar to that of Effelsberg (Fig. 4.26).
The cause is the same as in Effelsberg: the lever arm between the centre of gravity
of the BUS and the circular interface to the yoke disc.

   The coma is so dominant that the other structural deficiencies, which were
identified for the zenith load case, are barely visible. Looking into some details,
the print-through effect of the 20 supporting points between the BUS girders and the
yoke disc can be seen in the figure as small wiggles around the two central islands.
Also clear are the strong distortions at the edge of the reflector, which are difficult to
interpret.

   At this stage of the design process, assuming an alignment elevation angle of
55°, the design goal of better than about 60 μm rms (gravity only) was achieved.

5.3.4.3   The Deformation Behaviour of the Final Improved Design

Still, the difference between horizon and zenith deformation of more than a factor
two was unsatisfactory. At the beginning of the realisation phase, two further design
changes of the reflector structure were applied, which resulted in a more balanced
final deformation patterns with rms values of 61 and 83 μm in zenith and horizon
position, respectively (Fig. 5.12).

   The main reasons for these design changes were:

1. The *quadripod* shows in horizontal position a large sag (Fig. 5.13, left), which is
   partly caused by the cantilevers used for the connection of the quadripod legs to
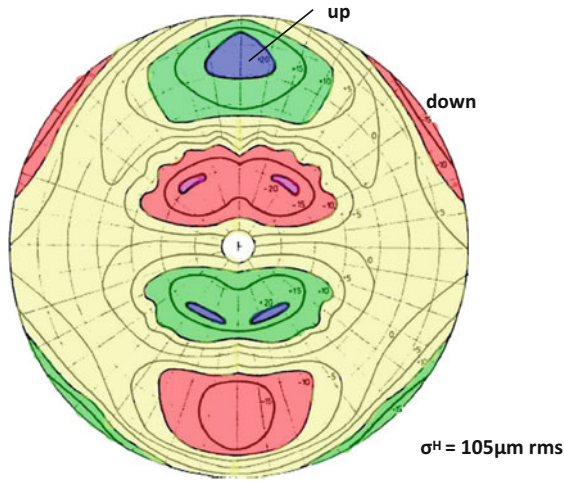   the elevation structure independent from the BUS structure, as implied by the

Fig. 5.11 Gravitational deformation pattern in horizon position shows a second-order coma with an rms error of 105 μm
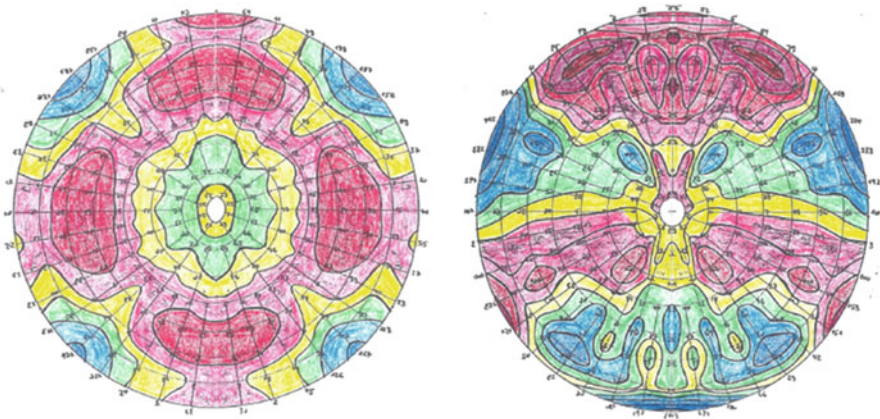

Fig. 5.12 "Hand-made" surface contour plots of the final design of the MRT with plot interval of 50 μm, zero between *pink* and *yellow*, reddish is positive. Shown is the gravity load case for zenith with 61 μm rms (*left*) and horizon with 83 μm rms (*right*)

Effelsberg design principle. A second significant contributor to the sag is the internal bending of the legs itself. This weakness has not only an influence on the gravity deformations but also on the dynamic behaviour of the whole reflector system. In the final design (Fig. 5.13, right), we breach the *independent support principle* and connect the quadripod legs directly and stiffly to the upper and lower chords of the four radial girders in the 45° planes of the BUS trusses. The resulting deformations at the footprints of the quadripod legs are visible in the deformation pattern in zenith (Fig. 5.12, left). The surface error is increased from
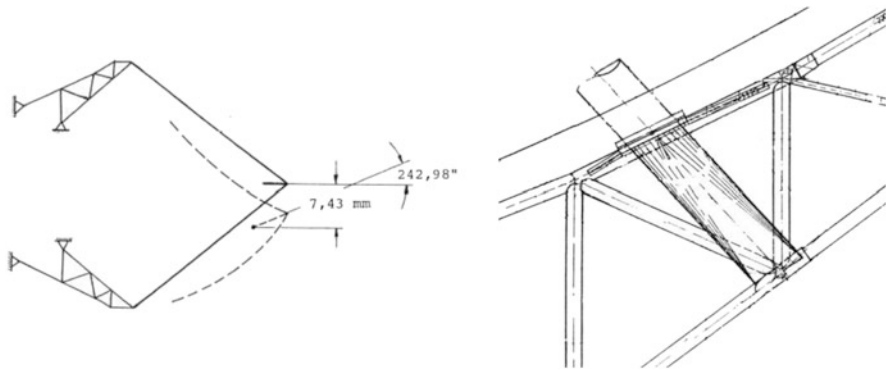
Fig. 5.13 Redesign of the quadripod attachment. In Version 6, the support on the ELS leads to large deformations of the quadripod and the reflector in horizon position (*left*). Attaching the quadripod directly to the BUS improved the pointing markedly but led to an increase in the reflector deformation in zenith position

44 to 61 μm rms, but this value is within the limits of the surface error requirement and could be sacrificed for the much better deformation and dynamic behaviour of the quadripod itself.

Once the independent support of the quadripod was abandoned, the engineers studied how the fixation of the quadripod would affect the pointing behaviour of the Cassegrain system. As mentioned earlier, an important requirement for the telescope is to show commensurate surface and pointing precisions. The final design of the quadripod arrangement within the overall BUS structure aimed at a balancing of surface and pointing error. A very good pointing behaviour over the elevation range was achieved by a compensatory effect between the bending of the main reflector and the quadripod. The static pointing error due to gravity between the zenith and horizon is 20 arcsec in the secondary focus, compared to 80 arcsec in the primary focus. These are stable values, which can be absorbed in the pointing model of the telescope. The advantage of a small error is the proportionally smaller varying error under wind influence. The calculated pointing jitter under wind of 12 m/s is less than 1 arcsec. This excellent behaviour has been confirmed in actual operation.

2. The second change concerned the higher order coma in horizon position. The designers were aware of the coma problem and introduced additional struts in the centre area (Fig. 5.14) that connect the BUS to the centre of the yoke in tangential direction. These reduced the offset of the forces transferring the weight of the BUS to the yoke (as explained for the Effelsberg reflector in Chap. 4). The coma-induced surface error in horizon position was thereby reduced from 105 to 83 μm rms. We have now achieved a better balance between the zenith (61 μm) and horizon (83 μm) deformations.
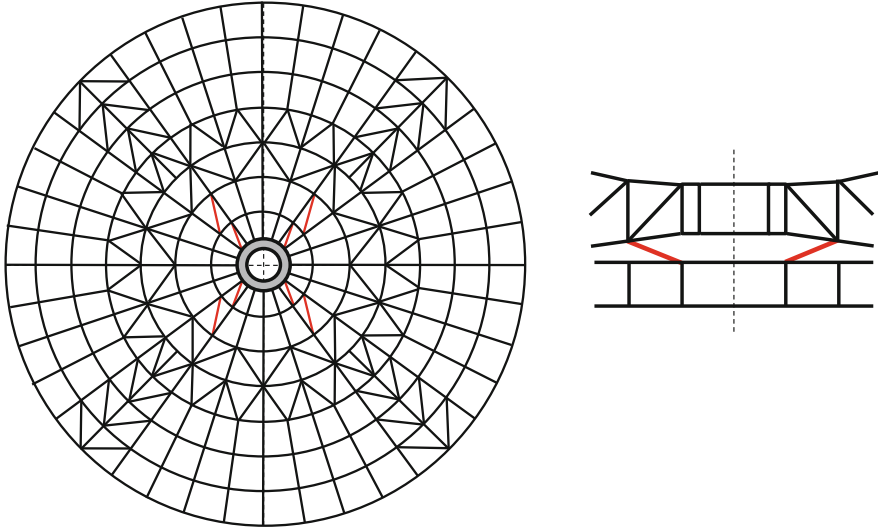
Fig. 5.14 Additional struts in the BUS–ELS interface (*red*) reduce the coma and improve the deformation pattern at the horizon significantly

5.3.5   *Overall Surface Error of the Actual Telescope*

The improvements between version 6 and the telescope as actually built, just mentioned, were relatively small but worthwhile and the remaining gravity-induced surface errors are, as explained, the radial bending of the BUS in the zenith and the second-order coma on the horizon. Further improvement was not necessary because the requirements had been satisfied (Eschenauer et al. 1977).

This is illustrated in Fig. 5.15, where the rms value of the gravitational deformation is shown as function of elevation angle. It is assumed here that the reflector surface has been adjusted at an angle of $50°$. We see that the maximum gravitational error has been reduced to 55 μm at the extreme positions of zenith and horizon. In practice, observations are rarely performed above an elevation of $80°$, where there is very little sky, and below $15°$, where the atmospheric absorption becomes prohibitive; this means a maximum gravitational error of 40 μm.

The computed deformations in the zenith and horizon positions are shown in the contour plots of Fig. 5.16. The deviations are predominantly large scale and stay well within the specification.

There are of course other causes for surface deformation, such as variations or gradients of temperature and wind forces. Fabrication errors of the surface panels, as well as alignment errors, are other important contributors to the final overall reflector quality of the antenna. We discuss these aspects in the following sections and will finally bring them together to look at the best compromises to obtain an optimum balance between technical effort and final performance.
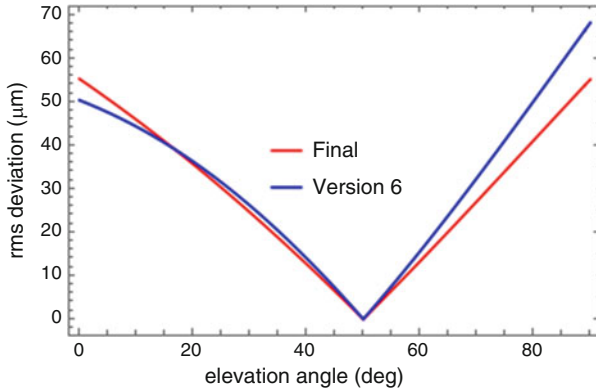
Fig. 5.15 The rms gravitational error as function of elevation angle for Version 6 and the final improved version of the design. It is assumed that the reflector has been perfectly adjusted at an elevation angle of 50°
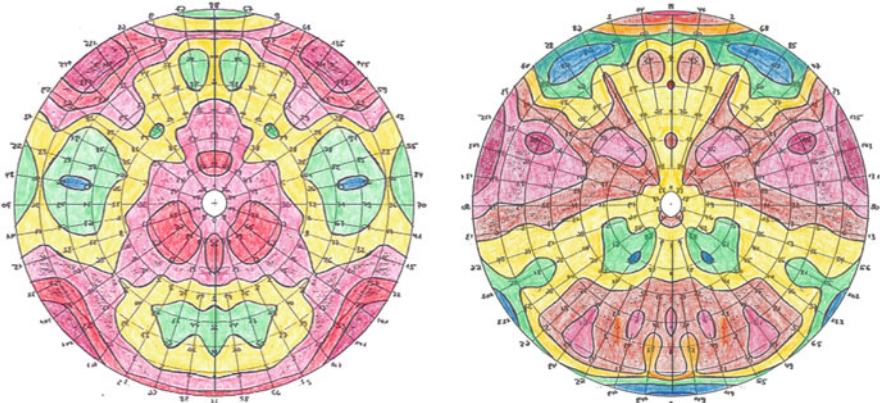

Fig. 5.16 Computed contour plots of the gravitational deformation of the MRT in horizon (*right*) and zenith (*left*) position for an adjustment angle of 50°. Contour interval is 50 μm with zero between *yellow* and *pink*. The rms value at these extreme angles is 55 μm

5.3.6   Thermal Effects and Their Control

We noted already that to reach the telescope specification, it would be necessary to minimise thermal effects. The main cause of outside disturbance in the thermal balance of a telescope is radiation. The surfaces are cooled by their own infrared radiation to the sky and immediate surroundings, which acts during day and night, and heated by the incoming solar radiation during day. Both effects are attenuated by convective heat exchange between the surfaces and the surrounding air. The thermal unbalance leads to a deterioration of the reflector surface precision and to pointing errors. An important parameter is the time constant of thermal changes in different sections of the telescope. Insulation and an appropriate surface treatment of structural members can decrease the magnitude of temperature variations in the structure.

The telescope is first of all subjected to the daily variation in ambient temperature. Then there is the direct radiation from the Sun during daytime, the radiation from the sky/atmosphere and the radiation of the different telescope sections towards the surrounding. The convective heat exchange with the environment is strongly dependent on the velocity of the wind. Considering that the telescope will change its position with respect to the sky and the environment during the day, there is an intricate interplay between the outside influences and the thermal parameters of the structure in reaching thermal balance. To achieve the required uniformity and stability of the structure, needed for the specified performance of the MRT, special measures must be taken, such as insulation, forced cooling/heating and special paint (Baars et al. 1988).

The design process indicated the need for a rather elaborate thermal control system for the BUS consisting of an insulating outside cladding and an air circulation system within the BUS. The large difference in the mass distribution (mass to surface ratio) between BUS and yoke (elevation cradle ELC) leads to a varying temperature difference between the two. This will cause differential expansion and hence lead to structural deformation. We look at the consequences of this now.

The pertinent data are listed in Table 5.2. The two time constants τ refer to a transient (subscript t) and periodic (subscript p) temperature variation; the total surface area of the outside cladding of the structure is denoted A_S.

The BUS is as a truss system of a rather filigree geometry with a lot of empty space between the structural members but with a relatively large outer surface area. The mass to surface ratio μ is

$$\mu_{BUS} = M_{BUS}/A_{BUS} = 79\,\mathrm{kg\,m^{-2}}$$

The ELC is a box-type girder, hence rather compact with a relatively small outer surface area. Here, the mass to surface ratio is

$$\mu_{ELC} = M_{ELC}/A_{ELC} = 760\,\mathrm{kg\,m^{-2}}$$

Table 5.2 Physical parameters of the steel structure of the MRT

Parameter	Unit	BUS	ELC
Heat capacity	$\mathrm{J\,kg^{-1}\,K^{-1}}$	470	470
Mass	10^3 kg	135	152
Total heat capacity	10^6 J $\mathrm{K^{-1}}$	63.5	71.5
Insulation	$\mathrm{kJ\,m^{-2}\,K^{-1}\,h^{-1}}$	4	4
Cladding area A_S	$\mathrm{m^2}$	1700	200
Heat throughput	$\mathrm{MJ\,K^{-1}\,h^{-1}}$	7.8	0.8
τ_t—transient	h	9.3	89.3
τ_p—periodic	h	4.5	5.8
α_s—atten. coeff.	–	0.37	0.04

about 10 times larger than that of the BUS. Consequently, the thermal time
constant for a transient load of the ELC is also about 10 times larger, as shown in
Table 5.2 (89.3 vs. 9.3 h).

It is clear that such different time constants will lead to time-dependent differ-
ences in the temperature of these major structural components. This is illustrated in
Fig. 5.17 for an assumed diurnal ambient temperature variation from −10 to +10 °C.
The ELC follows outside temperature changes with a phase lag of 6 h, but the
amplitude of the temperature change of the ELC structure is only 4% of the outside
changes. For the BUS, the attenuation coefficient α_s is 37%, and consequently, an
outside temperature change with 10 K amplitude results in a temperature change in
the structure of 3.7 K. Apart from two small intervals, there will always be a
significant, time variable temperature difference between BUS and ELC, which
leads to significant large-scale deformation of the BUS.

This simple example already shows that some form of thermal control of the
MRT will be necessary to achieve the specification. In fact, the difference in
temperature between BUS and ELC must be limited to <1 K. An obvious approach
for the improvement of the thermal behaviour of the BUS is to decrease the heat
throughput of the outside surface by increasing the insulation of the cladding (see
Table 5.2). There are practical limits to this. The value in the table pertains to the
actual 5-cm polyurethane foam insulation. Improving the insulation to reach the
required attenuation factor of 4% is beyond practical limits. For this reason, the
BUS of the MRT has been equipped with an active temperature control system. An
air circulation system within the BUS is realised by five large fans and a system of
radial, perforated ducts that creates a circumferential "wind" of about 2 m/s. The air
can be heated or cooled as required to keep the BUS at a temperature equal to that of
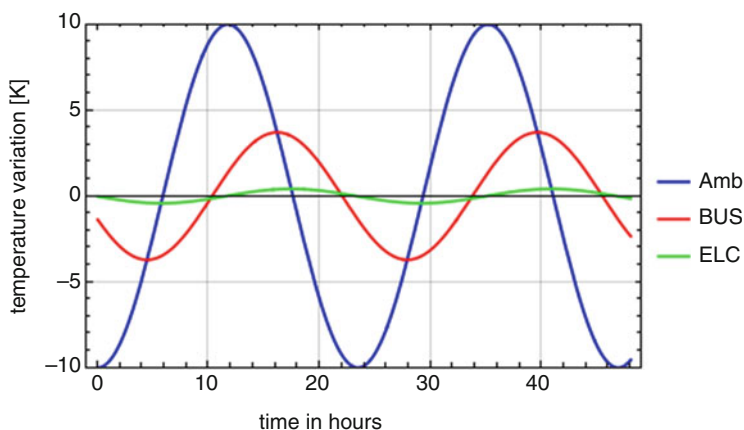the ELC to about 1 °C.

Fig. 5.17 A sinusoidal variation in ambient temperature of 10 K amplitude (*blue*) changes the
temperature of the BUS and ELC structure of the MRT as shown in *red* and *green*. The *red curve*
shows a damping to almost 40% and a time lag of 4.5 h. The *green curve* indicates a variation of
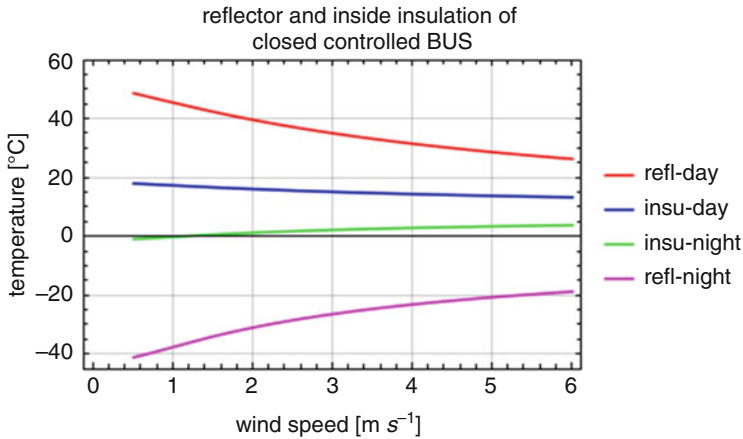the ELC of less than 1 K peak to peak

Fig. 5.18 Computed temperature of the reflector surface (refl) and the inside of the thermal insulation (insu) as function of the wind velocity for solar illumination (day) and clear sky (night), assuming ambient air at 0 °C. The control system keeps the BUS at 10 °C

The temperature of the quadripod is also controlled to equal the ELC temperature. In addition to a layer of thermal insulation, temperature-controlled glycol flows through a pipe spiralling along the length of the legs.

In Addendum, we summarise the theory behind the thermal control of the telescope and we calculate the temperature of the reflector and insulation as a function of the wind velocity for day and night situations. A summary of these calculations is shown in Fig. 5.18.

To improve the reflection of solar heat, the reflector surface is painted white, as is the outside surface of the insulating cladding that completely encloses the BUS. Insulation with an aluminium cover on the inside is also placed between the surface panel and the BUS frame. Figure 5.18 shows the dependence on wind velocity for the reflector surface (refl) and the inside of the insulation (insu) during day with solar illumination and at night with a clear sky. It is assumed that the BUS is kept at a temperature of 10 °C by the thermal control system. At night, the inside of the insulation remains below about 8 °C (green line) and the thermal control system must provide heat to keep the BUS structure at the required 10 °C. During the day, the temperature of the insulation rises above 10 °C and the control system switches to cooling the BUS to 10 °C. It should be noted that the control of the BUS temperature is not relevant for the outside panel temperature, as the figure clearly shows. The temperature of the reflector panels changes strongly during the day with very little influence on the BUS because the panels are outside the regulated system and have a very low heat conductance through their support bolts. The design of the panels and their support ensures a good surface quality throughout the day. The white paint reduces the panel temperature under solar heating compared to bare aluminium. The large emission coefficient of the paint causes a strong cooling at
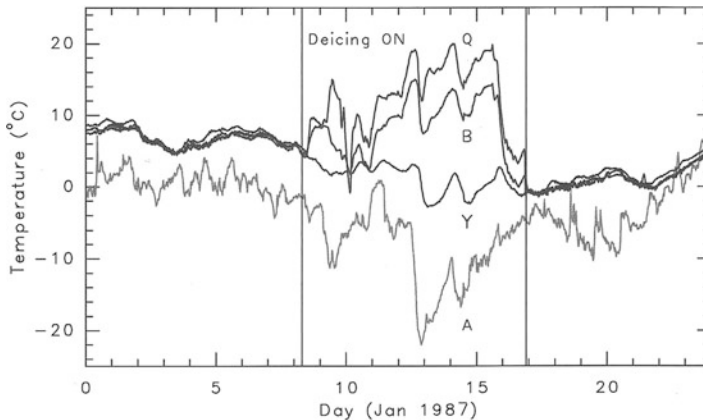
Fig. 5.19 A plot of the temperature over a full month of the ambient (A), yoke (ELC) (Y), BUS (B) and quadripod (Q). In the *left* and *right* parts of the plot, the telescope sections are kept closely at the same temperature by the control system. The centre part shows the situation during a severe winter storm during which the de-icing system is switched on. It keeps the telescope above freezing temperature, but the control system is not laid out to keep the sections at the same temperature (from Greve and Bremer 2010)

night. This can result in condensation and ice forming by the humidity of the ambient air.

The performance of the overall control system is shown in Fig. 5.19 (from Greve and Bremer 2010). With an operational control system, the MRT provides essentially constant performance with varying environmental conditions. This is shown in the left and right part of the figure. To battle occasional extreme winter conditions with snow and icing, the outside walls of the telescope, including the reflector surface, can be heated by elements imbedded in the insulation panels. This is the case in the centre part of the graph, and it clearly illustrates that the temperature control system cannot maintain equilibrium between the telescope sections. Despite the freezing weather, the telescope is kept at non-freezing temperatures, but the capacity of the control system is insufficient to keep the sections at an equal temperature. After switching, the de-icing off equilibrium is quickly restored. The control system is capable of limiting temperature differences during the extreme loads at dawn and dusk to about 1.5 K, which is within the specification.

In the course of early operation, it was noticed that under certain circumstances the reflector exhibited a significant astigmatism. The cause could be related to temperature differences between the membrane of the yoke and the massive ballast arms attached to the yoke. The ballast arms were some 5° cooler than the yoke membrane. A finite element analysis provided a quantitative pattern of the resulting astigmatism. This could be confirmed by a holographic surface measurement under a known thermal imbalance. In 2002, ventilators were placed in both the yoke and ballast arm structures. In addition, heating elements were installed in the ballast arms to create a homogeneous temperature distribution to about 1 K through the

structure from reflector BUS through the yoke to the ballast arms. This essentially removed the astigmatism of the reflector (Greve et al. 2005).

5.3.7   Conclusion

In the foregoing sections, we have dealt with the essential aspects of the design and performance of the MRT. The project also required the development of a method to determine the position of the reflector surface panels with a very high accuracy of better than 50 μm rms. The MRT was one of the first telescopes that depended on the method of *radio holography* for measuring the surface and has achieved a setting precision of the surface panels of 30 μm rms.

The deformations caused by wind were computed on the basis of measurements on a one-tenth model in the wind tunnel of the Technical University of Aachen. The largest deformation of about 26 μm (rms) occurs at an elevation angle of 60° with a frontal wind of 12 m/s. We showed earlier (Fig. 5.15) the advantage of setting the surface at an intermediate *rigging angle* of about 50°. This effectively balances the maximum wind deformation at that elevation angle against the increasing gravitational deformation at the lower and higher elevation angles.

The overall performance of the reflector is shown in Fig. 5.20, where all error components have been plotted as function of elevation angle. The thermal, panel manufacturing and panel setting accuracies are independent of elevation angle. The
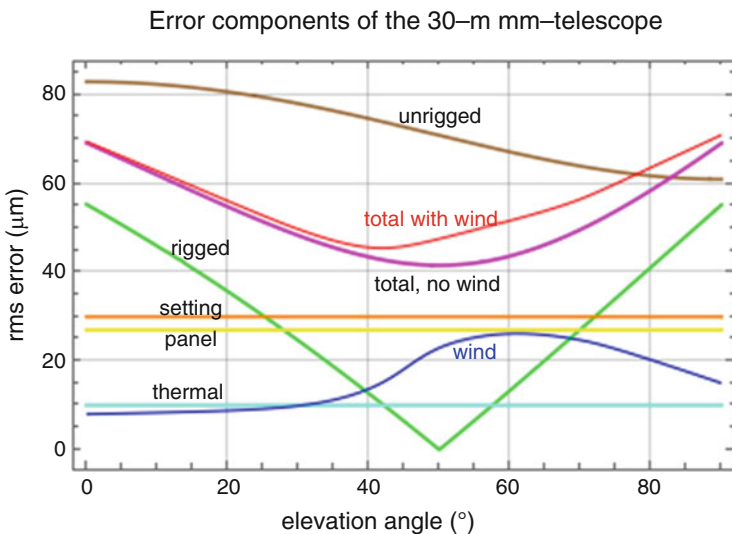

Fig. 5.20 Plot of the reflector error components as function of elevation angle. The curves "total" show the rss (root-sum-squared) value of the five components. Note the significant improvement by selecting a rigging angle of 50° and the fortuitous near coincidence of the gravitational minimum with the maximum wind deformation

wind and gravitational components show their elevation dependence. The curves "total" show the *root-sum-squared* value of the five error contributions. Note the rather small influence of the wind on the total error. For comparison, the curve "unrigged" displays the basic gravitational deformation as discussed in Sect. 3.4.

The 30-m telescope was realised beyond its specification, and further improvements have been made over the years in the surface precision by accurate radio holography and in the understanding and control of the thermal behaviour. Baars et al. (1994) have presented an overall review. After 30 years of operation, it remains a highly productive single dish mm telescope performing well at the submm atmospheric window near a wavelength of 850 μm.

5.4   The Large Millimeter Telescope

5.4.1   Conceptual Design Phase

In late 1994, the University of Massachusetts at Amherst (UMass) and the Mexican Instituto Nacional de Astrofísica, Óptica y Electrónica (INAOE) in Tonantzintla, Puebla, established a collaboration with the aim to jointly construct and operate a large radio telescope for millimetre wavelengths, for short the Large Millimeter Telescope (LMT), or in Spanish Gran Telescopio Millimétrico (GTM). The plan was to realise a telescope of 50 m diameter, operational to at least 300 GHz, located on a high mountain in Mexico. At that time, this was a far larger, highly accurate millimetre telescope than any in existence or planned. With a surface precision of 70 μm, the diameter to precision ratio is 700,000, about twice as large as that of the MRT.

It was believed to be impossible to economically construct such an accurate structure that would operate within specification while subjected to wind and temperature variations and also survive the extreme weather situations that occur at a high mountain site (storm, ice, snow). An important aspect was the experience of UMass with its radome-protected mm telescope of 14 m diameter, built by the company ESSCO of Concord, Mass. Thus, the project started with contracts for a conceptual design of a 50-m diameter telescope, placed in a closed radome. The company Toronto Iron Works (TIW) of Santa Clara, CA, together with the engineering design bureau Simpson, Gumpertz and Heger (SGH) of Waltham, MA, engaged in the structural design, while ESSCO looked into the reflector surface and the radome, areas of their expertise.

In February 1997, a full design proposal for a radome-enclosed antenna was delivered. A sketch is shown in Fig. 5.21. Remarkable features of the proposal include:

– The reflector is composed of hexagonal segments with active control of the surface shape.
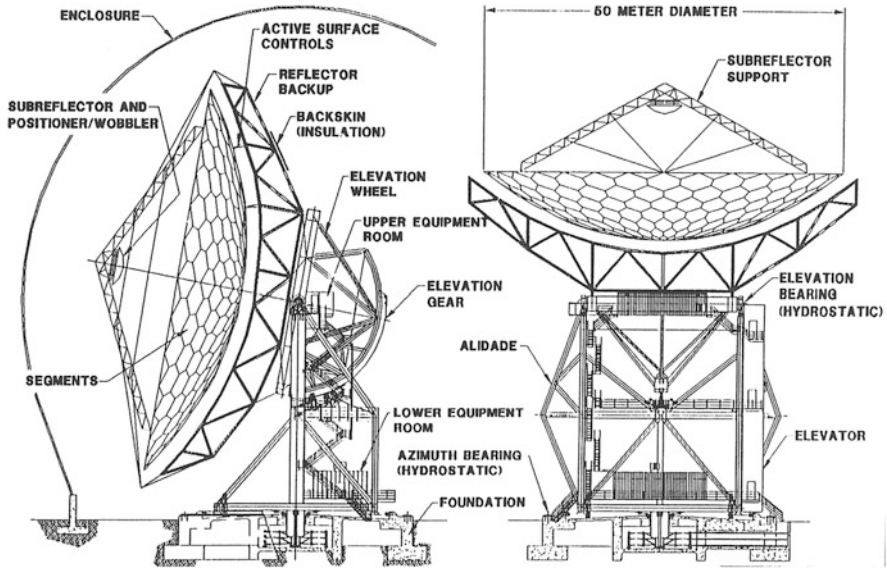– The BUS is supported by an umbrella-type elevation cradle.

Fig. 5.21 Sketch of the conceptual design for the radome-enclosed LMT (from TIW conceptual proposal to UMass)

– Hydrostatic bearings are used for both azimuth and elevation movement.

The surface layout was inspired by the optical Keck telescope of 10 m diameter, whose designers, J. Nelson and T. Mast, acted as consultants for the LMT design. The surface of the Keck telescope is actively controlled by means of edge sensors and motorised adjusters. A similar solution was envisaged for the LMT.

In the mount, we see the influence of NASA deep space antennas in the alidade and of the Effelsberg telescope in the elevation cradle. The hydrostatic bearings are surprising, because since their use in the Haystack and NRAO 140-ft telescopes (see Chap. 3) and the NASA Goldstone 64-m antenna, all built in the early 1960s, no other large antenna has applied these.

This proposal was found to be lacking in several aspects, some of which had emerged from parallel studies at UMass and INAOE. The first issue concerns the radome. A metal space frame that causes partial blocking of the aperture supports the skin. The skin absorbs a small part of the incoming radiation. It also exhibits a frequency-dependent reflection that is determined by the composition of the material. This is illustrated in Fig. 5.22. In a thorough study, Olmi and Mauskopf (1999) at UMass showed that the sensitivity of bolometer detectors would be significantly impaired by the vibrations of the radome skin in the ambient wind in addition to the loss by blocking and absorption.

At INAOE the option of an astrodome with open door was studied. It transpired that for thermal reasons the open area would need to be closed by a transparent
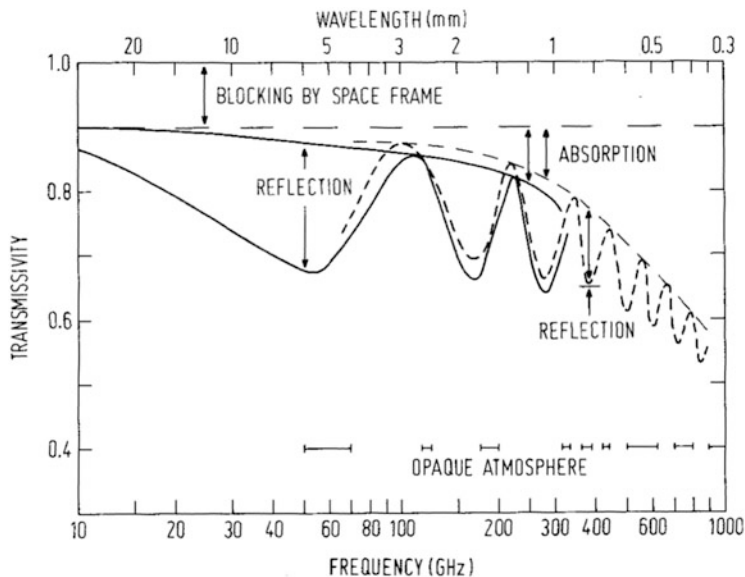
Fig. 5.22 Transmissivity of a typical ESSCO radome with Gore-Tex skin as function of frequency. The fixed blocking of the space frame is about 10%. The absorption increases monotonically with frequency. The reflection loss is a frequency-dependent component. The location of the minima can be tuned by the thickness of the membrane. The frequency regions where the atmosphere is opaque are indicated at the *bottom* (from Baars 1983)

screen similar to the solution for the JCMT on Hawaii. The support of such a huge sail turned out to be problematic, and moreover, the influence of the vibrations of the skin would be even more serious.

The hexagonal reflector layout, and in particular the active control of the surface shape, also posed problems. It was obvious that the fabrication of the hexagonal panels would be significantly more costly than of the usual trapezoidal panels of a surface consisting of concentric rings. More serious was the finding that the Keck solution with edge sensors would not function in this case, because the metal surface panels would exhibit uncontrollable temperature and hence local dimensional changes that would inhibit the active control of the overall reflector shape. The Zerodur glass of the panels on the Keck telescope avoids this problem.

Finally, the umbrella cradle made the provision of a large receiver cabin behind the primary mirror very difficult if at all possible. This would seriously limit the installation of multiple receiver units and thereby impair the flexibility of operation.

All these obstacles convinced the project leaders that the alternative of an open-air antenna should be considered. In the spring of 1997, a contract for a conceptual design study of such an antenna was placed with Vertex Antennentechnik in Germany. At about the same time, an unsolicited offer was received from MAN Technologie (now MT Mechatronics) for a similar concept study, which was also granted. The Project issued a Request for Quotation for the 50-m LMT in August

1997 in which it was left to the bidders to select either a radome/astrodome-enclosed antenna or an open-air telescope. All available study material, both from the project office and the concept proposals from the companies, was included in the document package. Three bids were received in December 1997: from TIW for the radome version and from each Vertex and MAN for the open-air alternative. The offer from MAN was selected for realisation.

5.4.2   *Towards a Final LMT Design*

The design of MAN was based on the experience with previous exposed telescopes. The first design sketches of the exposed telescope were submitted to the Project in early 1997 (Fig. 5.23). They show a wheel-on-track design with some major changes with respect to the TIW design. These are the elevated pintle bearing similar to the MERLIN antenna and the rear side BUS cladding similar to the MRT. The two ballast arms on the outside of the elevation bearings, which allow the arrangement of a large two-storey Nasmyth receiver cabin, resemble the design of the MRT and the IGN Yebes telescopes. Noticeable is also that at that stage the hexagonal panel concept of the TIW design was adopted.

The design involves an open-air alt-azimuth telescope of an appearance reminiscent of the MRT in Spain. The larger size of the antenna with even more stringent specifications regarding surface and pointing precision required several modifications and extensions to a straightforward upscaling of the MRT. In particular, the surface specification over the entire elevation range of the antenna could not be maintained without the introduction of a surface with actively controlled motorised adjusters. Also the pointing specification under operational wind would
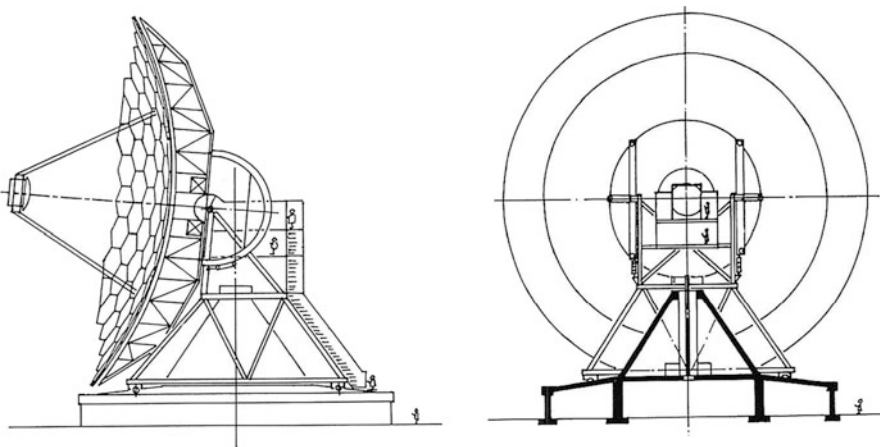

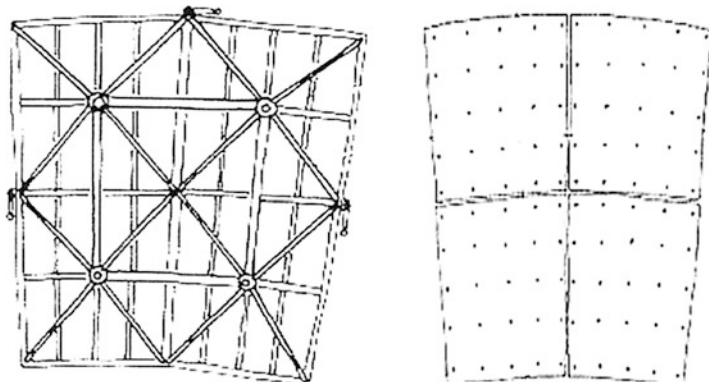**Fig. 5.23** Sketch of the initial MAN proposal for the LMT

Fig. 5.24 MAN's radial-circumferential reflector concept consists of an isostatic segment frame of about 5 m (*left*) that supports the reflector surface panels (*right*) through multiple adjustment screws. The frame is supported on the BUS at four points by motorised adjusters

require the incorporation of aspects of flexible body compensation (FBC), described below.

A closer look at the consequences of the hexagonal panel concept indicated a considerable increase in the number of different types of tiles and hence in the complexity of the support structure. The radial-circumferential topology of the backup structure truss system is easier and more conventional to manufacture in steel than the tetrahedron-octahedron topology required by the hexagonal partitioning of the reflector. The extra efforts in manufacturing and resulting increased cost would be significant. This, together with the understanding that the Keck scheme of active surface control would not work at the LMT, led MAN to select the traditional radial-circumferential partitioning of the reflector for their proposal. For the individual surface segments, a size of about 5 m was proposed. The sketches in Fig. 5.24 formed the basis for the final layout of the telescope surface.

5.4.3 The Final Design of the LMT/GTM

MAN obtained the order for the detailed design of the LMT/GTM from INAOE in December 1997. The contract involved the detailed design, up to manufacturing drawings, of the telescope plus a full plan for systems engineering and supervision of the fabrication and erection. It was envisaged that as much as possible of the fabrication would be done by Mexican industry. The final design shows the same features as the first sketches of the exposed concept. Only the reflector segmentation and related backup structure is changed from hexagonal to radial-circumferential topology. Of course, this is a significant change, as we have
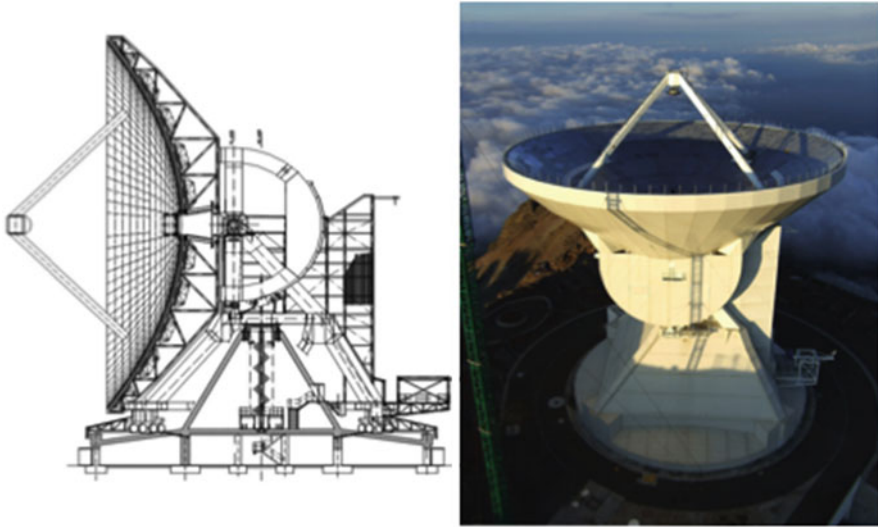
Fig. 5.25 Cross section of the LMT structural design and a picture of the telescope in 2012 (LMT Observatory)

explained above. The final design was completed in the fall of 1999 and is shown in Fig. 5.25. A general description is given by Kärcher and Baars (2000).

Different from the 30-m MRT and the 40-m ARIES XXI, the alidade of the LMT is of the wheel-on-track type. The transition from turning head to wheel on track is driven by the manufacturing limits for single-piece slewing bearings that were at the time in the range of maximally 6 m diameter. For a 50-m telescope, such a small diameter would result in a disproportionate overall design and lead to flaws in regard to stiffness and strength. The design applies the elevated pintle-bearing concept for more direct transfer of the lateral wind loads into the foundation via a conical concrete tower, as used for the MERLIN antenna. The wheel-on-track alidade allows the arrangement of a very comfortable external access to the receiver rooms via a staircase and an elevator.

The idea behind the design concept for the LMT structure (Fig. 5.26) is the four-point support principle as described previously for the 30-m MRT, the 32-m MERLIN and the 40-m ARIES XXI telescopes, and proposed already in 1965 by MAN for the Effelsberg telescope. As we have seen before, this naturally creates space for a large receiver cabin to the rear of the reflector apex that is stationary in elevation and provides plenty of room for several receivers and their focal plane optics.

The reflector truss system is connected only in the 45° symmetry plane to the four endpoints of the ballast girders by an interface structure, called by the drafts-men the "In Betweens". These "In Betweens" are visible from the outside at the erected telescope (see Fig. 5.24, right) and achieve the avoidance of astigmatic deformations as explained earlier. A *virtual ring girder* inside the backup truss
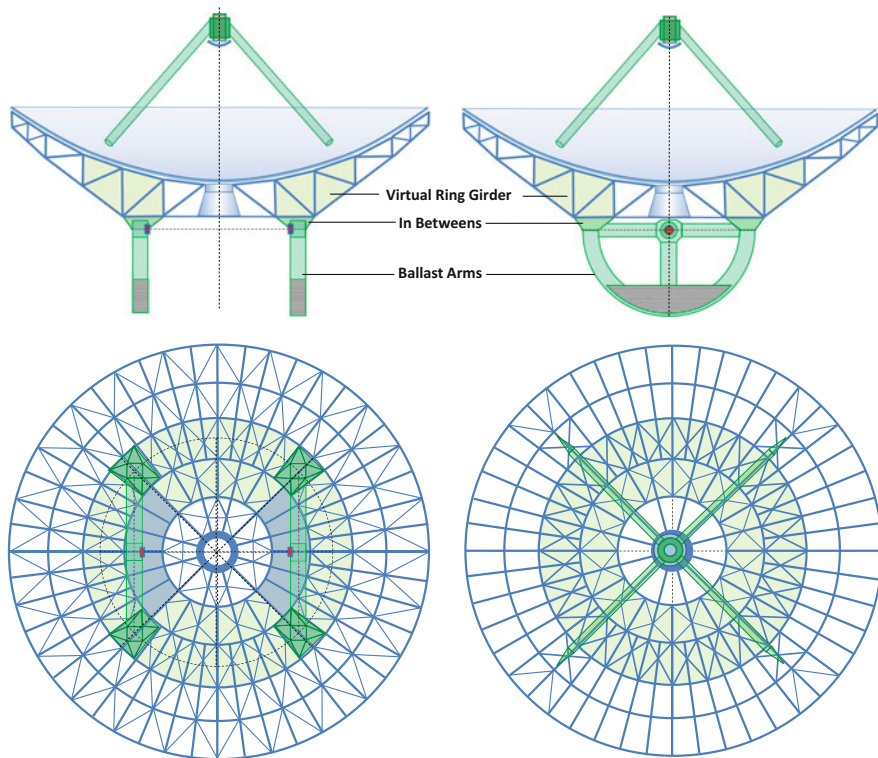
Fig. 5.26 Design concept of the LMT reflector backup structure and its connection to the elevation structure at the corners of the ballast girders

system, indicated in the figures by a light green shadowing, achieves the structural connection between the left and right ballast arm. It replaces the physical ring girder in the MERLIN design concept, or the "yoke disc" of the MRT design. The ring girder functionality is achieved by the diagonals in both the upper and lower chords of rings 2 and 3 of the truss system, closing the truss topology of these rings also in regard to torsional loads. In the upper chord of rings 1, 4 and 5, the diagonals are avoided, which eases the arrangement of the reflector segments (see next section). The diagonals in rings 2 and 3 are complicating the arrangement of the segment frames in these rings and form a drawback of the concept.

In view of the required surface accuracy of 70 μm rms, it was accepted from the beginning that an active surface would be necessary for the compensation of the environmental influences, gravity, wind and temperature. The computer-aided structural optimization yielded final gravity "switched on" deformations of $\sigma_Z = 316$ μm rms in zenith position and $\sigma_H = 415$ μm rms in horizontal position (Fig. 5.27). It was assumed that an active surface controlled in open loop could reduce the residual deformation to less than 5% of the absolute value.
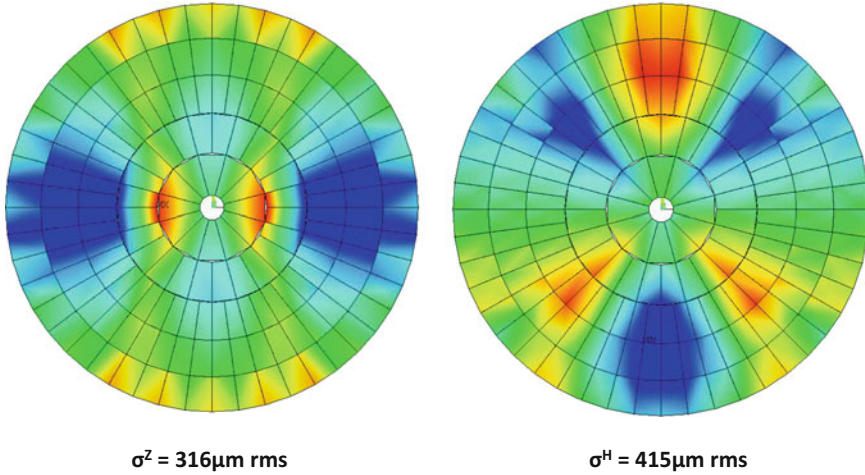
$$\sigma^Z = 316\mu m \text{ rms} \qquad\qquad \sigma^H = 415\mu m \text{ rms}$$

Fig. 5.27 Deformation patterns of the LMT structure under gravity loads. Gravity is switched on in zenith (*left*) and horizon (*right*)

5.4.4   Short Review of Surface Panel Technology

Similar to the 30-m MRT, the LMT applies a reflector design with separate *panel frames* between the panels proper and the backup structure. The reason is that highly accurate panels cannot be produced in sizes that fit to the dimensions of usual backup truss patterns.

The required surface precision often determines the manufacturing method for the panels, which then determines the limit on size and weight. Table 5.3 gives some typical values (status 2016).

The most economic aluminium cassette-type panels are produced by several fabricators in sizes up to 2.5 m with a precision upwards of 80 μm rms. The size limit is driven by transportation and handling issues, not by limitations imposed by the manufacturing process. The panels are produced in an economic way on universal jigs, adaptable to the required shapes.

The sandwich-type panels are replicated from dedicated cast iron or glass moulds. The aluminium deck sheets of the panels are stretch formed on the moulds; the deck sheets of the CFRP version are formed by replication technique on the moulds. Both methods were developed in the course of the construction phase of the Effelsberg, MRT and IRAM Plateau de Bure telescopes. The moulds are expensive and economically competitive only if a certain "mass production" of panels of the same shape can be established. The achieved panel precision is about twice the accuracy of the mould. Some examples will be shown in Chap. 7.

The electro-formed nickel technology is based on electrolytic deposition of nickel onto a steel mould. The Italian company Media Lario developed it for a space application under an ESA contract (X-ray Multi-Mirror telescope XMM).

Table 5.3 Typical design parameters of the most usual panel types (2016)

Type	Example	Maximum size (m)	Typical height (mm)	Typical weight (kg/m^2)	Precision (µm rms)
Aluminium cassette	Effelsb.	2.5	200	20	>80
Aluminium or CFRP sandwich	MRT HHT	1.2	50	10	25 6
Machined aluminium	ALMA (NA)	0.8	50	10	<10
Electroformed nickel	ALMA (EU)	1.2	30	10	<10

The technology has been used for the European ALMA antennas and the LMT. The panels are of sandwich type with top and rear deck sheets made from nickel and aluminium honeycomb core in between. The dimension of the manufacturer's production facilities allows panel sizes up to 1.2 m.

The machined aluminium panel technology was established for the production of panels of a surface accuracy much higher than the aluminium cassette panels without the need for moulds. The range of the milling machine on which the panels are produced limits the size. The German company Zrinski made the North American ALMA panels. A best precision of 3 µm rms for panels of up to a size of 1 m in the diagonal appears possible.

5.4.5 The Isostatic Reflector Segments of the LMT

The first approach to the radial-circumferential reflector segmentation of the LMT was based on the idea for a stiff frame between the nodes of the backup truss system (Fig. 5.24). The size of the segments was chosen at 5 by 5 m similar to the sizes of the first hexagonal panel segments of the first TIW design (Fig. 5.21). On each segment, four single panels of about 2.5 by 2.5 m were envisaged with 25 adjustors per panel to the frame.

A first analysis of the deformation behaviour of this concept showed that it was impossible under practical circumstances to bring the sag in centre of the segment down below 300 µm (Fig. 5.28, left). The remedy was to apply principles similar to homology or the isostatic support of large optical mirrors to the reflector segments of the LMT (Kärcher and Baars 2000; Kärcher 2006; Kärcher et al. 2012).

The isostatic frame (Fig. 5.28, right) does not suppress the overall sag of the segment but smoothens it by equal softness (mattress principle). This is achieved by the introduction of an additional *baseplate* that separates the panels from the sag of the frame. The load path of the weight of the panels and baseplate on the frame is separated into axial and lateral direction. The axial load is equally distributed onto eight axial bars; the lateral load is transferred into four lateral bars. Finite element
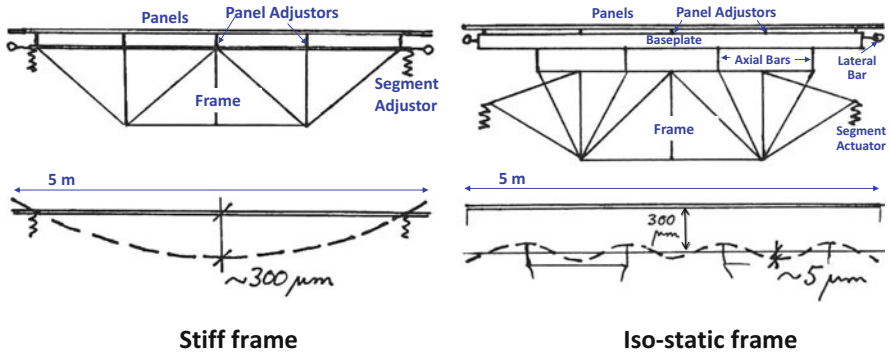
Fig. 5.28 Comparison of the stiff versus the isostatic panel support frame
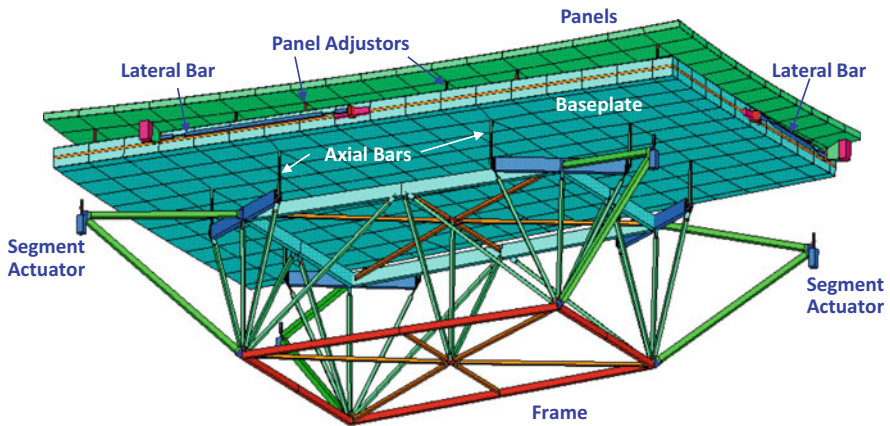

Fig. 5.29 Rendering of the FE model of the LMT panel segments

analysis showed that the accuracy under gravity load could be improved by an order of magnitude. Figure 5.29 shows a rendering of the finite element model of the final design, and Fig. 5.30 provides a view of the frame in the main truss structure.

The addition of panel frames complicates the structural system of the reflector significantly and causes a considerable cost increase over a standard system without these frames. It is only worthwhile for large reflectors with submillimetre wavelength capability and in combination with active optics.

5.4.6   Flexible Body Control (FBC)

The surface precision of a large telescope for short millimetre wavelengths is not the only challenge for the designing engineer. Also the pointing requirements are

Fig. 5.30 Rear view of the installed panel segments inside the backup truss
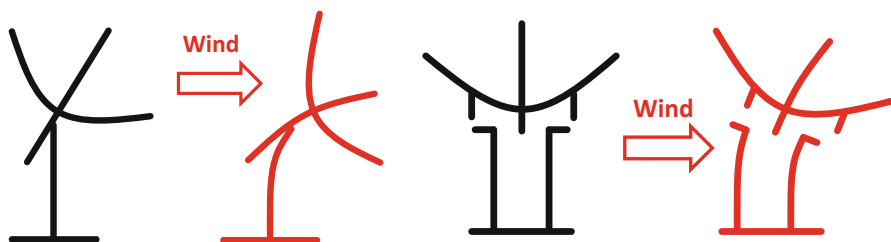

Fig. 5.31 The two main *deformation states* in elevation and cross elevation caused by wind

extremely demanding. Driven by the beamwidth at the maximum operational frequency of 300 GHz, the pointing accuracy has to be better than 1 arcsec rms under the specified operational wind speed of 10 m/s. Finite element calculations of the wind deformations showed that the maximal pointing deformations would be in the range of 5 arcsec, clearly too large as was the case with the gravity deformations of the reflector surface.

The remedy is again the application of active compensation; this time not at the surface but at the main axes drives. Figure 5.31 shows the main *deformation states* under wind loads in elevation and cross elevation. When the wind is blowing from the front or the rear, the reflector is making a nod-type deflection about the elevation axis. With the wind blowing from the side, the reflector shows a sideward roll type deflection orthogonal to the elevation axis. Both deflections are spread over the whole telescope structure and can be measured for instance by tilt meters attached to the alidade near the elevation bearings.

Using the readings of the tilt meters as input to the finite element model, we can derive the necessary corrections to the pointing. Similarly feeding the data of a set of temperature sensors throughout the structure to the finite element model will
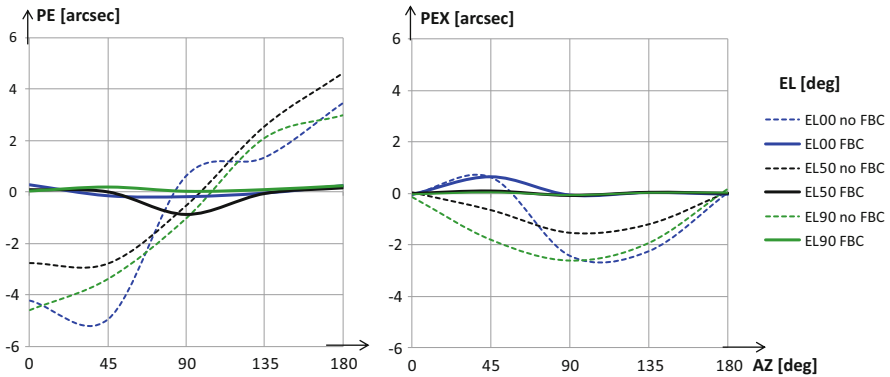
Fig. 5.32 Pointing error in elevation (PE) and cross elevation (PEX) as function of angle of attack (AZ) of the wind (10 m/s) for elevation angles 0°, 50° and 90°. *Full lines* with FBC and *dashed lines* without FBC

yield a deformation pattern from which pointing corrections can be derived. The method is generally called *Flexible Body Compensation* (FBC) and is used in some form in most of the recent radio telescopes as for instance ALMA (Chap. 6). The theoretical background is presented by Kärcher (1999), while Greve et al. (2005) discuss results of FBC application at the MRT.

Figure 5.32 shows the computed deformation of the LMT as function of wind attack angle for a wind speed of 10 m/s at three different elevation angles with FBC (full line) and without FBC (dashed). The improvement by FBC is about one order of magnitude.

5.4.7   Concluding Remark on the LMT/GTM

At the time of writing, early 2017, the construction of the LMT/GTM has not yet been completed. The project has suffered long delays for a number of reasons, such as problems in the fabrication of surface panels and subreflector, management errors and cost overruns. In June 2011 the reflector surface up to 32 m diameter had been installed and adjusted by holography and the basic axis control system was operational. A successful "first light" observation was made at 3.3 mm wavelength. Over the last three years time has been devoted to observations at 3 and 1.3 mm including successful participation in a few millimetre-VLBI observations.

In the meantime the panels for the outer two rings have been delivered and are being installed. It is foreseen that the full 50-m telescope can be completed towards the end of 2017. If the original specification can be met, the LMT/GTM will be a formidable addition to the available worldwide capacity for observations at short millimetre wavelengths.

5.5   The Nobeyama 45-m Millimeter Telescope

The last telescope to be mentioned in this chapter was the first large millimetre telescope to come into operation in 1983: the 45 m diameter reflector of the National Astronomical Observatory of Japan (NAOJ) (Akabane 1983). The antenna was designed and built by the Mitsubishi Company and is located at the Nobeyama Radio Observatory about 200 km West of Tokyo at an altitude of 1350 m (Fig. 5.33).

The telescope employs a wheel-on-track alidade of steel. The reflector backup structure is a truss frame, supported at a central hub, similar to the Parkes telescope (Chap. 3). A thermal insulation cladding shields the rear side of the BUS from direct sunlight. Some 40 fans continuously mix the air in the BUS volume. However, thermal effects noticeably influence the performance during daytime, in particular the pointing stability, and operation is usually restricted to the night.

Fig. 5.33 The 45-m diameter millimetre-wavelength telescope of the Nobeyama Observatory in Japan. It is the oldest large mm telescope (NRO/NAOJ)

The surface panels of the inner 30 m diameter are a composite of aluminium honeycomb core with outer sheets of CFRP; the precision is 60 μm rms. This was the first extensive use of CFRP in radio telescopes. In the course of time humidity penetrated the panels and led to delamination of the CFRP surface sheets destroying the surface accuracy. Since then all panels have been replaced by aluminium ones.

The telescope optics has a basic Gregorian geometry and employs a beam-waveguide system of mirrors to the focal point in the receiver cabin at base level in the alidade. A tripod, contrary to a quadripod in most radio telescopes, supports the subreflector. The optical layout is unusual for a radio telescope. Similar to a Nasmyth configuration it provides easy access to stationary equipment, but the multiple reflections in the beam waveguide cause a significant loss in signal.

The pointing and tracking control is realised through a master collimator, similar to the solution pioneered at the Parkes telescope. In this case the collimator, located at the crossing of the azimuth and elevation axes, employs an el-az layout with the coordinate transformation from celestial coordinates being performed by computer.

As is often the case improvements in the telescope performance have been obtained over the years. The current surface accuracy is about 0.10 mm, significantly better than the original specification. Under good conditions at night the pointing accuracy is 2–3 arcsec, just about acceptable for a beamwidth of 14 arcsec at 115 GHz. Most observations are made at frequencies below 115 GHz, in particular at 7 and 13 mm wavelength, where the performance is satisfactory.

5.6 Conclusion

The enormous richness of the sky at millimetre wavelengths has led to the construction of quite a number of mm telescopes, mostly located at good sites. In addition interferometer arrays of four to ten antennas with size between 6 and 15 m have been built in Japan, the USA and France. The culmination of this effort has been the construction of the ALMA array in Chile to be described in Chap. 6.

Addendum: Thermal Effects and Their Control

The thermal behaviour of the antenna structure is determined by the interaction of *radiation*, both onto and from the structure, *convection* by the wind and by forced air circulation inside a closed structure and *conduction* that depends on the thermal time constant of the structural members. The thermal balance between *radiation*, *convection* and *conduction* determines the actual temperature of the telescope. We discuss here the basic relations governing the thermal balance of the telescope. From these we can build *a thermal model* of the structure that will help us design a *thermal control system* to limit the thermal deformations to the specified values. This system may take the form of an outside cladding with thermal insulation and

possibly an additional air circulating system. Contrary to the static elastic behaviour of the structure, thermal effects are inherently time dependent. We summarise their role in the actual situation of a telescope operating under the influence of the environmental effects such as solar radiation and wind.

The daily variation in temperature is caused mainly by *solar radiation*. The effect of radiation on the thermal balance of the telescope structure is dependent on the emission and absorption characteristics of the material. These parameters depend on the temperature of the radiating body. Their values can be influenced by the treatment of the outer surfaces of the structure.

We distinguish three temperature regimes along with the wavelength of maximum radiated power:

1. The Sun at about 5800 K with its maximum at visible wavelengths (0.5 µm),
2. The cold sky in the range of 50–200 K, with a maximum in the far-infrared (30–60 µm),
3. The telescope at ambient temperature of the site, in the range of −30 to +30 °C, equivalent to 243–303 K, with its maximum in the infrared near 10 µm.

The energy balance of a surface under solar radiation requires that the absorbed solar power in visible light is equal to that radiated by the surface at infrared wavelength. The ratio of the absorption and emission coefficients for solar radiation and ambient surface temperature determines the heating of a surface under sunshine illumination. Note that at a given temperature the emission coefficient of a material is equal to its absorption coefficient (*Kirchhoff's Law*). In Table 5.4, we reproduce from Höfling (1978) typical values for the emission coefficients of treated surfaces used on telescopes. Here "aged surface" means a surface that has been exposed to the environment for a considerable time.

Inspecting the table we notice that colour-painted surfaces behave closely to being black. Clear metallic surfaces have small emission coefficients; they become very hot under sunshine. The white painted surface absorbs little solar heat but radiates strongly in the infrared. It can get colder than the ambient air even during sunshine!

The effects of radiation are counteracted by convection, that is, the effect of heat transport by the moving air (wind) along the surface of a body. It is a complicated physical process that is dependent on the shape and surface characteristics of the

Table 5.4 Emission coefficients of treated telescope surfaces

	New surface			Aged surface		
	ε_{sol}	ε_{amb}	$\varepsilon_{sol}/\varepsilon_{amb}$	ε_{sol}	ε_{amb}	$\varepsilon_{sol}/\varepsilon_{amb}$
White paint	0.12	0.85	0.14	0.50	0.95	0.53
Coloured paint	0.65	0.85	0.76	0.88	0.95	0.93
Aluminium bare	0.25	0.08	3.1	0.40	0.20	2.0
Aluminium treated	0.05	0.03	1.7	0.15	0.05	3.0
Zinc on iron	0.3	0.10	3.0	0.90	0.60	1.5
Black surface	0.85	0.87	0.98	0.98	0.98	1.0

body as well as the velocity and viscosity of the air. Fortunately, it is possible to perform calculations of the convective heat exchange with the use of a few characteristic parameters without complicated mathematics. The convective heat transfer between a solid body and a moving surrounding gas or fluid is proportional to the *Nusselt number* that is dependent on the size of the body and the speed of the wind as well as the Reynolds number, which characterises the state of turbulence of the air flow.

Calculation of Thermal Load Cases

With the knowledge of the emission coefficients of the materials and applying the convective parameters, we can design realistic measures to diminish temperature differentials in the telescope. The thermal exchanges in a reflector with backup structure (BUS) with attached insulation are sketched in Fig. 5.34. It depicts a schematic of all heat effects from the reflector surface at the top through insulation, the BUS containing structure and air and outside insulation. The general expression for the thermal balance at the surface of an antenna, both the reflector proper or a possible cladding around the remainder of the structure, can be stated as:

The sum of radiative input from Sun and sky equals output from surface by radiation and convection. Calculating the thermal balances at the various transitions between material and air, we can derive the equilibrium temperatures at the surfaces as a function of the wind velocity.

We present now the result for a few cases that apply to the MRT and LMT. The plots show the temperature change at a particular surface as function of wind speed with structural features (such as insulation and surface treatment) as parameter. We consider two different surface treatments that are common in reflector antennas (see Table 5.4):

– "Aged" white paint with $\alpha_{sol} = 0.50$ and $\varepsilon_{amb} = 0.95$ for outside reflector or cladding surface,
– "Aged" treated aluminium with $\alpha_{sol} = 0.15$ and $\varepsilon_{amb} = 0.05$ for both outside and inside surface.

Surface Temperature of a Free Versus Perfectly Insulated Reflector

Choosing a simple but instructive case we first consider a metal surface in two situations:

1. A metal plate supported above the earth and facing the Sun.
2. A similar plate but perfectly insulated on the rear side. It is the top part of Fig. 5.34 (blue-grey) without any conduction through the insulation. Thus, no heat energy is exchanged at the inner side of the surface. The solutions for the two cases are shown in Fig. 5.35 in dashed lines for the free plate and full lines for the insulated plate. Only the front side of the panel is painted white.

We note the following features. With solar input and very low wind speed, the insulated bare aluminium panel heats to a very high temperature near 120 °C. When the insulation is removed and heat exchange takes place also on the backside of the panel, the heating is limited to about 55 °C (red). With the painted panel, the
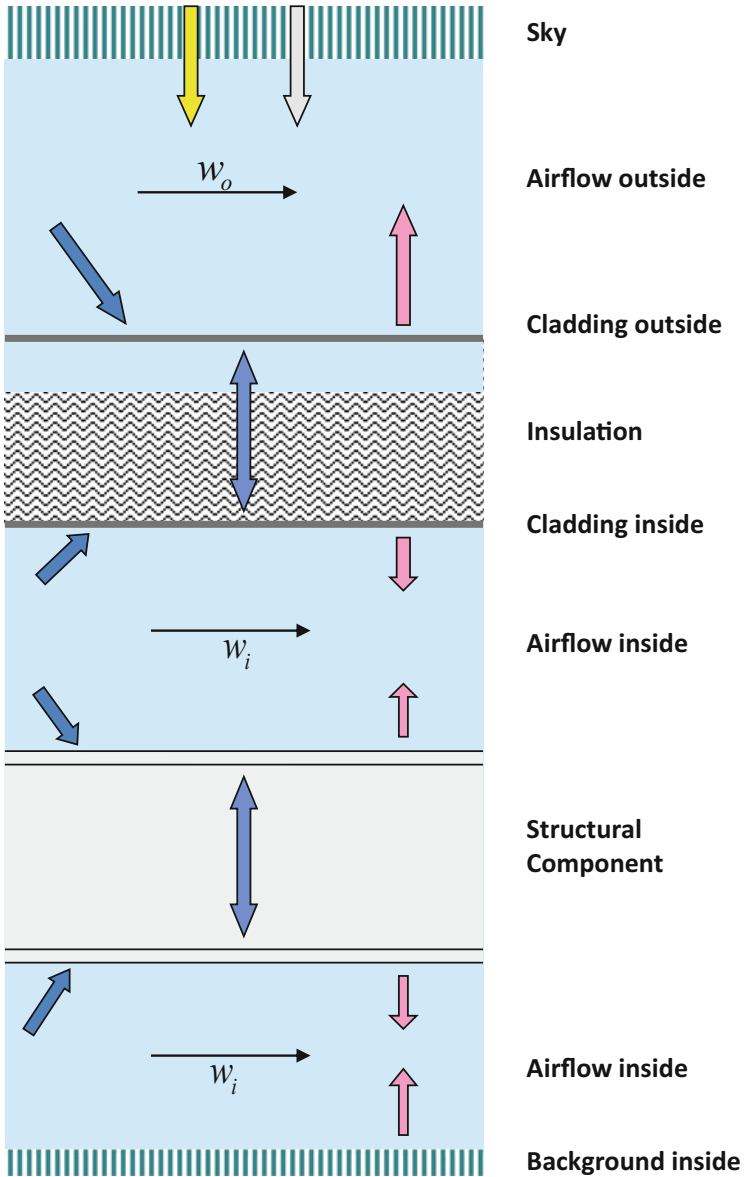
Fig. 5.34 Thermal effects in a reflector structure with insulation. Colour scheme: *blue* convection, *pink* radiation of structure at ambient temperature, *yellow* solar radiation input and *grey* sky radiation input. W is wind on reflector and inside the BUS
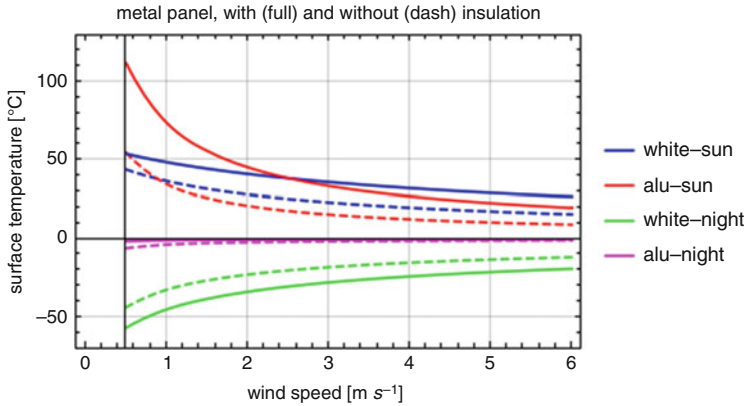
Fig. 5.35 Surface temperature of an aluminium panel with (*full lines*) and without (*dashed lines*) backside insulation for the situation SUN and NIGHT. Panel is painted (*white*) on front side or bare (alu)

radiation from the surface dominates the heat balance resulting in a lower maximum temperature and a small dependence on wind velocity (blue). At night, the dominant effect is radiation and the painted panel cools to low temperatures, well below freezing (green). This effect is increased by the presence of the insulation on the backside. The aluminium surface has a very low emission coefficient and remains essentially at the assumed ambient temperature of 0 °C (pink).

Temperature of Insulated Reflector with Open or Controlled BUS
We now take a more realistic case of a "panel" consisting of a metal outer plate to which insulating material of a finite thickness has been attached on the inside. This could be the actual reflector surface but also an insulating cladding around the backup structure (BUS). We now have a small heat conduction through the insulation in addition to the radiative and convective heat exchange.

We assume first that the BUS of the antenna is "open", exposed to the wind and at ambient temperature (no cladding). The results of the calculations for the panel outside temperature are displayed in Fig. 5.36 in full lines (open BUS). They are similar to the case of the perfectly insulated panel of Fig. 5.35.

The MRT, described above, has a completely enclosed and insulated BUS with an active system to control its temperature, independent of the ambient air temperature. Now the inside of the insulation of both cladding and panel will experience convective heat exchange with the BUS and enclosed air at a constant temperature. The resulting outside temperature of the panel is shown in Fig. 5.36 as dashed lines. As the figure shows, the control of the BUS temperature is not relevant for the control of the outside panel temperature. Its purpose it to keep the BUS temperature on the level of the yoke to avoid large-scale deformation of the BUS.

The temperature on the inside of the insulation is determined by the balance of the heat transported through the insulation and the convective transport from the
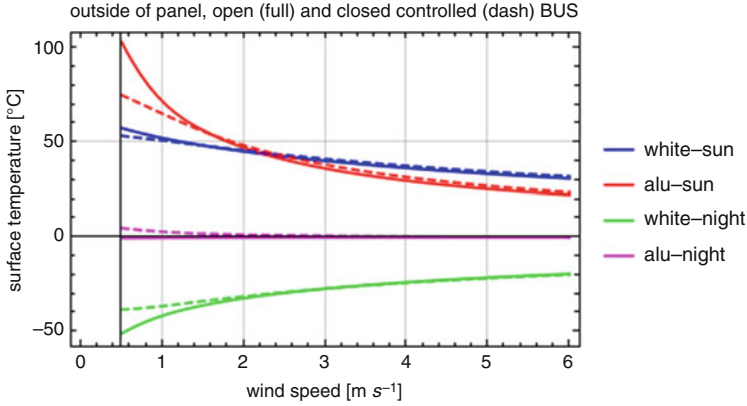
Fig. 5.36 The outside reflector temperature as a function of wind speed. The metal reflector panels are covered on the inside with a layer of insulation. The panels are connected to an open BUS without cladding (*full lines*) or to a completely enclosed and insulated BUS at a constant temperature of 10 °C (*dashed lines*)
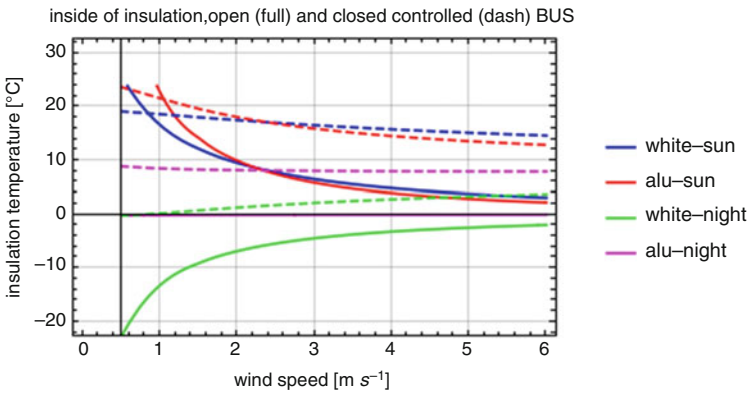

Fig. 5.37 The temperature on the inside of the insulation as a function of wind speed for the same layout as in figure. The BUS is kept at 10 °C by the control system

inside, assisted by the inside airflow (see Fig. 5.34). The BUS temperature is set to 10 °C. The results for this case are shown in Fig. 5.37.

Inspecting the three foregoing figures, we can draw the following conclusions:

1. Under solar illumination, the outside temperature of the realistic panel heats less at low wind speed than in the first example of perfect insulation because of the finite conduction of heat through the insulation.
2. We see a small influence of the controlled, constant temperature of the BUS on the outside temperature both at day (sun) and night at low wind velocities.
3. In the case of the controlled BUS, it is not surprising that the inner surface of the insulation is barely dependent on the wind speed. In the BUS, the air speed is fixed at 2 m/s.

4. Because the aluminium surface of the insulation panel has a low emission and absorption coefficient, it settles at night between T_{amb} and T_{BUS}, here at 8 °C. The strong cooling of the white outside at night causes the inside of the insulation to be below the BUS temperature of 10 °C (green dashed). This indicates that the BUS is being heated to keep it at its prescribed temperature.
5. The inside temperature of both a white and aluminium surface heats to well above the BUS temperature of 10 °C under sunshine. This implies that during daytime the BUS must be cooled to retain its temperature.

A summary plot for the MRT is shown in Fig. 5.18 of Sect. 5.3.6.

References

Akabane, K.: A large millimeter wave antenna. Int. J. Infrared Millimeter Waves. **4**, 793–808 (1983)

Baars, J.W.M.: Technology of large radio telescopes for millimeter and submillimeter wavelengths. In: Button, K.J. (ed.) Infrared and Millimeter Waves, vol. 9, pp. 241–281. Academic, New York (1983)

Baars, J.W.M., Greve, A., Hooghoudt, B.G., Peñalver, J.: Thermal control of the IRAM 30-m millimeter radio telescope. Astron. Astrophys. **195**, 364 (1988)

Baars, J.W.M., Greve, A., Hein, H., Morris, D., Peñalver, J., Thum, C.: Design parameters and measured performance of the IRAM 30-m millimeter radio telescope. Proc. IEEE. **82**, 687–696 (1994)

Brandt, P., Gatzlaff, H.: Design of the 30-meter millimeter-wavelength radio telescope. Tech. Mitt. Krupp Forschungsberichte. **39**, 111–124 (1981.) (in German)

Cogdell, J.H., et al.: High resolution millimeter reflector antennas. IEEE Trans. Antennaas Propag. **AP-18**(4), 515–529 (1970)

Eschenauer, H., Brandt, P., Schütz, K.: On the reflector accuracy of a high precision radiotelescope. Tech. Mitt. Krupp Forschungsberichte. **35**, 17–31 (1977)

Eschenauer, H., Gatzlaff, H., Kiedrowski, H.W.: Entwicklung und Optimierung hochgenauer Paneeltragstrukturen. Techn. Mitt. Krupp Forschungsberichte. **38**, 43–57 (1980)

Gordon, M.A.: Recollections of Tucson Operations, the mm-Wave Observatory of NRAO. Springer, Norwell (2005)

Greve, A., Bremer, M., Peñalver, J., Raffin, P., Morris, D.: Improvement of the IRAM 30-m elescope from temperature measurements and finite element calculations. IEEE Trans. Ant. Propag. **AP-53**, 851 (2005)

Greve, A., Bremer, M.: Thermal design and Thermal Behaviour of Radio Telescopes and their Enclosures, vol. ASSL 364. Springer, Heidelberg (2010)

Höfling, E.: Die Probleme der Erwärmung von Metallkonstruktionen durch Sonneneinstrahlung. Schweiz. Alum. Rundsch. **6** (1978)

Kärcher, H.J.: Enhanced pointing of telescopes by smart structure concepts based on modal observers. Proc. SPIE. **3668**, 998–1009 (1999)

Kärcher, H.J.: Iso-static mirror supports vs. homologue reflectors: a comparison. Proc. SPIE. **5495**, 147–158 (2006)

Kärcher, H.J., Baars, J.W.M.: The design of the large millimeter telescope/Gran Telescopio Milimetrico (LMT/GTM). Proc. SPIE Radio Telescopes. **4015**, 155–168 (2000)

Kärcher, H.J., Eisenträger, P., Süss, M.: Mechanical principles of large mirror supports. Proc. SPIE. **7733**, 201–212 (2012)

Olmi, L., Mauskopf, P.D.: A comparison of radome-and astrodome-enclosed large radio tele-
    scopes at millimeter wavelengths: The large millimeter telescope. Radio Sci. **34**, 733–746
    (1999)
Wilson, R.W., Jefferts, K.B., Penzias, A.A.: Carbon monoxide in the Orion Nebula. Astrophys.
    J. Lett. **161**, L43 (1970)

Chapter 6
Submillimetre-Wavelength Telescopes

About one-third of ALMA in a configuration of several hundred metres baselines [ALMA (ESO/NAOJ/NRAO), C. Padilla]

6.1   Introduction

Once the first larger mm telescopes had demonstrated the importance of the very high frequencies for astrophysical research, efforts were undertaken to open up the submillimetre-wavelength regime, i.e. frequencies from 300 GHz to 1 GHz or higher. From the best sites on earth, observations are possible up to about 1 GHz in the windows between the absorption lines of tropospheric water vapour (Fig. 6.1). Several institutes realised dedicated submm telescopes between 1987 and 1995, the three most significant being the JCMT and the CSO on Hawaii and the SMT/HHT on Mt. Graham in Arizona. An array of eight 6-m antennas, the Submillimeter Array (SMA) on Hawaii came into operation in 2004 (Ho et al. 2004). The definitive instrument is ALMA (Atacama Large Millimeter/submm Array), consisting of more than 60 antennas located at 5000 m altitude in northern Chile and covering the entire frequency range from 30 to 950 GHz. It began operation with a partial array in 2008 and construction was completed in 2014.

The requirements for good performance at 1 THz (wavelength 0.3 mm) are a reflector precision of better than 20 μm and a pointing accuracy of better than 1 arcsecond (aperture efficiency of 67% for $\varepsilon = 17$ μm, beamwidth $\approx$6 arcsecond for a 10 m reflector). While these are achievable by the current methods of structural optimisation, environmental effects of temperature and wind constitute major restrictions. In particular, limitation of deformations caused by temperature gradients is a prime necessity. A gradient of 1 °C over a length of 5 m in a steel
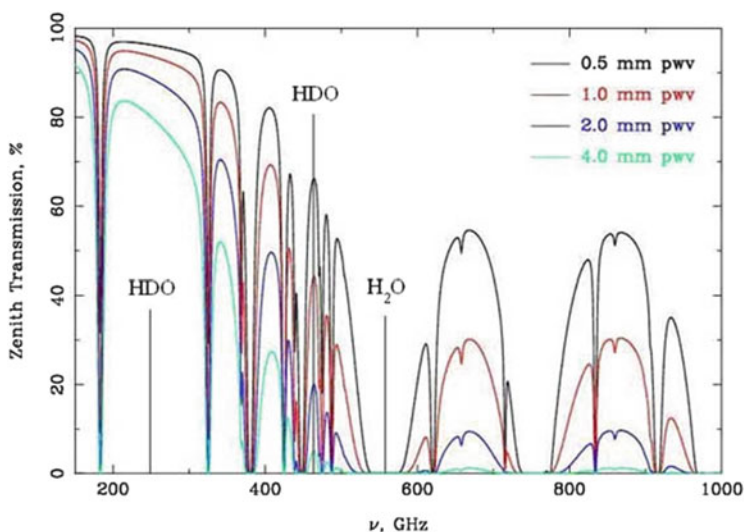

Fig. 6.1 Transmissivity of the earth's troposphere as function of wavelength. The three curves pertain to a precipitable water column height of 15 (*full*), 3 (*dashed*) and 1 (*stippled*) mm, which is typical for observatory altitudes of sea level, 2 and 4 km, respectively (Inst. Astronomy, Univ. of Hawaii)

support member leads to a deformation of about 50 μm. This indicates the need to control the temperature uniformity in a steel support structure to a few tenths of 1 K, which is difficult if at all practically possible.

The British-Dutch-Canadian James Clerk Maxwell Telescope (JCMT) employs a steel BUS and aluminium honeycomb panels, supported by motorised adjusters. The JCMT came into operation in 1987 and is located at 4000 m altitude on Mauna Kea, Hawaii. It has a diameter of 15 m and is placed in an astrodome, the front opening of which is covered by a cloth screen to keep the wind out and help stabilise the inside temperature regime. A detailed study of the thermal behaviour of the antenna was made (Bregman and Casse 1985), but the thermal control of the telescope has remained problematic. Normally, observations are restricted to the night-time because clouds hover over the site during the day. At night under a clear sky, the outside air reaches its maximum stability and the telescope can be operated to a highest frequency of about 700 GHz.

To satisfy the stringent specifications for the submm region, new design solutions and special materials need to be used. In the foregoing chapter, we met already the use of *carbon fibre reinforced plastic* (CFRP) with its low thermal expansion coefficient to confront the thermal effects. From the early 1980s onwards, this became the material of choice for the dedicated submillimetre telescopes despite its significantly higher price than steel. In the following sections, we describe the developments in design and technology by the examples of the CSO, IRAM, HHT and ALMA telescopes.

6.2   Leighton Dish and CSO Telescope

In the late 1970s, Robert Leighton at the California Institute of Technology devised an original way to manufacture a reflector of 10 m diameter with high precision. He used the existing large turntable, supported on an air bearing, on which the 5-m diameter glass mirror of the Palomar Telescope had been figured, as a base for the assembly of a backup structure (BUS) made of steel. The BUS consists of a triangular truss frame of precisely dimensioned rods (<0.1 mm length accuracy) with nodes in a regular triangular grid perpendicular to the optical axis (Fig. 6.2). Special care was taken that the lines of force of all members connected to a node intersect at a single point. The resulting structure behaves highly homologous. The total weight of the BUS is only 3600 kg (Leighton 1978).

The reflector surface consists of 84 hexagonal composite panels of aluminium honeycomb and surface skin. The panels are connected to each other at the corners; half of these (99) lie above a BUS node, where they are connected to the node by a 15 cm long adjuster. The total weight of the surface, including panel attachments, is 1300 kg.

After assembly, the surface presents a continuous membrane. The next step is to accurately figure the surface to the required paraboloid. Here use is made of the rotating air bearing support, which allows the use of a cutting tool attached to a fixed linear parabolic track (Fig. 6.2). Rotating the dish under the cutter and moving the cutter radially produces a paraboloidal surface. Note that the honeycomb panel core
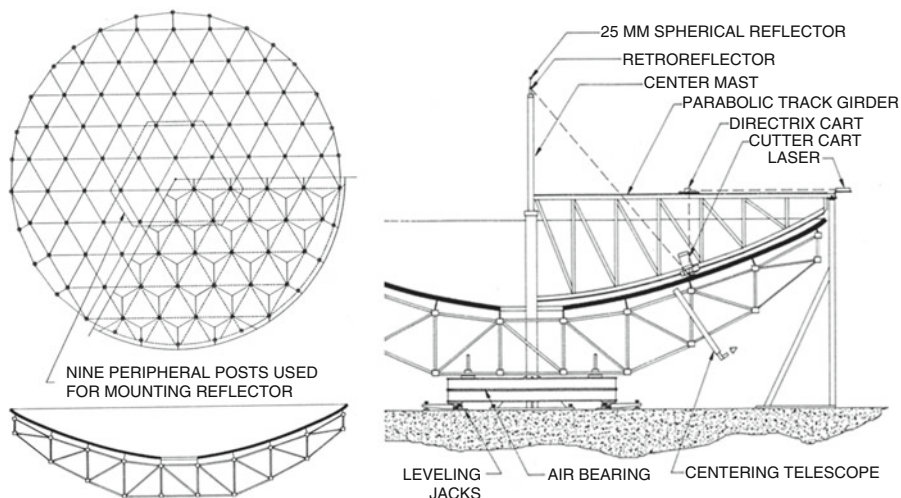
Fig. 6.2 The Leighton antenna. *Left*: Layout of the BUS and panels. *Right*: Template with moving cutter to figure the parabola. The BUS is rotated supported by an air bearing (from Leighton 1978)

was figured, not the aluminium sheet surface. A laser interferometer controls the correct setting of the track using the geometrical characteristic of the parabola. After a satisfactory accuracy of the cut has been achieved, the surface sheet is epoxied to the honeycomb. A final measurement of the continuous surface with the laser interferometer checks the accuracy and allows fine correction cutting where necessary.

An important design driver was the possibility of the full and accurate assembly of the reflector in the hall, a complete disassembly, transport of the singles pieces to the final site (Hawaii in case of the CSO submm telescope) and reassembly without loss in the original precision. This worked quite well, but additional surface measurement and adjustment was necessary to obtain the very high precision needed for the submillimetre region. A submm shearing interferometer was developed (Serabyn et al. 1991), and using astronomical sources, an overall accuracy of the CSO telescope of about 20 μm has been achieved.

At this accuracy, thermal deformations constitute a significant component of surface error. These are partially corrected by thermally changing the length of the panel support posts, based on a measurement of the temperature field in the reflector along with the calculated structural deformation (Woody et al. 1994). A photo of the CSO on Hawaii is shown in Fig. 6.3. The antenna is placed in an astrodome for environmental protection. The CSO was decommissioned in the fall of 2015.

Five identical antennas of somewhat lesser precision constituted the interferometer at the Owens Valley Radio Observatory (OVRO). In 2004, they were combined with nine 6-m antennas of the Berkeley-Illinois-Maryland-Array (BIMA) to form CARMA, the California Array for Millimeter Astronomy, located at 2200 m altitude in the Inyo Mountains of eastern California (Woody et al. 2004). After about 10 years of operation, this instrument was also decommissioned in 2015.
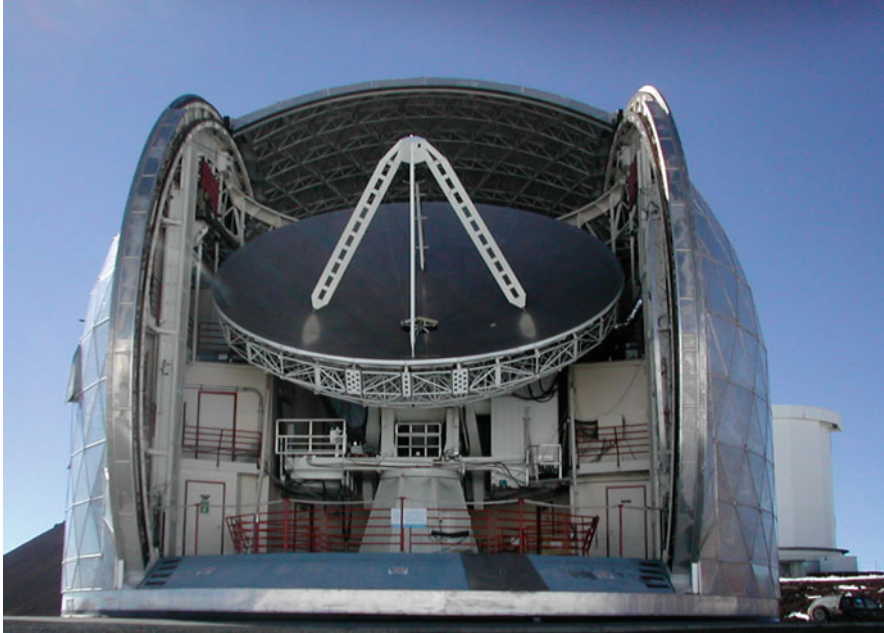
Fig. 6.3 The Caltech Submillimeter Observatory (CSO) on Hawaii. The 10.4-m diameter antenna is placed in a protective astrodome, which opens during observations (Courtesy, Sunil Golwala, Caltech)

6.3   CFRP Telescopes: IRAM 15-m and HHT

6.3.1   The IRAM Interferometer Antennas

Composite materials, in particular carbon fibre reinforced plastic (CFRP), have been extensively used for space applications since the early 1970s. CFRP possesses highly attractive characteristics. It exhibits a stiffness-to-weight ratio five times better than steel; hence, stiff and lightweight structures can be realised. Moreover, depending on the choice of fibre and its relative content in the composite matrix, the thermal coefficient of expansion can be varied. Most interestingly, this constant can be as small as a few times 10^{-6} (even zero or negative), reducing thermal deformations by an order of magnitude compared to steel or aluminium. Because of its high price, the use of CFRP in antennas and telescopes was initially restricted to space antennas, where both the weight and thermal behaviour were of great importance. Most communication satellites in those days operated at relatively low microwave frequencies (4 GHz), where the reflection coefficient of CFRP was sufficiently high to avoid the need for metallisation of the surface. Increased use of the material improved both its availability and decreased the cost, and around 1980, application of CFRP for accurate radio telescopes was being considered. As we have already mentioned in Chap. 5, both the subreflector of the MRT and the panels of the reflector of the Nobeyama 45-m telescope used CFRP sheets bonded to a honeycomb core of aluminium.

The 15-m antennas for the mm interferometer of IRAM had a surface specification of 70 μm (Guilloteau et al. 1992). During the design, it became clear that thermal deformations needed to be controlled to remain within specification. The antennas are transportable between baseline stations of hundreds of metres separation. There was thus a strong impetus to minimise the weight of the antennas. The two goals of lower weight and low sensitivity to temperature variations were realised by selecting CFRP for the majority of members of the BUS. The BUS is connected to the receiver cabin by a steel hub and the back-to-front members of the truss frame were realised in steel. The reflector of these antennas consists of six concentric rings of trapezoidal composite panels of aluminium honeycomb core and CFRP skins, fabricated by MAN Technology. They were made by replication from an accurately machined steel mould. A thin Hostaflon sheet (a plastic meant to protect the CFRP against a moist atmosphere) covered the surface; it was aluminised on the inside to provide the reflecting surface. This turned out to be an unsatisfactory solution. In the course of time, icicles and/or dust punctured the Hostaflon and water pressed itself between the foil and the CFRP surface, ruining the surface accuracy. Over the years, all panels have been replaced by lightweight, machined aluminium panels. The array of currently (2016) eight antennas operates with satisfactory efficiency at 350 GHz, higher than originally foreseen. It is being enlarged over the coming years to 12 elements under the name NOEMA (*NOrthern Extended Millimeter Array*). A picture of the antennas is shown in Fig. 6.4.
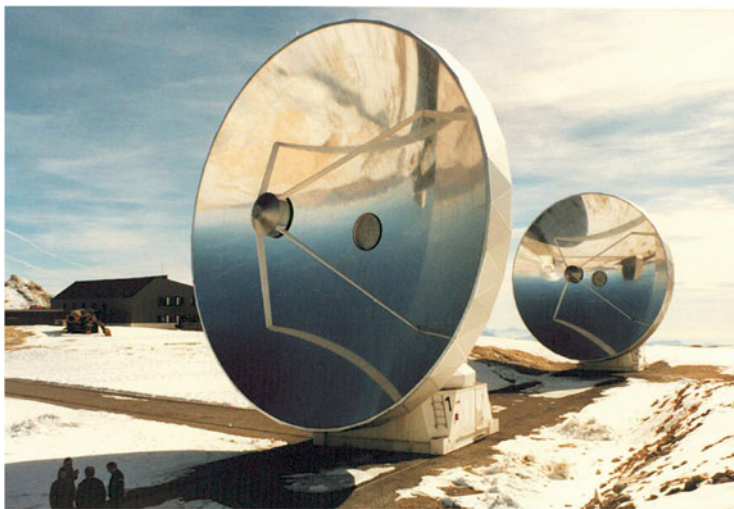

Fig. 6.4 The 15-m antenna of the IRAM millimetre array on Plateau de Bure, French Alps (IRAM)

6.3.2   The Heinrich Hertz (Submillimeter) Telescope (HHT)

Already during the construction of the MRT, preparations were made at the MPIfR for a small telescope dedicated to the shortest submillimetre waves that penetrate the atmosphere. As shown in Fig. 6.1, the window near 900 GHz is about 40% transparent under very good conditions at a very high (>3000 m) site. The CSO, discussed above, was located at such a site and its precision allowed observations at the shortest wavelength of about 0.3 mm (1 THz).

In the early 1980s, the MPIfR initiated a feasibility study with the companies Krupp and Dornier for an antenna of 10 m diameter with the best possible surface and commensurate pointing precision. Our aim was to reach a reflector precision of 17 μm, which at the shortest wavelength of 0.35 mm would yield an aperture efficiency of 70% with respect to a perfect surface. Not surprisingly, early in the design it became clear that the most critical aspect would be the avoidance of deformations caused by temperature variations. It was thus decided to realise the entire BUS, the reflector surface and the quadripod support of the subreflector in CFRP. Dornier proposed a box structure of CFRP plates for the BUS, in line with their experience in space modules and satellite antennas. Krupp with its extensive activity in truss-frame structures provided a BUS design of CFRP tubular members with invar steel nodes. The fabrication of CFRP nodes, where up to eight members may join, was considered too difficult and expensive. Although CFRP typically is a factor 4 to 5 lighter than steel, the total weight of the invar nodes was about as much as the weight of the CFRP members. The Krupp proposal was eventually realised.

The group at Krupp around Karl-Heinz Stenvers made an intensive study of the optimal material selection for the BUS members. The use of composite materials provides a number of free parameters in the choice of fibre, in particular its modulus of elasticity and thermal expansion coefficient, as well as the mixing ratio of fibre and resin and in the way the fibres are embedded in the resin. This opens the possibility of optimising the parameters of composite structural members in terms of stiffness and thermal and hygroscopic expansion coefficient. In close collaboration with the fibre manufacturer (Cellpac of Switzerland), optimisation methods were developed that allowed the simultaneous consideration of these parameters to obtain a structure with the required behaviour. These studies were augmented with measurements on prototype CFRP tubes. A comparison of computed and measured parameters of a CFRP member with invar end fittings is presented in Table 6.1 (Stenvers and Wilms 1989; Mäder et al. 1990). A satisfactory agreement between calculation and measurement is observed. It is of interest to mention that the CFRP tubes were pre-aged at 60 °C and 60% relative humidity for 6 months before they were cut at the required length. This rendered the tubes less sensitive to variations in humidity at the telescope site, which is at 3200 m altitude.

The BUS was pre-assembled at the company and subjected to a number of tests to check its stiffness and dynamic behaviour. Loading the structure and measuring its deformation determined the stiffness. The comparison between measurement

Table 6.1 Computed and measured parameters of a structural member of CFRP tube with invar steel node

Parameter	Calculation		Measurement	
	Tube	Member	Tube	Member
Compliance ($\mu m/kN$)	8.29	10.75	8.16	0.76
Thermal expansion coeff. ($10^{-6}/K$)	0.33	0.62	0.31	0.65
Swelling coeff. ($10^{-6}/\%rel.hum.$)	158	121	~120	–
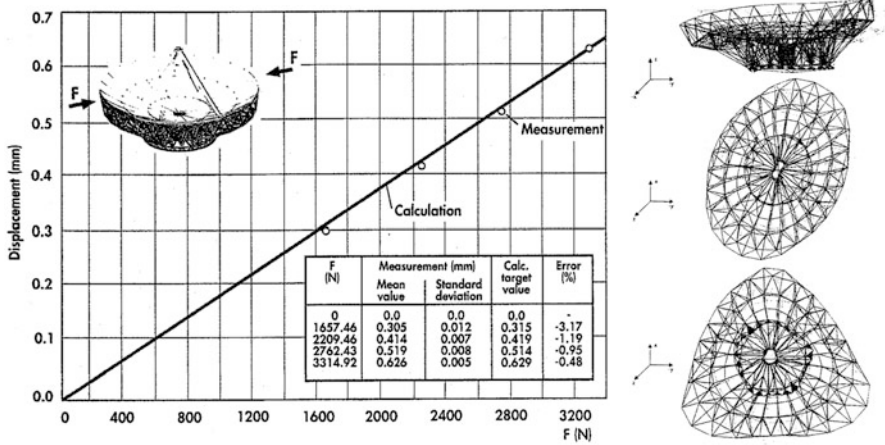
Fig. 6.5 *Left*: Measurements of the static deformation of the BUS compared to the computed relation. *Right*: Rendering of the three lowest BUS eigenfrequencies; numerical values in the text

and calculation is shown in Fig. 6.5 and confirms the high reliability of the design and the finite element analysis.

The first three natural frequencies of the BUS were measured and compared to calculated values with the result also shown in Fig. 6.5. The agreements are remarkably good with numerical values as follows:

Case	Calculation	Measurement	Difference
1	43.8 Hz	43.6 Hz	0.5%
2	46.4	47.5	2.3
3	72.3	74.1	0.3

The alt-azimuth mount is made of steel, covered by a layer of insulation. The BUS is attached along the circumference of the 4-m diameter top plate of the elevation structure by 20 "knife-edge" blades of steel. These effectively absorb the difference in thermal expansion between BUS and mount without introducing deformation into the BUS (see also Sec. 6.4.2). They can be seen in Fig. 6.6 where the black CFRP is attached to the white base plate of the mount.

Fig. 6.6 The quadripod, reflector and BUS attached to the upper flat plate of the mount. The antenna is placed in a protective enclosure. Here, the roof panels and doors are open for observations. The two dark windows in the building belong to the two instrument rooms with direct access to the Nasmyth focal points (J.Baars, SMT Observatory)

The quadripod for the support of the subreflector consists of rectangular pipes of CFRP. They are painted white to avoid solar heat and ultraviolet radiation from reaching the CFRP. The composite is sensitive to UV radiation and would disintegrate over time. For this reason, the BUS is wrapped in a white fabric shield around its back.

For the reflector panels, we turned to MAN Technologie, where at the time the panels for the IRAM interferometer antennas were under production. These panels reached a precision of about 15–20 μm, which was a factor two to three worse than we required for the HHT. The fabrication of panels for the three reflectors of the IRAM interferometer gave MAN a lot of experience and they offered a best effort for panels with a goal of 7 μm rms error provided a mould of 3 μm could be made available. This was possible through the collaboration with Steward Observatory of the University of Arizona in Tucson, where a large optics grinder had recently been installed and moreover an in-house facility for the production of Pyrex glass blanks had become operational. Pyrex moulds for the three panel rings with a surface precision of 3 μm rms were delivered from Tucson and MAN proceeded to fabricate the panels.

MAN devised a novel method to attach the aluminium front skin and simultaneously remove small-scale surface errors. A 40-μm thick aluminium foil was laid up on the mould and covered with a thin layer of epoxy on which the panel was lightly pressed down. This time the curing process was carried through at room temperature, thereby avoiding any buildup of internal stresses. The final set of

Table 6.2 HHT specified and achieved performance (in µm)

Error component	Specification	Achieved
Homology imperfection, assembly	7	<3
Space-frame residual deformation	7	<6
Panel fabrication	7	6
Panel residual deformation	7	<5
rss of structural/fabrication error	14	10
Reflector setting allowance	10	7
Overall rss error (µm)	17	12

panels showed an average surface precision of 6 µm rms, slightly better than the specification of 7 µm. Being able to fabricate panels of almost 2 m^2 at this accuracy was a significant step forward in the technology of accurate reflector surfaces.

Table 6.2 presents a comparison of the major parameters between specifications and achieved values. Using holography with a satellite signal source, the surface could be set to an overall precision of 12 µm rms. This was the best ever reached in the late 1990s and has only recently been repeated for the ALMA antenna of 12 m diameter.

Observations of planets, located near the Sun, showed the high quality and stability of the surface and pointing even when the Sun was illuminating part of the reflector (Baars et al. 1999). Several new technical methods and solutions were introduced and developed in this project that paved the way for later submillimetre telescopes such as ALMA, to be discussed next.

Early in the design of the HHT, it was decided to place the telescope in a protective enclosure in order to avoid the incorporation of survival conditions in the structural design (Fig. 6.7). The enclosure has the appearance of a co-rotating barn. During observations, the roof panels and the front doors are open, providing a clear view of the sky in the pointing direction, while normally offering some protection against wind.

6.4   Atacama Large Millimeter Array (ALMA) Antennas

6.4.1   Introduction

As we mentioned earlier, angular resolution comparable with or even better than optical telescopes can only be achieved at radio wavelengths by application of interferometry and aperture synthesis. Such telescopes for the millimetre-wavelength region were built between 1985 and 1995 in France (IRAM, see above), Japan and the USA. They consisted typically of three to ten antennas of 6–15 m diameter covering baselines to about 500 m. In the mid-1990s, proposals for much larger and more sensitive arrays were being developed in the USA, Japan and Europe. The concepts entailed up to 50 antennas of 8 to 15 m diameter to be spread

Fig. 6.7 The HHT in the opened protective enclosure. The hydraulically powered roof and door panels are closed during inclement weather (J.Baars, SMT Observatory)

over up to ten kilometres of baseline. All three groups identified the altiplano at 5000 m altitude near the 6000-m high Chajnantor Mountain in the northern Atacama Desert of Chile as the best and hence preferred site for the array. The atmospheric quality of this site would enable observations in all atmospheric windows up to 1 THz and the flat terrain allowed for the envisaged baselines of more than 10 km.

From 1997 onwards, plans were discussed to combine the three separate array proposals into one large, global Millimeter Array, actually working in the submillimetre domain up to 1 THz. This led in 2002 to the formation of ALMA, the *Atacama Large Millimeter Array*, with major partners North America (USA and Canada) and Europe (coordinated by ESO) each contributing 50% of the *basic instrument*, and East Asia (Japan, Taiwan and Korea) as third partner with a smaller contribution for so-called *enhancements*.

ALMA consists of the basic *synthesis array* of 50 antennas of 12 m diameter equipped with a cryogenically cooled system containing ten separate receiver cartridges covering the frequency region from 30 to 950 GHz [excluding the atmospheric absorption bands (Fig. 6.1)]. The enhancement consists of a set of four 12-m antennas plus a *compact array* of a dozen 7-m antennas for the measurement of the total intensity of extended object and coverage of the shortest baselines below the minimum separation between the 12-m antennas needed to avoid collision and excessive shadowing (Wootten and Thompson 2009).

Many of the dedicated single submm telescopes have been placed in some form of protective enclosure against the major influences of the environment, notably storm and snow or icing precipitation. Thus, the telescope proper could be optimised for operation under the relatively benign operational conditions without the need to accommodate survival loads. In the case of the multi-element ALMA telescope, a protective dome is out of the question. The main reason is that the antennas will be moved between stations over distances of more than 10 km. A dome-protected and transportable antenna is economically not viable. As a result, the ALMA antenna design must not only obey the stringent performance specification, but the structure must be able to withstand rather extreme survival loads without damage.

The requirements on the antennas are extremely high. The structural and electromagnetic performance specification is similar to that of the HHT but must be maintained in the open air under normal environmental conditions such as sunshine and relatively strong wind. There are some new specifications to cope with the particular difficulties of interferometry at millimetre wavelengths. The main obstacle to perfect observing conditions is the variation in the amount of water vapour in the line of sight of the antennas that causes phase changes in the received wavefronts. Even at the best sites on earth, such as the Chajnantor plateau, this often is a limiting factor to the achievable quality of synthesis imaging. To minimise the effects of atmospheric phase variations, the method of *fast switching* between the object under study and a nearby strong *calibration source* is used. The instrumental phase, including the atmospheric component, is derived from a short calibration measurement and is used to correct the main observation. Depending on the stability of the atmosphere, this might be done at intervals of the order of 10 s. The *fast switching* pointing specification aims at optimising this procedure in time and requires a high-quality servo-drive system with an advanced control algorithm.

At the highest frequency, the beamwidth of the antenna is about 6 arcseconds, which leads to a pointing precision requirement of $0.6''$ during the course of an observation. Wind and temperature effects may cause structural deviations that influence the pointing. For this reason, the regular observation is interspersed with short pointing calibrations on a nearby strong source with well-known position. This procedure is called *offset pointing*. Finally, for each pair of antennas, the measured phases of the correlated signal are also influenced by variations in the signal pathlength through each individual antenna's structure to its focal point. These can be caused by differential thermal expansion and gravitational or wind-induced bending of the structure. The specification for *pathlength stability* puts a limit on the allowable variation.

In view of the transportation between baseline stations, the minimisation of weight should be a goal. An important aspect for the design is of course the need for a series fabrication of more than 50 antennas, and finally, this must be achieved for an acceptable price. Competitive bidding is a usual way to obtain a reasonable price. The two ALMA partners (NSF/AUI/NRAO and ESO) agreed to each solicit bids for a prototype antenna, select different ones and place both products next to

each other for comparative testing. AUI/NRAO obtained an antenna from Vertex and ESO from the European consortium Alcatel-EIE-MAN (AEM).

For practical and economical reasons, the prototype antennas were erected on the site of the VLA in New Mexico, a site of inferior atmospheric quality for millimetre wavelengths (Fig. 6.8). The project was faced with the necessity to acquire the means to evaluate the performance of the antennas to a level of precision that would reliably determine their adherence to the specified performance and show any differences between the antennas. This process involved the development of new methods and equipment for the measurement of the reflector surface profile, of pathlength variations and pointing stability. We summarise these in the next section.

The antennas present rather different and interesting design aspects and technical features. A comparison between the most interesting aspects is presented below.

Political and administrative considerations led to the purchase of 25 "production" antennas from Vertex by AUI. ESO obtained 25 antennas from the Consortium Thales/Alenia Space—European Industrial Engineering (EIE)—MT Mechatronics, which we denote by AEM. Each company manufactured their own design. The Japanese partner in ALMA delivered 4 more 12-m antennas and a dozen of 7-m diameter dishes for the Atacama Compact Array (ACA), designed and manufactured by Mitsubishi. The major specifications of the ALMA antennas are listed in Table 6.3.

6.4.2 Test Program and Performance of the ALMA Prototype Antennas

As illustrated in Table 6.3, the specification of the ALMA antenna required a reflector surface precision of 25 μm with a goal of 20 μm along with a pointing and tracking precision of 0.6 arcsecond under all operational conditions. There are some additional specifications, which appear for the first time and are a result of the special requirements of interferometry at very short wavelength. We mentioned these already above: fast switching pointing, offset pointing and pathlength stability.

At large telescopes, operating at relatively long wavelengths (order cm) an overall calibration of the telescope system can often be obtained by the observation of a strong cosmic source of well-known intensity and celestial position (Sect. 8.5). At submm wavelengths with relatively small antennas like ALMA, this becomes essentially impossible.

The ALMA Antenna Evaluation Group devised several new methods and used state-of-the-art measuring equipment in an effort to quantify the actual values of the quantities listed in Table 6.3. The result of that work has been published in the open literature and in the following we summarise the methods and main results along with the references for details.

Fig. 6.8 Three ALMA prototype antennas on the test site at the VLA in New Mexico, USA. From *left* to *right*: the antenna from Mitsubishi, Japan, the North America antenna from Vertex and the European antenna from the AEM Consortium (NRAO/AUI/NSF)

Table 6.3 Specifications of ALMA antennas under operational condition

Reflector diameter	12 m
Reflector accuracy[a]	25 μm–goal 20 μm
Absolute pointing	2″ over all sky
Offset pointing	0.6″ over 2° radius (w.r.t. calibrator source)
Fast pointing switching	1.5° move in 1.5 s, settle to 3″ peak error
Pathlength stability	15/20 μm (non repeatable/repeatable)
Operating conditions	Temperature: −20 °C to +20 °C, ΔT_{amb}<0.6/1.8 °C in 10/30 min full solar loading, including solar observation average wind velocity: <6/9 m/s for day/night, respectively
Survival conditions	Temperature: −30 °C to +40 °C, wind: 235 km/h hailstones < 2 cm diameter with velocity 25 m/s ice on all exposed surfaces < 1 cm; rain 20 mm per hour snow 100 kg/m^2 on horizontal surfaces. The snow and ice loading and wind conditions have to be survived simultaneously.
Total weight should be minimised and limited to 100 tonnes, if at all possible	

[a]Includes main and subreflector, fabrication, gravity, wind and thermal deformation

The *reflector panels* were measured and set on the BUS with the aid of near-field radio holography (Chap. 8). At the elevation of the test transmitter of 7°, the surfaces of both antennas were set to 17 μm (Baars et al. 2007). Using a similar set-up on the construction site in Chile, the procedure was pushed to a measurement precision of better than 10 μm. Unfortunately, this measurement at a single elevation angle does not tell us what happens to the surface when the antenna points to high elevation.

Pointing behaviour of an antenna is routinely determined by the observation of a large set of radio sources, distributed over the sky, and deriving the parameters of the pointing model of the antenna, which accounts for deficiencies in the geometry such as non-perpendicularity of the azimuth and elevation axes (Sect. 8.5). At submm wavelengths, the dearth of sufficiently strong sources forces us to use stars as position reference. To this end, the antennas were equipped with an optical telescope mounted on the BUS and looking along the antenna axis through a hole in the reflector. This way it has been possible to determine absolute and offset (with respect to a nearby source) pointing accuracies, as well as the fast switching requirement. Very useful additional data regarding pointing and tracking variation under wind influence could be collected with a set of ten accelerometers, strategically placed on the reflector edge, the apex (focus) and vertex (centre of paraboloid) (Snel et al. 2007).

The *measurement of pathlength* variations has been attacked with the use of accurate laser-based distance measuring systems, such as the Automated Precision Inc. 5DOF instrument, which measures the three-dimensional coordinates of a point and the inclination angle of a surface containing the point with micrometer

accuracy. The critical distances in the antenna structure were monitored under varying conditions, in particular a change in temperature between day and night.

In this context, it is of interest to note that the temperature variation in the steel sections of the antenna, despite the insulation on the outside, causes significant changes in pointing and pathlength, which need to be corrected. For instance, a differential heating by the Sun of the two fork arms supporting the elevation axis and BUS/reflector structure will tilt the elevation axis in the cross-elevation direction causing a pointing error that will not be noticed by the axis-angle encoder. Alternatively to a direct measurement of the resulting length difference, it is possible to estimate the effect by measuring the temperature of the structure at a number of well-chosen points and feed the data into the finite element model of the structure to predict the length change and hence the pointing variation. The feasibility of this method has been demonstrated convincingly in the work on the ALMA prototype antennas as reported by Greve and Mangum (2008). The AEM antennas apply this method routinely in the production series of 25 antennas. In the Vertex antennas, a separate system of CFRP rods with displacement sensors provides the necessary corrections. Mangum et al. (2006) published a survey of the entire evaluation program, the applied methods and instruments along with the results. It was found that, within the limitations of the test program, both antennas satisfied the specifications.

6.4.3 Remark on the Circular BUS/ELC Interface Concept

The circular interface between the ELC and the BUS of the MRT (Chap. 5) was inspired by the umbrella cone of Effelsberg and had some influence on later telescope designs. It is particularly appropriate for telescopes where the BUS and the ELC are made from different materials. The prototype of this configuration is the Heinrich Hertz (submm) Telescope (HHT), discussed above. Its mount and elevation structure are made of steel, while the BUS is a space-frame structure of CFRP members and invar-steel nodes. Other examples of a steel elevation structure and a BUS of CFRP are the IRAM 15-m interferometer antenna and the US-ALMA antenna. These two materials show very different expansion behaviour under temperature changes.

For the prevention of temperature-induced tension forces, the interface points in the HHT are equipped with blade-shaped flexures (Fig. 6.9) which compensate differential deformations between the BUS and the yoke. In the case of the US ALMA antenna, the transition is made with a cone-shaped section made of invar steel.

(continued)

It should be kept in mind that the circular BUS/ELC interface does not solve all homology issues. There remain three effects, which have to be carefully examined as illustrated in Fig. 6.10.

1. The circular BUS/ELC interface does not prevent the influence of the elevation bearings on the reflector shape under gravity loads in zenith. The weight of the reflector shell may cause an astigmatic deformation depending on the ratio between the reflector diameter and the distance of the EL bearings and the offset of the ballast (upper left in Fig. 6.10). Optimising the ballast offset as shown for the MRT can minimise the effect.

2. A similar astigmatism may be caused by tension forces between the EL bearings themselves, which could be caused e.g. by a temperature difference between the yoke and the alidade. This may occur, for instance, if there is a temperature difference between the ELC and the fork arms of the mount (Fig. 6.10, lower left). This effect has been observed with the ALMA antenna from Vertex.

3. In horizon position, the circular BUS/ELC interface does not prevent the coma-type deformation pattern caused by the offset between the *centre of gravity* of the BUS weight (including reflector panels) and the circular interface (Fig. 6.10, right), as explained in Chap. 4 for the Effelsberg reflector. In the case of the MRT, these influences could be brought below the requirement limits by some additional struts, as described in Chap. 5. Clearly, designers should be aware of these effects to prevent unforeseen problems.

Fig. 6.9 Elevation Rotation Structure with circular BUS/ELC interface
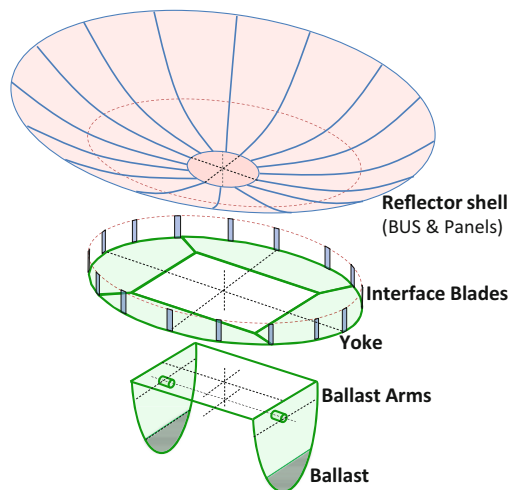
Fig. 6.10 Deformation
behaviour of an Elevation
Rotating Structure with
circular BUS/ELC interface
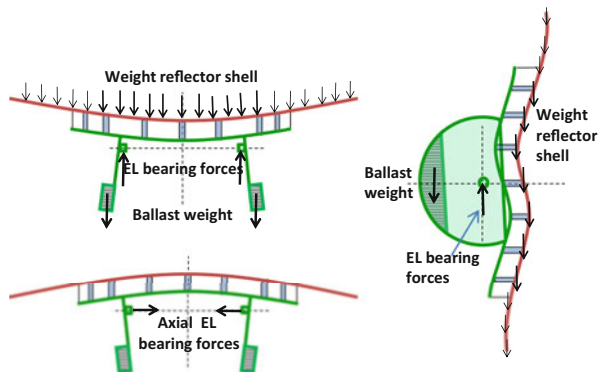
6.4.4   Comparison of the Designs from AEM/EIE and Vertex

As noted before, the "production" antennas for ALMA were designed and built in
three versions, all to an identical *requirement specification*. Nevertheless, the
results of the design activities of the individual engineering teams show interesting
differences. This provides us with the rare chance to compare the design approaches
and to gain an insight into different design philosophies by studying the details of
the different designs. We limit the discussion to the antennas from AEM
(European—EU part) and Vertex (North American—NA part) for which we have
abundant data available. These antennas are shown in Fig. 6.11. The visible
difference on the outside hides differences of detail, such as the drives, bearings
and surface panel technology.

The overview sketches of Fig. 6.12 enable us to identify these details. They are
drawn to the same scale and in an identical way to allow an engineering judgment in
a neutral manner.

The main purpose of our assessment is to see which of the differences are more
or less caused by "fashion" and experience of the engineering environment of the
designers, without consequences for performance and cost, and which of the design
differences have an impact on performance and cost.

6.4.4.1   Comparison of Structural Design

Because the *design* of the EU AEM antenna is essentially the work of EIE, we will
often refer to the EU antenna with the name EIE. Inspection of the sketches in
Fig. 6.12 allows us to identify the following commonalities or differences:

– Dimensions: the Vertex antenna is slightly more compact than the EIE antenna.
  The Vertex receiver cabin is smaller and the yoke arms are shorter, but the
  pedestal is higher. The diameter of the elevation drive and the azimuth bearing of
  Vertex is nearly half of that of the EIE antenna.

Fig. 6.11 Antennas from AEM (*left*) and Vertex (*right*) at the ALMA Assembly site (ALMA-ESO/NAOJ/NRAO)

- Structural materials: the elevation structure (backup structure and receiver cabin) of the EIE antenna is made completely of carbon fibre composites (indicated in the sketches by grey color), whereas that of the Vertex antenna is a combination of carbon fibre composites (backup structure in grey), of INVAR (the so-called INVAR cone in green) and of steel (the receiver cabin in light blue color).
- The subreflector supports (quadripod) are very different between the two antennas. The EIE quadripod consists of four single beams of oval cross section, arranged under ±45° against the EL axis and attached outside the rim of the reflector, thereby avoiding "spherical wave blocking" (see Chap. 8). The Vertex quadripod shows a complicated truss system and is arranged parallel and orthogonal to the EL axis. The design report states that the quadripod contributes to the overall stiffness of the reflector backup structure.
- The Vertex antenna employs 264 reflector panels arranged in 8 rings. The EIE antenna has 120 panels of larger size in 5 rings. Fabrication restrictions of the panel manufacturers are the cause of the difference. The Vertex antenna uses machined aluminium panels with a size of about of half a square metre, while the size of the EIE antenna panel is in the range of 1 square metre. These latter panels are made of electroformed nickel front and back skins with an aluminium honeycomb sandwich core. It provides sufficient stiffness for the larger area.

EIE antenna

Vertex antenna

EIE antenna
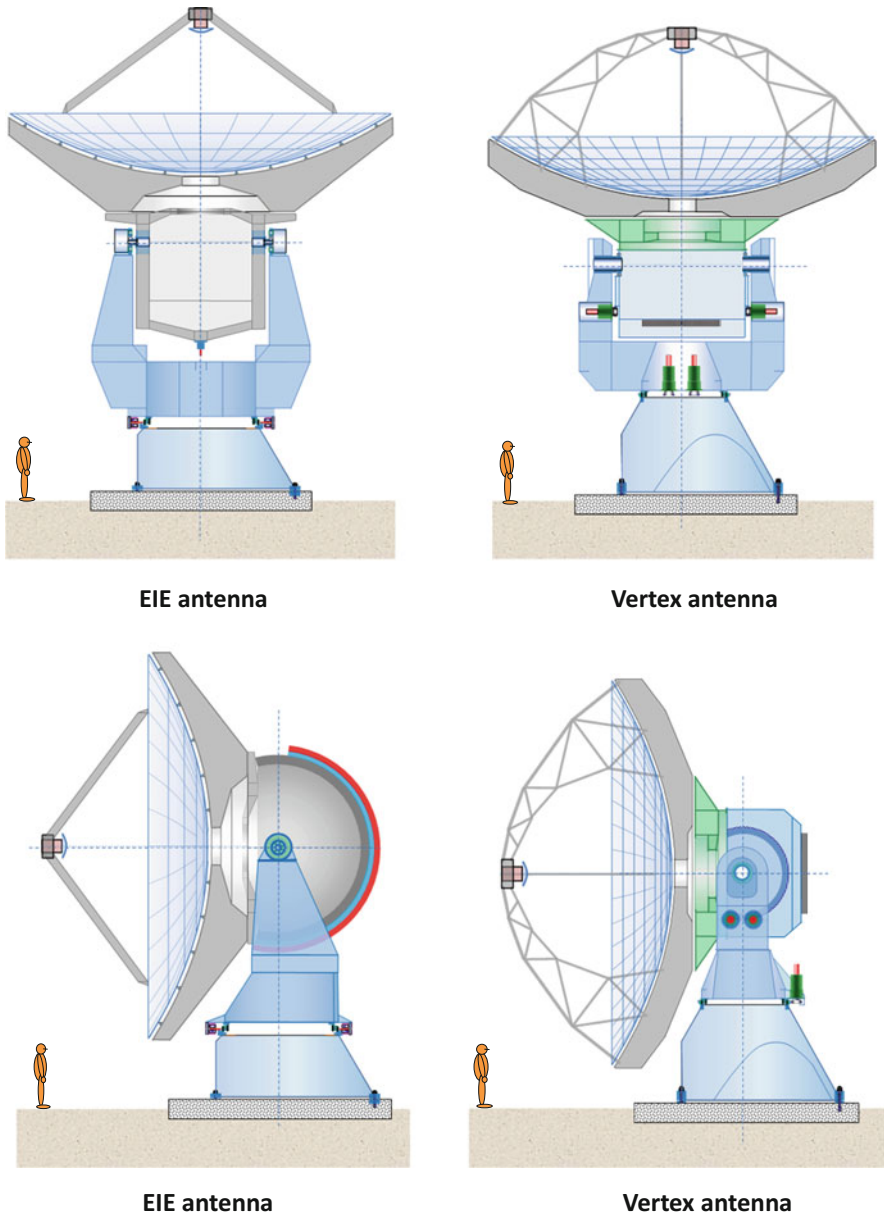
Vertex antenna

Fig. 6.12 A colour-coded comparison between the AEM/EIE (*left*) and Vertex (*right*) antennas *Grey* = carbon fibre composite; *green* = INVAR; *blue* = steel; *red* = drives/magnets

6.4.4.2 Weight

A weight breakdown of the antenna sections of the two designs is shown in Table 6.4. A comparison of the weights of the structural subsystems is of interest and leads to the following observations.

– The panel weight, including the panel adjusters, is about equal for both antennas. The overall surface weight is approximately 20 kg/m^2.
– The Vertex backup structure (BUS) is about 50% heavier than the EIE BUS. It is caused by differences in the application of CFRP technology. The EIE BUS is made of thin-walled CFRP "monocoque"-type boxes joined by glued flanges, whereas the Vertex BUS is composed of flat sandwich CFRP plates with aluminium honeycomb core, joined together by screws. A similar boxed panel providing additional stiffness and good thermal insulation closes the back of the EIE BUS. The back plane of the Vertex antenna is an aluminium sunscreen. The EIE receiver cabin is made fully out of CFRP boxed walls with superior thermal behaviour and high stiffness.
– The weight of the receiver cabin structure, including the invar cone, of the Vertex antenna is about three times that of the EIE antenna, which results from the different materials, steel vs. CFRP.
– The Vertex antenna needs more than four times the ballast of the EIE antenna. This is caused by the greater weight of the invar cone and BUS and the smaller depth of the receiver cabin resulting in a shorter lever arm for the ballast plates.
– Taken together, it leads to a big difference between the overall weights of the elevation structures, which is for the Vertex antenna more than twice that of the EIE antenna.
– The situation is reversed for the yoke and base of the azimuth structure. The EIE yoke plus base is 35% heavier than that of the Vertex antenna, which can be gleaned from the relative sizes in Fig. 6.12.
– Comparing the overall weight of both antennas, we notice that the Vertex antenna is 10% heavier than the EIE antenna. Both achieve to remain below the specification of 100 tons.

Table 6.4 Weights of the structural subsystems (tons)

	EIE	Vertex
Panels	2.1	2.2
Backup structure	5.0	7.8
Cabin, including drives	7.6	12.4
INVAR cone	–	9.1
Counterweight	3.4	15.9
Elevation section total	*22.0*	*47.4*
Yoke, including drive	50.1	34.9
Base	17.6	15.4
Overall total	*89.5*	*97.7*

Totals include some non-structural parts

6.4.4.3   Deformation Behaviour

The requirement specification for the ALMA antennas states an overall surface precision of 25 μm rms. Besides the manufacturing aspect of the panel surface, the main contributors to this are the gravity deformation of the BUS under varying elevation angle and deformations induced by temperature changes in the environment. A study of the deformation analysis of the two antennas gives us an idea about the quality of the structural design.

The deformation behaviour under gravity loads is characterised by the two *gravity-switched-on* load cases in zenith and horizontal position as explained in Chap. 4. The deformation patterns, taken from the design reports, are shown in Figs. 6.13 and 6.14 for the EIE and Vertex antenna, respectively.

For both load cases, the rms values are nearly the same, and the deformation patterns look quite similar. The EIE reflector shows in zenith position some sag along the elevation axis, which is hard to interpret. It may be caused by the not fully rotational symmetry and the stiffness of the connecting flanges to the receiver cabin. Such a feature is not apparent in the deformation pattern of the Vertex antenna, perhaps due to the stiffening function of the quadripod trusses.

In horizontal position, both antennas show the characteristic coma as explained for the Effelsberg reflector in Chap. 4. It is caused by the lever arm of the centre of gravity of the BUS against the circular interface to the receiver cabin. Here, it is the dominating effect in the overall gravity-induced reflector deformations and the related surface error budget. The slightly smaller values for the Vertex antenna may be a result of the stiffening influence of the quadripod.

For both designs, the gravity deformations are well within the allowed magnitude and no further structural optimisation was required.

$\sigma^H = 12.0$ μm rms $\sigma^Z = 6.8$ μm rms
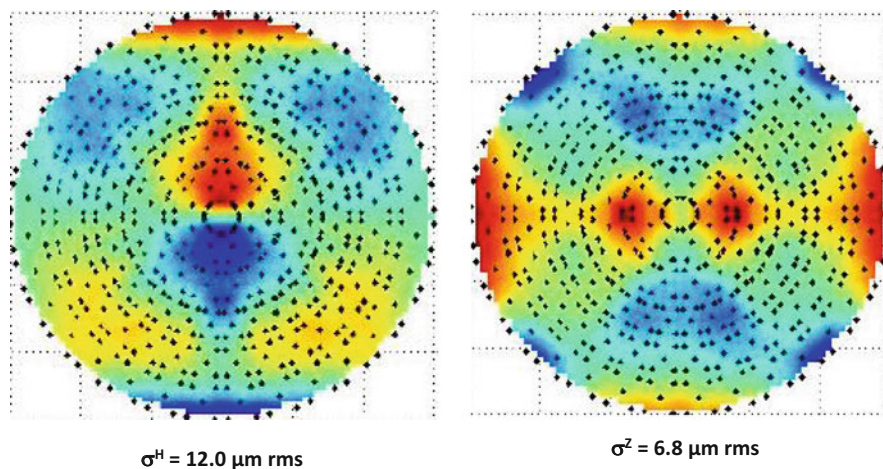
Fig. 6.13 Gravity deformation of the EIE antenna in horizon (*left*) and zenith (*right*) position (from EIE design report)

$\sigma^Z = 6.3\mu m$ rms $\sigma^H = 10.3\mu m$ rms
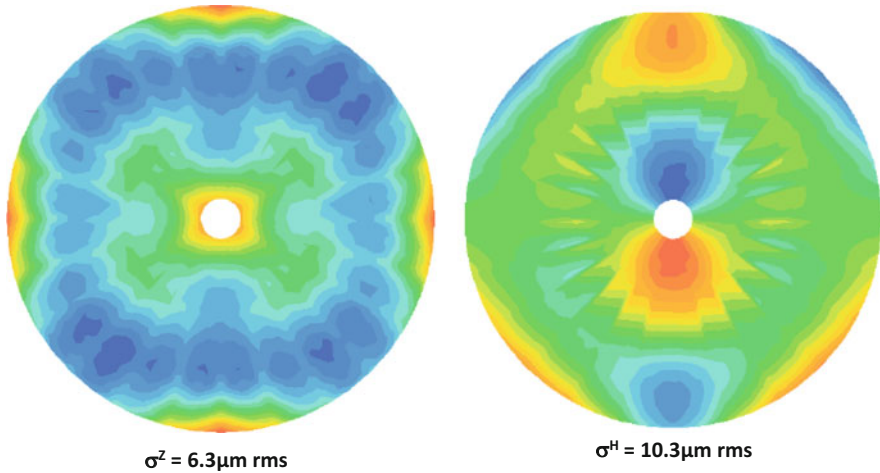
Fig. 6.14 Gravity deformation of the Vertex antenna in zenith (*left*) and horizon (*right*) position (from Vertex design report)

Once optimised for gravity influence, the structure is normally also optimised against wind-induced deformation. Because these are significantly smaller than gravity deformation, no separate optimisation for wind is necessary.

The situation is different when we consider thermal influences. Temperature-induced deformations may strongly disturb the surface error budget, as we have already mentioned earlier (Chap. 5). In fact, they are the major reason for the use of carbon fibre composites in the backup structure and the receiver cabin (in the case of EIE). The daily and seasonal change of the overall outside temperature is unavoidable. The computed deformation patterns of both antennas for a rather extreme 20 K decrease in temperature are shown in Fig. 6.15.

The rms values are equal and the deformation patterns are quite similar. Both are dominated by astigmatism, which is most likely caused by a thermal constraint between the elevation and the azimuth structure. While the computed values fall within the specified allowance, the measured effect has shown to be stronger on the Vertex production antennas as illustrated in Fig. 6.16, taken from Mangum (2015). Some of the Vertex antennas fail to meet the overall surface specification at the extreme end of the defined temperature region for primary operation (25 μm).

6.4.4.4   Interpretation of the Astigmatism from Basic Structural Mechanics

The deformation pattern is dominated by astigmatism, which is caused by the thermal constraint between the elevation and the azimuth structure. The astigmatic deformation patterns under temperature loads as well as the second-order coma under gravity in horizontal position are caused by the circular BUS interface and can be understood with basic structural mechanics.

$\sigma^{\Delta T=20K}$ = 5.2μm rms   EIE $\sigma^{\Delta T=20K}$ = 5.2μm rms   Vertex
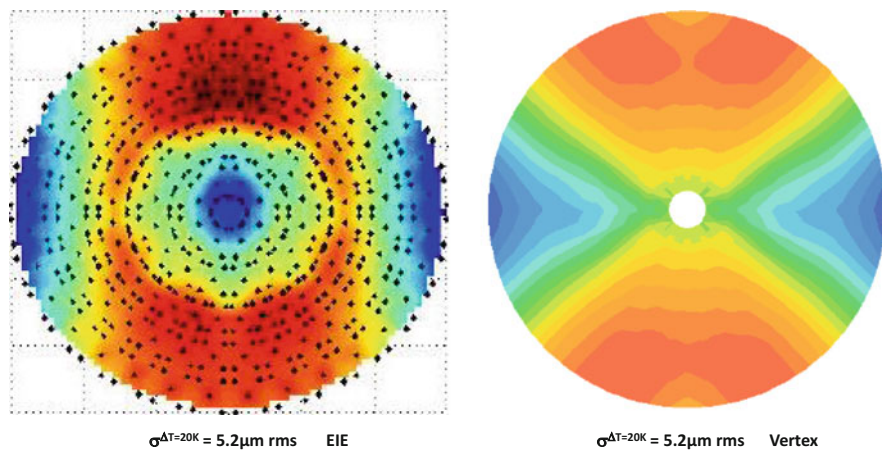
Fig. 6.15 Calculated surface deformation for a temperature change of 20 K (from EIE and Vertex design reports)
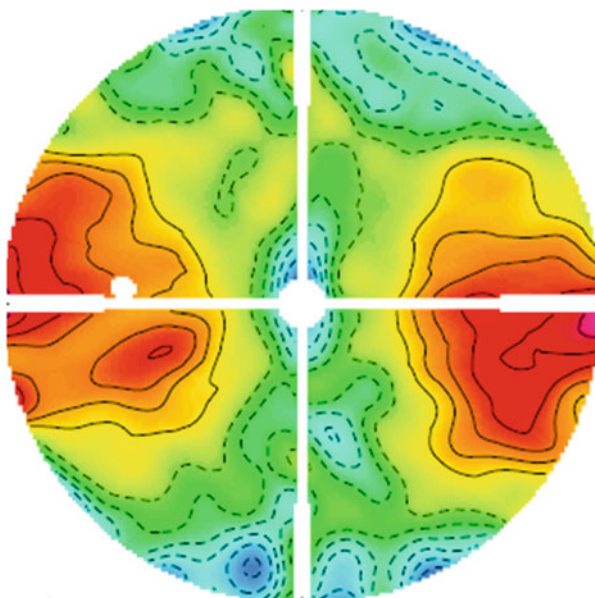
Fig. 6.16 Measured reflector surface pattern of a Vertex antenna. The astigmatism is caused by a large temperature difference between the setting and measurement epoch. (There is a colour swap with Fig. 6.15.) (ALMA—ESO/NAOJ/NRAO)

A closer look into the details of the structural design of the EL structure of the Vertex antenna (Fig. 6.17) allows an understanding of the astigmatism problem. The EL structure is composed of subsystems made of several materials with different thermal expansion behaviour. The thermal expansion coefficient of the
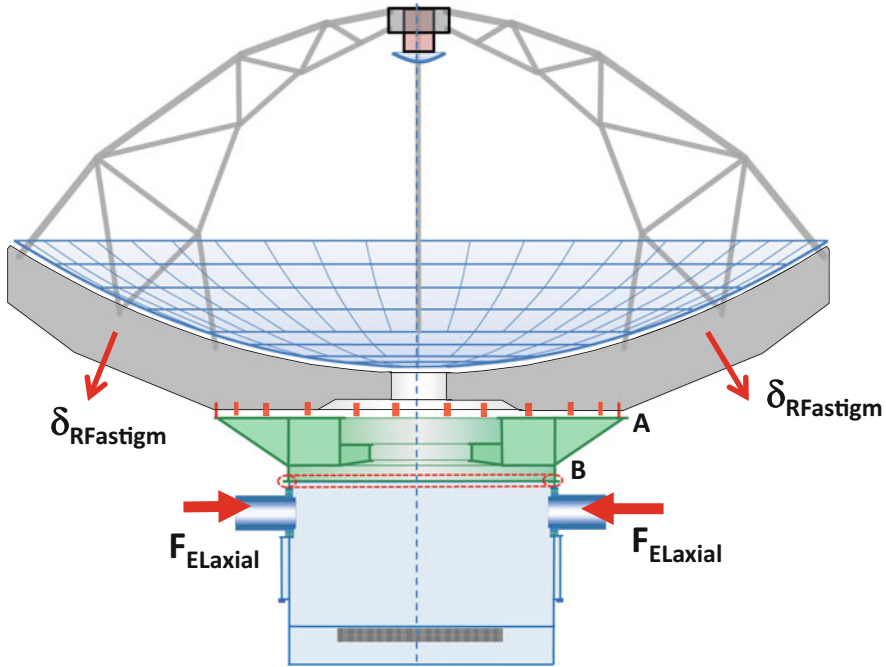
Fig. 6.17 Interpretation of the astigmatism of the Vertex antenna under temperature load

steel receiver cabin is more than ten times that of the INVAR cone or the CFRP backup structure. These differences result in thermal constraints, if the interfaces between the components are not carefully decoupled in a "thermally isostatic" way.

The design details in Fig. 6.17 show that the interface between the receiver cabin and the INVAR cone (indicated by "B") are configured as rigidly connected flanges, whereas the CFRP backup structure is connected to the INVAR cone via circularly arranged radial flexible blades (indicated by "A"). These blades are providing an isostatic decoupling between the BUS and the INVAR cone, which actually would be not necessary, because the thermal expansion of INVAR and CFRP is nearly the same.

The situation at the interface between the INVAR cone and the receiver cabin is very different. Here, a rigid flange connection is chosen, which implies a bimetallic effect between the two structural components. This will cause a curvature in the cone top layer that causes first of all a defocus, which could be effectively removed via the subreflector positioner. However, much more critical are the constraints with the yoke arms of the azimuth structure that exert a force ($F_{ELaxial}$) on the receiver cabin in axial direction via the EL bearings. Such axial forces will pull down the adjacent reflector area (deflections $\delta_{RFastigm}$) resulting in the observed astigmatic deformation. The circular blades between the BUS and the cone do not prevent the print-through of this effect onto the reflector surface. In the Vertex prototype, this effect was counteracted by a control system to maintain a uniform
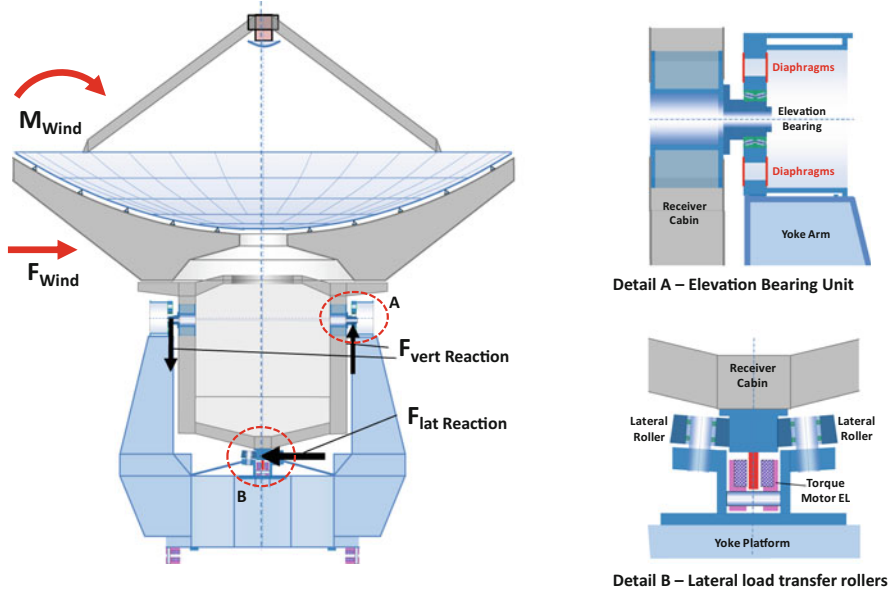
Fig. 6.18 Isostatic decoupling between elevation and azimuth structure of EIE antenna

temperature of the walls of the receiver cabin. It was abandoned in the series antennas for cost reasons.

The designers of the EIE antenna introduced a rather sophisticated and complicated solution for the isostatic decoupling between the elevation and the azimuth structure. We are not aware of anything similar in any other telescope mount (Fig. 6.18).

The elevation bearings of the EIE antenna contain two sets of diaphragms (right upper sketch) that prevent the transfer of axial loads via the bearings. This avoids the thermal constraint and the resulting astigmatic deformation of the antenna. A consequence of this is that other loads, introduced e.g. by wind, have to be transferred otherwise to the azimuth structure. The EIE engineers introduced therefore additional rollers in the centre of the yoke base (lower right sketch), which react there (force $F_{lat\ reaction}$) against the wind loads. The resulting turnover moments introduce vertical reaction forces ($F_{vert\ reaction}$) in the elevation bearings (Fig. 6.18, left). The EIE system appears somewhat intricate and probably is expensive but it fulfils its purpose of isostatic decoupling of the elevation section from the azimuth structure in regard to thermal effects.

6.4.4.5 Comparison of the Bearing and Drive Systems

As we noted above, the drive systems of the EIE and Vertex antenna are quite different. We compare these and the bearings in terms of realisation and performance.

The Vertex antenna uses a conventional geared drive with standard servomotors at high rated speed, which is reduced to antenna speed by a planetary gear train. The mechanically amplified motor torque is transferred to the antenna axis via pinions onto toothed gear rims, in azimuth integrated with the azimuth bearing (Fig. 6.19, left). For the prevention of the backlash in the teeth of the gears, the azimuth axis is equipped with two gear/motor units which are pre-tensioned during tracking via the control system, which means that only one motor unit is used for driving, and the second one is used for controlling the backlash. The two drive units are arranged on the rear side of the azimuth yoke platform. The driving force at the pinion tooth T_{drive}, which produces the torque about the antenna axis, activates a reaction force R_{react} in the radial rollers of the azimuth bearing (Fig. 6.20, left). When changing the movement direction, the role of the driving and pre-tensioning pinion as well as the reaction in the bearing rollers changes from one to the other side. This creates micro-movements in the teeth as well as the bearing rollers, which have influence on the tracking (jitter) and fast switching behaviour as well as the overall lifetime of the related components.

In the EIE antenna, any backlash and reaction forces on the bearing are avoided by the use of symmetrically arranged direct driving torque motors (Fig. 6.20, right). The azimuth motor consists of ten segments that produce the driving forces in tangential direction all in the same direction and avoid thereby a reaction on the bearing. The motor segments have two magnetic acting gaps (Fig. 6.19, right), in which the driving forces are produced. The magnetic field of the motor is produced by permanent magnets arranged on a "stator disc" attached to the fixed flange of the
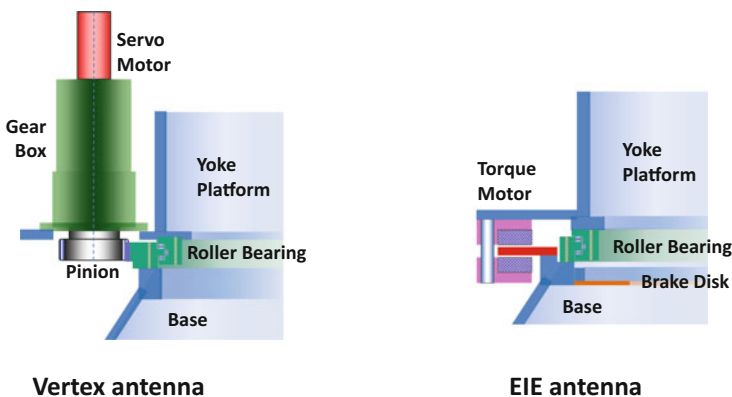
Fig. 6.19 Cross section through the azimuth bearing and drive of Vertex (*left*) and EIE (*right*) antenna
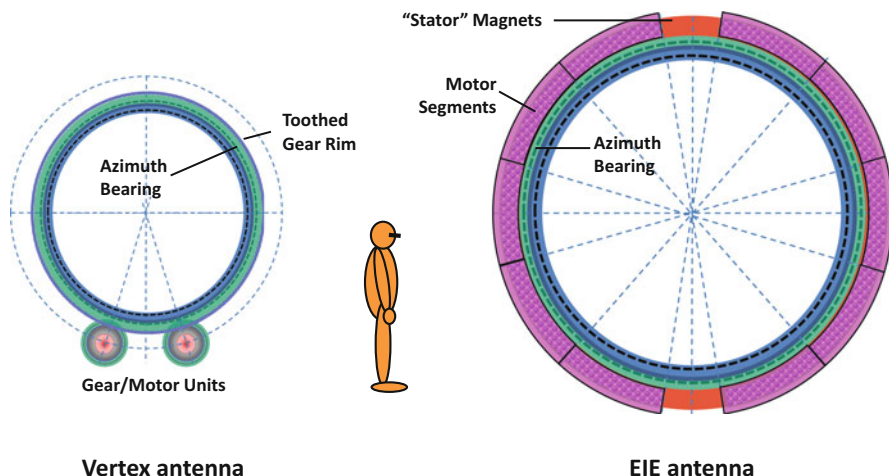
Fig. 6.20 Comparison of azimuth bearing and drive diameters of Vertex (*left*) and EIE (*right*) antenna (same scale)

base alongside the azimuth fixed bearing ring. The driving magnetic motor force is produced by the motor windings on top and bottom of the stator magnets by a current controlled by the amplifiers in the servo system. The distance from the axis to the magnetic gap, where the driving moment on the axis is produced by tangential magnetic forces distributed over the whole circumference, is about twice that of the toothed gear rim of the Vertex antennas, where the concentrated tooth forces of the driving pinions produce the driving moment on the axis. Due to this "smooth" arrangement, the required driving force inside one gap of one motor segment is in the range of only 1–2% of the driving force required at the pinion tooth of the Vertex antenna.

6.4.4.6   Dynamic Behaviour, Structural Resonance Frequencies

The tracking (jitter) and fast switching performance of an antenna is strongly dependent on the overall resonance behaviour of the antenna structure including the flexibility of the drives and is described by the "locked rotor" frequencies. The design reports give a lowest value of 7.1 Hz for the Vertex antenna and 9.3 Hz for the EIE antenna. The difference can be explained by the difference in weight of the structural masses (see Table 6.4) and the difference in stiffness of the drives as explained in the previous section.

The locked rotor frequencies, along with the free rotor frequencies, are the limiting factors for the layout of the position control algorithms. The overall position control and tracking behaviour of the EIE antenna are therefore expected to be somewhat better than that of the Vertex antenna. A quantified comparison can

only be done comparing the systems by equivalent end-to-end models and equivalent tests on the actual antennas. Such data are not (yet) available to us but can be expected to become available in due time.

Summarising the conclusions of this section, the comparison of the two ALMA antenna designs is somewhat similar to comparing a Harley-Davidson and a BMW motorbike. The Vertex antenna employs a conventional and proven design (the HHT experience; see Sec. 6.3.2), particularly in the drive system. The transition from the steel receiver cabin to the CFRP reflector backup structure via the invar cone seems to have some weakness. The EIE antenna has a very progressive drive system. The sophisticated structural design concept with optimum use of CFRP in the BUS resulted in an elevation structure with very low inertia.

From the system engineer's point of view—that is inspecting the available design information as described above—the Vertex antenna may be just at the specified limits, whereas the EIE antenna provides a significant engineering margin. A comparison of the difference in cost of the two systems against a possible performance difference is futile. Costs contain also political and administrative components. Its discussion goes well beyond the goal of this book.

6.4.5   Conclusion

In the fall of 2014, all 66 antennas of ALMA, equipped with the extensive receiver system, had arrived at the operations site at 5000 m altitude on the Llano de Chajnantor. Observations with the partially completed array had already been conducted since 2008 (see ALMA's web page www.almaobservatory.org). Figure 6.21 shows the four different types of antenna in the ALMA telescope. The two antennas in the foreground are the Vertex antenna (left) and the AEM antenna (right). Vertex delivered 25 antennas to the North American partner and AEM delivered another 25 antennas to the European partner. The two antennas in the background (centre) are the Mitsubishi 12-m antenna (left) and the Mitsubishi 7-m antenna (right). Mitsubishi delivered four 12-m antennas and twelve 7-m antennas to the East Asian partner. These 16 antennas form the Atacama Compact Array (ACA) (Iguchi et al. 2009).

All 12-m antennas underwent some small changes from the prototype version, based on experiences gained during the construction and operation of the prototypes. The performance of the production series has been summarised by Mangum (2015) for the North American antennas from Vertex and by Laing (2015) for the European antennas from AEM.

At the time of writing (early 2017), ALMA is in its fourth Observing Cycle with an essentially complete operational system. The front picture of this chapter gives an impression of the layout, although less than half of all antennas are shown. Observations with a partial and ever-growing array have been conducted for several years and have produced stunning results. The instrument is more than an order of magnitude more powerful than existing millimetre telescopes, in both sensitivity

Fig. 6.21 The four varieties of ALMA antennas. In foreground the 12-m antennas from Vertex (*left*) and Alenia-EIE-MT Mechatronics (AEM) (*right*). In background on right the 7-m antenna and on left the 12-m antenna from Mitsubishi [ALMA(ESO/NAOJ/NRAO), W. Garnier, ALMA]

and angular resolution. Baselines up to 15 km have been used providing angular resolution of 0.02 arcsecond, better than the Hubble Space Telescope.

In the submillimetre region, ALMA eclipses anything available at present, whereby the atmospheric quality at the high site adds significantly to the operational efficiency. The antennas perform almost entirely to specification. As noted above, some antennas develop slightly too high surface deformation at the extreme ranges of the operational temperature range, near $-20\ ^{\circ}$C. This situation arises rarely; nevertheless, actions are being undertaken to correct for this deficiency.

ALMA is likely to have an even greater impact on astronomy than the VLA in the 1980s. It provides the ultimate performance in the submillimetre range with the currently available technology. Any significant increase in performance of the instrument by improved receiver systems will need to include a method to determine the phase fluctuations caused by the earth's atmosphere with high precision.

Nevertheless, plans for other telescopes in the mm and submm region are being made. There are proposals and some design activities for a 25-m diameter single telescope that will allow observations between 1 and 2 THz, a 50-m antenna for up to 700 GHz and several 90–110-m telescopes for operation up to 100 GHz. None of these have been fully designed and costed nor funded at the time of writing.

References

Baars, J.W.M., Martin, R.N., Mangum, J.G., McMullin, J.P., Peters, W.L.: The Heinrich Hertz Telescope and the submillimeter telescope observatory. Publ. Astron. Soc. Pacific. **111**, 627–646 (1999)

Baars, J.W.M., Lucas, R., Mangum, J.G., Lopez-Perez, J.A.: Near-field radio holography of large reflector antennas. IEEE Antennas Propag. Mag. **49**(5), 24–41 (2007)

Bregman, J.D., Casse, J.L.: A simulation of the thermal behaviour of the UK-NL mm wave telescope. Int. J. Infrared mm Waves. **6**, 25 (1985)

Greve, A., Mangum, J.G.: Mechanical measurements of the ALMA prototype antennas. IEEE Antennas Propag. Mag. **50**(2), 66 (2008)

Guilloteau, S., et al.: The IRAM interferometer on Plateau de Bure. Astron. Astrophys. **262**, 624–633 (1992)

Ho, P.T.P., Moran, J.M., Lo, K.Y.: The submillimeter array. Astrophys. J. **616**, L1 (2004)

Iguchi, S., Morita, K., Sugimoto, M., Vila Vilaró, B., Saito, M., Hasegawa, T., Kawabe, R., Tatematsu, K., Sakamoto, S., Kiuchi, H., Okumura, S.K., Kosugi, G., Inatani, J., Takakuwa, S., Iono, D., Kamazaki, T., Ogasawara, R., Ishiguro, M.: The Atacama Compact Array (ACA). Publ. Astron. Soc. Jpn. **61**, 1–12 (2009)

Laing, R.: The performance of the European ALMA antennas. 36th ESA Antenna Workshop (2015)

Leighton, R.B.: A 10-meter telescope for millimeter and sub-millemeter astronomy. Technical Report of California Institute of Technology (May 1978)

Mäder, H.F., Stenvers, K.-H., Gatzlaff, H., Wilms, H.-F.: The 10-m submillimeter-wave telescope. Technische Mittelungen Krupp (Eng.) **1**, 27–42 (1990)

Mangum, J.G.: The performance of the North American ALMA antennas. 36th ESA Antenna Workshop (2015)

Mangum, J.G., Baars, J.W.M., Greve, A., Lucas, R., Snel, R.C., Wallace, P., Holdaway, M.: Evaluation of the ALMA prototype antennas. Publ. Astron. Soc. Pacific. **118**, 1257–1301 (2006)

Serabyn, E., Phillips, T.G., Masson, C.R.: Surface figure measurements of radio telescopes with a shearing interferometer. Appl. Opt. **30**, 1227–1241 (1991)

Snel, R.C., Mangum, J.G., Baars, J.W.M.: Study of the dynamics of large reflector antennas with accelerometers. IEEE Antennas Propag. Mag. **49**(4), 84–101 (2007)

Stenvers, K.-H., Wilms, H.-F.: Entwicklung und Optimierung eines tragenden CFK-Raumfachwerks für astronomische Teleskope. VDI-Berichte. **734**, 75–92 (1989)

Woody, D., Vail, D., Schaal, W.: Design parameters and measured performance of the Leighton 10.4-m-diameter radio telescopes. Proc. IEEE. **82**, 673–686 (1994)

Woody, D.P., et al.: CARMA: a new heterogeneous millimeter-wave interferometer. Proc. SPIE Millimeter Submillimeter Detect. Astron. II. **5498**, 30 (2004)

Wootten, A., Thompson, A.R.: The Atacama large millimeter/submillimeter array. Proc. IEEE. **97**, 1463–1471 (2009)

Chapter 7
Alternative Reflector Geometries
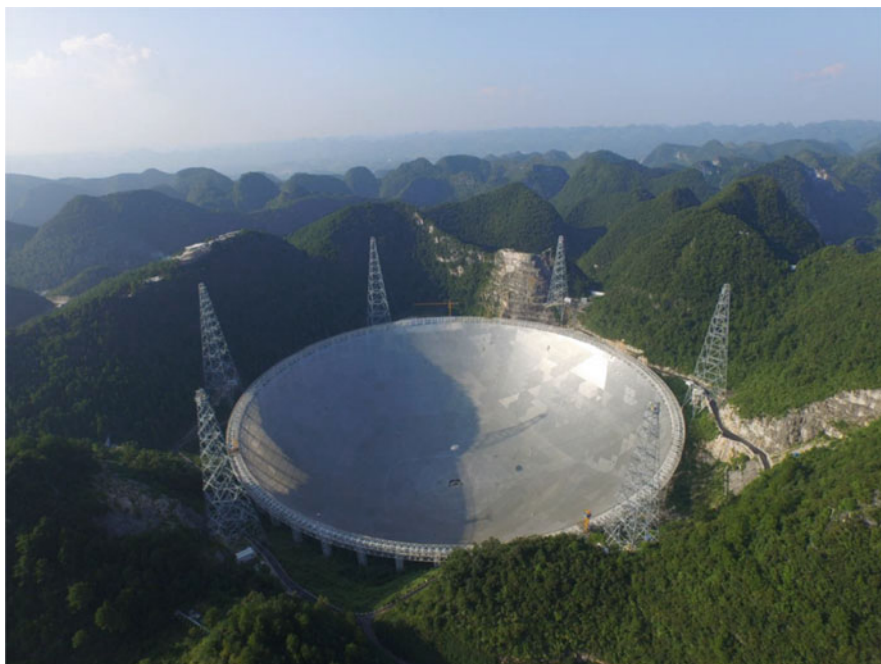
The FAST (500 m) fixed telescope in China in operation since 25 September 2016. The focus cabin, the white spot just above the centre, with its shadow at '4 o'clock', is supported and moved by six cables from the towers. It can be lowered to the centre hole of the dish for servicing (NAOC/CAS/China)

7.1   Telescopes with Fixed Main Reflectors

It is increasingly difficult and costly to increase the diameter of a reflector that is attached to a two-axis mount and maintains its accuracy in all attitude angles. After the completion of the Jodrell Bank giant, several ideas for a telescope of comparable or larger size, but very much cheaper, sprang up among radio astronomers and engineers. We shortly mention here the major examples.

Obviously, a large saving can be achieved if we avoid any movement of the primary curved surface. An early example (1947) of this was the 218-feet diameter wire-mesh paraboloid tied to the ground at Jodrell Bank. The big drawback of a stationary reflector is of course the very limited sky coverage. Apart from the rotation of the earth, which provides a daily trace of sky through the viewing direction, only a movement of the feed near the focus enables any increase in sky coverage. For a paraboloid, this is a very restricted region because of the strong coma effect of such a mirror (Chap. 8). The one at Jodrell Bank was specifically configured to observe the nearest galaxy M31, the Andromeda Nebula that passes near the zenith at Jodrell's latitude.

Around 1960, several telescopes with fixed reflectors were designed and built. A summary description of these is presented by Findlay (1964). The Arecibo spherical dish of 305 m diameter is the most impressive example of a stationary reflector (Fig. 7.1). Built in the early 1960s, it was originally devoted to ionospheric studies by radar backscatter, but it was soon also used for radio and radar astronomy (Gordon 1964). A spherical reflector creates a caustic, that is, a region of concentration of reflected rays, along a line focus at half the radius of curvature, independent of the direction of incidence with respect to the axis of the sphere. The bowl was constructed in a "Karst" hole near Arecibo, Puerto Rico. Cables from three towers on the surrounding hills suspended a platform near the focus. On this a line feed was mounted, which could be moved in two coordinates. An angle of about 30° with respect to the zenith could be reached, allowing an observing time of the order of 1 h for objects in the accessible declination zone. In 1997, the line feeds were replaced by a system of two Gregory-type shaped subreflectors allowing standard feed horns to be used (Kildal et al. 1994). The antenna is still in operation, now under management of SRI International.

At the University of Illinois, a *cylindrical paraboloid* was dug into the ground with dimensions of 400 × 600 ft. (122 × 183 m) (Swenson and Lo 1961). By phasing the log-period feeds along its axis, the beam could be steered along the meridian through an angle of 60°. Operating at a frequency of 610 MHz, the telescope produced a survey of the accessible sky, using the rotation of the earth as a "free" coordinate movement. It was closed in 1970 (Fig. 7.2).

John Kraus at Ohio State University devised yet another scheme: the radio equivalent of the *coelostat,* but restricted to function only as a transit instrument (Kraus 1963). Referring to Fig. 7.3, the telescope consists of a section of a paraboloid placed vertically on the ground. At some distance along the local meridian a flat reflector is placed, capable of tilting in elevation along the meridian. This enables radiation from a particular elevation direction in the sky to be directed

Fig. 7.1 The 315-m diameter stationary, spherical Arecibo dish in Puerto Rico. The domed structure under the moving platform contains optics to create a point focus (NAIC—Arecibo Observatory, a facility of the NSF)

at the paraboloid, which in turn concentrates the radiation towards its focal point, located just above the ground in front of the tilting reflector. At this position, the feed with receiver is located. This transit instrument also uses the rotation of the earth for azimuth coverage, while the tilting mirror selects the declination of the observed sky area. To provide a short tracking period, the feed system can be moved in the focal area over a short distance in azimuth.

Kraus built such a telescope, called the "Big Ear" around 1960 in Ohio (Fig. 7.4.). The focusing reflector was 21 m high and about 100 m wide. The telescope operated mainly at 21 cm wavelength. It was demolished in 1998 to make place for a golf course.

A similar telescope with a *spherical main reflector* was built in France and put into operation in 1967 (Ginat 1969). The size of the Nançay telescope is 30×300 m, and it has a larger tracking range because of the spherical reflector. It is still in full operation (Fig. 7.5).

The RATAN 600-m diameter Kraus-type antenna in the North Caucasus region of Russia offers several modes of operation by choice of various focal points, each using a certain part of the instrument (Fig. 7.6). Used at the full diameter, it has a beamwidth of half an arcminute at a wavelength of 8 cm (Korolkov and Pariiskii 1979).
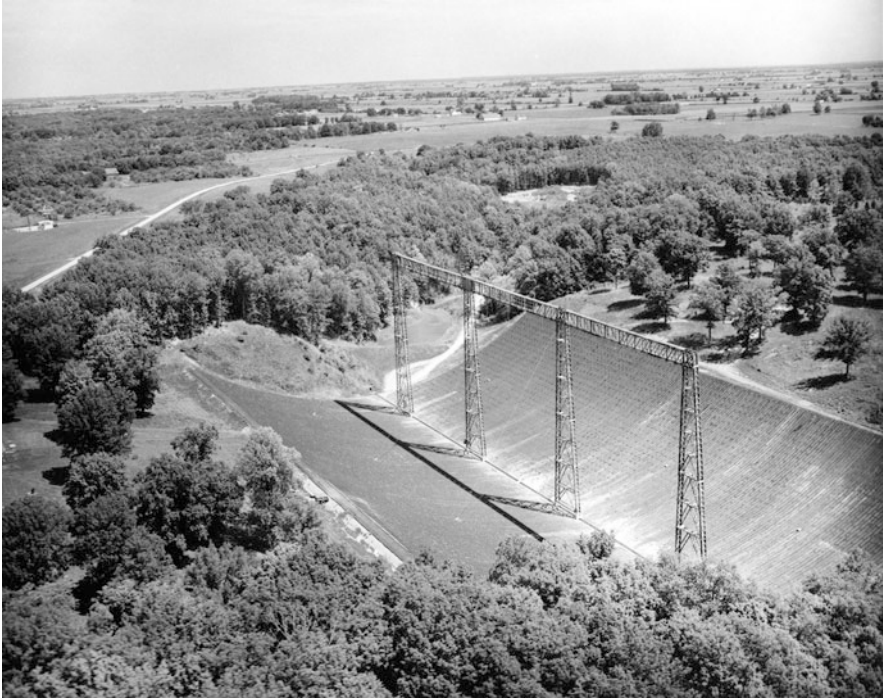
Fig. 7.2 The 600 × 400 ft. (183 × 122 m) cylindrical paraboloid of the Vermilion River Observatory. It operated at 610 MHz (Courtesy of the University of Illinois Archives)
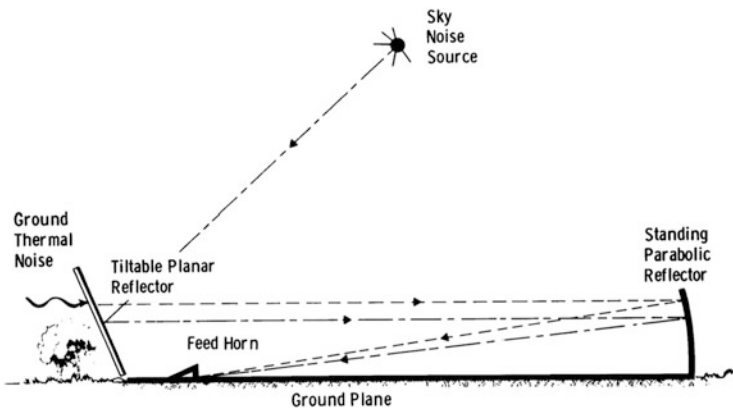
Fig. 7.3 Principle of the "Kraus-type" radio telescope. A section of a paraboloid is fixed to the ground (*right*). A tiltable flat mirror directs radiation from a certain elevation angle to the paraboloid, which reflects it to the focus near the ground in front of the tiltable mirror

Fig. 7.4 The "Big Ear" built by John Kraus in Ohio (Tom Root Air Photos, USA)

Fig. 7.5 The Nançay Radio Observatory Kraus-type telescope with fixed spherical reflector (*right*), which reflects the radiation coming from the flat, tiltable reflector at *left* to the focal area near the ground in front of the flat (*white cabin*) (Nançay Radio Observatory, France)

Finally, we mention the Chinese project FAST (*Five-hundred-meter Aperture Spherical Telescope*), shown on the front page of this chapter (Peng et al. 2009; Nan 2008). Similarly to Arecibo, it is located in a natural sinkhole (*Karst*) in the province of Guizhou in western China. The basic shape of the reflector is a sphere of 500 m diameter, of which a part of 300 m diameter will be illuminated during

Fig. 7.6 The 600-m diameter circular RATAN telescope. Several additional reflectors provide a number of different focal points. In the centre of the *circle* is a special reflector cone to concentrate the radiation onto a single horn feed. An angular resolution of 5 arcseconds can be achieved at the shortest wavelength of 1 cm (Special Astrophysical Observatory, Russia)

observation. This section is then actively deformed to a paraboloid by a system of motorised cables so that a single focal point, devoid of spherical aberration, is established. A lightweight cabin, supported and driven by six servo-controlled cables, plus an additional secondary system for fine adjustment, carries the receiver in the focal area and enables precise pointing and tracking. The zenith angle range is 40° with a tracking range of 4–6 h depending on the declination of the source. It will be used to a highest frequency of 3 GHz, where the angular resolution will be about 1.5 arcminute. The construction was completed in the summer of 2016 and test observations commenced on 25 September 2016.

7.2 The Giant Metrewave Radio Telescope (GMRT) in India

The GMRT is an indigenous project. Its design and realisation was carried out entirely by Indian scientists, engineers and industry. The instrument is an interferometric array of 30 large dishes of 45 m diameter, spread over an area of about

25 km diameter. It operates at long wavelengths from 8 m down to 21 cm. The National Centre for Radio Astrophysics (NCRA) of the Tata Institute of Fundamental Research (TIFR) has carried out the project. The GMRT is located near Pune (Swarup 1991; Swarup et al. 1991).

An important technological breakthrough was achieved in the design of lightweight dishes that enabled the realisation of the antennas at a relatively low cost. The design is based on what is being called the SMART concept—for *Stretched Mesh Attached to Rope Trusses*. The dish has been made lightweight and of low solidity by replacing the conventional backup structure by a series of rope trusses (made of thin stainless steel wire ropes) stretched between 16 parabolic frames made of tubular steel. The wire ropes are tensioned suitably to make a mosaic of plane facets approximating a parabolic surface. The lightweight thin wire mesh (made of 0.55 mm diameter stainless steel wire) with a grid size varying from 10×10 mm in the central part of the dish to 20×20 mm in the outer parts, stretched over the rope truss facets, forms the reflecting surface of the dish. The average deviation of the facets from the paraboloid is about 10 mm, which is a small fraction of the wavelength and hence impedes the performance only slightly (Chap. 8).

The low-solidity design cuts down the wind forces by a large factor and is particularly suited to Indian conditions where the site is free of snow. The overall wind forces and the resulting torques for a 45-m GMRT dish are similar to those for a 22-m antenna of conventional design, thus resulting in substantial savings in cost. The dish is connected to a cradle which is supported by two elevation bearings on a yoke placed on a 3.6-m diameter slewing-ring bearing secured on the top of a 15-m high concrete tower. The weight of the dish is about 80 tonnes and the counter-weight is about 40 tonnes (Fig. 7.7).

7.3 Large Horn Antennas

Because of its simple geometry, the horn antenna is amenable to an exact calculation of its gain. Consequently, so-called *standard gain horns* have been used extensively as a comparison device in the gain calibration of other antenna types. If a horn is made sufficiently large to reliably measure the flux density from a strong cosmic source, the true, absolute flux density of this source can be derived. This in turn can be used to establish the gain of a large, hitherto uncalibrated antenna (see Chap. 8). Then the measured signal from an unknown source with the now calibrated telescope can be assigned a true flux density to derive intrinsic source parameters. A description of these procedures can be found in Baars et al. (1977) and Baars (2014).

In the 1960s, several horn antennas were constructed for the purpose of measuring the absolute flux density of strong radio sources. The "Little Big Horn" (Fig. 7.8) at the NRAO in Green Bank made for many years almost daily observations of the strong source Cassiopeia A at 1440 MHz (Findlay et al. 1965).

Fig. 7.7 The GMRT array consists of 30 reflectors of 45 m diameter with a mesh surface. It operates from 38 to 420 MHz. The reflector is based on the SMART concept: Stretched Mesh Attached to Rope Trusses (Courtesy, G. Swarup, NCAR, India)

At the Bell Telephone Labs in Holmdel, NJ, a large fully steerable horn with an aperture of 6 × 6 m was constructed for studies of satellite communication (Crawford et al. 1961). Penzias and Wilson used it to make absolute measurements of radio sources (Fig. 7.9). In this process, they found a noise contribution of about 3 K from all directions (Penzias and Wilson 1965). This is the Cosmic Microwave Background, the cooled remnant of the Big Bang. The discovery earned them the Nobel Prize in Physics in 1978. Similar horn antennas were constructed at the Algonquin Observatory in Canada (Broten and Medd 1960) and Haystack Observatory in Massachusetts (Allen and Barrett 1967).

7.4   Offset Reflector Antennas

7.4.1   Introduction

Because the aperture of a horn is completely unobstructed, contrary to most reflector antennas, the beam is very clean with weak and symmetrical sidelobes. A similar situation can be achieved with a reflector by using a section of the

Fig. 7.8 The "Little Big Horn" at the NRAO in Green Bank, WV. It measures the absolute flux density of the strong source Cassiopeia A at 21 cm wavelength once a day when the source drifts through the beam. Over many years, an accurate measure of the secular decrease in Cassiopeia's intensity was also obtained (NRAO/AUI/NSF)

paraboloid that lies outside the optical axis. Now the feed can be placed in the focal point without its supporting structure blocking part of the main reflector. A complete electromagnetic design of this geometry was presented by Cook et al. (1965) at the Bell Telephone Laboratories, which was followed by the construction of an accurate 7-m diameter antenna, shown in Fig. 7.10 (Chu et al. 1978).

The most common prime focus offset antenna is the ubiquitous personal satellite dish for the direct reception of satellite-borne TV transmissions. Normally, large *offset antennas* are configured as dual-reflector Cassegrain or Gregorian systems.
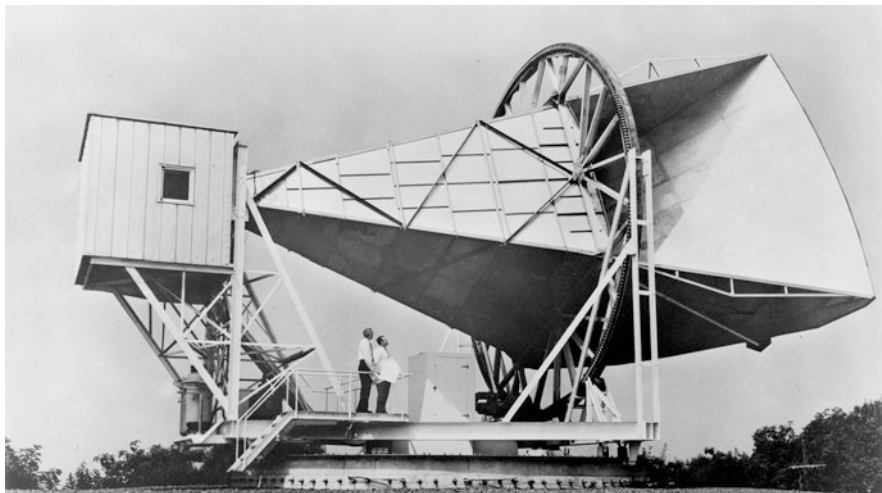
Fig. 7.9 The horn antenna at the Bell Labs in Holmdel, NJ, has an opening of 6×6 m and operates near 4 GHz. It was used for satellite communication experiments and for radio astronomy. A. Penzias and R. Wilson (not the persons on the platform) detected the Cosmic Microwave Background at 2.7 K with this instrument (Reprinted with permission of Nokia Corporation)

The electromagnetic advantages of a high efficiency and a clean beam with low sidelobes are somewhat offset (!) by polarisation effects, due to the asymmetry of the geometry, which are difficult to control, although Mizuguchi et al. (1978) and Dragone (1978) have shown ways to maintain good polarisation behaviour. Current comprehensive computer packages for electromagnetic field computations allow the design of a *combination of feed and shaped dual reflector* with optimised characteristics for the specific purpose of use.

The asymmetric layout renders the optimum application of homology in the structural design more difficult and normally results in the need to employ more material to reach a certain surface precision with unavoidable cost consequences. Thus, a compromise must be sought between the astronomical requirements, reflected in the EM performance, operational advantages and structural realisation. We illustrate this by a short description of several recent offset telescopes.

7.4.2   Allen Telescope Array (ATA)

The Allen Telescope Array (ATA), a project of the SETI Institute in Mountain View and the University of California Berkeley, employs dual-reflector offset antennas (Welch et al. 2009). The array is designed to have 350 elements. Up to now (2016), only 42 elements have been procured (Fig. 7.11). Since 2012, SRI International operates the array predominantly for the Search of Extra-Terrestrial Intelligence (SETI).

Fig. 7.10 The dual-reflector offset antenna at the Bell Labs. The accurate 7-m diameter reflector could be used at millimetre wavelengths. The Cassegrain subreflector is to the left on the support structure. The focus with the feed is in the cabin under the lower edge of the main reflector and Nobel laureate Arno Penzias in front (Reprinted with permission of Nokia Corporation)

The antennas are Gregorian offset systems with a paraboloidal primary and ellipsoidal secondary reflector. The main dish is a single piece of aluminium with a diameter of 6.1 m with a stiffened rim. The 2.4-m secondary reflector is supported at the rim by a shroud that prevents ground radiation to reach the feed, thereby helping to realise a very low system temperature. The reflectors are shaped by hydro forming on a mould, figured in the right contour with the aid of photogrammetric measurements. The reflector is connected to a simple El-Az mount with a screw drive for the elevation motion. A single broadband log-periodic feed provides an operational bandwidth from 0.5 to 10 GHz.

7.4.3 *MeerKAT and Square Kilometre Array (SKA)*

The global radio telescope project *Square Kilometre Array* (SKA) will contain a low-frequency (50–350 MHz) aperture synthesis array, consisting of hundreds of thousands of log-periodic dipoles to be located at the Murchison Radio Observatory in North-western Australia, and an array of several thousands of reflector antennas of 15 m diameter, operating from 350 to 15,000 MHz (Hall 2005). The *dishes* will

Fig. 7.11 Dual-reflector offset antennas of the Allen Telescope Array (ATA). A shroud that shields the system from ground radiation supports the secondary reflector (Rick Forster, SETI Org.)

be shaped dual-reflector offset antennas, and most of them will be located in the Karoo desert of the Northern Cape Province of South Africa with array stations in several countries in Southern Africa to attain baselines of up to 3000 km. Next to the electromagnetic advantages, mentioned above, an important argument in favour of the offset geometry is the possibility to locate a large receiver package containing several separate units on a rotating platform near the focal point without causing aperture blocking.

The *MeerKAT* telescope array (Jonas 2009) is an initiative of the South African SKA Project and is an official *precursor* of the SKA. It consists of 64 antennas, located in the centre area of the future South African part of the SKA and spread over an area of 8 km diameter. The array became operational in 2016 and will be integrated after a few years in the first phase of SKA.

The antenna of MeerKAT is configured as an *Offset Gregorian* dual-reflector system with a primary reflector of 13.5 m diameter and a secondary reflector of 3.8 m diameter (Fig. 7.12). The primary surface consists of 40 aluminium panels supported on a steel backup structure and the subreflector is a one-piece composite structure. The backup structure is of a standard design using finite element methods to achieve the required performance with minimum weight. As is clear from the

Fig. 7.12 The first MeerKAT antenna of 13.5 m diameter in the Karoo desert of South Africa. The full array will contain 64 antennas spread over an area of 8 km diameter (J. Jonas, SKA-SA)

picture, a rather strong *boom* is needed to support the large subreflector. The boom also provides support for the receiver platform near the secondary focal point.

The MeerKAT antennas have been designed to reach an overall surface accuracy of 0.6 mm, which provides excellent performance up to 20 GHz. The El-Az mounting employs a circular, toothed azimuth bearing with pinion drive, while the elevation angle is set by a linear rack drive. The pointing accuracy under optimal conditions is 5 arcseconds, decreasing to 25 arcseconds in a more normal, windy situation. The weight of the antenna is only 42 tons. At the time of writing (summer 2016), the construction at the site is in progress. Tests of the first units have shown conformity with the specifications and an array of 16 antennas has produced some impressive first astronomical results.

The SKA antennas will be 15 m in diameter with a geometrical layout similar to that of MeerKAT. Prototyping for this antenna has been going on for some time. A design for a lightweight single-piece reflector from CFRP was realised in Canada. MT Mechatronics of Germany with the Chinese company CETC54 proposed an alternative design for a highly modular all-metal version. This proposal has been selected for prototype realisation because of its lower cost and reduced risk in the choice of material, assembly and transportation. A rendering of the antenna is shown in Fig. 7.13. The reflector consists of 66 triangular aluminium panels supported by a truss-frame BUS. The BUS has a tetrahedron geometry composed of steel tubes bolted to steel nodes. Only a few types of nodes and length of tubes are employed, which eases manufacturing and assembly, while requiring a

Fig. 7.13 A rendering of the design of the SKA 15-m diameter antenna (SKA Organisation)

minimum in transportation volume. The weight of the antenna is about equal to that of the smaller MeerKAT antenna. A total of 133 dishes will be combined with MeerKAT for the first phase of the SKA. The plan for the full SKA comprises some 2000–3000 reflectors.

7.4.4   Green Bank Telescope (GBT)

As we pointed out earlier, for a certain deformation tolerance the offset antenna requires more material than the symmetric reflector, which will increase the cost. This disadvantage did not prevent the NRAO from replacing the collapsed 300-ft transit telescope (Chap. 3) with a fully steerable offset reflector of 100-m aperture

diameter, the Green Bank Telescope (GBT). The primary argument in favour of the offset configuration was the *clean beam* with very low sidelobes, which would enable high-quality mapping of very weak extended objects. The choice of diameter was understandably determined by the desire for a telescope at least as big and powerful as the Effelsberg 100-m antenna. The need to slightly enlarge the diameter of an offset reflector in one direction to obtain an effective circular aperture would increase the size to 110 m in one coordinate, and hence, the telescope would be bigger than Effelsberg, certainly a good "selling point".

The decision to build an offset antenna had significant consequences as we listed above. Early in the design phase, it was realised that the goal of a surface accuracy of 0.4 mm rms could only be realised with an actively controlled surface. Also the pointing requirement would be very difficult to achieve without special provisions to measure and counteract wind influences in real time. As a result of these considerations, it was decided to develop and install an elaborate optical reference and measurement system to control both surface shape and pointing direction in real time. Thus, the GBT would be the first radio telescope with *closed loop active deformation control*. This complete system has not been successfully employed up to now. Actually, using other approaches, in the area of *open loop active control*, the telescope functions satisfactorily.

The construction was started in 1991 and the telescope came into operation in 2002 (Prestage et al. 2009). A picture of the GBT is shown in Fig. 7.14.

Fig. 7.14 The Green Bank Telescope (GBT) with an effective diameter of 100 m. The Gregorian optics enables operation from both the primary and secondary focus (NRAO/AUI/NSF)

Structural Design of the GBT

The structural design of the Green Bank Telescope is dominated by the choice of the offset geometry for the optics. As illustrated in Sect. 2.2.3, the focus of such an arrangement is about twice farther from the reflector than in a circularly symmetric layout. Consequently, a large support tower for the secondary reflector or primary focus equipment is necessary. Fortunately, it can be as bulky as needed, because it does not cause aperture blocking. The projection effect of the offset geometry necessitates an increase in the diameter of the reflector of about 10% in the direction normal to the elevation axis.

The structural system of the GBT consists, as that of conventional rotational symmetric telescopes, of three major subsystems:

1. The reflector backup structure supporting the reflector surface panels through motor-controlled adjusters;
2. The elevation cradle that connects the reflector backup structure with the elevation bearings and the elevation drives; it includes the supporting tower for the secondary reflector and receiver room;
3. The alidade that connects the elevation bearings and drives with the azimuth bogies and the azimuth pintle bearing.

Consequences of the Offset Approach for the Elevation Structure

The sketches in Fig. 7.15 and the picture in Fig. 7.14 show that the backup structure is in radial direction larger and more flat than that of a rotationally symmetric reflector. The shape of the reflector panels and the related topology of the backup truss system are adapted to the overall radial-circumferential geometry of the parent paraboloid. This achieves identical panel shapes in each circumferential ring, a clear advantage in the manufacturing process.

Dedicated isostatic interface points between the backup structure and the elevation cradle (shown in Fig. 7.15) achieve a certain level of homology. However, the project planned from the beginning an active surface for the main reflector to push the overall system accuracy beyond conventional passive reflectors. Hence, homology was not a primary concern.

The cantilevered structure for the support of the secondary reflector and the receiver room requires huge overhanging trusses in the elevation cradle that increase the weight of particularly this subsystem compared to conventional telescopes. It also requires a large amount of counterweight.

Remarks on the Design of the GBT Alidade

The alidade of the reference design in the proposal phase of the project (Fig. 7.16) presented a conventional structural concept with large box beams arranged in the direction of the load paths of the forces such as gravity and wind, similar to most large radio telescopes.

The alidade of the actually built telescope (Figs. 7.14 and 7.15) is composed of a dense filigree truss system. This concept is hard to understand from the viewpoint of structural mechanics. It was probably driven by manufacturing and transportation considerations, such as avoiding large welded box beams.
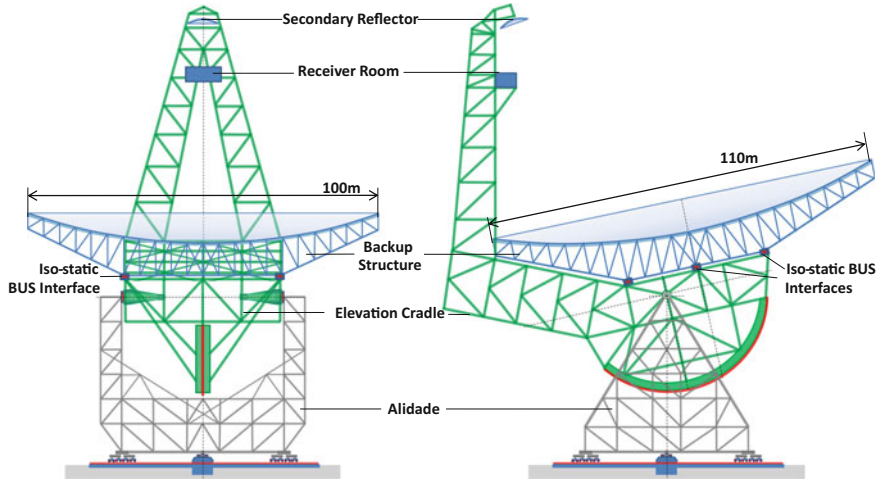
Fig. 7.15 The structural subsystems of the GBT
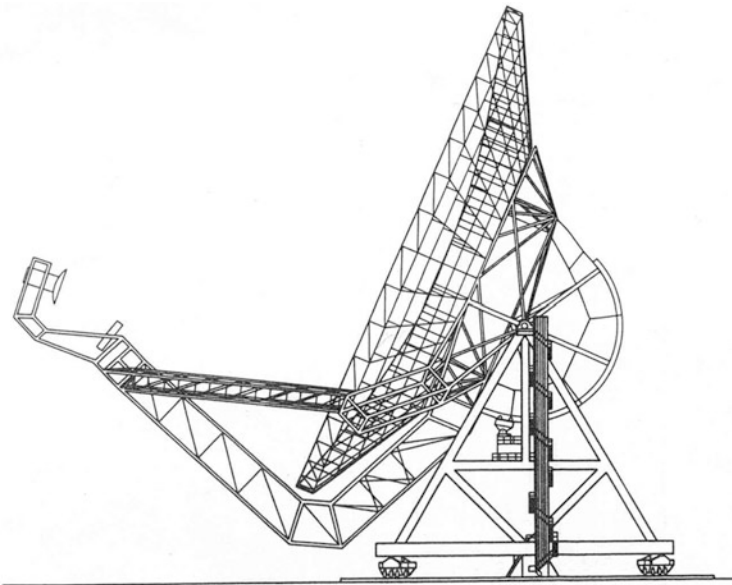
Fig. 7.16 The original reference design of NRAO during the proposal phase of the GBT project (NRAO/AUI/NSF)

The alidade resembles somewhat the alidade of the 76-m Lovell telescope (Chap. 3). The original alidade of the Lovell of 1956 (Fig. 7.17 left) showed some weakness in lateral direction parallel to the El axis. In 1976, diagonal bracings were added equivalent to the diagonals of the Effelsberg alidade (Chap. 4).

The overall deformation behaviour of the first Lovell alidade in lateral direction is equivalent to a sideward bending of a U-shaped beam (Fig. 7.18 left). Because the diagonals are missing, the bending (fixing) moment at the bottom of the two arms causes an S-type bending of the alidade base indicated by the green lines. The additional diagonal braces that were added later (Fig. 7.18 right) assure the transfer of lateral loads directly to the pintle bearing in the centre and eliminate the bending of the alidade base truss system.

In the GBT alidade (Fig. 7.19), the base truss system is even larger and more complex than in the Lovell telescope. It is difficult to imagine how the loads may be transferred from the El bearings and drives to the Az bogies and pintle bearing. A truss member may or may not contribute to the overall stiffness. Those not contributing and therefore superfluous members add weight and costs.

From the viewpoint of the structural designer, the U-shaped beam model as illustrated for the Lovell telescope gives a first hint to the deformation behaviour of the GBT alidade, but a realistic understanding can only be obtained by computer-aided finite element modelling. The designers of the GBT alidade have presumably made such a computer-aided structural optimisation, but the weight of the actually built telescope is nevertheless more than twice that of Effelsberg. This is not only caused by the offset optics but surely also by the decision for the filigree-trussed alidade.
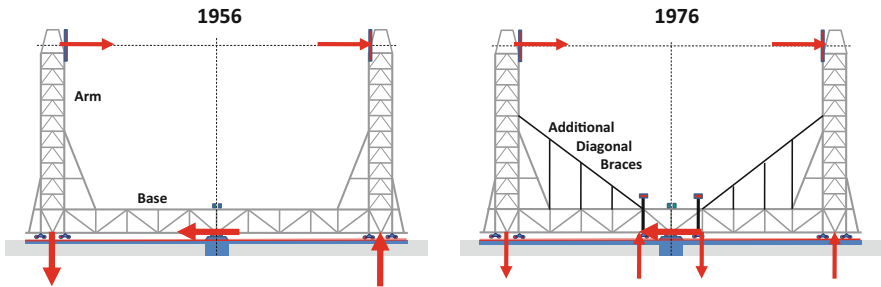
Fig. 7.17 The Lovell alidade before (*left*) and after (*right*) enhancement
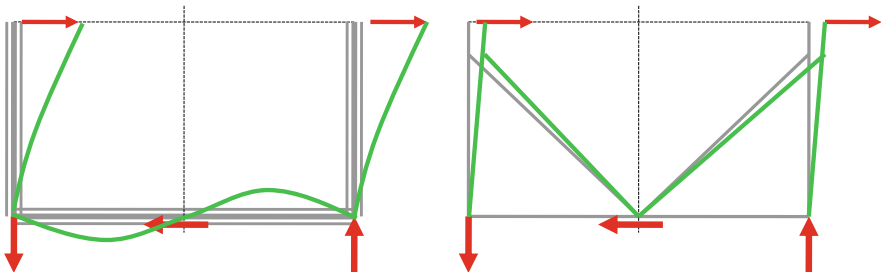
Fig. 7.18 Deformation features of the Lovell alidade before (*left*) and after (*right*) enhancement. *Thin red arrows* indicate the wind forces and *thick red arrows* the reaction forces. The deformed situation is shown in *green*
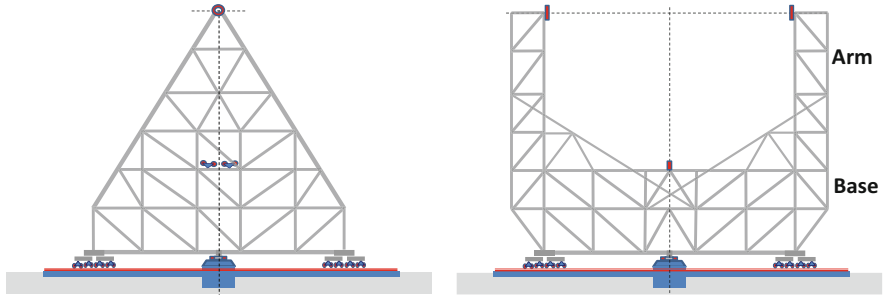
Fig. 7.19 The GBT alidade. The pintle bearing is located at the *centre* in *blue*

Closing Remark on the GBT
After its initial commissioning, the GBT, as several other large telescopes, has faced a number of serious and time-consuming problems. The significantly higher weight than originally designed and the chosen design of the azimuth bogies required a full replacement of the azimuth rail track.

The active control of the reflector shape is realised by feeding the finite element model with extensive data of the BUS temperature distribution and regular updates of the large-scale profile of the reflector from holographic measurements. These data are used to adjust the surface panels to the best-fitting paraboloid. Under benign wind conditions, the GBT functions near its original specification.

Addendum: Remarks on Wheel-On-Track Systems

Wheel-on-track systems for the azimuth movement are a feature of large radio telescopes. Nowhere else in the field of wheel-on-track applications are such huge loads per wheel applied as in radio telescopes. Examples are 100 tons per wheel for the Effelsberg telescope and 475 tons per wheel for the Green Bank telescope. The only somewhat similar application in other technical areas exists in the field of hydraulic steel constructions, but the requirements there are very different in regard to accuracy and life cycle loads. The wheel-on-track system of a radio telescope is an important and sensitive subsystem with an impact on reliability and performance. We summarise some of its essential features.

The first huge radio telescope in Jodrell Bank used for its azimuth axis system the best available technology, a wheel-on-track system based on standard railway tracks. The problem of the large loads was solved by a large number of wheels on bogies, and by more than one track (in the final construction status three), and by two railway rails per track. The rails were mounted discontinuously in segments with bolts and gusset plates connecting the joints, as was usual in railway technology. The system has worked well over more than 50 years with adequate maintenance by the Jodrell Bank crew.

The main issues for the design of a wheel-on-track system are the optimisation of the rolling behaviour of the wheels on the track and the handling of the high stresses in the contact area between the wheels and the track. Both issues have a big impact on pointing performance and lifetime of the telescope.

A number of bogies normally located at the four or six corners of the alidade transfer the weight of the telescope via the track to the foundation. For the relatively small telescopes, only one wheel per alidade corner may be sufficient (e.g. Dwingeloo, see Chap. 3). With large telescopes, the contact stress problem forces the use of two or more wheels per corner, and the load distribution between the wheels is achieved by sequentially arranged levers (Fig. 7.20). The very large telescopes have four (Green Bank) or even eight (Effelsberg) wheels per corner.

The rolling behaviour of a wheel on the track depends on two angles of the wheel axis; the *steering* angle determines the direction of the rolling movement and the *chamfer* angle determines the curvature of the movement. For an accurate rolling behaviour, both angles have to be precisely aligned during assembly and commissioning.

For fine alignment of the steering and the chamfer angles, it is important to understand their influence on the rolling behaviour of the wheels. A misalignment of the steering angle causes a skew symmetric runout of the wheels on the track (Fig. 7.21 top), while a misalignment of the chamfer angle causes a symmetric runout of the wheels (Fig. 7.21 bottom). This different behaviour can be easily identified during commissioning of the drive system of the azimuth axis, for instance via dial gauges between the bogie body and the load spreader.

Two different design approaches for the wheel axis alignment evolved in the advancement of radio telescopes, one with self-aligning features for the chamfer angle (developed by JPL for the Deep Space antennas and used also for the GBT) and the other with alignment levers for both angles with some similarities to the steering mechanisms of car wheels (developed by MT Mechatronics for the LMT (Chap. 5) and the Sardinia Radio Telescope. The Effelsberg bogies use a third alignment concept, based on sliding blocks that can be interpreted as a predecessor of the alignment levers.

The self-aligning features of the GBT bogies (Fig. 7.22 left) are achieved by triangular flexures, which separate the body of the bogie from the load spreader. A misalignment of the wheels against the track, caused e.g. by local inaccuracies of

Effelsberg   Green Bank

Fig. 7.20   The lever systems for the bogies of Effelsberg and Green Bank telescopes
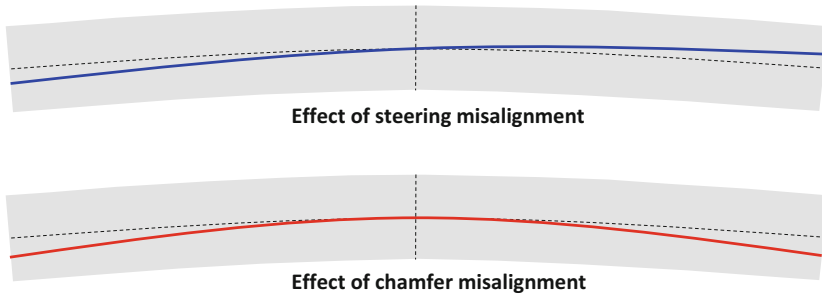
Fig. 7.21 Influence of misalignment of the bogies on the rolling behaviour. *Top*—steering, *bottom*—chamfer

Fig. 7.22 Two different design approaches for the wheel axes alignment. *Left*: *GBT* Green Bank Telescope; *right SRT* Sardinia Radio Telescope

the track surface, is compensated by a bending of the triangular flexures. This bending causes a reaction moment in the contact area of the wheel on the track and a related edge pressure (Fig. 7.23 left).

The design philosophy of the SRT bogies is completely different (Fig. 7.22 right). It has a crowned wheel. The crowning diameter is chosen in such a way that a slight deviation of the chamfer angle does not cause edge pressure but moves the centre of the contact area a little sideward (Fig. 7.23 right). The self-aligning features of the GBT concept are not needed here.

The coarse alignment of the chamfer angle during assembly of the telescope is done in the GBT by shims and in the SRT by a tappet at the end of an alignment lever at the bogie. For the GBT system, realignment requires releasing the loads on the wheels via jacks. The SRT system allows very fine realignment by the tappet during slight movement of the telescope without jacking.
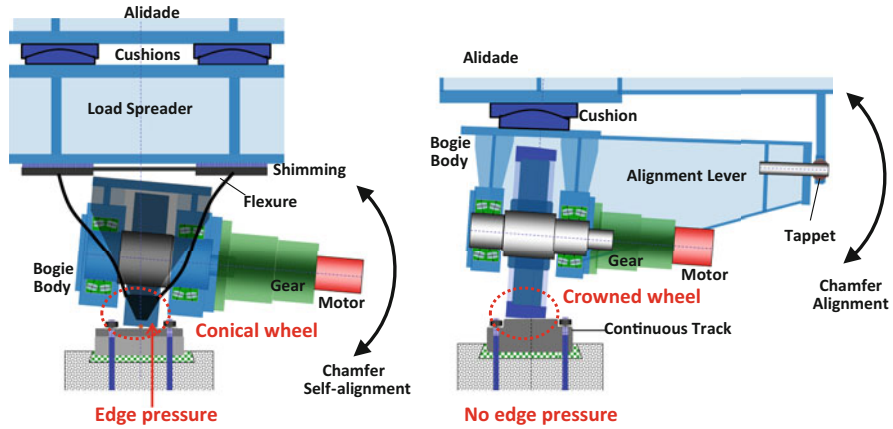
Fig. 7.23 Comparison of chamfer alignment features. Same scale; *left*: *GBT* Green Bank Telescope; *right SRT* Sardinia Radio Telescope
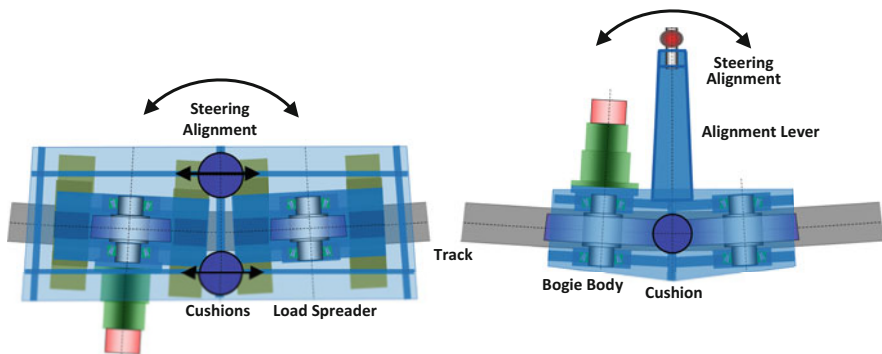
Fig. 7.24 Comparison of steering alignment features drawn at same scale. *Left*: *GBT* Green Bank Telescope; *right*: *SRT* Sardinia Radio Telescope

The alignment lever of the SRT system is also used for the alignment of the steering angle (Fig. 7.24 right). In the GBT, the alignment of the steering angle is done during assembly by lateral alignment of the cushions (Fig. 7.24 left). A realignment of the steering angle would necessitate removing the loads on the wheels by jacking.

A large runout of the wheels on the track causes a lateral restraining force between the wheels and the track that can become very high, above the limits set by friction between the wheels and the track. In such a case, the lateral forces parallel to the wheel axis (not the rolling forces) can suddenly release and cause an impulse type vibration of the complete telescope structure. Clearly, such an instance should be avoided.

References

Allen, R.J., Barrett, A.H.: Absolute measurements of the radio flux from Cassiopeia a and Taurus a at 3.64 and 1.94 cm. Astrophys. J. **149**, 1–13 (1967)

Baars, J.W.M.: History of flux density calibration in radio astronomy. URSI Radio Sci. Bull. **348**, 47–66 (2014)

Baars, J.W.M., Genzel, R., Pauliny-Toth, I.K.K., Witzel, A.: The absolute spectrum of Cas A: an accurate flux density scale and a set of secondary calibrators. Astron. Astrophys. **61**, 99–106 (1977)

Broten, N.W., Medd, W.J.: Absolute flux measurements of Cassiopeia A, Taurus A, Cygnus A at 3200 Mc/s. Astrophys. J. **132**, 279–285 (1960)

Chu, T.S., Wilson, R.W., England, R.W., Gray, D.A., Legg, W.E.: Comstar experiment: the Crawford Hill 7-meter millimeter wave antenna. Bell Syst. Tech. J. **57**, 1257–1288 (1978)

Cook, J.S., Elam, E.M., Zucker, H.: The open Cassegrain antenna. Bell Syst. Tech. J. **44**, 1255–1300 (1965)

Crawford, A.B., Hogg, D.C., Hunt, L.E.: A horn-reflector antenna for space communication. Bell Syst. Tech. J. **40**(4), 1095–1116 (1961)

Dragone, C.: Offset multireflector antennas with perfect pattern symmetry and polarization discrimination. Bell Syst. Tech. J. **57**, 2663–2684 (1978)

Findlay, J.W.: Radio telescopes. IEEE Trans. Antennas Propag. **12**, 853–864 (1964)

Findlay, J.W., Hvatum, H., Waltman, W.B.: An absolute flux density measurement of Cassiopeia A at 1440 MHz. Astrophys. J. **141**, 873–884 (1965)

Ginat, M.: The Nancay radio telescope. In: Mar, J.W., Liebowitz, H. (eds.) Structures Technology of Large Radio and Radar Systems, pp. 55–63. MIT Press, Cambridge, MA (1969)

Gordon, W.E.: Arecibo ionospheric observatory. Science. **146**, 26030 (1964)

Hall, P.J.: The square kilometre array: an international engineering perspective. Exp. Astron. **17**, 5–16 (2005)

Jonas, J.L.: MeerKAT – the South-African array with composite dishes and wide-band single-pixel feeds. Proc. IEEE. **97**, 1522–1530 (2009)

Kildal, P.-S., Baker, L.A., Hagfors, T.: The Arecibo upgrading: dual-reflector feed system. Proc. IEEE. **82**, 714–724 (1994)

Korolkov, D.V., Pariiskii, I.N.: The Soviet RATAN-600 radio telescope. Sky Telescope. **57**, 324–329 (1979)

Kraus, J.D.: The large radio telescope of Ohio University. Sky Telescope. **26**, 12–16 (1963)

Mizuguchi, Y., Akagawa, M., Yokoi, H.: Offset Gregorian antenna. Trans. Inst. Electron. Commun. Eng. Jpn. **61B**(3), 166–173, 1978 (also in IEEE AP Symp. Digest., 2–5, 1976)

Nan, R.: Introduction to FAST: five hundred meter Aperture Spherical radio Telescope. Proc. SPIE 7012, Ground-based and Airborne Telescopes II, August 27 (2008)

Peng, B., Jin, C., Wang, Q., Zhu, L., Zhu, W., Zhang, H., Nan, R.: Preparatoryr study for constructing FAST, the world's largest singel dish. Proc. IEEE. **97**, 1391–1402 (2009)

Penzias, A.A., Wilson, R.W.: A measurement of excess antenna temperature at 4080 Mc/s. Astrophys. J. **142**, 419–421 (1965)

Prestage, R.M., Constantikes, K.T., Hunter, T.R., King, L.J., Lacasse, R.J., Lockman, F.J., Norrod, R.D.: The Green Bank telescope. Proc. IEEE. **97**, 1382–1390 (2009)

Swarup, G.: Giant Metrewave Radio Telescope (GMRT). In: Radio Interferometry: Theory, Techniques, and Applications. Proc. 131st IAU Colloquium, pp. 376–380 (1991)

Swarup, G., Ananthakrishnan, S., Kapahi, V.K., Rao, A.P., Subrahmanya, C.R., Kulkarni, V.K.: The giant meter-wave radio telescope. Curr. Sci. **60**, 95–105 (1991)

Swenson, G.W., Lo, Y.T.: The University of Illinois radio telescope. IRE Trans. Antennas Propag. **9**, 9–16 (1961)

Welch, W.J., et al.: The Allen Telescope Array: the first widefield, panchromatic, shapshot radio camera for radio astronomy and SETI. Proc. IEEE. **97**, 1438–1447 (2009)

Chapter 8
Electromagnetic Aspects of the Reflector Antenna

James Clerk Maxwell

Heinrich Rudolf Hertz

Oliver Heaviside

$$\nabla * H + i\omega\epsilon E = j \quad \nabla \cdot E = \rho$$
$$\nabla * E - i\omega\mu H = 0 \quad \nabla \cdot H = 0$$

Heaviside notation of Maxwell equations

The originators of electromagnetic waves and radio

8.1 Introduction

The purpose of the reflector antenna is to concentrate the radiation from a desired direction as effectively as possible in the focal point while suppressing interfering signals from other directions. The electromagnetic (EM) analysis of the antenna provides the basis for the definition and specification of the geometrical layout. This in turn has a strong influence on the structural and mechanical design and realisation of the antenna. Therefore, we devote this chapter to a summary of the main aspects of the electromagnetic theory of the reflector antenna. In particular, we present quantitative information on the relation between EM parameters and the resulting requirements on the hardware realisation of the antenna. The electromagnetic characteristics of even the largest radio telescope reflector cannot be properly described by geometrical optics only, as is usual for optical telescopes. A wave-based EM diffraction analysis is required to derive the parameters of the antenna: in particular its beam shape with sidelobes, polarisation state, gain and beam efficiency.

The theory is based on Maxwell's equations, shown on the cover page of this chapter. During the intensive work on the development of radar during World War II, a detailed analysis of reflector antennas was carried out that resulted in the book *Microwave Antenna Theory and Design*, volume 12 of the MIT Radiation Laboratory Series, edited by Silver (1949). It is still a basic text for the subject although many other books have appeared since. Significant contributions to the theory and practice of reflector antennas have been provided by radio astronomers, notably in the area of antenna calibration with the aid of radio sources.

In Chap. 2, we mentioned the different types of telescope geometry. The great majority of radio reflectors have a *paraboloidal* main reflector. We can place a detector in the primary focus or employ a secondary reflector to form a *Cassegrain* or *Gregory* system. At the start of a new telescope project, the definition of the geometry of the optical system is the first activity. The geometrical layout influences both the electromagnetic characteristics and the structural and mechanical layout of the antenna. The latter is most influenced by the choice of the optical configuration. We have presented the geometry of the telescope and the choice of optical parameters, such as focal ratio and magnification, in Chap. 2.

In the following sections, we introduce the terminology of important antenna beam parameters, such as *beamwidth, directivity* and *gain*. This should benefit the structural engineer, who encounters these terms in discussions with future users of the antenna. Our main purpose is to illustrate in a quantitative graphical form how the beam parameters are influenced by imperfections in the geometry of the antenna system. Examples of these are *defocus, area blocking* and *surface deviations*. From this knowledge, we can derive requirements for the structural, mechanical and thermal tolerances of the antenna that form the practical conditions for the structural design. For instance, we indicate the required precision of the reflector surface and the focus stability for satisfactory performance at a particular wavelength. The subject of this chapter is extensively treated by Baars (2007).

8.2   Radiation Pattern of a Circular Aperture

We now describe the antenna radiation pattern of a circular aperture. In this, we make use of the so-called *reciprocity theorem*. It states that the parameters of the antenna are independent of the choice one makes in considering the antenna in a receiving or transmitting situation. The terminology generally refers to the transmitting mode because mainly radar physicists and engineers developed the theory. The reader should keep in mind that the discussion applies equally to the receiving case that is used in radio astronomy.

The physical situation is as follows. A radiator, called *feed* in the focal point of the reflector, *illuminates* the reflector. The reflected waves form an outgoing *wavefront* along the axis of the reflector. This propagating wavefront develops into the *radiation pattern*, also called *beam*, of the antenna. *Diffraction effects*, caused by the finite size of the reflector, determine the beam characteristics. In particular, the angular width of the beam is proportional to the quotient of the wavelength and the reflector diameter.

The wavefront in the aperture plane of the reflector created by the feed is called the *illumination function*, which we assume to have rotational symmetry. We write its amplitude A as function of the radial coordinate r in the aperture as

$$A(r) = \tau + (1 - \tau)(1 - r^2) = 1 - (1 - \tau)r^2. \qquad (8.1)$$

This is the so-called *quadratic on a pedestal* distribution with a level $\tau(0 \leq \tau \leq 1)$ at the rim of the reflector. This level is called the *taper* of the aperture illumination. Full taper, i.e. an edge illumination of zero, occurs with $\tau = 0$, while for $\tau = 1$ we have a uniform aperture illumination. The taper is often expressed in decibel; thus, the taper at the edge $T_e = 20\log(\tau)$. Practically obtained illumination functions from a *horn feed* are well represented by the function of Eq. (8.1). It is more realistic than an often-used alternative of a Gaussian distribution (see e.g. Baars 2007, Ch. 4).

The basic theory of the radiating aperture (our reflector antenna) can be found in the books by e.g. Silver (1949) or Baars (2007). Using the illumination function of Eq. (8.1), the basic *power radiation function*, also called the *gain function*, *antenna pattern* or *antenna beam*, is given by the following expression:

$$g(u) = \left[\tau \frac{J_1(u)}{u} + 2(1 - \tau) \frac{J_2(u)}{u^2} \right]^2. \qquad (8.2)$$

This antenna beam $g(u)$ is rotationally symmetric with the normalised polar angle u, where $u = (\pi d / \lambda)\sin\theta$, and d is the reflector diameter, λ is the wavelength and θ is the polar angle with respect to the beam axis. The functions $J_1(u)$ and $J_2(u)$ are Bessel functions of the first kind and order one and two, respectively.

The value of the taper has a noticeable influence on the beam characteristics, as illustrated in Fig. 8.1. The beam pattern near the axis is plotted for uniform illumination ($\tau = 1$), for a quadratic illumination without pedestal ($\tau = 0$) and for
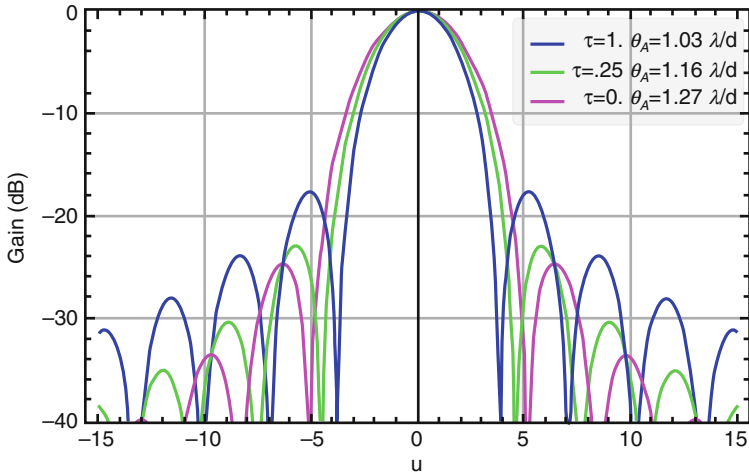
Fig. 8.1 Power pattern (in dB) of a circular aperture with a quadratic illumination function with values $\tau = 1$ (uniform), $\tau = 0.25$ (-12 dB) and $\tau = 0$ (full quadratic, zero) edge illumination. The resulting beamwidth is indicated in the inset
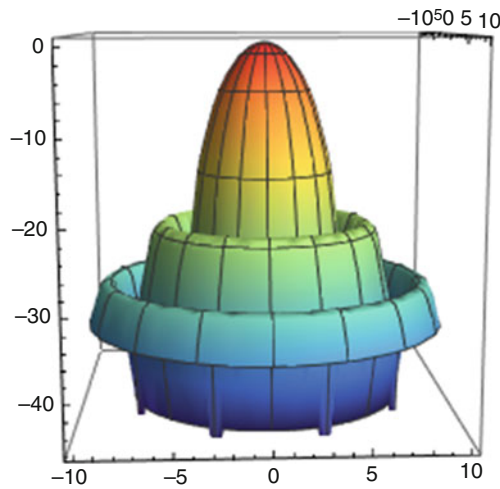
Fig. 8.2 A three-dimensional plot of the antenna beam and two sidelobes. The intensity scale is logarithmic. The first sidelobe level is about 20dB below the peak

$\tau = 0.25$, a quadratic function on a pedestal at the edge of the reflector. We see that the beamwidth θ_A increases with a stronger taper, while the first sidelobe level decreases from -17.6 dB to -23.0 dB and -24.6 dB for $\tau = 1$, $\tau = 0.25$ and $\tau = 0$, respectively. A three-dimensional rendering of the beam is shown in Fig. 8.2.

The choice of taper depends on the purpose of use. A communication satellite ground station looks at a single satellite with a well-defined signal. Here, one wants to optimise the amount of power received or transmitted, and as long as the direct

surroundings are not occupied with similar satellite transmitters, the sidelobe level is of secondary importance. Thus, an illumination function with a light taper is used.

In the case of a radio telescope, observing a weak source that is located in the neighbourhood of a strong source, the sidelobes can pick up a sizeable amount of signal, which by the noise-like nature of the radiation cannot be distinguished from the signal from the source under study and thus will influence the output of the telescope in an unknown way. In such a case, a stronger taper is preferred. A value of $\tau = 0.25$ is often used, which provides a good compromise between sidelobe level and beamwidth. A full discussion of this subject can be found in Baars (2007).

In the following sections, we introduce the most important parameters of the beam pattern. We then discuss the influence on the overall antenna performance by variations in the illumination taper as well as imperfections in the geometry of the feed–reflector combination.

8.3   Major Parameters of the Reflector Antenna

The definitions of the major parameters of an antenna that are important for the characterisation of its performance are listed in Table 8.1. Some of these are illustrated in Fig. 8.3. Because these terms will be used in discussions between the structural designer and the future user, we comment shortly on their meaning.

Beamwidth
The major interest of the user of the antenna is to maximise the sensitivity of reception and the accurate knowledge of the direction of arrival of the signal. The latter is determined by the beamwidth of the antenna, which is proportional to the ratio of wavelength to aperture diameter. The *half-power beamwidth*, written as HPBW, is the angle θ_A at which the power level has decreased to half (-3 dB) of

Table 8.1 The major parameters of an antenna

Parameter	Definition	Comment
Beamwidth	$\theta_A = 1.2\lambda / d$	HPBW in radian
Aperture efficiency	$\eta_A = A / A_g$	A_g—geometrical aperture area
Gain	$G = 4\pi A / \lambda^2$	A—effective aperture area
Antenna solid angle	$\Omega_A = \int_{4\pi} g(\theta, \phi) d\Omega$	Full pattern
Main beam solid angle	$\Omega_m = \int_{\Omega_m} g(\theta, \phi) d\Omega$	Main beam to first null
Beam efficiency	$\eta_B = \Omega_m / \Omega_A$	–
Scatter efficiency	$\eta_s = \exp[-(4\pi\varepsilon/\lambda)^2]$	"Ruze" loss,—ε rms error
Blocking efficiency	$\eta_b = (1 - A_{bl}/A_g)^2$	A_{bl}—blocked area
Defocus	Lateral	Coma sidelobe, pointing error
Defocus	Axial	Gain loss

Fig. 8.3 Sketch in polar coordinates of the full beam pattern of an antenna, including sidelobes. The half-power beamwidth (HPBW) and beamwidth to first null (BWFN) are indicated
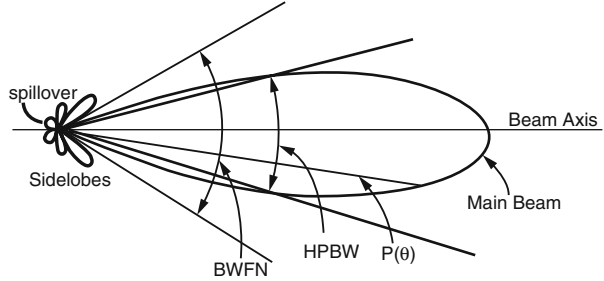
the on-axis value: $\theta_A = a\lambda / d$ (radian), where λ is the wavelength and d the diameter of the reflector aperture. As we illustrated above, the coefficient a is dependent on the illumination function. The HPBW is a measure of the angular resolution; it indicates the minimum angular distance between two sources in order to be seen separately: the so-called Rayleigh criterion. For example, an antenna of 25 m diameter, operating at 20 cm wavelength, has an HPBW of about 0.5°; an antenna of 12 m diameter for the submillimetre wave band has an HPBW of less than 8 arcseconds at 0.4 mm wavelength.

Aperture Efficiency and Gain

The basic parameter *aperture efficiency* indicates the sensitivity of the antenna. It is defined as the ratio of the *effective absorption area* to the *geometrical aperture area* of the reflector. It is the preferred quantity used by radio astronomers. Radar and communication engineers normally express the sensitivity in terms of the antenna *gain* G, defined in Table 8.1. We see that the gain increases with the effective area and with the inverse of the wavelength squared. The concepts of gain and aperture efficiency are useful for observations of point sources, i.e. sources of negligible angular width compared to the beamwidth of the antenna.

Antenna Solid Angle and Beam Efficiency

The directional radiation power pattern is often called the *gain function*, denoted by $g(\theta,\phi)$, where θ and ϕ are the angular polar and azimuthal coordinates with respect to the beam axis, respectively. Usually, we normalise the pattern by defining $g(0, 0) = 1$. The integral over the entire unit sphere, i.e. 4π steradians, is called the *antenna pattern solid angle* (Table 8.1).

As sketched in Fig. 8.3, we can separate the total pattern solid angle Ω_A into the main beam Ω_m (extending to the first null in the antenna pattern) and the combined sidelobe solid angle Ω_s so that $\Omega_A = \Omega_m + \Omega_s$. For the observation of sources of finite angular extent, the parameter $\eta_B = \Omega_m / \Omega_A$, called *main beam efficiency*, is useful. In practice, we have $\eta_B \approx 1.2\eta_A$.

8.4   Influence of Imperfections on Performance

Now we discuss without theoretical derivation the important factors that determine the beam characteristics and efficiency of the antenna. These are of high interest to both the designer and the user of the antenna. The major parameter *aperture efficiency* can be broken down into several components, each representing a basic characteristic or a deviation from the perfect situation. This enables us to set conditions on these imperfections for a given loss of efficiency, and these can be directly introduced into the design of the structural, mechanical, thermal and electromagnetic realisation of the antenna. The imperfections in the antenna structure determine the "quality" of the beam, which in turn influences the reliability of the received signal. We now write the *aperture efficiency* as the product of a number of individual efficiency contributions:

$$\eta_A = \eta_i \cdot \eta_s \cdot \eta_p \cdot \eta_r \cdot \eta_e \cdot \eta_a \cdot \eta_f \cdot \eta_b, \tag{8.3}$$

where

η_i = illumination efficiency of the aperture by the feed function (*taper*)
η_s = spillover efficiency of the feed (and subreflector, if present)
η_p = polarisation efficiency of the feed–reflector combination
η_r = radiation efficiency of the reflector surface (ohmic loss)
η_e = small-scale surface error efficiency (Ruze loss), also called scattering efficiency
η_a = large-scale surface error (aberration) efficiency
η_f = focus error efficiency (due to both lateral and axial defocus)
η_b = blocking efficiency due to aperture blocking by quadripod, subreflector, etc.

The first three terms are fully determined by the electromagnetic design of the reflector and feed combination. The remaining terms depend on the structural deviations from a perfect situation due to material and environmental restrictions such as finite stiffness of structural members and the influence of gravity, wind and temperature variations. We describe the consequences of these deviations for the EM performance of the antenna. *These relations form the background for the discussion between the user and the structural designer about the desired performance and the structural and financial feasibility of a telescope or antenna project.*

8.4.1   Illumination, Spillover and Polarisation Efficiency

The *illumination efficiency* η_i represents the degree to which we utilise the reflector area. Ideally, we would like to have a uniform illumination function over the aperture, which yields the maximum possible illumination efficiency of one.

Unfortunately, it is physically impossible to construct an illuminating element (the *feed*) that exhibits a constant sensitivity up to the edge angle of the reflector and falls sharply to zero at the edge. As we have illustrated in Sect. 8.2, a tapered function decreases the achievable aperture efficiency. With a finite edge illumination level, some of the power will "spill over" the edge and be lost. In terms of reception, this causes a signal contribution from the area surrounding the reflector, either the ground for the primary reflector or the sky for the subreflector.

This effect is captured by the *spillover efficiency*, which is varying inversely to the illumination efficiency. Thus, depending on the specific performance in mind, a compromise is necessary by a judicious choice of the taper value. (In §8.7.2, we mention a method to increase η_i while keeping spillover small.) The efficiency of the illumination function (Eq. 8.1) as function of the taper value is shown in Fig. 8.4. In radio telescopes, a *taper* of -12 to -15 dB is usually applied. Communication engineers often aim at maximising the G/T_S ratio (gain to system temperature). Note that T_S contains a contribution from spillover and hence is also influenced by the illumination taper.

A good feed will have *polarisation efficiency* close to one and we ignore it further on.

The last five efficiency terms in Eq. (8.3) are a consequence of imperfections in the structural and mechanical realisation of the antenna. It is essential to determine the relation between these terms and the magnitude and character of the mechanical deviations.
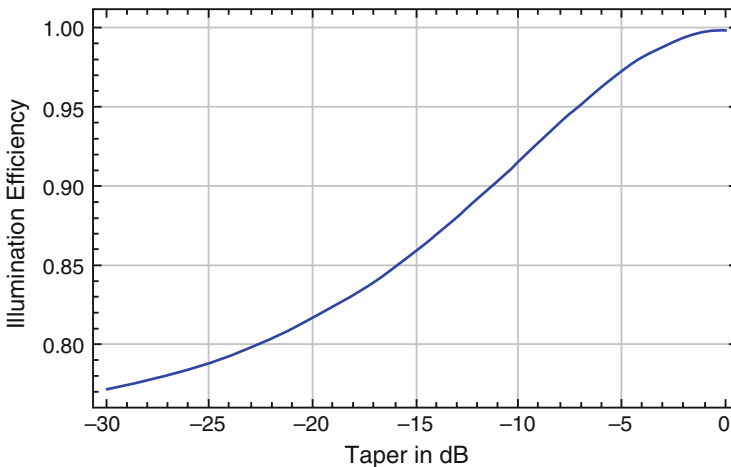
Fig. 8.4 Illumination efficiency as function of taper value according to Eq. (8.1)

8.4.2   Radiation Efficiency

The *radiation efficiency* is a measure of the ohmic loss in the reflecting or radiating structures, i.e. the reflector surface and the feed. For most metallic surfaces, this loss is very small up to the highest radio frequencies, normally less than 1%. This quantity is usually ignored in the design and operation of terrestrial antennas, although it plays a significant role in space-borne, cooled telescopes. A one-percent loss in reflectivity causes a system temperature increase of 1% of the physical temperature of the reflector.

8.4.3   Small-Scale Surface Error (Scattering) Efficiency

In Eq. (8.3), we discern between small-scale and large-scale deviations of the reflector from the prescribed geometrical form. These deviations cause phase errors over the aperture that result in less than perfect addition of the reflected wavefronts in the focus and hence to a loss in aperture efficiency. The power that is removed from the forward beam direction is distributed over the sidelobes of the antenna pattern. Depending on the spatial character of the surface deviations, different effects may occur as, for instance, asymmetrical sidelobe structure, main beam broadening and wide-angle sidelobe enhancement.

The distortions are caused by fabrication errors in the reflector panels, imperfect localisation of the panels on the backup structure and deformations of panels and backup structure under influence of gravity, wind and temperature differences. In the chapters on structural design, much attention has been given to methods to minimise these deformations.

The separation between small-scale and large-scale deviations is based on their different nature. We discuss first the influence of small-scale errors that are correlated over areas of the order of the surface panels or less. They are caused by manufacturing error and local deformation of the individual panels due to gravity or temperature as well as the errors in the adjustment of the panels to the prescribed reflector contour. As far as these errors can be considered randomly distributed over the aperture with an rms value ε and with a correlation length c, the distance over which the errors are spatially correlated, that is much larger than the wavelength and much smaller than the reflector diameter, their effect can be described by the *tolerance theory* of Ruze (1952, 1966). As will be obvious, the gain loss depends on the ratio of the error ε to the wavelength λ. The relation, often called *Ruze formula*, is given by

$$\eta_e = \exp\left[-\left(\frac{4\pi\varepsilon}{\lambda}\right)^2\right] + \left(\frac{c}{d}\right)^2 \cdot \left\{1 - \exp\left[-\left(\frac{4\pi\varepsilon}{\lambda}\right)^2\right]\right\}, \qquad (8.4)$$
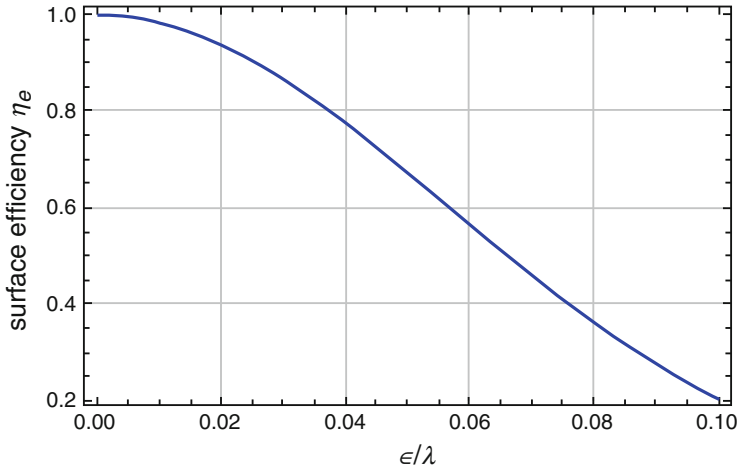
Fig. 8.5 Surface efficiency η_e as function of the ratio rms error to wavelength

where c is the correlation length and d the reflector diameter. The radiation, scattered by the errors and removed from the main beam, appears as a wide, low-level error pattern, the width of which is dependent on the correlation length c. The first term in the above formula represents the loss in gain, and the second term represents the maximum level of the *error pattern*. Generally, the contribution of the second term is negligible, less than 1% for $c/d < 0.1$. Then the application of the Ruze formula can be restricted to the first term as illustrated in Fig. 8.5. We see that with an rms error of only one-twentieth of the wavelength, we experience a drop in efficiency of more than 30%.

The ratio of power in the error pattern to that in the main beam is only dependent on the magnitude of the rms error and shown in Fig. 8.6. For an error of 0.05 wavelength, the power in the error beam is about half of that in the main beam, which is equivalent to a loss in main beam gain of one-third, in accordance with Fig. 8.5.

As shown by Eq. (8.4), the peak level of the error pattern relative to the main beam level is proportional to the square of the ratio c/d. A small value of c, that is, many small independent error patches, produces a very weak but also very wide error pattern. Few large correlated areas cause a narrow error beam with an increase of its peak level. Often, the reflector consists of concentric rings of surface panels supported on the backup structure and several error patterns may be discerned due to intra-panel, panel-to-panel and ring-to-ring correlation lengths. As an example, we show in Fig. 8.7 a measurement of the beam pattern of the IRAM 30-m millimetre radio telescope (Kramer et al. 2013). Next to the diffraction pattern (blue), three error beams can be fitted to the measured pattern (red). The narrowest error beam is caused by large-scale deformation of the reflector with a correlation
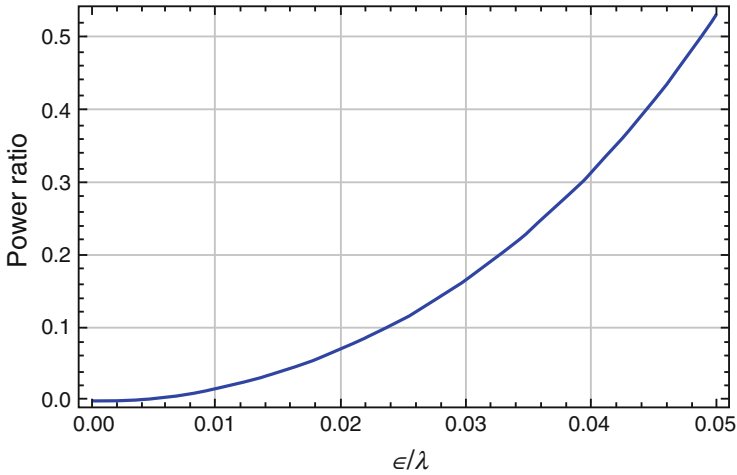
Fig. 8.6 The ratio of the power in the error pattern to that in the main beam as function of the surface error in units of the wavelength
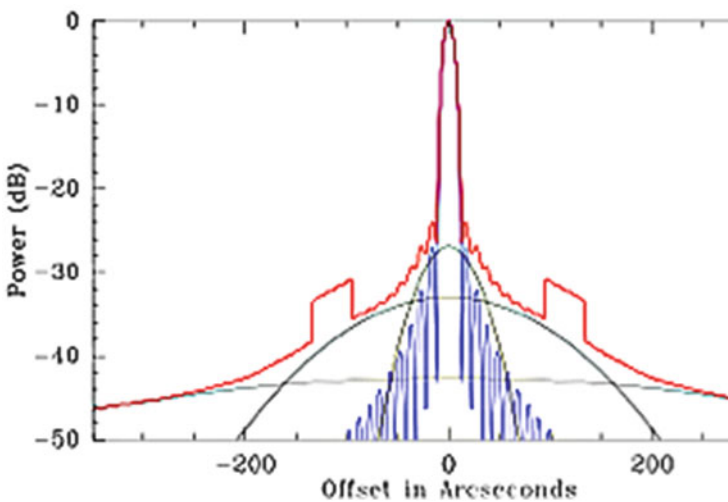
Fig. 8.7 Beam pattern of the IRAM 30-m telescope at 1.1 mm wavelength (*red*). The pure diffraction beam is shown in *blue*. Three error beams can be discerned (*black*). Their widths indicate correlation lengths of about 6, 1.5 and 0.5 m (IRAM Internal Memo 2013)

length of about 6 m. It originates mainly from variations in the temperature distribution of the BUS.

The next error beam indicates a correlation length of about 1.5 m, which is close to the average size of the panel frames of 2 m. Finally, the widest error beam can be identified with small-scale errors within the individual panels that are supported on

the panel frame at 50 cm interval. The "ring" of enhanced level at about 120 arcseconds from the axis is caused by systematic buckling of the panel frames under a temperature gradient within the frame. This results in the *grating effect* of the ring.

It should be remarked that from practical experience, supported by theoretical work by Greve (1980), the formal restrictions imposed by Ruze for the validity of his theory appear to be quite flexible. Often an rms error is derived from large-scale, semi-systematic deformations and used in Eq. (8.4) with acceptable conformance to the measured gain decrease.

8.4.4 Large-Scale Deformation: Representation by Zernike Polynomials

We now direct our attention to the effects of large-scale deformations of the reflector surface that originate in the supporting structure for the reflector and possibly in the mount. These are directly related to the *quality of the telescope structure* in regard to manufacturing and alignment accuracy, and the deformation behaviour under environmental influences including gravity. Thus, the analysis and mathematical description of these deformations provide a direct connection between structural design methods such as *finite element analysis* (FEA) and the resulting distortion of the antenna beam pattern known as *aberrations*. The primary aberrations of an optical telescope were described by Seidel (1856) on the basis of geometrical optics. They carry the names *distortion, coma, field curvature, astigmatism and spherical aberration*. It is important to realise that these aberrations represent deviations of the imaging optical element, in our case the reflector and perhaps the feed. Thus, they cause pathlength changes across the reflected EM field on its way to the focus, which is equivalent to stating that the wave field suffers phase errors. If the phase function can be determined, either by calculation or measurement, and is inserted into the basic radiation integral, the resulting beam pattern will show deviations in shape and intensity. We call the pattern *distorted*.

It would be useful to decompose any measured distortion function into components represented by the primary aberrations. From this one might glean an insight into the mechanical or structural causes of the error. Frits Zernike (1888–1966) achieved such decomposition in 1934 during his work on phase-contrast microscopy for which he received the Nobel Prize in Physics in 1953. He found a set of orthogonal polynomials, the *Zernike polynomials* that represent the distorted wave field. We present a short introduction to the subject in the *Addendum* to this chapter.

The shape of the four major aberrations is sketched in the 3D representation of Fig. 8.8. These are plots of the Zernike polynomials pertaining to the specific aberration. They show the shape of the reflected wavefront produced by the distorted reflector.
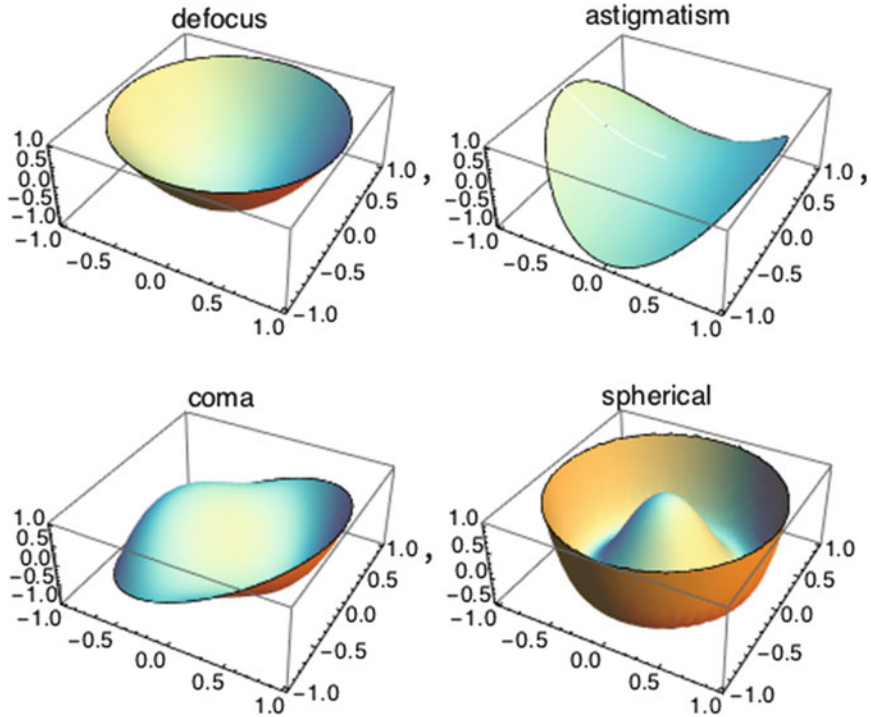
Fig. 8.8 A 3D representation of the major optical aberrations defocus, astigmatism, coma and spherical aberration. Note that the vertical axis range runs from -1 to $+1$

A result of great practical value is the identification of the primary Seidel aberrations with a single Zernike term. Table 8.4 in the Addendum lists these. In earlier chapters, we have seen that several of the primary aberrations are directly caused by external influences on the mechanical structure, specifically gravity. The structural engineer can easily include the mathematical description of these aberrations by the appropriate Zernike polynomial in his finite element structural analysis.

The influence of a large-scale aberration on the shape of the antenna beam is shown in Fig. 8.9 for coma and astigmatism (top and bottom). The aberration functions are shown on the left. The contour plot of the resulting beam is plotted on the right on a logarithmic scale. The coma lobe is the crescent-shaped sidelobe on the right side of the central beam. The saddle-like distortion of astigmatism leads to an asymmetric beam and sidelobe structure.

The convenience of the Zernike representation has contributed to a growing tendency among designers and users of radio telescopes to characterise the overall deformation picture of the surface by a set of Zernike polynomials.
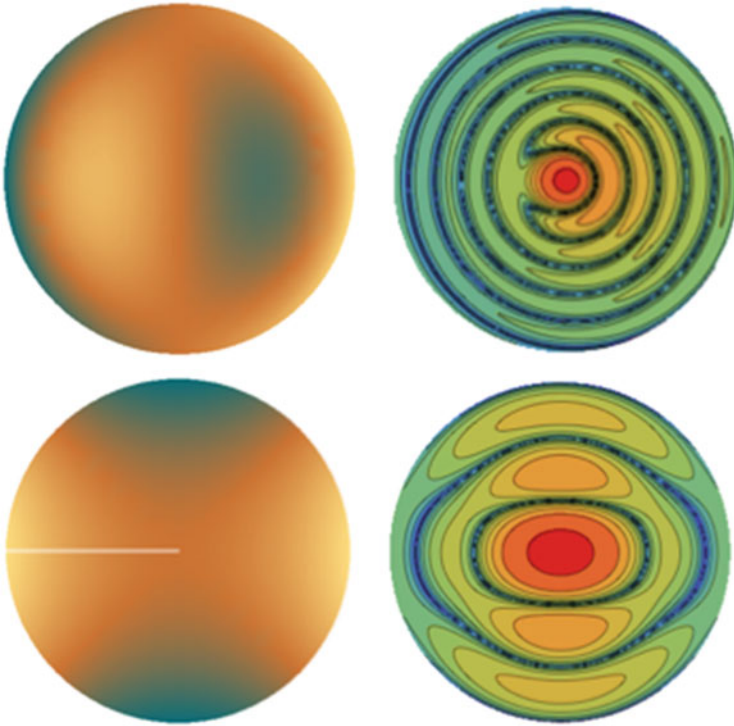
Fig. 8.9 Two major aberrations at work. The aberration function is shown in a density plot on the *left* (*dark* is *up*, *light* is *down*). The contour plot of the beam is plotted on the *right* on a logarithmic scale. *Top* shows coma. Clearly visible is the coma lobe, the crescent-shaped sidelobe on the right side of the beam. The first sidelobe to the left is suppressed. *Bottom* panels show the case of astigmatism. The saddle-like distortion is shown on the left and the beam contour plot on the right. The beam is now asymmetric and shows an asymmetric sidelobe structure

8.4.5 Blocking Efficiency

Aperture blocking is caused by the shadow projected onto the reflector by the structure that supports the feed and electronics, or the subreflector in a dual-reflector system, in the primary focus. The usual method of accounting for this obstruction on the antenna efficiency is to consider the obstructing area to impose a *negative beam* onto the perfect beam (Ruze 1968). The analysis leads to a simple Eq. (8.5) for the blocking efficiency η_b (not to confuse with the beam efficiency η_B of Table 8.1):

$$\eta_b = \left(1 - A_b/A_g\right)^2, \tag{8.5}$$

where A_b is the total blocking area and A_g the geometric area of the aperture. A geometrical blocking of 5% of the aperture will cause a loss in efficiency of 10%.

Fig. 8.10 The projected
area of the blocking
elements onto the aperture
plane: the central circular
area, the plane-wave
rectangular quadripod and
the curved area of the
spherical-wave blocking
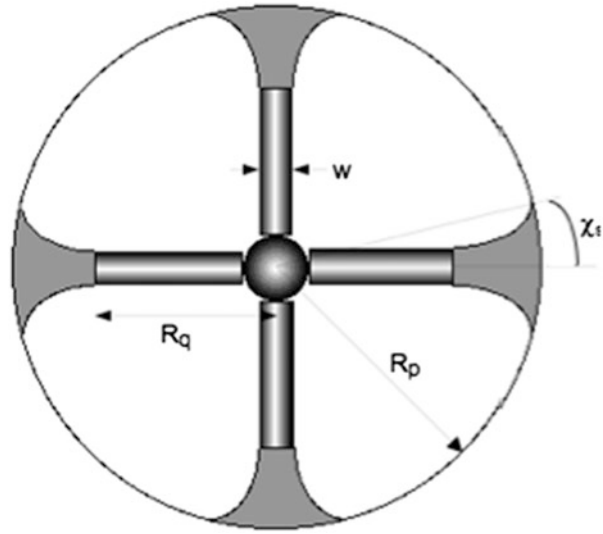
Normally, the blocking area consists of three components, illustrated in Fig. 8.10:
the central area of the Cassegrain secondary reflector or the prime focus instrument
box, the projected area of the support legs of width w that block the incoming plane
waves and finally the wedge-like shadows outside the legs from the waves reflected
from the outside area of the reflector. One can envisage this by placing the eye in the
primary focus and looking outwards along the quadripod starting at the bottom. The
shadowed section of the reflector widens as one moves upwards as shown in the
sketch of Fig. 8.10. This is called *spherical-wave blocking*. If the quadripod
penetrates the reflector surface at a small radius R_q, the spherical-wave blocking
may be the major component. On the other hand, a quadripod supported at the rim
of the reflector avoids spherical blocking. The detailed expressions for the blocking
areas can be found e.g. in Baars (2007, Sect. 4.5).

   As examples we show in Fig. 8.11 a cut through the beam pattern in the plane of
the quadripod leg and a plot of the blocked area for three radio telescopes: the
Westerbork telescope and the ALMA antennas from AEM and Vertex. The odd
numbered sidelobes (red) are stronger; the even numbered ones weaker than in the
unblocked pattern (blue). The WST quadripod penetrates the surface at about half
the reflector radius leading to a considerable spherical-wave blocking and a con-
comitant relatively low blocking efficiency of 83%. The 12-m diameter ALMA
antennas have narrow legs (8–10 cm) and a better geometrical layout and obtain a
blocking efficiency of 95%. Note that the AEM antenna supports the quadripod at
the edge of the reflector, thereby avoiding the spherical shadow. The spherical-
wave blocking of the Vertex antenna is offset by a slightly thinner cross section of
the legs and the final blocking efficiencies are equal. In these examples, we have
assumed a uniform illumination function. In practice, the illumination will have a
taper towards the edge of the reflector (Eq. 8.1) and the blocking can be weighted
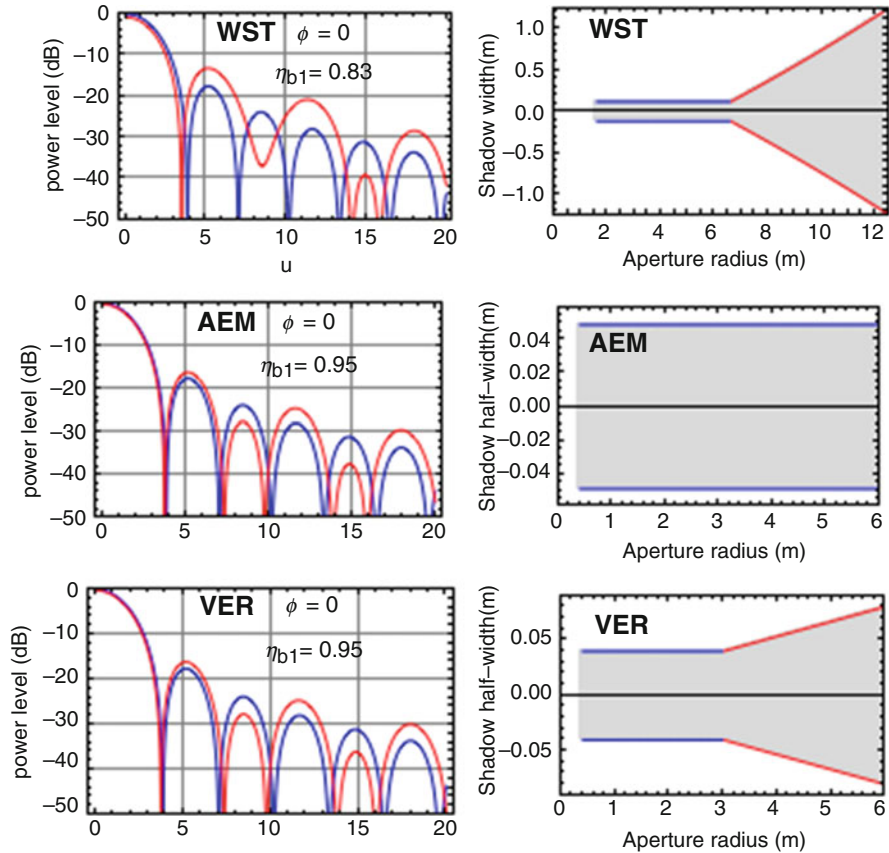
Fig. 8.11 Geometrical shape of the blocking area (*grey*) for three radio telescopes and the resulting cut through the beam pattern in the plane of the support structure (*red*) versus the unblocked pattern (*blue*). Blocking efficiency is indicated

according to the level of illumination, which leads to a smaller contribution of the outer blocked areas and an improved blocking efficiency.

8.4.6 Lateral and Axial Defocus: Gain Loss

A displacement of the feed from the focal point of the reflector will cause a systematic, large-scale phase error over the aperture. It is easy to see that a shift along the axis (*axial defocus*) causes a rotationally symmetric phase error over the aperture. The phase error is approximately proportional to the square of the radial coordinate. This functional form is similar to the aberration called *defocus* earlier. The name is now clear: a reflector distortion of this form can be corrected
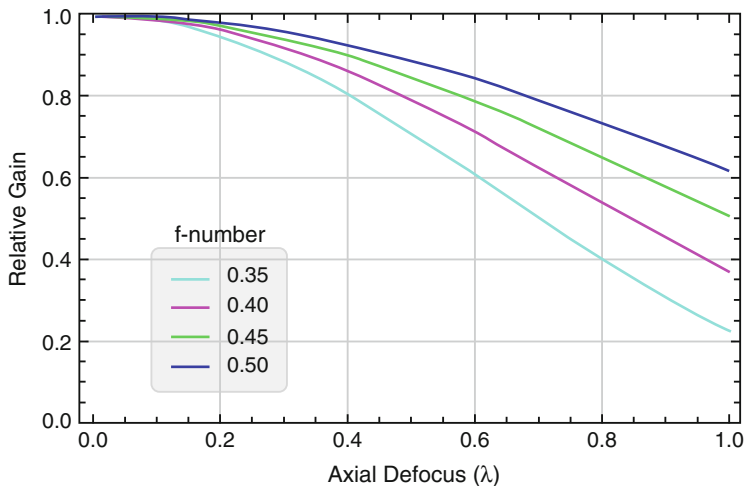
Fig. 8.12 Decrease in gain as function of axial defocus in units of wavelength for several values of the *f/d* ratio

effectively by adjusting the location of the feed along the axis to the position of maximum signal. The amount of shift necessary for a certain phase error is dependent on the focal ratio of the reflector. In addition, there is an influence of the illumination taper. The decrease in aperture efficiency as function of the defocus for a tapered illumination of -12 dB is shown in Fig. 8.12. We see a strong dependence on the focal ratio. A defocus of only one-third of a wavelength causes a drop in gain of typically 10%. Many large antennas exhibit significant changes in focal length as function of elevation angle. If the feed can be adjusted along the axis with a mechanical focusing stage, most of the gain loss can be recovered.

A shift of the feed in radial direction, perpendicular to the reflector axis (*lateral defocus*), causes an asymmetric phase error over the aperture that is proportional to odd powers of the radial coordinate with an angular variation proportional to the cosine of the azimuth angle (Ruze 1965). This is reminiscent of the case of *coma* distortion described earlier. Indeed, the beam now exhibits the *comalobe*, a high sidelobe on the side of the beam towards the reflector axis. A reasoning similar to the one in the previous paragraph shows that the effect of a structural coma distortion can be counteracted by a lateral shift of the feed. Thus, a well-designed focus arrangement will also allow lateral adjustments. A lateral defocus will cause a pointing error that needs to be corrected by a pointing change of the antenna. An illustration of the change in the beam pattern is shown in Fig. 8.13.

The loss in gain in this case is relatively small; for a lateral defocus of one wavelength, it is only 5%. But the comalobe level rises from the perfect situation of -23 dB to the uncomfortable high value of about -16 dB. The comalobe level as function of the lateral defocus is shown in Fig. 8.14, again for a typical tapered illumination. The comalobe intensity is somewhat dependent on the focal ratio, as illustrated in the figure, and only slightly on the illumination function.
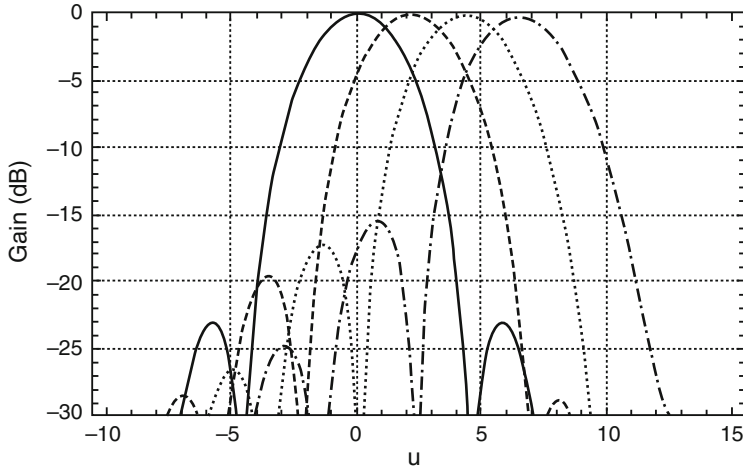
Fig. 8.13 Radiation patterns for a lateral feed displacement of up to one wavelength for an illumination function with -12 dB taper
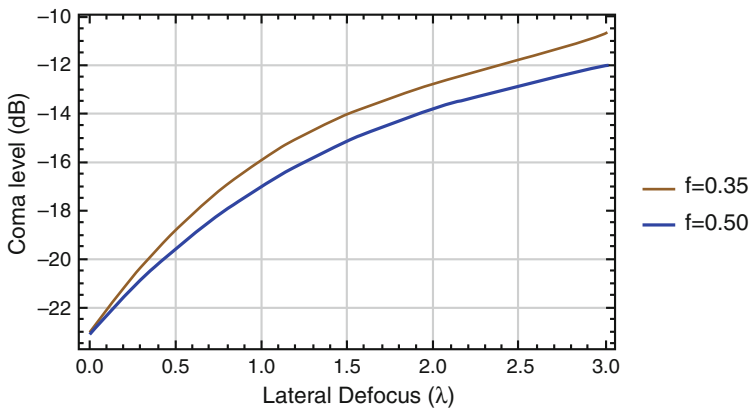
Fig. 8.14 The level of the coma lobe (first sidelobe near the antenna axis) as function of the lateral defocus in wavelength for *f*-ratios of 0.35 and 0.5

The foregoing discussion on defocus is applicable to prime-focus operation of the antenna. The situation in the case of Cassegrain optics is somewhat different. Any change in the position of the subreflector, which is located near the primary focus, has about the same effect as a change of the feed in the prime-focus case. However, the situation in the secondary focus is much relaxed because of the *magnification* (*m*) of the Cassegrain system. The parameters in the secondary focus are to first order equal to those in a prime-focus antenna with a focal length *m* times that of the actual paraboloid. This virtual reflector is called the *equivalent paraboloid* (Chap. 2).
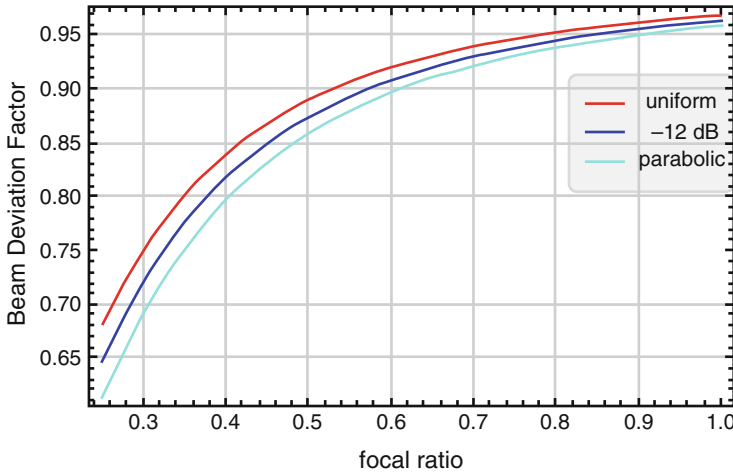
Fig. 8.15 The BDF for fully tapered (*cyan*), $a_\tau = 0.25$ (-12 dB) taper (*blue*) and uniform (*red*) illumination as function of the focal ratio of the reflector

8.4.7   Beam Deviation Factor (BDF)

It is obvious that a lateral shift of focus also introduces a change in pointing direction. Its magnitude is determined by the relation between the physical shift of the feed from the axis and the resulting change in the pointing direction of the beam maximum towards the sky. If the reflector were a flat plate, the change in pointing angle would be equal to the angular shift of the feed with respect to the axis. With curved reflector geometry, the pointing direction changes less than the angular feed displacement and the ratio between these is called the *beam deviation factor* (BDF), a number smaller than one. Clearly, the BDF will be dependent on the focal ratio of the reflector, and from inspection of the geometry, it is clear that a deeper reflector will exhibit a smaller BDF. Also the taper of the illumination function will influence the value of the BDF. A full derivation can be found in Baars (2007, Ch. 4). The plot of Fig. 8.15 shows the BDF as function of focal ratio for three values of the taper. This plot is needed whenever we discuss pointing errors caused by structural deformations.

8.4.8   Conclusion

In Table 8.2, we summarise the tolerance requirements as they have been presented in this chapter. Clearly, the structural stiffness and stability are subjected to tight tolerances. The requirement on the pointing error appears rather benign. One should keep in mind however that this only pertains to the signal loss. A pointing error

Table 8.2 Summary of tolerances requirements

Imperfection	Specification	Tolerance	Figure
Surface error	10% gain loss	$\lambda/40$	8.5
Defocus-axial	10% gain loss	$\lambda/3$	8.12
Defocus-lateral	−19 dB comalobe	$\lambda/2$	8.14
Defocus-lateral	10% gain loss	1.5 λ	8.13
Blocking	10% gain loss	5% of area	Eq. (8.5)
Pointing error	10% gain loss	0.4 HPBW	8.1

results in assigning a wrong position to the celestial source, which might make a positive identification with an underlying optically visible object difficult if not impossible.

8.5   Measuring Antenna Parameters with Cosmic Sources

8.5.1   Antenna Gain and Beam Pattern

The exact calculation of the radiation pattern of a reflector antenna is difficult because of the unavoidable imperfections in geometry and fabrication. Thus, there is a great interest in the direct measurement of the major parameters of the antenna. For this a sufficiently strong signal source is required located at a large distance from the antenna. Radio astronomers built the first large reflector antennas, and a natural step for them was to use the newly detected cosmic radio sources as test transmitter for the measurement of antenna parameters. These sources are certainly far from the antenna, they have a small angular size, and by their daily movement along the sky, they offer a possibility to make measurements over a substantial elevation range. If the absolute intensity of a few cosmic sources would be accurately known, the gain of the antenna could be determined.

In fact, the absolute flux density of the strongest radio sources has been determined over a wide frequency range with the use of relatively small absolutely calibrated antennas, such as a horn or dipole array. The derived *absolute radio spectrum* (the intensity as function of wavelength) is then used for the measurement of the gain of large, uncalibrated antennas. The establishment of such an absolute flux density scale has reached an accuracy of a few percent over the radio frequency range from 20 MHz to 300 GHz. The strongest radio source of small angular size is Cas A, named after the celestial constellation Cassiopeia in which it is located, and it has served as the primary standard for the absolute flux density scale for frequencies up to 25 GHz (Baars et al. 1977). For higher frequencies, up to 900 GHz, the planet Mars is used as primary calibrator (Perley and Butler 2013). In Fig. 8.16, we show the absolute spectra of the four strongest sources, published by Baars et al. (1977). A review of the history of absolute calibration in radio astronomy has been presented by Baars (2014).
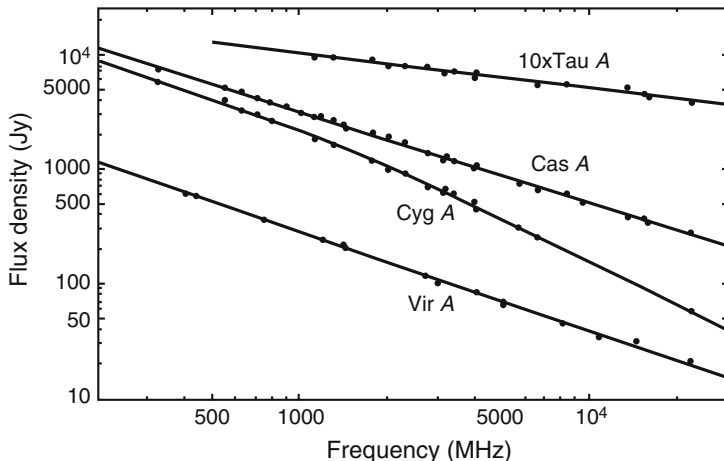
Fig. 8.16 The absolute spectra of the four strongest radio sources in the frequency range 200–30,000 MHz

8.5.2 Antenna Pointing

As we have seen in the discussion of the structural design, in particular with the use of homology, structural deformations lead to deviations in the reflector surface and also to errors in the pointing direction. The *pointing error* is defined as the difference between the *indicated (encoder readout) and commanded (true target coordinates)* position of the antenna. The pointing error results from shifts in the orientation of the best-fit reflector and focus position (*homology*) and from mis-alignments of the telescope axes, errors in zero point and linearity of the angle encoders, gravitational bending of the mount structure and refraction by the earth's atmosphere. We need to determine the necessary corrections to the commanded position to ensure that the antenna beam is directed precisely in the desired direction. To this end, we measure the apparent position of a large number of sources with accurately known celestial position that are distributed over the entire visible sky. The measured differences between indicated and true position form the input data for the establishment of a *pointing model* of the telescope.

The pointing model consists of a set of physically reasonable relations representing the known or expected geometrical and structural imperfections of the antenna system. The coefficients of their terms are found from the set of pointing observations by a least squares procedure. These resulting coefficients are called the *pointing constants*. They might vary over time due to ageing effects in the structure, variable wind forces and diurnal or seasonal temperature variations. Thus, for reliable antenna pointing it will be necessary to regularly check the constants for their actual value. Stumpff (1972) has presented the theory of the pointing model and the essential equations can be found in Baars (2007). Normally, eight constants are sufficient for adequate performance. They represent physically

realistic situations, such as perpendicularity of the telescope and beam axes (2), inclination of the azimuth axis with respect to the vertical (2), angle encoder offsets (2), gravitational bending of the structure (1) and atmospheric refraction (1).

As we have seen in foregoing chapters, the large telescopes operating at millimetre wavelengths attain a beamwidth of less than 10 arcseconds. This requires a pointing precision of less than 1 arcsecond. Time variable outside influences, such as wind, atmospheric refractivity and temperature gradients, might easily introduce errors of this magnitude that cause the beam to drift away from the source during a longer observation with a resulting loss of signal. To avoid this, the astronomer intersperses his observations with short *pointing checks* on a nearby position calibration source, a procedure called *offset pointing*. Depending on the circumstances, such a procedure may be done every 10 s or several minutes. Clearly, minimising the angular distance to the calibrator and the time needed to make the calibration are of prime importance. This has a noticeable influence on the design of the mechanical and control subsystems of the telescope (see the description of the ALMA antennas in Chap. 7). We illustrate the procedure by the example of Fig. 8.17.

1. An observation starts by slewing the telescope to the nominal position of the source to be observed. The current *pointing model* is applied for this initial positioning.
2. If the telescope is equipped with flexible body control (FBC), as described in Sect. 5.4, the FBC is applied using the data from the "state sensors" to calculate the pointing correction. The telescope is in a state of "blind pointing" that will have a certain positional error.
3. Now the astronomical offset pointing is performed, checking the position of a nearby reference source. This eliminates slowly variable structural and atmospheric disturbances and increases the pointing accuracy upon returning to the object of observation.
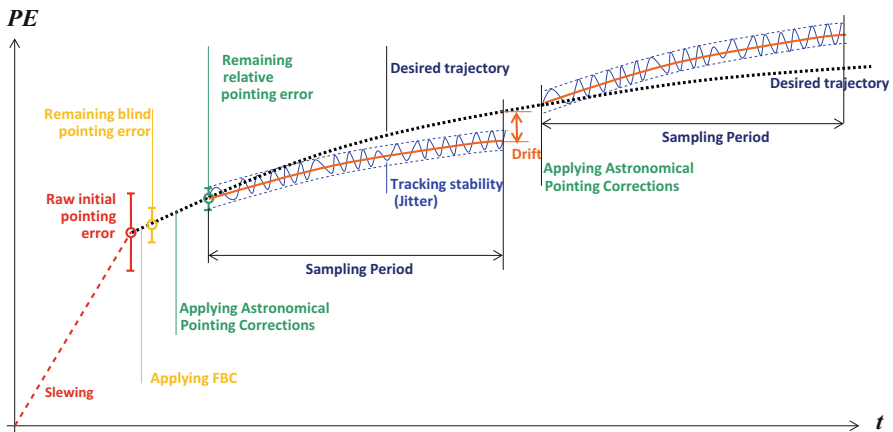
Fig. 8.17 Scenario of an *offset pointing* observation. Plotted is the position change as function of time

4. The telescope collects the incoming signal for a certain *integration time* during which it tracks the sidereal trajectory of the source. Any correction from the FBC is immediately applied. There will be a residual time-dependent error caused by jitter in the drives and by wind gusts, as well as drift caused by atmospheric fluctuations and deficiencies in the thermal modelling.
5. Depending on the actual situation and the quality of the modelling, the error will reach a value at which the observer decides to interrupt the observation with another offset pointing procedure. The optimum time interval between offset pointings is dependent on the many parameters involved and must be estimated by the observer.

The availability of the strong and absolutely calibrated radio sources along with a large set of sources with accurately known celestial position (from interferometric observations) enables the accurate characterisation of a large reflector antenna. Its use is not only customary in radio astronomy but also in the area of ground stations for satellite communication and deep space probes. Kuz'min and Salomonovivh (1966) have written a book with the title *radio astronomical methods of antenna measurement*. Further summaries of these methods have been presented by Baars (1973, 2007, Ch. 5).

8.6   Radio Holographic Measurement of Reflector Profile

The reflector normally consists of a set of panels that are supported on the backup structure by adjusters. A last activity in the delivery of the antenna is the measurement and setting of the surface with a specified accuracy to the desired reflector profile, usually a paraboloid. The desired measuring and setting accuracy must be of the order of 2–3% of the shortest wavelength. For a 25-m telescope operating at 10 cm wavelength, the measuring accuracy should be about 1 mm. For a 12-m submillimetre telescope operating at 0.3 mm, we would need 6 μm measuring accuracy, i.e. better than a millionth of the reflector diameter.

Variations of the classical *geodetic* method measuring angle and distance have been widely used. They have been shortly reviewed by Baars (1983). Photogrammetry was applied to the early Green Bank telescopes (Chap. 3) as early as 1962 (Findlay 1964). There is a resurgence of this method with the recent fully digital systems that allow a measuring accuracy of about 30 μm for reflectors of 10–20 m diameter.

Where a high accuracy is required, the method of choice is the technique of *radio holography*. As sketched in Fig. 8.18, there exists a *Fourier Transformation* relationship between the field function in the aperture $A(x,y)$ of an antenna and the radiation field (beam pattern) at large distance $F(\theta,\varphi)$. Where normally we calculate the beam pattern from the known aperture illumination function, we can turn this around and obtain the aperture illumination function from a known beam pattern.

Fig. 8.18 The principle of radio holography. The far-field pattern $F(\theta, \phi)$ is measured in both amplitude and phase over a sufficiently large solid angle. A Fourier Transformation (FT) delivers the aperture distribution $A(x, y)$; the phase function $\Phi(x, y)$ is a representation of the reflector surface contour

Far-field pattern

$F(\theta, \varphi) = A(\theta, \varphi) \exp[\,i\Phi(\theta, \varphi)]$

Aperture distribution

$A(x,y) = a(x,y) \exp[\,i\phi(x,y)]$

aperture

$$\text{FT}$$
$$F(\theta, \varphi) \Leftrightarrow A(x,y)$$
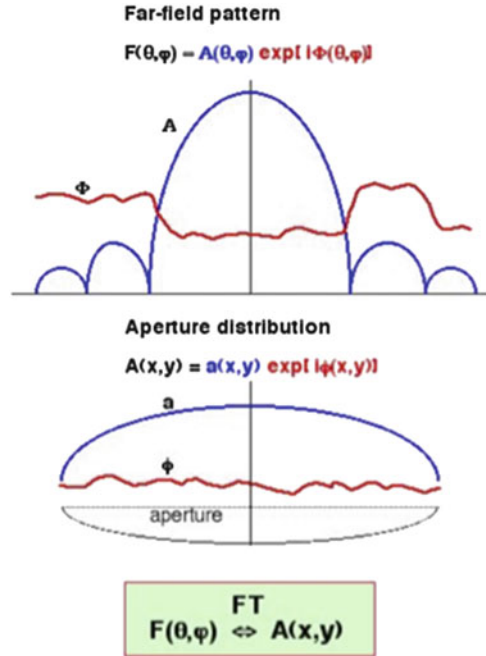
Strictly speaking, for this to work we need a knowledge of the amplitude and phase of the entire (4π steradians) radiation pattern. A Fourier Transformation of this will deliver the field distribution over the aperture plane, also in amplitude and phase.

We want to relate the acquired phase map over the aperture with the deviations from a perfect reflector contour. Realising that a perfect paraboloid reflecting a plane wave will produce a constant phase function over the aperture, we project the phase deviations in the measured distribution upon the reflector and identify these with structural deviations from the prescribed contour. This gives us a map of surface deviations along the direction of the antenna axis. The deviation at the position of the adjusters is obtained by interpolation of the measured deviation map. This delivers a table of the necessary adjustments of the panels. Thus, the spatial resolution of the aperture field need not be better than of the order of the distance between adjusters. Invoking the sampling theorem, we find that for a resolution of n points across the antenna diameter the pattern must be measured to an angle of n HPBWs from the axis. With n of the order of several tens, the pattern intensity at the edge will be very low and a strong source signal is required. The beacon on communication satellites in the 11 GHz band has been a favourite signal source. Also the method has been extended to the use of an earth-bound signal source at short distance. Measuring accuracies of better than 10 μm have been achieved for telescopes of 10–30 m diameter. We illustrate this by the example of Fig. 8.19.

This technique was first described in detail by Bennett et al. (1976), although the principle had been indicated by Jennison (1966) in an appendix to his popular text

Fig. 8.19 Holographic maps of an ALMA antenna with an rms error of 11 μm (scale in μm). The difference between two consecutive measurements is typically a few μm rms. These data were obtained with a transmitter at 300 m distance at a frequency of 100 GHz. Note the blocked area of the quadripod and subreflector, as well as two faulty panels which were removed from the data before analysis (from Laing 2011, ESO)
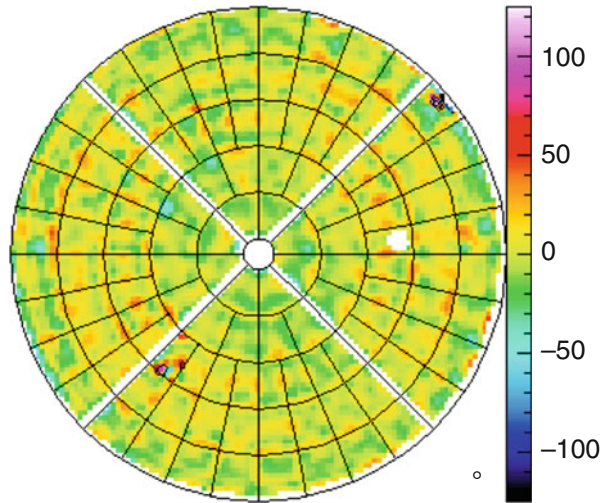
Introduction to Radio Astronomy. Scott and Ryle (1977) applied the method to the antennas of the Cambridge synthesis array, using to their advantage the powerful reference signal from the full-size reference antenna of the array. From there onwards, the method has widely been used and several variations of the basic scheme were introduced depending on the availability of equipment and other circumstances. A full description of the method is presented by Baars (2007, Ch. 6).

8.7 Progress in Electromagnetic Design

8.7.1 Historical Introduction

From the moment the new Jodrell Bank radio telescope made its great public splash with the reception of signals from the Russian space probe Sputnik in November 1957, the interest in large reflector antennas widened from radio astronomy to the fields of space exploration and satellite communication. The tracking of and data collection from space probes as well as communication and spy satellites required sensitive ground stations. Reflector antennas were a natural choice. Simultaneously, the need to design and fabricate small antennas for the space vehicles became an active field of development. This spurred an increased activity in the area of the electromagnetic analysis and design of reflector antennas. Without going into detail, we mention here some of the aspects of this work along with references, so the curious reader might find his way to the pertinent literature. A special issue of the *Proceedings IRE* in January 1958 was devoted to the subject. Ramsay (1958) contributed a review of *Microwave antenna and waveguide techniques before 1900*.

The *Contributions to the antenna field during World War II* were summarised by Van Atta and Silver in the *Proceedings IRE* in (1962).

Significant activity occurred in the 1960s with the construction of large ground stations for space probe tracking and satellite communication. The NASA Deep Space tracking antennas of 64 m diameter came into operation around 1966. The parallel intensive activity at the Jet Propulsion Laboratory (JPL) into the electromagnetic and structural aspects of large antennas has been summarised by Imbriale (2003) and Levy (1996), respectively. Earlier, large radio telescopes had come into operation, such as the Australian 210-ft and NRAO 140-ft antennas described in Chap. 3. From 1967 onwards, the realisation of a 100-m diameter, highly accurate reflector was the main goal of the newly established Max-Planck-Institut für Radioastronomie in Bonn, Germany, featured in Chap. 4.

8.7.2   Radio Astronomy and Communication Approaches Differ

A difference in design philosophy between radio astronomy on the one hand and space exploration and satellite communication on the other should be pointed out. The signal received in radio astronomy is essentially *white noise*, either over a continuous spectrum as synchrotron or thermal radiation or in the form of spectral lines from atoms and molecules, which occur at their specific frequencies in the radio spectrum. Thus, a radio telescope is used over a wide frequency range limited only by its mechanical-structural parameters. The sensitivity increases proportional to the square root of the observation time.

The situation is different in communication and space probe tracking. Here, the signals are *modulated* and contain information transmitted in a relatively small bandwidth at fixed frequencies. Efforts towards improvement in performance may thus be concentrated at a single frequency over a narrow bandwidth. Normally, maximising the ratio of antenna gain to receiver noise temperature is the major goal. Clearly, improving the illumination efficiency by a flat illumination pattern over the aperture would be effective. To this end, Galindo (1964) proposed *shaping* the reflectors of a Cassegrain system. First, the shape of the hyperboloidal subreflector is changed to direct the higher sensitivity of the central cone of the feed pattern to the outer, larger area regions of the main reflector, essentially creating an almost uniform illumination over the aperture. The unavoidable systematic phase errors incurred by this procedure are corrected by a counteracting deviation of the primary reflector from the paraboloidal form, so that the total pathlength from the aperture plane to the focal point remains constant. The result is an increase in the efficiency of the antenna.

Most radio observatories did not adopt this feature, because in the earlier analyses it appeared that the procedure would be frequency dependent, notably due to the relatively small diameter of the secondary reflector (measured in

wavelengths). The VLA of NRAO applied mild shaping. The three 20-m dishes of the Korean VLBI Network also are shaped Cassegrain systems (Minh et al. 2003). The success here might be due to the fact that the 2-m diameter subreflector is quite large reckoned in wavelengths and geometrical optics procedures are sufficient for the design analysis.

In the global project, Square Kilometre Array (SKA) (Hall 2004) several thousands of reflector antennas of 15 m diameter will be deployed. The current design foresees the use of Offset-Gregorian-Shaped reflectors (Chap. 7). This difficult electromagnetic design problem can currently be attacked successfully with the aid of comprehensive computer programs, "*electromagnetic solvers*", in which the detailed design of the feed can also be included in the optimisation of the system.

Both radio astronomers and communication engineers have been active in the development of high efficiency feeds, for both prime-focus and Cassegrain focus illumination. A primary goal was the attainment of a circular beam of high polarisation purity, preferably providing an optimum illumination function with a flat top and steep slope close to the edge of the aperture. These feeds are based on hybrid-mode corrugated horns and the wide-angle so-called scalar horn. Many details can be found in the collection of papers *Electromagnetic Horn Antennas* edited by Love (1976) and a review by Clarricoats and Poulton (1977). Goldsmith (1998) edited a collection of major papers in the area of *Quasioptical Systems*.

8.7.3   Exploiting the Focal Plane

8.7.3.1   Multi-feed System with Independent Pixels

As we have indicated before, the early radio telescopes operated with a single feed in the primary focus of the paraboloid; they were "single-pixel" instruments, in stark contrast to the imaging capabilities of optical telescopes. The major obstacle to the exploitation of the focal plane is the strong coma of the reflectors with a small focal ratio. The increasing choice of the Cassegrain configuration with its large effective *f*-number and hence much better imaging capability opened the possibility of installing multi-feed receivers in the secondary focal plane. This increased the efficiency of observing extended objects and carrying out systematic large-scale sky surveys. A pioneering example is the 32-pixel array of the University of Massachusetts (Erickson et al. 1999). The separate data of each feed are used to construct a map of the sky brightness over the angular area covered by the multi-beam system (Fig. 8.20, left).

A further impetus came from the development of highly sensitive bolometers and superconducting Kinetic Inductance Detectors (KID) as detectors of broadband millimetre-wavelength radiation. A 295-element bolometer array (Fig. 8.20, right), developed at the Max-Planck-Institut für Radioastronomie, operates at 870 μm wavelength on the APEX telescope at 5000 m altitude in Chile (Siringo et al. 2009).
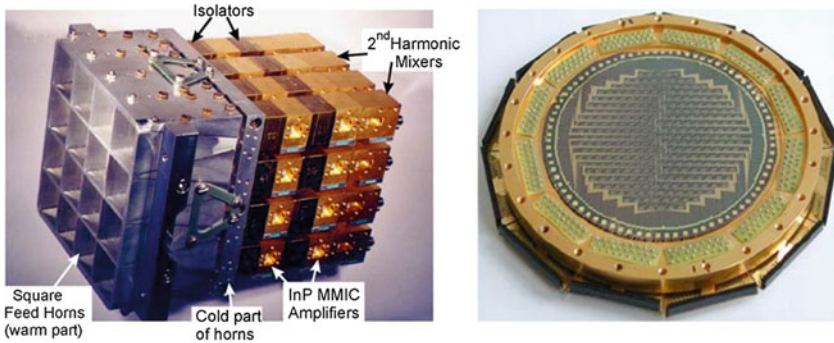
Fig. 8.20 Multi-feed receivers. *Left*: SEQUOIA array of 16 dual-polarisation feeds with MMIC amplifiers for 85–115 GHz (FCRAO, Univ. Massachusetts). *Right*: LABOCA, a 295-element bolometer (within the central polygon) operating at 870 μm wavelength. It is a primary instrument of the APEX submillimetre telescope (MPIfR)

These developments have inspired the originators of some recent telescope proposals to use a *Ritchey–Chrétien* (RC) optical arrangement. We give the geometrical parameters of the RC in Chap. 2. The RC telescope is a modified Cassegrain with both mirrors in the shape of a hyperboloid. By a proper selection of the eccentricities of the reflectors, one can obtain a system that does not suffer from coma and spherical aberration. A consequence is that some astigmatism cannot be avoided. The primary reflector remains close to a paraboloid, and the resulting phase variation over the aperture is corrected by adjusting the eccentricity of the secondary reflector. This is another version of *shaping*, this time to increase the field of view rather than the on-axis efficiency. It should be noted that methods for profile measurements of the reflector surface that use the specific geometry of the parabola need a correction device in the RC telescope. In optics, this is called the *null corrector*. An error in the null corrector caused the wrong figure in the shaping of the Hubble Space Telescope primary mirror that required later extensive focal plane correctors to obtain an error-free focal area. Similar problems might arise with measuring devices for radio telescopes.

8.7.3.2   Phased-Array Feeds (PAF)

Recently, highly interesting developments have produced so-called *phased-array feeds* (PAF) that sample the primary focal plane sufficiently dense to realise several tens of adjacent beams. Here, a considerable area of the focal plane, including the first diffraction ring, is covered by a two-dimensional array of adjacent feeds. Using beam forming, all elements of the PAF are combined into compound beams. Interestingly, the disturbing effect of coma can be effectively suppressed by this method. Thus, the system can be deployed in the primary focal plane of a paraboloid with a small focal ratio. The beam forming weights can be optimised in various ways, for example to maximise sensitivity, reduce sidelobes, suppress RFI

Fig. 8.21 The Phased-Array Feed APERTIF in the focal plane of a WSRT antenna (*left*, ASTRON) and the Australian PAF (*green* feature in the inset) mounted on ASKAP in Western Australia (ASKAP/CSIRO)

or optimise polarisation performance (Jeffs et al. 2008; van Ardenne et al. 2009). Phased-Array Feeds for radio astronomy received an increasing attention in the early 2000s with the development of a PAF demonstrator (Ivashina et al. 2004). A major breakthrough of PAF technology was triggered by the availability of affordable all-digital processing back ends, tools for electromagnetic modelling and optimising PAF systems (Ivashina et al. 2006) and competitive room temperature low-noise amplifiers. First successes with such systems in interferometers have been obtained with APERTIF at ASTRON/Westerbork in the Netherlands (van Cappellen and Bakker 2010) and with ASKAP at CSRIO in Western Australia (DeBoer et al. 2009). Figure 8.21 shows pictures of the PAFs used by these groups, as placed in the WSRT and ASKAP.

8.8 Conclusion

As we have seen in this chapter, it is important for a successful antenna system that the interplay between structural and electromagnetic imperfections be understood and properly accounted for in the design of all components. This aspect received increasing attention in the 1960s, notably by the work of John Ruze at MIT. His results, as presented in Sect. 8.4 above, enabled a practical approach to the required structural-mechanical design. Together with the seminal work by von Hoerner (1967) on homologous deformations (Chap. 4), great progress was made in the translation from astronomical performance requirements to mechanical, structural and electromagnetic specifications. The radio astronomer needed to develop a feeling for the structural and mechanical limitations in defining his specifications on the basis of electromagnetic parameters. The structural engineer was much helped by an understanding of the important antenna parameters and their sensitivity to structural imperfections.

From about 1970, advanced finite element analysis enabled structural models to be optimised by computer. Increasingly, sophisticated computer programs for the analysis of the electromagnetic analysis of reflector telescopes became available, greatly improving the design of optimally matched feed horns. Reviews by Rusch (1984, 1992), poetically titled *the current state of the reflector antenna art*, summarise the situation well. Rusch also mentions hardware aspects and material choices for both earth-bound and space-borne antennas and the use of composite materials such as *carbon fibre reinforced plastic* (CFRP). By the time of the 1992 review paper, many advances in the technology of individual radio telescopes had been published. This includes the important area of accurate measurement and setting of the reflector surface, particularly the progress in radio-holographic reflector profile measurement. The significance of the advances obtained in the design and construction of radio telescopes is reflected in several special issues of the *Proceedings IEEE* devoted to *Radio and Radar Astronomy* in September 1973, *Radio Telescopes* in May 1994 and *Advances in Radio Telescopes* in August 2009.

Addendum: Aberrations and Zernike Polynomials

Here, is a summary of the mathematical procedure, developed by Zernike, which allows us to separate any distorted wave function into a number of components that contain a description of the primary and possibly higher order aberration terms. We depart from the general mathematical statement that the distorted wave field, or equivalently the distorted reflector surface, defined over the aperture area of the reflector, can be expanded into a series of orthogonal polynomials. Thus, for the deviation δ at any point with coordinates (ρ, ϕ), we can write $\delta(\rho, \phi) = \sum_i a_i Z_i(\rho, \phi)$, where Z_i is the ith polynomial and a_i the factor with which the polynomial contributes to the total deviation. In 1934, Frits Zernike (1888–1966) found a particularly elegant set of polynomials with separate radial and azimuthal terms that are suitable for the description of telescope aberrations and surface errors. The *Zernike polynomials* appear in even and odd form and are written as:

$$Z_n^m(\rho, \phi) = R_n^m(\rho) \cos(m\phi) \quad \text{even term}$$
$$Z_n^{-m}(\rho, \phi) = R_n^m(\rho) \sin(m\phi) \quad \text{odd term}$$

$$\text{where} \quad n \geq m \qquad \text{non-negative integers}$$
$$0 \leq \rho \leq 1 \qquad \text{normalised radial coordinate}$$
$$0 \leq \phi \leq 2\pi \qquad \text{azimuthal angle}$$

Details about these polynomials, including their generating functions, can be found in Born and Wolf (1999, Ch. 9 and Appendix VII). A main feature is their orthogonality, which is expressed as

$$\int_A Z_i \cdot Z_j dA = |Z_i|^2 \quad \text{for} \ i = j$$

$$\text{and} \quad \int_A Z_i \cdot Z_j dA = 0 \qquad \text{for} \ i \neq j,$$

where the integration is extended over the aperture area A.

The orthogonality condition allows the simple calculation of the contribution factor (a_i) of the individual *Zernike modes* by integration over the aperture area of the deviations multiplied with the polynomial:

$$a_i = \frac{1}{|Z_i|} \int_A \delta(\rho, \phi) \cdot Z_i(\rho, \phi) dA. \tag{8.6}$$

This equation can be used as the basis for the development of algorithms for deformation calculations with FEA programs or for analysis of measurement data from alignment or acceptance tests.

We used above two counting systems for the Zernike polynomials: the sequential numbering scheme represented by index i and the dual numbering scheme with indexes m, n. The latter scheme reflects some special symmetry features which are of interest particularly in regard to corresponding symmetry features in the basic gravity load cases of mechanical structures.

Figure 8.22 shows the shape of the Zernike modes indicated by the sequential and the dual numbering scheme in a way that regularities in the symmetries are
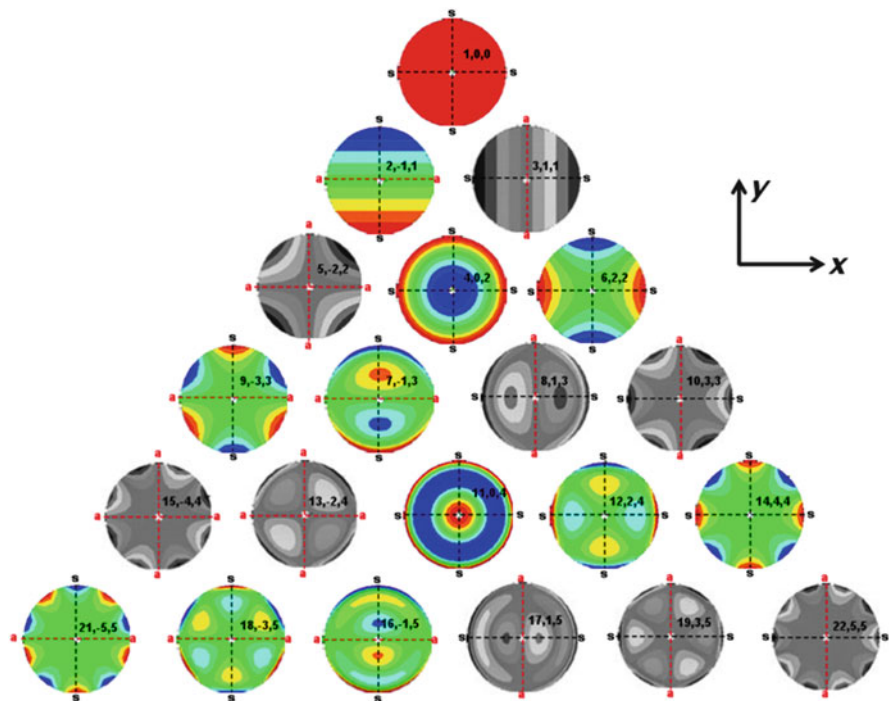
Fig. 8.22 Symmetry features of the Zernike polynomials

visualised. *Even* symmetry about the coordinate axes is indicated by a black dashed line denoted s—s, and *odd* (skew) symmetry is indicated by a red dashed line denoted a—a. The first number is the sequential i; the second and third are the dual numbers m, n. There are four symmetry classes of the Zernike polynomials: SS denotes even symmetry about the x- as well as the y-axis; SA even symmetry about the x-axis, but odd symmetry about the y-axis; AS odd symmetry about the x-axis and even symmetry about the y-axis; AA means odd symmetry about both axes, x and y. The Zernike polynomials of symmetry classes SS and AS are shown in Fig. 8.22 in colour. They correspond to the symmetry classes of the basic gravity deformation states of an antenna in zenith and horizon position. The Zernike polynomials of symmetry classes SA and AA are shown in the figure in grey. They have no correspondence with the gravity deformation states but may occur under wind and temperature influences.

Seidel's *primary aberrations*, as mentioned in the main text, can be identified with the corresponding Zernike components. We list these with their name, sequence number i and Zernike numbers m, n in Table 8.3.

Table 8.4 contains the mathematical form of the major aberrations with the representation in Zernike polynomial and explicit algebraic form. A plot of four of these functions has been shown in Fig. 8.8.

Table 8.3 Seidel primary aberrations with corresponding Zernike components

Name	Seq. i	m, n	Characteristic
Piston	1	0, 0	Solid body shift along z-axis
Tip	2	−1, 1	Solid body rotation about x-axis
Tilt	3	1, 1	Solid body rotation about y-axis
Defocus	4	0, 2	*alias* field curvature, quadratic in r
Astigmatism	5; 6	−2, 2; 2, 2	Not rotationally symmetric
Coma	7; 8	−1, 3; 1, 3	Not rotationally symmetric
Trefoil	9; 10	−3, 3; 3, 3	Threefold symmetry
Spherical aberration	11	0, 4	Rotationally symmetric

Table 8.4 Zernike polynomial representation of primary aberrations

Type of aberration	n	m	Zernike representation	Explicit form
Distortion (tip-tilt)	1	1	$A_{111}R_1^1(r) \cdot \cos\phi$	$A_{111} \cdot r \cdot \cos\phi$
Defocus (curvature)	2	0	$\frac{1}{\sqrt{2}}A_{120}R_2^0(r)$	$\frac{1}{\sqrt{2}}A_{120} \cdot (2r^2 - 1)$
Astigmatism	2	2	$A_{022}R_2^2(r) \cdot \cos(2\phi)$	$A_{022} \cdot r^2(2\cos^2\phi - 1)$
Coma	3	1	$A_{031}R_3^1(r) \cdot \cos\phi$	$A_{031} \cdot (3r^3 - 2r) \cdot \cos\phi$
Spherical aberration	4	0	$\frac{1}{\sqrt{2}}A_{040}R_4^0(r)$	$\frac{1}{\sqrt{2}}A_{040} \cdot (6r^4 - 6r^2 + 1)$

References

Baars, J.W.M.: The measurement of large antennas with cosmic radio sources. IEEE Trans. Antennas Propag. **21**, 461–474 (1973)

Baars, J.W.M.: Technology of large radio telescopes for millimeter and submillimeter wavelengths. In: Button, K. (ed.) Infrared and Millimeter Waves, vol. 9, Ch. 5, pp. 241–281. Academic Press, New York (1983)

Baars, J.W.M.: The Paraboloidal Reflector Antenna in Radio Astronomy and Communication. Springer, New York (2007)

Baars, J.W.M.: History of flux density calibration in radio astronomy. URSI Radio Sci. Bull. **348**, 47–66 (Mar 2014)

Baars, J.W.M., Genzel, R., Pauliny-Toth, I.K.K., Witzel, A.: The absolute spectrum of Cas A: an accurate flux density scale and a set of secondary calibrators. Astron. Astrophys. **61**, 99–106 (1977)

Bennett, J.C., Anderson, A.P., McInnes, P.A., Whiteaker, A.J.T.: Microwave holographic metrology of large reflector antennas. IEEE Trans. Antennas Propag. **24**, 295–303 (1976)

Born, M., Wolf, E.: Principles of Optics, 7th edn, Seidel Aberrations, Ch. 5, 236; Zernike Polynomials, Ch. 9, 523, Appendix VII, 905. Cambridge University Press (1999)

Clarricoats, P.J.B., Poulton, G.T.: High-efficiency microwave reflector antennas—A review. Proc. IEEE. **65**, 1470–1504 (1977)

DeBoer, D.R., et al.: Australian SKA pathfinder: a high-dynamic range wide-field of view survey telescope. Proc. IEEE. **97**, 1507–1521 (2009)

Erickson, N.R., Grosslein, R.M., Erickson, R.B., Weinreb, S.: A cryogenic focal plane array for 85-115 GHz using MMIC preamplifiers. IEEE Trans. MTT. **47**, 2212–2219 (1999)

Findlay, J.W.: Operating experience at the National Radio Astronomy Observatory. In: Large Steerable Radio Antennas. Annals of the New York Academy of Sciences, vol. 116, pp. 25–40 (1964)

Galindo, V.: Design of dual-reflector antennas with arbitrary phase and amplitude distributions. IEEE Trans. Antennas Propag. **12**, 403–408 (1964)

Goldsmith, P.F. (ed.): Quasioptical Systems: Gaussian Beam Quasioptical Propagation and Applications. IEEE Press, New York (1998)

Greve, A.: Strehl number degradation by large-scale systematic surface deviations. Appl. Opt. **19**, 2948–2951 (1980)

Hall, P.J. (ed.): The Square Kilometre Array: an international engineering perspective. Exp. Astron. **17**, 1–3 (2004, also in book by Springer, 2005)

Imbriale, W.A.: Large Antennas of the Deep Space Network. Wiley, Hoboken, NJ (2003)

Ivashina, M., Bij de Vaate, J.G., Braun, R., Bregman, J.D.: Focal plane arrays for large reflector antennas: first results of a demonstration project. Proc. SPIE. **5489**, 1127–1138 (2004)

Ivashina, M.V., Kehn, M.N.M., Kildal P.S., Maaskant, R.: Control of reflection and mutual coupling losses in maximizing efficiency of dense focal plane arrays. First European Conference on Antennas and Propagation, Nice, 1–6 (2006)

Jeffs, B.D., Warnick, K.F., Landon, J., Waldron, J., Jones, D., Fisher, J.R., Norrod, R.: Signal processing for phased array feeds in radio astronomical telescopes. IEEE J. Sel. Top. Sign. Process. **2**, 635–646 (2008)

Jennison, R.C.: Introduction to Radio Astronomy. Newnes, London (1966)

Kramer, C., Peñalver, J, Greve, A.: Improvement of the IRAM 30 m Telescope Beam Pattern. IRAM Internal Memo (2013)

Kuz'min, A.D., Salomonovivh, A.E.: Radioastronomical Methods of Antenna Measurements. Academic Press, New York (1966)

Laing, R.A.: The Performance of the European ALMA Antennas. ESA Workshop on Antennas (2011)

Levy, R.: Structural Engineering of Microwave Antennas. IEEE Press, Piscataway, NJ (1996)

Love, A.W. (ed.): Electromagnetic Horn Antennas. IEEE Press, New York (1976)

Minh, Y.C., Roh, D.-G., Han, S.-T., Kim, H.-G.: Construction of the Korean VLBI Network (KVN). In: New technologies in VLBI, Proceedings of a Symposium of the International VLBI Service for Geodesy and Astrometry. ASP Conference Series, vol. 306, pp. 373–381 (2003)

Perley, R.A., Butler, B.J.: An accurate flux density scale from 1 to 50 GHz. Astrophys. J. Sup. Series **204**, 19 (20 p) (2013)

Ramsay, J.F.: Microwave antenna and waveguide techniques before 1900. Proc. IRE. **46**, 405–415 (1958)

Rusch, W.V.T.: The current state of the reflector antenna art. IEEE Trans. Antennas Propag. **32**, 313–329 (1984)

Rusch, W.V.T.: The current state of the reflector antenna art – entering the 1990s. Proc. IEEE. **80**, 113–126 (1992)

Ruze, J.: The effect of aperture errors on the antenna radiation pattern. Suppl. al Nouvo Cimento. **9**, 364–380 (1952)

Ruze, J.: Lateral feed displacement in a paraboloid. IEEE Trans. Antennas Propag. **13**, 660–665 (1965)

Ruze, J.: Antenna tolerance theory – a review. Proc. IEEE. **54**, 633–640 (1966)

Ruze, J.: Feed support blockage loss in parabolic antennas. Microwave. J. **11**, 76–80 (Dec 1968)

Scott, P.F., Ryle, M.: A rapid method for measuring the figure of a radio telescope reflector. Mon. Not. Roy. Astron. Soc. **178**, 539–545 (1977)

Seidel, L.: Astr. Nachr. **43**, 289, 305, 321 (1856)

Silver, S.: Microwave Antenna Theory and Design MIT Radiation Lab Series, vol. 12. McGraw-Hill, New York (1949)

Siringo, G., Kreysa, E., Kovács, A., Schuller, F., Weiß, A., Esch, W., Gemünd, H.-P., Jethava, N., Lundershausen, G., Colin, A., Güsten, R., Menten, K.M., Beelen, A., Bertoldi, F., Beeman, J. W., Haller, E.E.: The large APEX bolometer camera LABOCA. Astron. Astrophys. **497**, 945–962 (2009)

Stumpff, P.: Astronomische Pointing Theorie für Radioteleskope. Kleinheubacher Berichte. **15**, 431–437 (1972)

van Ardenne, A., Bregman, J.D., van Capellen, W.A., Kant, G.W., Bij de Vaate, J.G.: Extending the field of view with phased array techniques: results of European SKA research. Proc. IEEE. **97**, 1531–1542 (2009)

Van Atta, I.C., Silver, S.: Contributions to the antenna field during WW II. Proc. IRE. **50**, 692–697 (1962)

van Cappellen, W.A., Bakker, L.: APERTIF: phased array feeds for the Westerbork synthesis radio telescope. IEEE International Symposium on Phased Array Systems and Technology, Waltham (MA), USA, pp. 640–647 (2010)

von Hoerner, S.: Design of large steerable antennas. Astron. J. **72**, 35–47 (1967)

Chapter 9
Concluding Review and a Dialogue on Management Aspects
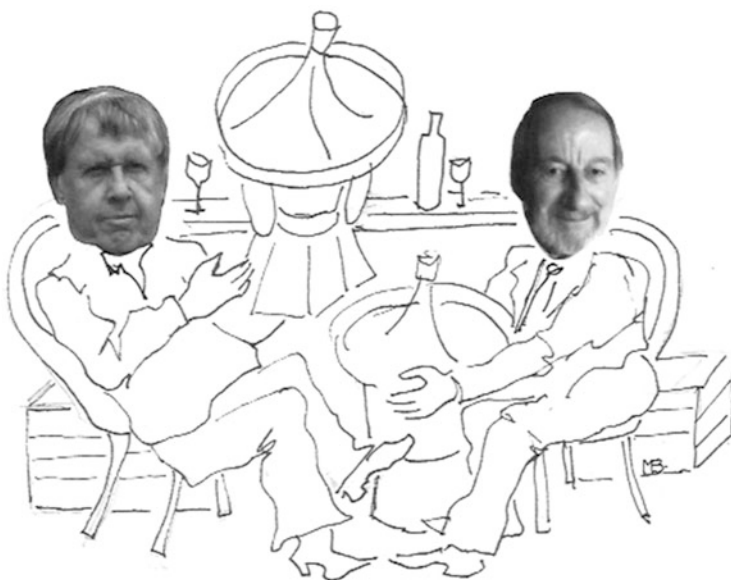
The authors, HK—*left* and JB—*right*, at work. Drawing by Marja Baars

9.1 Concluding Review

When we started to discuss the content and style of this book several years ago, we decided not to cover design aspects that had not been matured into a working telescope. However, some of the telescopes that we would like to feature because of their advanced design were still under construction, in particular the LMT/GTM in Mexico (Chap. 5) and ALMA in Chile (Chap. 6). Since then, our writing has been interrupted sufficiently by other duties, so that these instruments could be given the attention they deserve.

We have painted in this book the technical development in a new branch of astronomy—radio astronomy—that arose in the 1940s from a serendipitous discovery of long-wavelength radio radiation from the centre region of our Milky Way by Jansky in 1932. With the exception of the 21-cm spectral line of neutral hydrogen, detected in 1951, the early observations of the general "background" radiation from which some strong "localised sources" stood out were hard to interpret. The extremely course angular resolution of the radio telescopes made it impossible to identify the received signals with an optical counterpart. When through the use of interferometry a few discrete sources could be identified with supernova remnants and distant galaxies, the significance of the radio regime for the science of astronomy had been established. In the late 1940s and early 1950s, proposals for large radio telescopes were advanced in several countries, notably the Netherlands, England, Australia, Germany, Canada and the USA (Table 9.1).

In most cases, the proposal entailed a fully steerable parabolic reflector of as large a size as technically and/or financially possible. The choice is easy to understand. The geometry of the reflector requires only a single detection element in the focal point and allows operation at any wavelength. In addition, most proposers already had experience with such a reflector through the use of the German "Würzburg Riese" radar antenna, left after the war along the European coastline. Of course, the German engineers who designed and built these 7.5-m diameter antennas were not available for help. Thus, the early radio astronomers, typically physicists and engineers from the radar laboratories, turned to mechanical and structural engineers working in the area of bridges (Jodrell Bank, Parkes), railroads (Dwingeloo) and airplanes (Stockert).

These "bridge builders" were faced with a number of new and stringent requirements for a radio telescope. The reflector needed to be directed to any point of the sky and moreover be able to follow that point on its diurnal path along the firmament. Thus, the reflector would have to be placed on a two-axis mount that provided precisely controlled angular movement about the axes. In addition, the parabolic shape of the reflector needed to be maintained with varying tilting angle to an accuracy of a small part (less than 5–10%) of the observing wavelength. The important hydrogen line at 21 cm wavelength determined the minimum operational wavelength of the early large telescopes mentioned above and described in Chap. 3. Thus, the requirement for the reflector precision was set at about 1 cm.

The designers went to work and presented three very different solutions for the support of the reflector by the mount. The Jodrell Bank reflector was part of the load-bearing structure and connected to the elevation bearings by a stiff outer hoop. The

Table 9.1 Data on radio telescopes described in this book

Name—Institute	Location-altitude (m)	Year	Mount—Drive	Optics	Diameter (m)	Minimum Wavelength	Weight (tonnes)	Remarks
Reber—private	Wheaton, USA—?	1937	Transit	Par—PF	9.6	10 cm		
Würzburg—NFRA	Kootwijk, NL—50	1950	El-Az—turret	Par—PF	7.5	10 cm		21 cm hydrogen line detection
Dwingeloo—NFRA	Dwingeloo, NL—25	1956	El-Az—wheel on track	Par—PF	25	10 -> 6 cm	120	Upgraded 1972
Stockert—Univ. Bonn	Stockert, D—435	1957	El-Az—king-post	Par—PF	25	10 cm	90+base	Upgraded to Cassegrain in 1967
Jodrell/Lovell—Univ. Manchester	Jodrell Bank UK—80	1957	El-Az—wheel on track	Par—PF	76	20 -> 6 cm	3200	Upgraded in 1976 and 2002
Parkes—CSIRO	Parkes, Aus—415	1961	El-Az—turret	Par—PF	63	6 cm	1000	Master equatorial, upgraded in 2003
300 ft—NRAO	Green Bank, USA—800	1962	Transit	Par—PF	92	6 cm	600	Collapsed in late1988
Arecibo—NAIC/RSI	Arecibo, USA—500	1963	Fixed—to zenith	Sphere—line feed	305	10 cm		Upgraded in 1997 to point focus layout
Haystack—MIT/Lincoln Lab	Westford, USA—130	1964	El-Az—turret—hydrostatic bearing	Par—Cass	37	30 -> 3 mm	305	In radome
140 ft—NRAO	Green Bank, USA—800	1965	Polar—hydrostatic bearing	Par—PF	43	2 cm	2700	Changed to Cassegrain in 1973
36 ft/12 m—NRAO	Kitt Peak, USA—1940	1967	El-Az—turning head	Par—PF -> Cass	11 -> 12	1 mm	55	In astrodome, new reflector in 1983
WSRT—NFRA/ASTRON	Westerbork, NL—16	1970	Polar—4-point support	Par—PF	25	6 cm	124	Array of 14 antennas, PAF in 2017
Effelsberg—MPIfR	Effelsberg, D—320	1971	El-Az—wheel on track	Par—PF and Greg	100	7 mm	3165	Homology, active subreflector in 2006
45 m—NRO	Nobeyama, J—1350	1983	El-Az—wheel on track	Par—Greg, Coudé	45	2 mm	700	CFRP surface panels, master collimator

(continued)

Table 9.1 (continued)

Name—Institute	Location-altitude (m)	Year	Mount—Drive	Optics	Diameter (m)	Minimum Wavelength	Weight (tonnes)	Remarks
MRT—IRAM	Pico Veleta, ES—2850	1985	El-Az—turning head	Par—Cass	30	0.8 mm	732	Full thermal control
CSO—Caltech	Mauna Kea, USA—4140	1986	El-Az—turning head	Par—Cass	10.4	0.35 mm	35	In astrodome
IRAM Interferometer—IRAM	Plateau de Bure, F—2550	1988	El-Az—turning head	Par—Cass	15	0.8 mm	100	CFRP—array of 6 -> 12 (NOEMA)
MERLIN—Univ. Manchester	Cambridge, UK—15	1990	El-Az—wheel on track	Par—Cass	32	1.2 cm	300	Part of MERLIN array
GMRT—NCRA/TIFR	Pune, India—650	1992	El-Az—turning head	Par—PF	45	20 cm	116	Array of 30, lightweight
HHT/SMT—MPIfR/ARO	Mt. Graham, USA—3200	1994	El-Az—turning head	Par—Cass	10	0.3 mm	50	CFRP structure and panels—astrodome
GBT—NRAO/GB observatory	Green Bank, USA—800	2002	El-Az—wheel on track	Par—PF and Greg	105	7 mm	7600	Active surface
ARIES XXI—IGN	Yebes, ES—1350	2005	El-Az—turning head	Par—Cass	40	3 mm	764	
ALMA—global collaboration	Pl. Chajnantor, Chile—5000	2013	El-Az—turning head—direct drive	Par—Cass	12	0.3 mm	90	CFRP structure—array of 50
SRT—INAF	Sardinia, It—600	2013	El-Az—wheel on track	Par—Greg, Coudé	64	3 mm	3300	Active surface
FAST—NAOC	Guizhou, China—1000	2016	Fixed—to zenith	Sphere—PF	500	10 cm		Uses 300 m actively shaped to paraboloid
LMT—INAOE/UMass	Sierra Negra, Mex—4640	2017	El-Az—turning head	Par—Cass	50	1 mm	3000	Active surface
MeerKAT—SKA/SA	Karoo, S. Africa—1300	2017	Az-turret/El-linear rack drive	Par—Greg	13.5	1.3 cm	42	Offset reflector geometry—array of 64

Dwingeloo reflector was supported by a truss frame and connected to the elevation bearings about midway between centre and rim. This arrangement is optimal for the distribution of gravitational deformation (Chap. 4) and has been used for most large telescopes. These two telescopes have a wheel-on-track azimuth movement that has been selected for most telescopes from about 40 m diameter upwards.

The designers of the Stockert and Parkes telescopes took a completely different approach. Here, the reflector is supported at the centre by a stiff hub that is connected to a compact elevation–azimuth mount placed on top of a concrete tower. This type is often called a turning head mount. When large slewing bearings, currently up to 8 m diameter, became available, the central hub could be enlarged enabling a better support of the reflector structure at the elevation bearings. The turning head design has been widely applied to telescopes up to a diameter of 30–40 m.

The gravitational deformation pattern of the reflector is quite different between these three approaches for the support structure. The best compromise is reached with a solution similar to that used in the Dwingeloo telescope, where extreme, large-scale deformations can be avoided.

The early radio telescopes were essentially designed to provide sufficient stiffness against gravitational deformation as function of elevation angle. They had a reflector surface of metallic mesh that significantly reduced the force of the wind. Thus, the influence of wind and possible temperature gradients on the reflector precision and the pointing behaviour could essentially be ignored for the envisaged wavelengths of observation.

The story told in this book limits itself to the development of large and accurate reflector antennas. It should be understood that progress in the science of radio astronomy was not uniquely due to the emergence of large reflectors. The extremely poor angular resolution (half a degree, the size of the moon, for a 25-m reflector at 20 cm wavelength) led to the use of interferometers from the early days. These operated at relatively long wavelengths of 1–3 m and consisted of arrays of dipoles or a cylindrical paraboloid with a wire-mesh reflector. These instruments produced the first catalogues of discrete radio sources with reasonably good positions. The new large single reflectors enabled detailed study of these objects at shorter wavelength. The "radio sky" presented the astronomers with unexpected objects such as supernova remnants and clouds of ionised hydrogen in our Milky Way and many sources outside our Galaxy, so-called extragalactic objects. Some of these could be identified with a known optical galaxy, but many remained enigmatic until larger telescopes would become available. Around 1960, interferometric observations showed angular fine structure in sources that spurred an increased activity towards telescopes with very high angular resolution, essentially interferometers at cm wavelength, and high sensitivity, hence large and precise reflectors for the short cm wavelengths.

The first in the latter class is the NRAO 140-ft equatorially mounted telescope with a design minimum wavelength of 3 cm. We have discussed its features in Chap. 3. It incorporates several original aspects, such as hydrostatic bearings, welded aluminium reflector structure and the choice of polar mount. None of these have become standard features of later telescopes. The 140-ft delivered great science but also showed technical shortcomings. With a beamwidth of only

a few arcminutes, its unpredictable pointing variations became a serious impediment. These were caused by differences and gradients in the temperature of the structure. The avoidance and/or control of structural temperature variations became an essential condition in the design of all future telescopes with an angular resolution less than an arcminute.

With the experience of the first large telescopes in the early 1960s, it became also clear that bigger and simultaneously more precise antennas for operation at shorter wavelengths could not be realised in an economic way without new design methods that would significantly reduce the weight for a given reflector precision. Fortunately, around this time the first computer programs for finite element analysis of structures became available. The Haystack antenna mentioned in Chap. 3 provided a successful demonstration of their capabilities.

A breakthrough was achieved in 1966 by the introduction of the principle of homologous deformation, shortly called *homology*, by Sebastian von Hoerner. The idea is as simple as it is genius: let the structure deform under gravitational load but in such a way that the surface retains a parabolic shape for all elevation angles, while allowing a change in focal length and axis direction. The price to pay is the adjustment of the detector to the changing position of the focal point.

The idea was proven to be practically feasible and was applied in the design of the Effelsberg 100-m telescope. For equal weight, the minimum wavelength of a homologous telescope can be more than an order of magnitude smaller than with a classical design based on stiffness. It is interesting to recollect here that, once homology became known among telescope users, several older telescopes showed some homologous behaviour that could be exploited by adjusting the detector to the "best focus" location depending on the elevation angle.

Because the subject of this book is concerned with the structural design of reflector antennas of increasing size and precision, hardly any mention has been made of the large interferometric arrays that have been realised since 1970. These so-called aperture synthesis telescopes combine the signals of an array of two-element interferometers to a picture of the brightness distribution of the observed object. The large number of elements (typically from about 10 to as many as 40) pushed for a most economic antenna design and normally resulted in a "standard" antenna such as used for the 27 elements of 25 m diameter of the VLA in New Mexico. The original features of the polarmounted 25-m antennas of the WSRT have been presented in Chap. 4, and in Chap. 7 we mentioned the "indigenous" GMRT with 30 wire-mesh antennas of 45 m diameter in India. These instruments achieve an angular resolution of the order of arcseconds. Much better resolution is obtained by the VLBI (very long baseline interferometry) networks, where the signals from globally distributed antennas are combined to attain milli-arcsecond resolution.

Nevertheless, there remained a push to shorter wavelengths, not only originating from the desire to improve the angular resolution but also to explore the astrophysical domain of the millimetre wavelengths. Several extragalactic sources showed an unusual increase in intensity with decreasing wavelength pointing to possibly interesting hitherto unknown physical processes. NRAO took the initiative for an 11-m diameter reflector with a precision goal of 50 μm, a value barely achieved by

two 4.5-m diameter dishes in Texas and California (Chap. 5). Similarly to the experience with the 140-ft, the contractor did not manage to satisfy the surface specification; it came out at 0.1 mm, good enough for observations at wavelengths longer than 2 mm. As mentioned in Chap. 5, the detection of the carbon monoxide molecule in interstellar space and star forming regions opened a Pandora's box of discoveries of tens of molecules and turned "millimetre astronomy" into one of the most intensely researched subfields of astronomy.

In the early 1970s, the company ESSCO of Concord, Massachusetts, well known for its radome-enclosed radar antennas, offered an integrated radome-enclosed mm-wavelength antenna of 13.7 m diameter with a surface precision of 0.3 mm that over time was improved to 0.15 mm. A number of radio observatories acquired such a telescope (in Brazil, Sweden (20 m diameter), Univ. of Massachusetts, Finland, Spain, China, Korea). Most of the sites were marginally suitable for work at 3 mm wavelength, where the reflector already showed a significantly decreased efficiency. With the exception of the UMass telescope, the astronomical output has been limited, but the interest in millimetre-wavelength astronomy certainly grew through the use of these instruments.

Around the mid-1970s, several proposals for the construction of a large telescope for short mm wavelengths (1–4 mm), located at a high and dry site, were submitted in Japan, Germany, England, France and the USA. The reflector precision of these would be in the range of 50–100 μm. The application of homology and advanced finite element methods made it possible to design a reflector structure with such small deformation behaviour for diameters up to 30–40 m. But it now became clear that the influence of wind and temperature variation would become the limiting factor in the achievable precision of reflector surface and antenna pointing. This posed new challenges to the structural engineer who needed to involve aspects of thermal control and advanced servo control in his design work. But it was also necessary to adapt the beautiful highly symmetric homologous "umbrella" support of the Effelsberg reflector. The requirement to accommodate an accessible receiver cabin behind the reflector was incompatible with the umbrella concept at the smaller size of the telescope. Still one needed homology to satisfy the performance requirements. Most mm telescopes employ a yoke structure at the elevation bearings to provide a support interface to the homologous reflector backup structure and leave space for a receiver cabin between the arms of the yoke (Chaps. 4 and 5).

The realisation of a full thermal control was pioneered in the IRAM 30-m telescope (Chap. 5). In the 50-m LMT (Chap. 5), it was necessary to include real-time active control of the reflector shape by motorised adjusters of the surface panels, as well as of wind-induced pointing errors. This is called flexible body control (FBC) and is described in Chap. 5.

By the end of the 1980s, the importance of millimetre-wavelength observations for the understanding of a number of astrophysical problems had been solidly established. Proposals were made for telescopes to extend the wavelength range to the smallest wavelength where the earth's atmosphere is sufficiently transparent from the highest and driest places on earth (Hawaii, Northern Chile, South pole). At

such a wavelength (~0.3 mm), the required reflector precision is about 20 μm and a 12-m diameter antenna would have a beamwidth of 6 arcseconds requiring a pointing precision and stability of 0.6 arcsecond. The possible high-altitude sites (4000–5000 m altitude) have abundant sunshine and are normally windy. Clearly, the influence of variations in temperature and wind would again need to be minimised. Early studies indicated that budgetary realities would pose a limit of 10–15 m on the reflector diameter. Installing an elaborate and bulky temperature control system such as on the MRT (Chap. 5) appeared unwieldy. An alternative structural material with low thermal expansion was needed. Such a material had become available in the form of carbon fibre reinforced plastic (CFRP). It is a lightweight and strong material with a thermal expansion about an order of magnitude smaller than steel. It had been extensively used in space-borne systems. Its increasing use in consumer products and industry lowered the price to a level where it could be considered for a telescope on earth. A 10-m diameter reflector support structure of CFRP with CFRP surface panels was pioneered by Krupp/MAN for the MPIfR. The HHT telescope is described in Chap. 6.

The poor angular resolution of radio telescopes compared to their optical counterparts remained with the new mm telescopes. Thus, several interferometer arrays were put into operation from 1985 onwards in Japan, the USA and France. By the mid-1990s, mm astronomy had become a productive and fruitful part of astronomy and astronomers discussed the need for a truly large telescope such as the Very Large Array in New Mexico that operates to a shortest wavelength of 7 mm. As described in Chap. 6, independent proposals for a "millimetre VLA" were prepared in Japan, the USA and Europe. Eventually, these were amalgamated into the ALMA telescope now in full operation at 5000 m altitude in the Atacama Desert of northern Chile. ALMA consists of 54 submm antennas of 12 m diameter, plus a dozen smaller ones of 7 m diameter, which can be distributed over an area of more than 10 km diameter. The telescope is equipped with receivers for the entire wavelength band from 0.3 to 10 mm (Chap. 6).

The specification for reflector precision and pointing is comparable to that of the HHT mentioned above, but a number of additional requirements challenge the designers. Being fully exposed to the environment, the survival of extreme weather conditions must be guaranteed. In addition, special observing schemes to suppress atmospheric disturbances put very high demands on the drive and position control system. This has consequences for the stiffness of the structure and the choice of the drive system. Finally, the large quantity of antennas requires great attention to be paid to cost-saving methods of fabrication, transport and assembly. Considering the clear impact of ALMA on astronomy, even in a state of partial completion, it can be concluded that the astronomers conceived of a truly magnificent observing tool and that the engineers met their challenges and delivered an instrument satisfying the specifications.

The reader might ask himself: are the radio astronomers now satisfied with all these telescopes or do they want more? The not surprising answer is: we are quite happy with what we have but we need more! We mentioned in Chap. 7 the Square Kilometre Array (SKA), a global effort for a gigantic multifaceted radio telescope

that will cover wavelengths from several metres down to a few centimetres. Construction of a first phase will start within a few years and completion of the full instrument could be beyond 2030.

On a smaller scale, there are several plans for telescopes that could be classified as "extrapolations" of the current situation. China is very active in this area. We mentioned the 500-m diameter FAST fixed spherical "bowl" in Chap. 7. The Xinjiang Astronomical Observatory in Urumqi has been given green light for the construction of an "Effelsberg-type" telescope of 110 m diameter, again a little bit larger! Use at a shortest wavelength of 3 mm is foreseen. In the USA, there is a design, at the moment without funding, for a 25-m diameter submillimetre telescope that will penetrate into the wavelength regime of 0.2 mm. The Japanese radio astronomers propose a 50–60-m diameter reflector that should work down to 0.4 mm. Studies have begun at NRAO for an extension of the VLA to fill the wavelength and angular resolution gap between the SKA and ALMA. Finally, several 12-m class submm telescopes are being realised or planned (in Argentina/Brazil, China/South pole and the Netherlands/Namibia), all located at high sites. Added to the existing submm telescopes in Hawaii, Arizona, Europe (Spain, France) and Chile, they will complete a powerful network for VLBI observations at short mm wavelengths. This network, called the Event Horizon Telescope (EHT), aims at observing the shadow of the presumptive massive black hole in the centres of our Galaxy and other external galaxies.

9.2   A Dialogue on Management Aspects

In this final section, we leave the realm of technology to discuss aspects of the realisation of a state-of-the-art radio telescope project. We have seen how the development of radio telescope reflectors has taken its course over the last 70 years, beginning with the adaptation of wartime radar antennas to the present large and highly accurate telescopes that need an integrated approach to structural design, mechanics and related control systems to achieve their specification.

The process of advance is a continuous interplay between the requirements or wishes of the astronomers and the capabilities of the design and fabrication engineers in industry. The conversation can only be fruitful if the participants speak a common language or at least have a basic understanding of each other's desires and capabilities. For a project to be successful, it is necessary that the *customer*, the scientist in the astronomical institute, can describe and explain his wishes in a way that is comprehensible to the *contractor*, the engineer who will translate these wishes into design and manufacturing proposals that include an estimate of the cost. To this end, it is customary to appoint *project managers* on both sides of the contract who, apart from managing their own groups of workers, assure that there exists a good communication between customer and contractor. The *system engineers* of the two parties carry out the particular task of creating a full mutual understanding of requirements and limitations. The authors of this book

have spent most of their career in such a role, including collaborating on a few projects. Based on our experiences in this area, we will now comment on the nontechnical aspects of a telescope project. As in the introductory chapter, we choose the form of a dialogue, where JB represents the customer and HK the contractor.

9.2.1   Customer and Contractor

JB: upon my arrival at the MPIfR in Bonn in September 1975 the finances for a mm-telescope of 30 m diameter had been secured and the project was ready to embark on discussions with prospective companies. I had been hired by Peter Mezger, the director for mm-astronomy, to act as Project Manager for the new telescope. At that time Otto Hachenberg, the originator of the 100-m Effelsberg telescope, was handling the antenna part of the new mm-wavelength efforts. He was nearing retirement and it had been agreed that I would assume the management of the project at that moment. Considering the success of the Effelsberg telescope it was natural to approach the two companies, Krupp and MAN, who had jointly designed and built that telescope.

The companies were invited to embark on the new project in a joint effort, a so-called Arbeitsgemeinschaft, a consortium. In principle they were open to such an arrangement. All parties, the Institute and Krupp/MAN were entering new territory in "specification space". It was agreed to start with a conceptual design phase during which each company would independently develop a few concepts. This guaranteed a diversity of proposals to emerge, which we thought would be helpful in defining a final design. The companies were given a set of performance specifications indicating the major parameters of the instrument we would like to have. We mentioned these in Chap. 5. *Here it is important to note that these were not detailed specifications on the structure. Rather they were boundary conditions to which the structure of the telescope should be matched for the planned astronomical research program.*

It was of course necessary to assure that no misinterpretation of these conditions would result in an unacceptable design. To this end regular face-to-face meetings between the contractor and the customer were held. I thought the process worked well and each company presented three conceptual designs that indeed showed rather large differences.

HK: Shortly before this project was introduced to the companies I had joined the design department of MAN-Gustavsburg and was assigned the role of systems engineer for the mm-telescope project. During the conceptual design phase a good interaction between customer and contractor was established that worked well throughout the entire project. Already in this phase the companies had

appointed a project manager. The customer had a leader but a formal organisation with a project manager was not obvious. Rather the group consisted of experienced physicists and engineers who had acquired experience in other telescope projects. I would like to go somewhat deeper into the aspects of project management and system engineering.

9.2.2   Project Management and System Engineering

HK: Large international institutions such as the European Southern Observatory ESO, or the European Space Agency ESA, carry out very big projects. Professional managers run these using management methods and tools that are taught in business schools. In "normal" telescope projects the project management is usually the task of a science staff member with some previous experience and interest in management, not necessarily following a formalized process of project control. Often on the customer's side of the project the same person handles management and system engineering. This is not ideal, because engineering and management issues should be handled with equal attention, which is difficult for a single person.

In industry the personal separation of project management and system engineering is the rule. These functions carry different responsibilities and any conflict of interest has to be resolved in an amicable way. The task of the project manager is to finish the project in time and on budget with acceptable technical outcome. The task of the system engineer is to find the best technical system based on available technology or, if this technology is not available, to initiate new technical development, bread boarding, prototyping and testing. The final outcome is always a compromise between best technical solutions and limited budget.

JB: The distinction between project management and system engineering is indeed important. In my case with 30-m telescope, despite being named project manager, I was really more the institute's system engineer. The contractual and financial aspects of the project were handled by the administration of the Institute, so my task in that area was mainly reporting on the progress and any technical problems that needed resolution. As I said earlier, we started the project with a conceptual design phase. At the end a single concept was adopted for the next phase. It is here that system engineering and a close contact between the engineering people at the customer and contractor play a decisive role in the project's success. Could you elaborate on that?

HK: As you already pointed out, the astronomer must formulate his vision in the form of requirement specifications. At this point the creative part of the system engineering starts. One will first look, whether previous solutions exist. If, to the joy of the creative engineer, previous solutions do not exist, he has to create new ones. The engineering process is similar to Darwin's evolution, with sometimes an

ingenious idea, but also a lot of trial and error. The standard methods in structuring large new projects take this into account and the projects are divided in project phases: (1) conceptual design, (2) preliminary design, (3) detailed design. Then follows (4) the construction phase (manufacturing, assembly), (5) commissioning (including acceptance testing) and finally the (6) operational phase carried out by the customer.

In the conceptual design phase, alternative design concepts should be established, analyzed and assessed in regard to performance, cost and risk, and at the end one concept should be selected for further elaboration. One frequent error is to start with only one concept introduced by convenience, orders from the boss, tradition or previous experience. In the conceptual design phase the most far-reaching technical decisions are made, and the best way to avoid a "one way street" is to compare alternatives! The project of the 30-m telescope followed this route.

In the preliminary design phase, the selected concept is further developed. Performance and technical risks are indentified by engineering analysis, bread boarding or prototyping. Normally at the end of this phase the total cost can be reliably determined and a fixed-price contract for the full construction is signed.

In the detailed design phase the design is finalized up to a level, that the construction phase can be planned, including reliable scheduling and cost control. In the construction phase the systems have to be built, commissioned and tested. During this phase the system engineer obtains his most important feedback for future projects.

9.2.3   Technological Aspects

JB: Your last remark brings me to the issue of technical requirements and their solutions for which the contractor may not be equipped and may be hesitant to engage in those areas solely for this "one off" delivery. An obvious example is the need to measure and adjust the surface of the reflector to a very high accuracy in the micron-range.

Normally, the customer—a radio astronomy observatory—will have a technical department for the development and construction of the electronic receiver systems and other parts of the operational telescope. Therefore such equipment is rarely part of the large industrial contract for the telescope. This despite the fact that the final acceptance of the telescope cannot be carried out without the use of these "customer provided" parts of the overall telescope system.

In the 30-m telescope project we encountered several critical points where the contractor did not have an existing solution available. These were in particular the

measurement of the reflector surface shape, the extremely high demands on the position control system and the thermal control of the structure. In these areas a close cooperation was established in which the customer developed methods and equipment needed to achieve the performance specification and the contractor accepted the results of these efforts as valid data for the determination of the telescope's performance. One specific example is the measurement of the surface. The contractor delivered a surface with a precision of about 200 μm, as agreed in the contract, and the customer used his own equipment to measure and adjust the surface with an accuracy of about 30 μm to a precision of 80 μm, well within the specification.

The control system for the accurate positioning and movement of the telescope was developed and realised in a joint effort of the Institute and the contractor with additional help from a university department. This was a highly successful endeavour that strengthened the contractor's standing in this field and saved the customer money while co-creating an advanced control system. The thermal control, a first of this magnitude, was jointly designed with and realised by a specialised company.

The close collaboration between the system engineers throughout the project was essential for a successful completion of the work.

HK: I agree with your statement. Let me add a warning for this procedure. A change of the system engineer at the contractor between the design and the construction phase should definitely be avoided. The designer may stop his engagement before the design is mature, and the fabricator may blame the designer as an excuse for his own deficiencies. Much of the success of these "state-of-art" projects depends on an atmosphere of trust and acknowledged professionalism between the parties.

9.2.4   Industrialisation Aspects, Costs

HK: The large telescopes are single, "one-off" projects, normally financed and realised with local resources. The continuity of growing know-how and its transfer from one project to the next is not guaranteed. If it fails it often causes extra cost and frustration. This is where industry has its role; industry is the best avenue to transfer know-how over time and projects. It gives the astronomer the role as customer and the fabricator as contractor. The relationship between astronomer and fabricator can be organized in different ways. The traditional Anglo-American way is for the customer to appoint a principal Architect or Engineer, who has major technical authority and is placed between customer and contractor. The Continental, may be German, method is to locate this Engineer with the contractor. For the customer this is tantamount to placing a turnkey contract with the contractor. It

minimises the managerial effort and budgetary risk for the customer. It involves a great confidence in the competence of the contractor!

The overall telescope System Engineer, covering also optics, mechanics and user interface is normally better located on the customer side, because his tasks are densely interwoven with the scientific goals, the science instrument design and later operation. The structural system engineer will be located in industry, because his engineering field is too different from the astronomical business. Sometimes the outcome of the structural system engineering is independently checked by outside specialists, expert consultants, located in the customer's project office.

JB: This is clear to me. You can't have your cake and eat it! It seems that a turnkey contract is preferable if you have the money. But in a totally new design for a telescope with extremely high requirements on precision you must be very confident that the contractor knows what he is doing and will be doing the right thing. It is very difficult to interfere in his process, because the contractor will immediately charge for extra work. In my view the model we used in the 30-m telescope project is a good middle road between the American and German way of project handling. The contractor was fully responsible for satisfying the specifications but the customer helped him to achieve and to demonstrate that. Both parties gained from the experience.

Radio telescopes, and satellite ground stations also, are normally located in a remote, radio quiet place. The mm-telescopes moreover tend to go to the highest place affordable. This brings to mind how one best decides on aspects like manufacturing, transportation and assembling the telescope. Can you illuminate this subject based on your experience with telescopes all over the world?

9.2.5   Manufacturing in Foreign Countries

HK: It is an interesting question and there is no general, uniform answer to it. The telescope structure is a rather big and heavy item, built and assembled with rather traditional, mature and simple technologies. The mechanical subsystems such as bearings and drives, and particularly the electrical and control system, consisting of motors, sensors, computers and software, are relatively small units, using highly sophisticated and ever developing technologies. Therefore it makes sense to look for the fabrication and assembly of the steel structure to local manufacturers in the vicinity of the site of the telescope, or at least in the country where the project is located and the money is provided. Cost issues may influence this choice; because for large structures the costs of detailed design engineers and draftsmen in addition to labour by technicians and fitters form a significant part of the overall cost.

Presently it is difficult to find a steel construction company in central Europe to built these structures for reasonable prices. When I started my career 35 years ago,

MAN Gustavsburg and other companies were manufacturing such structures and upper management was proud of its production capabilities. Today qualified manufacturing workshops are no longer available in Germany. The telescope engineering team of MAN (now named MT Mechatronics) survived by adapting its business concept to design and system engineering developments for the world market.

Identifying an appropriate local partner in a foreign country requires a careful assessment of his organizational structure and manufacturing quality. Often he needs assistance in setting up the necessary workshop processes, quality assurance systems and management, scheduling and cost control. This is difficult and the necessary efforts are often underestimated by the main contractor, lured by the low quotations of the local companies and believing in the power of fixed price contracts. To complete a project within specification, on time and in budget requires not only knowledge of the technical issues, but with equal importance attention to training, quality control and technical help for the local subcontractor. There are of course also the human aspects of social interaction with people of different cultural background that may speak a foreign language. To me these aspects make my projects especially exciting!

9.2.6   Product Delivery, Commissioning

JB: We are nearing the end of our story. There is one point that should be mentioned that is particular to the type of projects we have been discussing. Upon completion of the assembly of the telescope the contractor is not yet in a position where he can deliver his product with a documented proof of the required performance. The best way in which this proof can be established is to successfully carry out an astronomical observation. It is thus clear that final delivery of the industrial product will occur after a period of commissioning where all operational requirements have passed a test of full functionality. Normally, the customer takes charge of this activity with application of his own equipment and measuring methods, but the participation of the contractor will be required.

As we have mentioned at several places in this book, there are two major specifications that can only be satisfied with help from the customer. These are: (i) the measurement of the correct shape of the reflector and the adjustment of the reflector panels to this shape, and (ii) the establishment of a pointing model and confirmation of the correct behaviour of the servo-controlled pointing system (Sect. 8.8). Both activities are time consuming and normally need several iterations to obtain a final and satisfactory result.

The commissioning also involves the test of the receiver systems and the correct operation of the software for the control of the telescope and receivers, as well as

the data collection and eventual preliminary analysis in real time. This latter feature is essential for a timely completion of the iterative actions such as adjustment of the surface.

Ideally both system engineers from the customer and the contractor will participate in the initial commissioning to assist in analysing any unexpected outcomes. It is during this period that they learn most about the success or failure of their work. To the contractor's system engineer this knowledge will be most useful for his next project. The customer's system engineer will need it to answer questions from the astronomers when they experience odd behaviour of the telescope.

Acronyms and Abbreviations

ACA	Atacama Compact Array (Chile)
AEM	Alenia/Alcatel—EIE—MT Mechatronics consortium
ALMA	Atacama Large Millimeter Array (Chile)
APERTIF	Aperture Tile in Focus
ARGE	Arbeitsgemeinschaft (Consortium)
ASKAP	Australian SKA Precursor
ASTRON	Netherlands Institute for Radio Astronomy
ATA	Allen Telescope Array (USA)
AUI	Associated Universities Incorporated (USA)
Az	Azimuth
BDF	Beam Deviation Factor
BIMA	Berkeley Illinois Maryland Array (USA)
BUS	Backup structure
CAD	Computer-Aided Design
CAMRAS	C. A. Muller Radio Astronomy Station (Netherlands)
CARMA	California Array for Millimeter Astronomy
CCD	Charge-Coupled Device
CD	Cradle
CFRP	Carbon fibre reinforced plastic
CSIRO	Commonwealth Scientific and Industrial Research Organisation (Aus.)
CSO	Caltech Submillimeter Telescope Observatory (Hawaii)
E-ELT	European Extremely Large Telescope (ESO, Chile)
EIE	European Industrial Engineering (Italy)
El	Elevation
El-Az	Elevation over azimuth mount
ELC	Elevation cradle
ELT	Extremely Large Telescope
EM	Electromagnetic
ERS	Elevation rotating structure

ESA	European Space Agency
ESO	European Southern Observatory
ESSCO	Electronic Space Systems Corporation (USA)
FAST	Five-hundred-meter Aperture Spherical Telescope (China)
FBC	Flexible Body Compensation/Control
FDR	Final Design Review
FEA	Finite Element Analysis
FRAN	Framed Structures Analysis Program
FOV	Field of View
GBT	Green Bank Telescope (USA)
GMRT	Giant Metrewave Radio Telescope (India)
GMT	Giant Magellan Telescope (Chile)
GTM	Gran Telescopio Millimétrico (LMT) (Mexico)
HHT	Heinrich Hertz Telescope (USA)
HPBW	Half-power beamwidth
IGN	Instituto Geográfico Nacional (Spain)
INAOE	Instituto Nacional de Astrofísica, Óptica y Electrónica (Mexico)
INVAR	Very low expansion steel
IRAM	Institute for Radio Astronomy in the Millimeter Range (France)
JCMT	James Clerk Maxwell Telescope (Hawaii)
JPL	Jet Propulsion Laboratory (USA)
LBT	Large Binocular Telescope (USA)
LES	Lincoln Laboratory Experimental Satellite
LFST	Largest Feasible Steerable Telescope
LMT	Large Millimeter Telescope (GTM) (Mexico)
MAN	Maschinenfabrik Augsburg Nürnberg (Germany)
MERLIN	Multi-Element Radio Linked Interferometer Network (UK)
MIT	Massachusetts Institute of Technology (USA)
MPG	Max-Planck-Gesellschaft (Germany)
MPIfR	Max-Planck-Institut für Radioastronomie (Germany)
MRT	Millimeter Radio Telescope
NAOC	National Astronomical Observatory of China
NAOJ	National Astronomy Observatory of Japan
NASA	National Aeronautics and Space Administration
NOEMA	Northern Extended Millimeter Array (IRAM, France)
NRAO	National Radio Astronomy Observatory (USA)
NRL	Naval Research Laboratory (USA)
NSF	National Science Foundation (USA)
OVRO	Owens Valley Radio Observatory (USA)
PAF	Primary Focus Array
PDR	Preliminary Design Review
RC	Ritchey–Chrétien
RS	Reflector surface
SETI	Search for Extra-Terrestrial Intelligence

SKA	Square Kilometre Array
SMA	Submillimeter Array (Hawaii)
SMT	Submillimeter Telescope (USA)
SOW	Statement of Work
SRT	Sardinia Radio Telescope (Italy)
STAIR	Structural Analysis Interpretive Routine
TIW	Toronto Iron Works (USA)
TMT	Thirty Meter Telescope (optical)
UMass	University of Massachusetts at Amherst (USA)
VLA	Very Large Array (USA)
VLBI	Very Long Baseline Interferometry
VLT	Very Large Telescope (ESO)
VWF	Volkswagen Foundation (Germany)
WSRT	Westerbork Synthesis Radio Telescope (Netherlands)

Glossary

Antenna Device to receive or transmit electromagnetic radiation. Here used as an alternative for reflector or radio telescope.

Aberration Deviation of perfect behaviour by the telescope caused by shifts or deformations of the optical system.

Alidade Section of the telescope that provides azimuth movement and carries the elevation structure and reflector

Angular resolution Measure for the "sharpness" of view of the telescope; the angle on the sky where two stars can just be seen separately (see beamwidth).

Aperture Area over which a telescope captures radiation.

Aperture efficiency Percentage of power entering the aperture that actually reaches the focus.

Astigmatism Saddle-like deviation of reflector leading to a distortion of the beam with different foci in perpendicular planes

Astrodome Protective enclosure for the telescope that opens over the width of the telescope during observation. It co-rotates with the telescope.

Azimuth Angle along the horizontal plane. Normally, starting with zero in the North and advancing through East from 0 to 360 degrees

Backup structure (BUS) Support structure between reflector and elevation structure.

Beam The representation of the relative sensitivity of the antenna over all directions.

Beamwidth Angular width of the "main beam" over which the antenna collects most radiation. The half-power beamwidth (HPBW) is the angle where the sensitivity has decreased to half w.r.t. the peak value. It is used as a basic parameter characterising the angular resolution of the antenna.

Blocking Area of the aperture that radiation cannot reach by structural obstruction, such as a quadripod support of a secondary reflector.

Carbon fibre reinforced plastic (CFRP) Composite material of carbon fibres embedded in an epoxy matrix. Advantages are a large strength-to-weight ratio and a very small coefficient of thermal expansion.

Cassegrain optics Telescope with two mirrors. A hyperbolic secondary mirror reflects the radiation from the primary paraboloid back to a secondary focus, often behind the primary, reached through a central hole in the primary reflector. Named after its proposer Cassegrain.

Cladding Cover on the outside of the telescope structure providing protection from weather. Often includes thermal insulation.

Coma Up-down (or left-right) large-scale deviation of reflector leading to a shift in the beam direction and a strong asymmetric sidelobe.

Commissioning Process of testing to determine the specified performance of a telescope

Direct drive An electric motor directly drives the telescope axis without any intermediate gears.

Elevation Angle in the vertical plane from 0 degree at horizon to 90° in the zenith (overhead).

El-Az Shorthand for Elevation—Azimuth, indicating the two axes about which the telescope is rotated to reach a chosen direction on the sky.

El-Az-mount Telescope with movement in azimuth (around the vertical azimuth axis) and elevation (around the horizontal elevation axis).

Elevation structure Connection from BUS to the elevation bearings.

Feed Element in the focus, often a horn, that captures the radiation and transfers it to the receiver.

Field of view Angular area of sky available to the telescope beam.

Finite element Aanalysis Method to mathematically analyse the behaviour of a large physical system by dividing it into small, more easily analysed elements.

Flexible Body Control Method to counteract deformation of a flexible body through the use of data collected by sensors located on or near the body.

Focus The location where the radiation received by the telescope is concentrated.

Gain A measure for the sensitivity of the antenna or telescope, proportional to the effective aperture area.

Gregorian optics Telescope with two mirrors (see Cassegrain). In this case, the secondary mirror is an ellipsoid. Named after its proposer Gregory.

Homology Design method to control structural deformations so as to preserve the paraboloidal shape as function of orientation allowing a change in focal length and axis direction.

Horn Element to radiate or receive electromagnetic radiation, widely used as feed (see there) in the focus of the telescope. Parameters of a horn can be accurately calculated; hence, the horn is used for absolute calibrations of antenna sensitivity (gain).

Interferometer The signals of two or more separated antennas are combined to form an interference pattern that provides angular resolution proportional to the largest distance between the antennas.

Load/loading Force exerted on the structure from gravity, wind and thermal expansion.

Master equatorial Mechanical/optical device to transform celestial coordinates to instrument (azimuth–elevation) coordinates.

Mount/mounting Telescope structure that carries the reflector and enables the movement in azimuth and elevation.

Offset optics The primary reflector is a section of a larger paraboloid outside the symmetry axis of this paraboloid. Thus, the focus lies outside the aperture and blocking of the aperture is avoided. Example is the small dish for home reception of TV satellites.

Pintle bearing Central bearing on the telescope's azimuth axis.

Pointing The direction of viewing represented by the readings of the axis angular encoders (elevation and azimuth angle).

Pointing model Set of parameters representing inaccuracies in the telescope's geometry to adjust the commanded pointing direction to coincide with the true pointing direction.

Polar/equatorial mount Telescope with one axis parallel to the earth axis, allowing tracking a star by rotation about this axis only. The second axis sets declination.

Prime-Focus Array (PAF) Multi-element feed in the focal plane to increase the field of view and project a number of beams on the sky.

Quadripod Four-legged support of the secondary reflector or the primary focus equipment in the focus of the primary reflector (sometimes a tripod).

Radio holography Method to measure the geometrical shape of the reflector with the aid of a radio signal. The measured deviations from the theoretical shape are used to adjust the reflector to the correct curve.

Radome Fully closed protective structure for the telescope: a space-frame truss covered with a fabric that is transparent to the radio radiation.

Receiver Electronics that amplify and process the received radiation.

Reflector Essential part of the telescope that reflects the incoming radiation to the focal point.

Ritchey–Chrétien optics Telescope with two hyperbolic reflectors without coma aberration, thereby providing a large field of view.

Scattering efficiency Percentage of power that is scattered away from the main beam by imperfections in the geometrical shape of the reflector.

Sidelobe Secondary, normally weak, feature around the central beam.

System Engineer Person responsible for a complete and technically adequate realisation of a project

Zenith Point on the sky directly overhead from the viewer's position.

Name Index

A

Aerospace Corporation, 108
Alcatel, 165
Alcatel-EIE-MAN (AEM), 165, 166, 168, 170–181, 223
Alenia-EIE-MT Mechatronics (AEM), 182
Alenia Space, 165
Algonquin Park, 49, 50
Allen Telescope Array (ATA), 194–196
Allen, R.J., 192
ALMA, 6, 140, 145, 154, 155, 162–182, 223, 230, 233, 244, 246, 250, 251
Altmann, H., 76, 82, 83, 88
APEX, 137, 167, 236
Apollonius, 10
Archimedes, 1, 2, 10
Arecibo, 67, 186, 187, 189, 245
Ashton, E.L., 53
ASKAP, 237
ASTRON, 237, 245
Atacama Compact Array (ACA), 165, 181

B

Baars, J.W.M. (JB), 26, 96, 127, 132, 134, 137, 140, 162, 167, 191, 210, 211, 213, 223, 227–229, 231, 233
Becker, F., 73
Bell Laboratories, 33, 109, 194, 195
Bennett, J.C., 232
Berkeley-Illinois-Maryland-Array (BIMA), 156
Bliss Company, 55
Bolton, J.G., 49
Bowen, E.G., 47

Brandt, P., 82, 118
Bregman, J.D., 155
Bremer, M., 130
Bristol Steel and Iron, 56
Broten, N.W., 192
Caltech Submillimeter Observatory (CSO), 154–157, 159, 246
CAMRAS, 31, 38
Cassegrain, L., 12, 17, 19–21, 26–28, 42
Chajnantor, 6, 163, 164, 181, 246
Chu, T.S., 193
California Array for Millimeter Astronomy (CARMA), 156
Cook, J.S., 193
Crawford, A.B., 192
CSIRO, 47–49, 51, 52, 245

C

DeBoer, D.R., 237
Dornier, 116, 159
Dragone, C., 194
Dwingeloo, 3, 23, 31, 36–41, 44, 45, 50, 81, 204, 244, 245, 247

E

Effelsberg, 4, 21, 41, 54, 64, 65, 71–95, 101, 106, 112–116, 118–122, 124, 133, 137, 139, 168, 169, 174, 199, 201–204, 245, 248, 249, 251, 252
Erickson, N.R., 235
ESA, 18, 139, 253
Eschenauer, H., 82, 117, 125
ESO, 163–165, 233, 253

Subject Index

A

Aberration, 12, 17, 121, 125, 133, 134, 146, 151, 154, 163, 190, 215, 220–222, 224, 236, 238, 240

Absorption area, 214

Accelerometer, 167

Adjuster, 117, 133, 135, 136, 155, 173, 200, 231, 232, 249

Air mass, 127

Alidade, 74, 80, 114, 116, 118, 119, 133, 137, 142, 144, 145, 169, 200–204

Antenna
    Cassegrain, 26
    communication, 115
    deep-space, 133
    measurement, 231
    offset, 21, 193–196, 198
    reflector, 2, 6, 26–28, 108, 147, 192–203, 210, 211, 213–218, 220, 221, 223, 225, 227–229, 231, 233–240, 247, 248
    solid angle, 213, 214
    temperature, 42, 111, 156, 168, 174–177, 182, 195

Aperture
    blocking, 42, 196, 200, 215, 222
    illumination, 211, 231
    integration, 239

Array, 17, 28, 60, 96–98, 100, 113, 154, 158, 162–182, 190, 192, 194–197, 228, 233, 235–237, 245–248, 250

Astigmatism, 45, 55, 99, 101, 121, 130, 131, 169, 175–178, 220–222, 236, 240

Astrodome, 133, 135, 155, 156

Atmosphere, 5, 15, 16, 18, 127, 134, 158, 159, 164, 182, 229, 249

Atmospheric fluctuation, 117, 231

Axis
    azimuth, 5, 18, 19, 32–35, 37–41, 43, 45, 46, 49–53, 57, 59, 78–80, 111, 113, 115, 118, 133, 135, 145, 167, 170, 173, 175, 177–180, 187, 197, 200, 203, 204, 225, 230, 247
    elevation, 18, 19, 195, 197
    encoder, 168
    polar, 18, 53–55, 96, 97, 99

B

Back focal distance, 26, 29

Backlash, 179

Backscattering, 186

Backup structure (BUS), 23, 29, 37, 39, 41, 43, 46, 49, 50, 53–55, 59, 74, 76, 78, 80–95, 100–102, 104, 111, 116, 119, 136, 138, 139, 144, 147, 149, 155, 171, 173, 175, 177, 181, 191, 196, 200, 217, 218, 231, 249

Baseline, 98, 158, 162–164, 182, 196, 248

Beacon, 232

Beam
    efficiency, 210, 213, 214, 222
    pattern, 211, 213, 214, 218–220, 223–225, 228, 231
    shift, 46
    solid angle, 213, 214

Beam-deviation-factor (BDF), 227

Beamwidth, 52, 65, 142, 145, 154, 164, 187, 210, 212–214, 230, 247, 250

Bearing
    hydrostatic, 53, 54, 133, 247